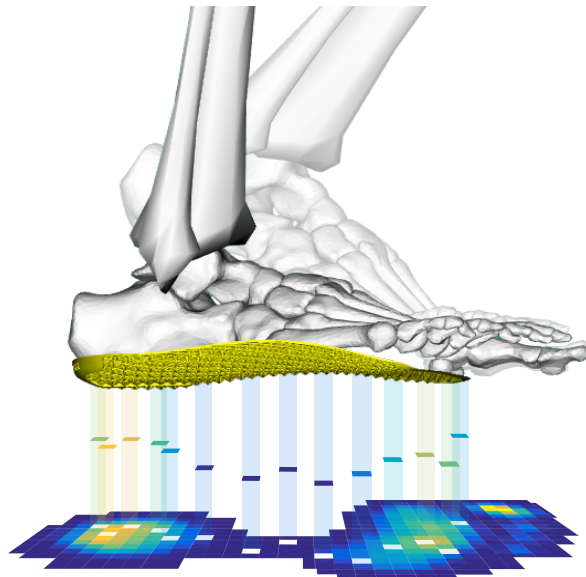


A combined multibody and plantar pressure approach to estimate and predict foot kinematics applied to 3D-printed insoles



Tiago de Melo Malaquias

Supervisors:

Prof. dr. ir. J. Vander Sloten
Prof. dr. I. Jonkers
Prof. dr. ir. F. De Groot

Dissertation presented in partial fulfillment of the requirements for the degree of Doctor of Engineering Science (PhD): Mechanical Engineering

May 2019

A combined multibody and plantar pressure approach to estimate and predict foot kinematics

applied to 3D-printed insoles

Tiago DE MELO MALAQUIAS

Examination committee:

Prof. dr. ir. R. Puers, chair

Prof. dr. ir. J. Vander Sloten, supervisor

Prof. dr. I. Jonkers, supervisor

Prof. dr. ir. F. De Groote, supervisor

Prof. dr. ir. G.H. van Lenthe

Prof. dr. B. Vanwanseele

Prof. dr. med. S. Clockaerts

(AZ Groeninge Kortrijk)

Prof. dr. ir. C. Mazzà

(University of Sheffield, United Kingdom)

Dissertation presented in partial fulfillment of the requirements for the degree of Doctor of Engineering Science (PhD): Mechanical Engineering

May 2019

© 2019 KU Leuven – Faculty of Engineering Science
Uitgegeven in eigen beheer, Tiago de Melo Malaquias, Celestijnenlaan 300C box 2419, B-3001 Leuven (Belgium)

Alle rechten voorbehouden. Niets uit deze uitgave mag worden vermenigvuldigd en/of openbaar gemaakt worden door middel van druk, fotokopie, microfilm, elektronisch of op welke andere wijze ook zonder voorafgaande schriftelijke toestemming van de uitgever.

All rights reserved. No part of the publication may be reproduced in any form by print, photoprint, microfilm, electronic or any other means without written permission from the publisher.

Acknowledgements

A retrospective analysis of these four years allowed me to understand the importance of the people surrounding me, without their support I could not have achieved this milestone. A Ph.D. is the top of a staircase which I have now reached, but behind me, there is a group of people that made this climb possible. So, I will dedicate this section to acknowledge everyone that in some way helped me to attain this major life accomplishment.

I must start by thanking the most fantastic trio of promoters Jos, Ilse, and Friedl; you were the main responsible for this achievement. You allowed me to come to Leuven to pursue a dream; for that, I will be forever thankful. For the past four years, you have guided me in such a harmonious way that I could not have asked for better. You always directed me to the right path; there was never a moment of uncertainty. Moreover, you balanced the supportive and demanding sides of a promoter until the last minute perfectly.

Besides your brilliant technical quality displayed through the insightful meetings with had through the years, each one of you brought to this thesis crucial and different contributions. Jos your joyfulness, experience and management skills give you the incredible capacity to have an overview of so many different topics and students. The pleasure you still take from research is admirable and that is transmitted to each one of us. You are one of the main responsible for the best working environments anyone could ask for: *BMe*. I will keep fond memories of your kind words of support and respect. Ilse, you are one of the most determined, caring and dedicated persons I have met in my life. I highly admire your determination, it makes you a force to be recognized. Your dedication to research and to your research group is visible from your innovative interdisciplinary work and from the people around you. Everyone in your research group knows, how much you care about us: Together wE Achieve More. I am truly thankful for the time you have dedicated to my thesis, you went '*above and beyond*'. Friedl your kindness and altruism are admirable; you always have time to help, and you always do it with a smile on your face. Your

capacity to understand the technical nuances of our projects is incredible, which in my case I know it was not always easy. I am sure that your future academic career will be incredible, especially when surrounded by excellent examples.

It was a pleasure and honour to have worked with you for the past four years. I have learned so much from you. I am looking forward to follow your future collaborations. A sincerely Dank je wel/Obrigado!

I would also like to thank all the members of my examination committee. Prof. Robert Puers, thank you for chairing the committee and for taking care of the administrative parts. Prof. Van Lenthe, Dr. Stefan Clockaerts, and Prof. Benedicte Vanwanseele thank you for your efforts and your willingness to read this thesis and help me improve it. Your excellent feedback and comments were invaluable in making this a more complete and comprehensive work. I would especially like to thank Prof. Claudia Mazzà, whom it was my honour to have as an external jury member. Thank you for your feedback as well as your availability and kindness to be a part of my Ph.D.

Greta, thank you for your insight in starting the Foot-Ankle funding chair and for your vision to collaborate not only with medical doctors but also with engineers.

A special appreciation goes to Baron Jean-Pierre Berghmans for partially supporting this research financially through the Foot-Ankle funding chair. Your donations have been essential for this work, and it gave us the freedom needed to perform this research.

Work presented in this project was also partially funded by the *Aladyn* project (*IWT*). Therefore I would also like to acknowledge the contributions of Lode and Dennis of *RSPrint*, Fien and Sartje of *RSscan*, and Tom of *Materialise*. Their technical support and their insightful view over the project were truly important during the development of this thesis. To Lode, Fien, and Sartje I must explicitly thank you for the provided measurement data, which was crucial for the conclusion of this thesis.

Furthermore, I would like to thank Walter Coudyzer of the radiology department of the UZ Leuven for his great help with the 4D CT scans measurements.

Wouter thank you so much for all the support provided during the entire Ph.D. If I could write one more name on this thesis, it would be yours. All the time you spent guiding me, discussing new ideas, explaining the different concept, providing technical support was crucial for the completion of this thesis. I will never be able to thank you enough. You were a true mentor.

Tassos, during the first days of my Ph.D. I attended your public defence, and, at that moment, I was so amazed that during the night I dreamed about my

public defence. Well, that day has arrived, and it is time for me to make my family and friends proud like I felt for you. Thank you for the great support and mentoring during the time we worked together, and to have introduced me to my favourite bar till this day in Belgium (*Fiere Margriet*).

Tuur, Carolina, Martina, Giacomo, Fabio, Cederic, Thomas, Jacoba, Joran, Jeffreyn and Niek it was a great pleasure to work with you. I was lucky to have worked with such great persons. You all contributed to this thesis and to my wonderful experience as a Ph.D. student.

Kurt, Thij, Xianyi, Maarteen, Sam, Tom, Mariska, Lianne, Hans, Hoa, Jente, Jill, Lorenzo, Azin, Wannes and Wei you always made me feel welcome at FaBeR, even though I would only go there occasionally. You are an amazing group to work with, thank you for all the nice discussions, constructive critics and most of all for the great work environment that you create.

Stefan, Mr. S., you still owe me a night out in Eindhoven! Four years have passed, and we haven't been there together. We had great times together in Leuven that included long and deep conversations at 5 a.m. in Grote Markt. I am now waiting for your Public Defence invitation.

Antoine, I am now waiting for a Michelin star meal that was promised four years ago, so wrap it up. You were the first person I met in Belgium and looking back seems like an eternity ago. Four years full of great experiences, and still on the top of my list is that day in Liège. It was so good that I haven't gone back not to ruin the idea. Maybe next time I'll go there will be for a bigger celebration, something like a wedding. It has been great sharing these Ph.D. years with a fantastic person like you.

Hannelore, my 'feet' friend, and work confident, among holidays, conferences, coffee breaks and 'weird' experiments we had fun over the last four years. I think when we get old, we will tell stories about how we used to drive cadaveric specimens to the hospital to give life to them again, stories like *Dr. Frankenstein*. We even appeared on TV to talk about these experiences! Good luck finishing your Ph.D., you will nail it.

BMe was my second home for the last four years and could not have asked for a better group of people to share this time. From day one I felt welcome and happy at work. I will always cherish the memories I made with you and how much fun we've had. Nele, Heleen, Julie, Sanne, Pim, Quentin, Karen, Haniyeh, Steven, Gabrijel, Marija, Vule, Zhaoyin, Lilibeth, Annaclaudia, Dimitris, Laura, Klaas, Amelie, Steffi, Lauranne, Hans, Diego, Tommy, Mar, Apeksha, Jorge, Marie-Mo, Darshan, Patricia, Dario and Stefan thank you for these wonderful times. This is not a 'Goodbye.' however, rather a 'See you soon!'.

Rita, you were presented to me as the secretary *BMe*, soon I realized that you were the moving force of the division, the information centre, the every-problem solution, the travel agency and I could go on for pages to reach one conclusion, you spoiled us all! Thank you for your amazing competence.

Ivo, the problem solver, I will always remember the day you helped me and Hannelore using the blowtorch you always carried in your pocket. To this day I am still impressed by the perfect timing of that moment. This is just one example of how grateful I am to have shared your last four years at *BMe*.

Kristel and Jana you had '*big shoes to fill*', but you did an amazing job with your sympathy and joyful spirit. Thank you so much for all the help, especially in the last months with all the defences organization.

Boys from 04.114, Mojtaba, Satanik, Fernando, Ali, and Alex it has been a pleasure sharing the office with such amazing people. From the endless discussions about the environment, traffic, weather, religion, culture, and daily life hacks, to the weekly supply of candies; guys we have created a world multicultural legacy in the office.

Dries, my dear friend, you were by far the person I spent the most time in the last four years, a nine to nine routine throughout the Ph.D.: Work, Cycle, CrossFit and repeat! I have so many things to thank you for. You were one of the main responsible for my integration in the Flemish society, which includes the day you welcomed Markos and me into your family house. You convinced me to start CrossFit, which brought the opportunity to challenge myself in a new sport as well as a whole new group of friends. We spent amazing holidays together from the west (New York and Montreal) to the east (Budapest and Satu Mare), and I believe it was with one of these trips that you conquered Agnesia with the perfect shopping adventure. We can discuss the truthfulness of the last statement in October!

Markitos, my true '*malakas*' (yes, this word is written on my thesis!), we started this adventure together and what a ride it has been. As an expat, you always tend to have someone in the back of your mind in case everything goes wrong, your secret safeguard, the person you believe it will do anything to help you. From the moment we met you carried (without knowing) that load. You always know how to keep calm and how to deal with problems and people. Last year just showed how good you are at that, truly proud of your personal achievements, you are a brave man! You, Maria and Alkis (*mi patronzito*) are my awesome Greek family.

Andrea, the '*Maverick*', and I am the '*Goose*' to your Leuven flights! It has been a pleasure sharing these past years with you; you brought a breath of fresh air to the office with an Italian scent. I love hearing your adventures, to know

that your warm Italian spirit has not been overshadowed by harsh northern winters. Next time you host me, you know I will revert the score you have saved in *FIFA*. Keep your happy and joyful spirit; we all need it!

Michel, the '*mooie boy*' of the office, that crazy, wonderful and colourful mind of your always baffles me, and you are such a box of surprises. I appreciate that you trust us to share what's going on up there every day. I think you have now realised that you have been adopted by a southern family (Portugal, Italy, Greece, and Spain) and I hope by now you have learned how to give/receive a proper hug. One thing that I still think we have failed is the lunch situation, please stop the sprinkles!

Rebeca, you are a crucial piece of the group, a peaceful and reasonable person that can hear and laugh about the strangest conversations. It is always a pleasure to share the first 10 min of my working day with you. You always have a kind word to say — best of luck for the rest of your Ph.D.

Orçun, my 'lost Turkish family', the most joyful character in *BMe*, you brought a smile to my face every single time you passed by the office with your positive attitude. You are amazing person to hang-out and to work with, and I know you will achieve everything you want. However, your next achievement should be a trip to Portugal to meet the rest of the family!

Wout my step-in to Belgium, you have been a great part of this wonderful experience. From the first day, I felt at home mostly because of you, you made my integration so much easier. I will forever be grateful for that.

Björn, my big Icelandic bear, what a ride it has been! Sharing three of the best years of my life with you has been wonderful. Your friendship, companionship and support created such a cosy environment to live in that I truly feel at home with you. The mutual respect we have for each other is fantastic. I am super proud of what you accomplished in Belgium, a Master's degree and now a Ph.D., it has been a pleasure being a part of your success. In four years, I hope to be celebrating with you one more accomplishment!

Lima tudo começou com um encontro aleatório num autocarro em Bruxelas e desde esse dia temos partilhado momentos memoráveis juntos. Em três anos criámos uma associação que está representada em três países, fomos ao outro lado do mundo vivenciar uma das melhores experiências da nossa vida, sobrevivemos à noite louca de Budapeste e espalhamos toda a nossa história com o mundo num podcast, isto enquanto trabalhávamos no nosso Ph.D. A vida é feita para encontrar-mos amigos como tu, com quem podemos sempre contar e com quem podemos partilhar estes grande momentos! Este texto fica aquém daquilo que foram na realidade os últimos anos mas o importante agora é saber qual é a próxima aventura?!

Aninha, uma amizade tão inigualável que sobreviveu a partilhar uma casa por um ano sem nunca (mas mesmo nunca) nos termos chateado. Sem dúvida a melhor colega de casa que alguém podia encontrar. És uma pessoa fantástica com quem adorei partilhar os últimos anos. A ligação é tão forte que até defendemos o doutoramento com apenas 24h de difereça. Partilhámos mil e um momentos entre outras mil ideias incríveis. De todos eles, três que vou de certeza guardar para sempre: criação de uma associação que está representada em três países, uma viagem mágica a Budapeste e por um momento que será único nas nossas vidas - a final do Euro 2016! O que virá a seguir?

Aqueles que sempre estiveram presentes, o *Café Mensal* e as *Belas e os Gordos* (ou qualquer que seja o nome neste momento), Leitão, Guedes, Moncada, Marta, Tatiana, Lopes, Luisa, Daniel, André, João, Dantas, Titi, Lamas, Frazão e Francisca; um enorme obrigado por termos mantido uma amizade intocável apesar da distância física. É muito por vossa causa que voltar a Algés será sempre a melhor sensação do mundo.

Filipa, ou Ana como eu gosto de te chamar, és, foste e serás sempre parte da família. Uma amizade com mais de 25 anos, creche, primária, básica, secundária, universidade, vida 'adulta', casamento e doutoramento. Mesmo com 2000 km pelo meio, continuas a ser o meu grande apoio, nunca me deixaste sentir essa distância, muito mas muito obrigado *chéri!*

Dade e Zé este sucesso é partilhado com vocês, uma presença excepcional na minha vida, a família que eu adoptei e que me adoptou. Todos os nossos sucessos, meus, do Diogo e da Catarina, são também vossos.

Avó, tios e malta jovem: Margarida, Rodrigo, Maria e Henrique, sei que não é fácil estarmos afastados por tanto tempo mas acreditem que o vosso apoio foi e será sempre importante para o meu sucesso. Todas as vossas chamadas e mensagens foram essenciais para concluir mais esta etapa da minha vida. Obrigado por todo o apoio nesta aventura.

Diogo e Tó, comigo fazemos o trio dos irmãos emigrantes. Tó trilhaste este caminho primeiro, mostraste-nos e deste-nos motivação para seguir um caminho semelhante. Foi sempre com orgulho que olhei para o teu percurso e devo-te a ti o bichinho do doutoramento. Diogo, uma vida partilhada contigo, as vitórias são dos dois e para os dois, sempre alcançámos os nossos objectivos esta tese é mais um. Mais virão!

Mãe e Pai, não sei o quão difícil deve ser para vocês viverem tão longe de nós, se é difícil para mim quando tenho um mundo inteiro para descobrir e conquistar, para vocês deve ser muito mais. Sei que sempre acreditaram que devíamos partir à descoberta, atingir os nossos objectivos, lutar pelos nossos sonhos, mesmo que isso nos leve para o outro lado do mundo. A conclusão do

doutoramento é uma vitória que é totalmente vossa e este esforço todo é muito em parte para vocês. Obrigado por me terem dado todas as oportunidades possíveis para fazer este dia acontecer!

Catarina, só duas pessoas 'estranhas' aceitariam ultrapassar dois doutoramentos em três países diferentes e acreditar que no fim tudo ia ficar bem. Nós acreditámos, e aqui estamos no fim dessa aventura a lutar por novos objetivos e desafios em conjunto. Depois de escalar esta montanha acredito que seremos capazes de atingir todos os nossos sonhos. No meio de toda esta comoção passaram dez anos desde que te conheci, e hoje mais que nunca acredito que não existe melhor companheira/amiga/namorada para partilhar esta montanha russa que é a vida. Obrigado por todo o teu apoio!

Obrigado! Thank you! Dank je wel!

Tiago

Abstract

In Europe, over 200 million people suffer from disabling foot and ankle pain caused by a variety of pathologies as overloading injuries, degenerative joint disorders and systemic diseases (*e.g.* diabetes). Foot orthoses (FOs) or insoles are a popular conservative treatment to alleviate pain and prevent further deterioration of the pathological condition; the goal is to optimize a patient's foot function by relieving symptoms and slow down or even arrest the progression of the pathology (*e.g.* rearranging pressure distribution in diabetic patients to prevent foot ulcers). Currently, the process of patient assessment for insole design and manufacturing relies on subjective decision making and time-consuming handicraft work by the clinician. The design of these orthoses is primarily based on the capture of the foot shape using traditional techniques such as plaster casting.

3D-printed insoles reduce the manufacturing time and allow efficient production of subject-specific insoles. It allows for the local adjustment of mechanical properties so that the insole can optimally guide the movement of the foot. Therefore, it is crucial to understand the biomechanical effect of the insole on the foot. The overall aim of this thesis was to develop the different steps necessary for the creation of a fully objective and automated digital workflow that goes from foot biomechanics assessment to the production of subject-specific insoles.

Computer multibody models can describe the causal relations between input parameters (*i.e.* kinetics) and model response (*i.e.* kinematics) given a known geometrical structure. Only a limited number of detailed musculoskeletal foot models for use in dynamic simulations were described in literature. Moreover, the number of accessible detailed musculoskeletal foot models is even smaller, this is a major limitation to reproduce results or to use the reported models in different studies. In the present work, two detailed *OpenSim* 3D multibody foot-ankle models generated based on CT scans using a semi-automatic tool, are described. The proposed models consist of five rigid segments (talus, calcaneus, midfoot, forefoot, and toes), connected by five joints (ankle, subtalar, midtarsal,

tarsometatarsal and metatarsophalangeal), one with 15 DOF and the other with 8 DOF. The calculated kinematics of both models were evaluated using motion capture and compared against literature, both presenting realistic results. An inverse dynamic analysis was performed for the 8 DOF model, again presenting dynamic results similar to literature.

The 8 DOF foot model was then used with *in-vivo* gait analysis measurements of flat feet and control subjects using different footwear while walking. The differences in kinematic and kinetic parameters between control and flat feet subjects were estimated in barefoot and shoe walking. In parallel, the influence of subject-specific 3D-printed insoles on kinematics and kinetics of flat feet subjects was compared to the influence of a subject-specific Ethylene-Vinyl Acetate (EVA) molded insole. The flat feet subjects presented an increase in forefoot dorsiflexion and abduction while walking barefoot. The use of EVA and 3D-printed insoles corrected the aberrant flat feet-related kinematics and kinetics presented during the minimalistic shoe condition: arch height increased, as reflected by the decreased forefoot dorsiflexion and abduction. Both insoles provided similar correction, thereby confirming the suitability of 3D-printed insoles in the correction of flat feet kinematics and kinetics.

The use of plantar pressure measurement systems to evaluate foot and ankle pathologies is well established in clinical practice. Although relevant to detect local tissue (over-)loading, to date, plantar pressure data cannot be used to evaluate ankle-foot kinematics. In this thesis, we present a least squares optimization algorithm that minimizes the weighted difference between simulated and measured plantar pressure using different marker-sets data. Both, marker positions and plantar pressures are simulated in *OpenSim* using the previously described 8 DOF foot model coupled with an ellipsoid based elastic foundation contact model. It was concluded that a minimum of four markers combined with pressure data was needed to estimate the kinematics with accuracy comparable to the full marker approach. The ability of estimating full foot kinematics using a simplified set-up that relies on a limited number of reflective markers combined with plantar pressure measurements has significant time and economic implications for both research and clinical applications. It will allow a more accessible, objective clinical evaluation of foot pathologies.

With the introduction of 3D-printed insoles came the ability to manufacture insoles with mechanical properties that are tailored to specific subjects in a time efficient manner. However, our understanding of how insoles' mechanical properties influence the dynamic behavior of the foot during movement is limited. So, a torque driven forward simulation framework was developed to evaluate the effect of different insoles' properties on the kinematics of the foot. In this thesis the effect of different insole stiffnesses on foot kinematics during walking was evaluated. The torque driven forward simulations were computed in *OpenSim*.

again using the 8 DOF foot model. The model was coupled with an elastic foundation foot-ground contact model. The insoles were modeled using bushing forces connecting the calcaneus to the forefoot. Increased bending stiffness mostly independent from torsional stiffness led to kinematic adaptations that have the potential to partially correct low foot longitudinal by increasing forefoot adduction.

This thesis demonstrates the potential of detailed foot musculoskeletal models to be used for kinematic acquisition in a clinical environment and for the improvement of insoles design. These advances can lead to improved orthopaedic patient care, improving both the evaluation as well as the treatment prescription process.

Beknopte Samenvatting

In Europa lijden meer dan 200 miljoen mensen aan voet en enkel klachten die veroorzaakt zijn door verschillende pathologieën zoals overbelasting, degeneratieve gewrichtsaandoeningen en systemische ziektes (bv. diabetes). Voetortheses of steunzolen zijn een populaire conservatieve behandeling om pijn te verminderen en verdere ontwikkeling van de pathologie tegen te gaan met als doel de patiënt zijn voetfunctie terug te optimaliseren. Hiermee worden de symptomen van de pathologie onderdrukt of zelfs uitgesteld (zoals het voorkomen van voetzweren bij diabetes patiënten door het herorganiseren van de drukverdeling). In de huidige praktijk wordt het ontwerp van de zool en de productie hiervan afgesteld op de subjectieve beslissing van de clinicus. Daarnaast worden deze ook met de hand gemaakt, wat een tijdrovende activiteit is. Het ontwerp van de zolen is voornamelijk gebaseerd op de vorm van de voet, die wordt opgemeten met traditionele methodes zoals een gipsafgietsel.

De ontwikkeling van 3D-geprinte zolen laat toe om subject specifieke informatie efficiënt op te nemen in het productieproces en zorgt voor een verminderde productietijd. Bovendien kunnen de mechanische eigenschappen van de zool lokaal aangepast worden zodat de zool de voet optimaal kan begeleiden tijdens een beweging. Daarom is het cruciaal om het biomechanische effect van de zool op de voet te begrijpen. Het globale doel van deze thesis is de ontwikkeling van een stappenplan dat kan gebruikt worden om volledig objectief en automatisch een analyse van voet biomechanica om te zetten in de productie van subject-specifieke zolen.

Computer gebaseerde musculoskeletale modellen laten toe om een causale relatie te beschrijven tussen input parameters (kinetica) en de respons van het model (kinematica) indien er een gekende geometrische structuur bestaat. In de literatuur zijn slechts een beperkt aantal gedetailleerde musculoskeletale modellen van de voet beschreven die gebruikt werden in dynamische simulaties. Dit maakt het moeilijk om resultaten uit voorgaande studies te reproduceren of om de gebruikte modellen over te nemen in andere studies. In deze thesis worden

twee gedetailleerde 3D voet-enkel modellen gecreëerd in *OpenSim* aan de hand van een semiautomatische methode gebaseerd op CT beelden. De voorgestelde modellen bestaan uit vijf rigide segmenten (talus, calcaneus, middenvoet, voorvoet en tenen) die verbonden zijn via vijf gewrichten (enkel, subtalaire, midtarsaal, tarsometatarsaal en metatarsophalangeaal gewricht). Eén van de modellen heeft 15 vrijheidsgraden en het andere heeft 8 vrijheidsgraden. De kinematica werd berekend met beide modellen en vergeleken met een marker-gebaseerde ganganalyse en met de literatuur. Beide modellen toonden realistische resultaten. Bovendien vertoonde de inverse analyse uitgevoerd met het model met 8 vrijheidsgraden ook overeenkomstige resultaten met de literatuur.

Het model met 8 vrijheidsgraden werd hierna gebruikt voor een *in-vivo* ganganalyse van proefpersonen met platvoeten en gezonde controlessubjecten tijdens het dragen van verschillend schoeisel. De verschillen in kinematica en kinetica werden bestudeerd tussen de twee groepen voor blootvoets wandelen en wandelen met schoenen. Daarnaast werd de invloed van subject-specifieke 3D geprinte zolen en subject-specifieke Ethyleen-Vinyl-Acetaat (EVA) zolen op de kinematica en kinetica van proefpersonen met platvoeten bestudeerd. De proefpersonen met platvoeten vertoonden een gestegen voorvoet dorsiflexie en abductie tijdens het blootvoets wandelen. Zowel de EVA zool als de 3D geprinte zool verbeterden de verstoerde kinematica gerelateerd aan platvoeten tijdens het wandelen met een minimalistische schoen: de hoogte van de voetboog nam toe, zoals weerspiegeld in de gedaalde voorvoet dorsiflexie en abductie. Beide zolen gaven eenzelfde correctie, waardoor bevestigd wordt dat 3D geprinte zolen kunnen gebruikt worden door personen met platvoeten voor de correctie van de kinematica en kinetica tijdens het gaan.

In de klinische praktijk worden voet en enkel pathologieën vaak geëvalueerd aan de hand van plantaire druk opgemeten door drukplaten. Dit systeem laat toe om te bestuderen hoe het weefsel lokaal (over)belast wordt, maar op dit moment kan het nog niet gebruikt worden voor het evalueren van de voeten-enkel kinematica. In deze thesis presenteren we een kleinste kwadratenmethode optimalisatie algoritme dat het verschil tussen gesimuleerde en opgemeten plantaire druk gaat minimaliseren aan de hand van verschillende marker-sets data. Zowel de positie van de markers als de plantaire druk worden gesimuleerd in *OpenSim* met het voorafgaand beschreven voet-enkel model met 8 vrijheidsgraden. Dit model is gekoppeld met een elastisch contact model gebaseerd op een ellipsoïde. We konden concluderen dat een minimum van vier markers in combinatie met plantaire druk is nodig om kinematica te berekenen die in nauwkeurigheid overeenkomstig is met een volledig marker-gebaseerde oplossing. De mogelijkheid om de kinematica van de volledige voet te voorspellen aan de hand van een vereenvoudigde opstelling met een beperkt

aantal reflectieve markers in combinatie met een meetsysteem voor plantaire druk kan een significante invloed hebben op tijd en economische aspecten voor onderzoeks- en klinische toepassingen. Het zal toelaten om een eenvoudigere en objectieve klinische evaluatie van voet pathologieën uit te voeren.

Met de introductie van 3D geprinte zolen is er de mogelijkheid om zolen met subject specifieke mechanische eigenschappen te ontwikkelen op een tijds-efficiënte manier, maar onze kennis van hoe deze mechanische eigenschappen het dynamische gedrag van de voetbeweging beïnvloeden is nog beperkt. Daarom werd een werklijn ontwikkeld voor koppel gedragen voorwaartse simulaties om de invloed van verschillende eigenschappen van de zolen op de kinematica van de voet te bestuderen. In deze thesis hebben we de invloed van de stijfheid van de zool op de voetkinematica tijdens het wandelen geëvalueerd. De voorwaartse simulaties werden opnieuw uitgevoerd met het model met 8 vrijheidsgraden gekoppeld met het elastische contact model. De zolen werden gemodelleerd als ‘bushing forces’ die de calcaneus met de voorvoet verbinden. Een gestegen stijfheid in de buigrichting (meestal onafhankelijk van een torsionele stijfheid) leidde tot kinematische veranderingen dat mogelijk de voet in de longitudinale richting kan verbeteren door de voervoet adductie te doen toenemen.

Deze thesis toont dat gedetailleerde modellen de mogelijkheid hebben om kinematica op te meten in een klinische omgeving en om het ontwerp van zolen te verbeteren. Deze vooruitgang kan leiden tot een verbetering van de behandeling van orthopedische patiënten door zowel het proces van de evaluatie als de voorschrijving van de behandeling te verbeteren.

List of Abbreviations

1M	1 Markers
2M	2 Markers
3D	Three-dimensional
3DMFM	3D multi-segment foot model
4D	Four-dimensional
AM	Additive manufacturing
AMP	All Markers+ Pressure
BIO	Blake inverted orthosis
CT	Computed tomography
DOF	Degree of freedom
EFM	Elastic foundation modeling
EVA	Ethylene-vinyl acetate
FE	Finite element
FEM	Finite element model
FFO	Functional Foot orthosis
FMMM	Foot musculoskeletal multibody models
FO	Foot orthosis
FWO	Research Foundation - Flanders
GRF	Ground reaction forces
HU	Hounsfield units
IMU	Inertial measurement unit
LMM	Linear mixed model
<i>meanabsdiff</i>	Mean absolute kinematics difference
MFM	Milwaukee foot model
MO	Markers Optimization
MRI	Magnetic resonance imaging
OFM	Oxford foot model
P1	Phase one of stance phase of gait (from initial contact (0%) to foot flat (16%))
P2	Phase two of stance phase of gait (from foot flat (17%) to midstance (42%))
P3	Phase three of stance phase of gait (from midstance (43%) to heel off (66%))

P4	Phase four of stance phase of gait (from heel off (67%) to toe off (100%))
<i>peakabsdiff</i>	Peak absolute kinematics difference
PiG	Plug in Gait
PiGe	Plug in Gait extended
PLA	Polylactide
RMS	Root mean square
ROM	Range of motion
SD	Standard deviation
ST	Soft tissue
VSC	Flemish Supercomputer Center
<i>withinstd</i>	Within the standard deviation

List of Symbols

Chapter 3: Extended foot-ankle musculoskeletal models for application in movement analysis

ρ	Density
n	Volume mesh element
i	Foot segment
HU	CT scan greyscale Hounsfield units
a	Line's slope of the linear relation between the CT scan's greyscale and the correspondent density value
b	Y-intercept of the linear relation between the CT scan's greyscale and the correspondent density value

Chapter 4: A multi-segment foot-model based kinematics and kinetics analysis on the influence of 3D-printed insoles in flat feet subjects

X_{Phase}	Dependent variable for each of the four phases of stance
$Condition$	Fixed effect for each conditions (barefoot, <i>Labshoes</i> , <i>EVA Molded</i> , <i>3D-printed</i>)
$Side$	Fixed effect for each leg (Left or Right)
$Subject$	Random variable

Chapter 5: Plantar pressure based estimates of foot kinematics during gait – a least squares optimization approach

pp_{norm}	Matrix (64 x 64) of the sum of the plantar pressure over the stance phase normalized to the maximum value
\hat{pp}	Matrix (64 x 64) of measured plantar pressure

i	Time step
nT	Number of time steps
s	Scaling factor for the measured pressure
A_s	Area of the sensors
A, \dots, J	Ten parameters of the ellipsoid conic algebraic equation
q	Kinematics
f_{pp}	Pressure error
pp	Matrix (64 x 64) of simulated plantar pressure
f_M	Marker error
M	Simulated marker positions
\hat{M}	Measured marker positions
s_M	Scaling factor of the markers error
w_P	Weight of the pressure error in the cost function of the optimization algorithm
w_M	Weight of the markers error in the cost function of the optimization algorithm
ϵ_{marker}	Distance between the measured and simulated marker
r	Trial
s	Subject
nR	Number of trials
nS	Number of subjects
d_{marker_i}	Distance between measured and the simulated marker
nM	Number of markers

Chapter 6: Predictive simulations of the corrective effect of controlled stiffness 3D-printed insoles during the stance phase of gait

f	Stress
ε	Strain
ε_l	Initial strain
ε_p	Yeld strain
k_L	Stiffness of the ligaments
a	Cross sectional area of the ligaments
L_0	Length of the ligaments at zero load
\hat{pp}	Matrix (64 x 64) of measured plantar pressure
pp	Matrix (64 x 64) of simulated plantar pressure
i	Time step
nT	Number of time steps
q	Kinematics
f_{pp}	Pressure error
f_M	Marker error

M	Simulated marker positions
\hat{M}	Measured marker positions
s_M	Scaling factor of the markers error
f_F	Vertical ground reaction force error
F	Simulated vertical ground reaction force
\hat{F}	Measured vertical ground reaction force
f_K	Penalization for large joint angles
w_P	Weight of the pressure error in the cost function of the optimization algorithm
w_M	Weight of the markers error in the cost function of the optimization algorithm
w_F	Weight of the vertical ground reaction force error in the cost function of the optimization algorithm
k_T	Torsional stiffness
k_B	Bending stiffness
k_p	Position error gain of the correction controllers
k_v	Velocity error gain of the correction controllers
X_{Phase}	Dependent variable for each of the four phases of stance
$Condition$	Fixed effect for each insole stiffness
$Side$	Fixed effect for each leg (Left or Right)
$Subject$	Random variable

Appendix A: Contact Model

\hat{pp}	Matrix (64 x 64) of measured plantar pressure
pp	Matrix (64 x 64) of simulated plantar pressure
i	Time step
nT	Number of time steps
s	Scaling factor for the measured pressure
A_s	Area of the sensors
A, \dots, J	Ten parameters of the ellipsoid conic algebraic equation
I	Interval for the ten equally distant time steps of the stance phase
q	Kinematics
f_M	Marker error
M	Simulated marker positions
\hat{M}	Measured marker positions
s_M	Scaling factor of the markers error
f_F	Vertical ground reaction force error
F	Simulated vertical ground reaction force
\hat{F}	Measured vertical ground reaction force

w_M	Weight of the markers error in the cost function of the optimization algorithm
w_F	Weight of the vertical ground reaction force error in the cost function of the optimization algorithm

Contents

Abstract	ix
Beknopte Samenvatting	xiii
List of Abbreviations	xvii
List of Symbols	xix
Contents	xxiii
List of Figures	xxix
List of Tables	xxxix
1 General Introduction	1
1.1 Foot Orthoses	5
1.1.1 Types of foot orthoses	6
1.1.2 Materials used for foot orthoses fabrication	7
1.1.3 Foot orthoses mechanical properties assessment	7
1.2 Dynamic measurement systems	9
1.2.1 3D Stereophotogrammetry	9
1.2.2 Inertial measurement units	12

1.2.3	Plantar pressure	12
1.3	Foot musculoskeletal models	14
1.3.1	Finite elements musculoskeletal models	14
1.3.2	Foot musculoskeletal multibody models	15
1.3.3	Forward predictive simulations	19
1.4	Summary of the state-of-the-art limitations	21
2	General Aim	23
2.1	Research Objective	24
2.2	Thesis Outline	26
3	Extended foot-ankle musculoskeletal models for application in movement analysis	27
3.1	Abstract	28
3.2	Introduction	28
3.3	Methods	29
3.3.1	Surfaces and volume meshes generation	29
3.3.2	Computation of the local coordinate systems	29
3.3.3	Anthropometric properties computation	31
3.3.4	Model creation	31
3.3.5	Marker set protocol and Acquisition	32
3.3.6	Decomposition of ground reaction forces	34
3.3.7	Validation	34
3.4	Results	34
3.5	Discussion	37
3.6	Conclusion	38
3.7	Supplementary material	38
3.8	Acknowledgements	38

4 A multi-segment foot-model based kinematics and kinetics analysis on the influence of 3D-printed insoles in flat feet subjects	41
4.1 Abstract	42
4.2 Introduction	42
4.3 Methods	44
4.4 Results	47
4.4.1 Kinematics	47
4.4.2 Kinetics	48
4.5 Discussion	52
4.6 Conclusion	54
4.7 Acknowledgements	55
5 Plantar pressure based estimates of foot kinematics during gait – a least squares optimization approach	57
5.1 Abstract	58
5.2 Introduction	58
5.3 Methods	59
5.3.1 Marker set protocol and acquisition	59
5.3.2 Foot musculoskeletal model	60
5.3.3 Contact Model	60
5.3.4 Estimation of kinematics	63
5.3.5 Validation	64
5.4 Results	67
5.5 Discussion	72
5.6 Conclusion	75
5.7 Acknowledgements	75
6 Predictive simulations of the corrective effect of controlled stiffness 3D-printed insoles during the stance phase of gait	77

6.1 Abstract	78
6.2 Introduction	79
6.3 Methods	80
6.3.1 Marker set protocol and acquisition	80
6.3.2 Insoles mechanical testing	80
6.3.3 Foot musculoskeletal model	81
6.3.4 Ligaments	81
6.3.5 Contact model	82
6.3.6 Estimation of Kinematics	84
6.3.7 Residual Reduction Analysis	85
6.3.8 Insoles Modeling	85
6.3.9 Forward Simulations	85
6.3.10 Outcome Variables	86
6.4 Results	87
6.5 Discussion	90
6.6 Conclusion	92
6.7 Acknowledgements	93
7 General conclusion and Future work	95
7.1 Individual contributions	95
7.1.1 Study 1: Extended foot-ankle musculoskeletal models for application in movement analysis - Chapter 3	95
7.1.2 Study 2: Multi-Segment foot kinematics and kinetics analysis on the influence of 3D-printed insoles on flat feet subjects - Chapter 4	96
7.1.3 Study 3: Plantar pressure based estimates of foot kinematics during gait – a least squares optimization approach - Chapter 5	97

7.1.4 Study 4: Predictive simulations of the corrective effect of controlled stiffness 3D-printed insoles during the stance phase of gait - Chapter 6	98
7.2 General discussion	98
7.3 Future perspectives	102
7.3.1 Simulation-based insole design, the route to application	102
7.3.2 Pressure-based kinematic simulations for broader biomechanics applications	104
A Contact model computation	107
A.1 Geometry and position	107
A.2 Stiffness optimization	110
B Sensitivity analysis: ellipsoids scaling factor	113
C Extended results of Chapter 5	117
D Extended results of Chapter 6	129
Bibliography	137
Curriculum Vitae	163
List of publications	165

List of Figures

1.1	(A: Standard clinical procedure from patient assessment of foot pathologies to conservative treatment using insoles (A.1, A.2, A.3, A.4 and A.5). B: Envisioned clinical procedure from patient assessment of foot pathologies to conservative treatment using insoles (B.1, B.2, B.3, B.4, B.5 and B.6). Purple double lined arrows: Methodologies used in research environments to evaluate foot pathologies and insoles effectiveness. Yellow dashed arrows: Possibility of bringing research methodologies into clinical care.	3
1.2	(A) Whitman's FO; (B) Robert-Whitman's FO; (C) Levy's FO; (D) Root's FO and (E) U.C.B.L. FO. Figure adapted from Kirby, K. and Green, D., 1992 [137].	5
1.3	Most used 3D multisegment foot models - 3DMFMs: (A) Milwaukee Foot Model (MFM) adapted from Kidder <i>et al.</i> (1996) [73, 136]; (B) Oxford Foot Model (OFM) adapted from Carson <i>et al.</i> (2001) [50].	11
1.4	Finite Element (FE) model described in Cheung and Zhang 2005 adapted from [58]: (A) soft tissues; (B) bony and ligamentous structures and (C) flat and custom-molded insoles.	15
1.5	Different foot musculoskeletal multibody models (FMMM). (A) Chow and Jacobson (1971) adapted from [188]; (B) Hatze (1976) adapted from [104]; (C) Delp <i>et al.</i> (1990) adapted from [72]; (D) Scott and Winter (1993) adapted from [217]; (E) Morlock and Nigg (1991) adapted from [168] and (F) Bruening <i>et al.</i> (2012) adapted from [38].	18
1.6	Elastic Foundation method formulation adapted from A. Pérez-González <i>et al.</i> (2008) [192].	20

3.1	Cutting planes used to divide the soft tissue and anatomical landmarks selected in <i>Mimics® Innovation Suite</i>	30
3.2	Extended foot models (<i>OpenSim</i>). Left) 8 DOF model and Right) 15 DOF model. Depicted segments: Cyan - Talus; Purple - Calcaneus; Green - Midfoot; Yellow - Forefoot; Red – Toes. The dashed lines depict the joint axes.	32
3.3	Results: (A) Kinematic results - Angles (degrees) between the two specified bodies for the 8 DOF model (green), 15 DOF model (red) and Lundgren <i>et al.</i> (2008) [152] (blue) during the stance phase of gait; (B) Inverse Dynamics results - Joint normalised moments (Nm/Kg) obtained for the 8 DOF model during the stance phase of gait; (C) Ligaments - Elongation of the right foot ligaments (% of their resting length) during the stance phase of gait. The solid lines represent the mean of the trials and the dashed lines \pm 1SD.	36
4.1	A) Minimalistic shoes (<i>Labshoe</i>), B) <i>EVA Molded</i> insoles and C) <i>3D-printed</i> insoles.	46
4.2	Mean joint angles between calcaneus and forefoot for each phase of the stance phase for the barefoot and <i>Labshoe</i> condition. Orange – Control barefoot; Light Green – Control <i>Labshoe</i> ; Pink – Flat Feet barefoot; Light Blue – Flat Feet <i>Labshoe</i> . The black lines represent significant difference (p – value $< 0.05/8$). The box plots do not depict eventual outliers.	49
4.3	Mean joint angles between calcaneus and forefoot for each phase of the stance phase for the different conditions of the flat feet group. Light Blue – Flat Feet <i>Labshoe</i> ; Blue – Flat Feet <i>3D-printed</i> ; Dark Blue – Flat Feet <i>EVA Molded</i> . The black lines represent significant difference (p – value $< 0.05/8$). The box plots do not depict eventual outliers.	49
4.4	Mean joint angles between calcaneus and forefoot for each phase of the stance phase for the different conditions of the control group. Light Green – Flat Feet <i>Labshoe</i> ; Green – Flat Feet <i>3D-printed</i> ; Dark Green – Flat Feet <i>EVA Molded</i> . The black lines represent significant difference (p – value $< 0.05/8$). The box plots do not depict eventual outliers.	50

4.5	Mean joint moments (ankle, midtarsal and tarsometatarsal) for each phase of the stance phase for the barefoot and Labshoe condition. Orange – Control barefoot; Light Green – Control <i>Labshoe</i> ; Pink – Flat Feet barefoot; Light Blue – Flat Feet <i>Labshoe</i> . The black lines represent significant difference ($p - value < 0.05/8$). The box plots do not depict eventual outliers.	50
4.6	Mean joint moments (ankle, midtarsal and tarsometatarsal) for each phase of the stance phase for the different conditions of the flat feet group. Light Blue – Flat Feet <i>Labshoe</i> ; Blue – Flat Feet <i>3D-printed</i> ; Dark Blue – Flat Feet <i>EVA Molded</i> . The black lines represent significant difference ($p - value < 0.05/8$). The box plots do not depict eventual outliers.	51
4.7	Mean joint moments (ankle, midtarsal and tarsometatarsal) for each phase of the stance phase for the different conditions of the control group. Light Green – Control <i>Labshoe</i> ; Green – Control <i>3D-printed</i> ; Dark Green – Control <i>EVA Molded</i> . The black lines represent significant difference ($p - value < 0.05/8$). The box plots do not depict eventual outliers.	51
4.8	Representation of the foot weigh bearing mechanism during the midstance of gait. A) Flat feet subjects bear weight in the midfoot as well as in the calcaneus, forefoot and toes. B) Control subjects bear weight do not bear weigh in the midfoot. C) Both flat feet and control subjects bear weigh in the midfoot when using insoles.	54
5.1	Musculoskeletal lower leg model (<i>OpenSim</i>). Depicted segments: Cyan – talus; Purple – calcaneus; Green – midfoot; Yellow – forefoot; Orange – toes.	60
5.2	Ellipsoid contact geometry computation. Step A - Selection of different pressure areas (3D clouds of virtual points) and scaling of pressure; Step B – Conversion of scaled pressures to clouds of virtual points; Step C – Ellipsoid fit: Least squares optimization.	62
5.3	Example of the foot model with the optimized location of the ellipsoid contact geometries.	63

- 5.4 Musculoskeletal model with the different markers combinations used to quantify: 1) the influence of pressure as an input for the kinematics estimation and 2) the influence of the number of markers on the plantar pressure-based kinematics estimation. Green: Markers Optimization (*MO*) - Entire marker set (Table 5.2) without contact geometries ($w_P = 0\%$ and $w_M = 100\%$); Dark Blue: All Markers + Pressure (*AMP*) - Entire marker set with contact geometries ($w_P = 60\%$ and $w_M = 40\%$); Orange: *PiG* - *PiG* marker set with contact geometries ($w_P = 80\%$ and $w_M = 20\%$); Yellow: *PiG* extended (*PiGe*) - *PiG* marker set plus one marker in the hallux with contact geometries ($w_P = 80\%$ and $w_M = 20\%$); Blue: 2 Markers (*2M*) – One marker in the calcaneus and in the hallux with contact geometries ($w_P = 70\%$ and $w_M = 30\%$); Light Blue: 1 Marker (*1M*) – One marker in the head of the second metatarsal with contact geometries ($w_P = 80\%$ and $w_M = 20\%$). All the reduced combinations maintain four markers in the tibia.

66

5.5 Kinematics results for the 8 DOF. Green: *MO* – Mean kinematics computed with the entire marker set without contact geometries ($w_P = 0\%$ and $w_M = 100\%$) with standard deviation; Dark Blue: *AMP* – Mean kinematics computed with the entire marker set with contact geometries ($w_P = 60\%$ and $w_M = 40\%$) with standard deviation. Full line – Mean of the five subjects, four trials and both feet (40 different trials).

68

5.6 Kinematics results for the 8 DOF. Dark Blue: *AMP* – Mean kinematics computed with the entire marker set with contact geometries ($w_P = 60\%$ and $w_M = 40\%$) with standard deviation; Orange: *PiG* – Mean kinematics computed with the *PiG* marker set with contact geometries ($w_P = 60\%$ and $w_M = 40\%$); Yellow: *PiGe* - Mean kinematics computed with the *PiG* marker set plus one marker in the hallux with contact geometries ($w_P = 80\%$ and $w_M = 20\%$); Blue: *2M* – Mean kinematics computed with one marker in the calcaneus and in the hallux with contact geometries ($w_P = 70\%$ and $w_M = 30\%$); Light Blue: *1M* – Mean kinematics computed with one marker in the head of the second metatarsal with contact geometries ($w_P = 80\%$ and $w_M = 20\%$). All the reduced combinations maintain four markers in the tibia. Full line – Mean of the five subjects, four trials and both feet (40 different trials).

69

5.7 Dark Blue line – Kinematics differences between the means of the <i>MO</i> and the <i>AMP</i> approaches for the 8 DOF. Green Bar – The mean kinematics of the <i>AMP</i> approach is within the standard deviation of the <i>MO</i> approach. Red Bar – The mean kinematics of the <i>AMP</i> is not within the standard deviation of the <i>MO</i> approach.	70
5.8 Yellow line - Kinematics differences between the means of the <i>AMP</i> and the <i>PiGe</i> approaches for the 8 DOF. Green bar – If the mean kinematics of the <i>PiGe</i> approach is within the standard deviation of the <i>AMP</i> approach. Red bar – If the mean kinematics of the <i>PiGe</i> approach is not within the standard deviation of the <i>AMP</i> approach.	70
6.1 Descriptive framework used to predict ankle-foot kinematics under the effect of different insole stiffness using torque driven forward dynamic simulations. (1) Marker set protocol, pressure and ground reaction forces (GRF) acquisition. (2) Insoles mechanical tests: Left – Three-point bending test, Right – Torsional test. (3) Musculoskeletal lower leg model (<i>OpenSim</i>). Depicted segments: Cyan – talus; Purple – calcaneus; Green – midfoot; Yellow – forefoot; Orange – toes. (4) Foot model with the ellipsoid based contact geometries. (5) Ligaments visualization. (6) Visual summary of the optimization algorithm used to compute the kinematics. (7) A simple representation of the RRA algorithm. (8) Insoles model: Top - The different types of insoles: A) Pure torsional (Stiffnesses: 1 to 6 Nm/rad); B) Pure bending (Stiffnesses: 10 to 90 Nm/rad) and C) Combination of both. Bottom - Bushing forces representation: Left) Connection between the calcaneus and the forefoot; Right) Springs representation resisting relative rotation.	83
6.2 Calcaneus-Midfoot (Midtarsal) kinematics (joint angles). Each square represents the mean angular difference between the barefoot and insole condition, over all subjects, all trials and both legs per phase of stance. The white squares represent insoles that did not cause a significant difference ($p - value < 0.05/69$). For the exact means and standard deviation values consult and Appendix D.	88

6.3 Midfoot-Forefoot (Tarsometatarsal) kinematics (joint angles). Each square represents the mean angular difference between the barefoot and insole condition, over all subjects, all trials and both legs per phase of stance. The white squares represent insoles that did not cause a significant difference ($p - value < 0.05/69$). For the exact means and standard deviation values consult and Appendix D. The highlighted square depicts an example of the mean kinematics of the barefoot and the insole with the highest combined values of bending and torsional stiffness ($T=6 \text{ Nm/rad}$, $B=90 \text{ Nm/rad}$) during the entire stance phase. The dots represent the mean of each phase (P1, P2, P3 and P4).	89
6.4 Example of control adaptation. Top) Tarsometatarsal kinematics (joint angles). Each square represents the mean angular difference between the barefoot and insole condition, over all subjects, all trials and both legs per phase of stance; Bottom) Tarsometatarsal correction controllers. Each square represents the mean joint correction controller computed for each insole condition, over all subjects, all trials and both legs per phase of stance. The white squares represent insoles with no significant difference ($p - value < 0.05/69$).	92
A.1 Ellipsoid contact geometry computation. Step A - Selection of different pressure areas (3D clouds of virtual points) and scaling of pressure; Step B – Conversion of scaled pressures to clouds of virtual points; Step C – Ellipsoid fit: Least squares optimization.	109
B.1 Joint angles for the ankle, subtalar and metatarsophalangeal plantarflexion/dorsiflexion degrees of freedom during the stance phase of gait for different scaling factors. Dark Blue – 2cm scaling factor; Orange – 2.5cm scaling factor; Blue - 3cm scaling factor; Green – No contact geometries.	114
B.2 Mean optimization function value (f) computed using the kinematics estimation method detailed in Section 5.3.3 for each trial and leg. These values were obtained using ellipsoid contact geometries generated with the 2 cm scaling factor.	115
B.3 Mean optimization function value (f) computed using the kinematics estimation method detailed in Section 5.3.3 for each trial and leg. These values were obtained using ellipsoid contact geometries generated with the 2.5 cm scaling factor.	115

B.4 Mean optimization function value (f) computed using the kinematics estimation method detailed in Section 5.3.3 for each trial and leg. These values were obtained using ellipsoid contact geometries generated with the 3 cm scaling factor.	116
C.1 Kinematics results for the 8 DOF for Subject 1. Green: MO – Mean kinematics computed with the entire marker set without contact geometries ($w_P = 0\%$ and $w_M = 100\%$); Dark Blue: AMP – Mean kinematics computed with the entire marker set with contact geometries ($w_P = 60\%$ and $w_M = 40\%$). Full line – Mean of the four trials and both feet (8 different trials).	118
C.2 Kinematics results for the 8 DOF for Subject 1. Dark Blue: AMP – Mean kinematics computed with the entire marker set with contact geometries ($w_P = 60\%$ and $w_M = 40\%$); Orange: PiG – Mean kinematics computed with the PiG marker set with contact geometries ($w_P = 60\%$ and $w_M = 40\%$); Yellow: $PiGe$ – Mean kinematics computed with the PiG marker set plus one marker in the hallux with contact geometries ($w_P = 80\%$ and $w_M = 20\%$); Blue: $2M$ – Mean kinematics computed with one marker in the calcaneus and in the hallux with contact geometries ($w_P = 70\%$ and $w_M = 30\%$); Light Blue: $1M$ – Mean kinematics computed with one marker in the head of the second metatarsal with contact geometries ($w_P = 80\%$ and $w_M = 20\%$). All the reduced combinations maintain four markers in the tibia. Full line – Mean of the four trials and both feet (8 different trials).	119
C.3 Kinematics results for the 8 DOF for Subject 2. Green: MO – Mean kinematics computed with the entire marker set without contact geometries ($w_P = 0\%$ and $w_M = 100\%$); Dark Blue: AMP – Mean kinematics computed with the entire marker set with contact geometries ($w_P = 60\%$ and $w_M = 40\%$). Full line – Mean of the four trials and both feet (8 different trials).	120

- C.4 Kinematics results for the 8 DOF for Subject 2. Dark Blue: *AMP* – Mean kinematics computed with the entire marker set with contact geometries ($w_P = 60\%$ and $w_M = 40\%$); Orange: *PiG* – Mean kinematics computed with the *PiG* marker set with contact geometries ($w_P = 60\%$ and $w_M = 40\%$); Yellow: *PiGe* - Mean kinematics computed with the *PiG* marker set plus one marker in the hallux with contact geometries ($w_P = 80\%$ and $w_M = 20\%$); Blue: *2M* – Mean kinematics computed with one marker in the calcaneus and in the hallux with contact geometries ($w_P = 70\%$ and $w_M = 30\%$); Light Blue: *1M* – Mean kinematics computed with one marker in the head of the second metatarsal with contact geometries ($w_P = 80\%$ and $w_M = 20\%$). All the reduced combinations maintain four markers in the tibia. Full line – Mean of the four trials and both feet (8 different trials). . . 121
- C.5 Kinematics results for the 8 DOF for Subject 3. Green: *MO* – Mean kinematics computed with the entire marker set without contact geometries ($w_P = 0\%$ and $w_M = 100\%$); Dark Blue: *AMP* – Mean kinematics computed with the entire marker set with contact geometries ($w_P = 60\%$ and $w_M = 40\%$). Full line – Mean of the four trials and both feet (8 different trials). . . . 122
- C.6 Kinematics results for the 8 DOF for Subject 3. Dark Blue: *AMP* – Mean kinematics computed with the entire marker set with contact geometries ($w_P = 60\%$ and $w_M = 40\%$); Orange: *PiG* – Mean kinematics computed with the *PiG* marker set with contact geometries ($w_P = 60\%$ and $w_M = 40\%$); Yellow: *PiGe* - Mean kinematics computed with the *PiG* marker set plus one marker in the hallux with contact geometries ($w_P = 80\%$ and $w_M = 20\%$); Blue: *2M* – Mean kinematics computed with one marker in the calcaneus and in the hallux with contact geometries ($w_P = 70\%$ and $w_M = 30\%$); Light Blue: *1M* – Mean kinematics computed with one marker in the head of the second metatarsal with contact geometries ($w_P = 80\%$ and $w_M = 20\%$). All the reduced combinations maintain four markers in the tibia. Full line – Mean of the four trials and both feet (8 different trials). . . 123
- C.7 Kinematics results for the 8 DOF for Subject 4. Green: *MO* – Mean kinematics computed with the entire marker set without contact geometries ($w_P = 0\%$ and $w_M = 100\%$); Dark Blue: *AMP* – Mean kinematics computed with the entire marker set with contact geometries ($w_P = 60\%$ and $w_M = 40\%$). Full line – Mean of the four trials and both feet (8 different trials). . . . 124

- C.8 Kinematics results for the 8 DOF for Subject 4. Dark Blue: *AMP* – Mean kinematics computed with the entire marker set with contact geometries ($w_P = 60\%$ and $w_M = 40\%$); Orange: *PiG* – Mean kinematics computed with the *PiG* marker set with contact geometries ($w_P = 60\%$ and $w_M = 40\%$); Yellow: *PiGe* - Mean kinematics computed with the *PiG* marker set plus one marker in the hallux with contact geometries ($w_P = 80\%$ and $w_M = 20\%$); Blue: *2M* – Mean kinematics computed with one marker in the calcaneus and in the hallux with contact geometries ($w_P = 70\%$ and $w_M = 30\%$); Light Blue: *1M* – Mean kinematics computed with one marker in the head of the second metatarsal with contact geometries ($w_P = 80\%$ and $w_M = 20\%$). All the reduced combinations maintain four markers in the tibia. Full line – Mean of the four trials and both feet (8 different trials). . . 125
- C.9 Kinematics results for the 8 DOF for Subject 5. Green: *MO* – Mean kinematics computed with the entire marker set without contact geometries ($w_P = 0\%$ and $w_M = 100\%$); Dark Blue: *AMP* – Mean kinematics computed with the entire marker set with contact geometries ($w_P = 60\%$ and $w_M = 40\%$). Full line – Mean of the four trials and both feet (8 different trials). . . . 126
- C.10 Kinematics results for the 8 DOF for Subject 5. Dark Blue: *AMP* – Mean kinematics computed with the entire marker set with contact geometries ($w_P = 60\%$ and $w_M = 40\%$); Orange: *PiG* – Mean kinematics computed with the *PiG* marker set with contact geometries ($w_P = 60\%$ and $w_M = 40\%$); Yellow: *PiGe* - Mean kinematics computed with the *PiG* marker set plus one marker in the hallux with contact geometries ($w_P = 80\%$ and $w_M = 20\%$); Blue: *2M* – Mean kinematics computed with one marker in the calcaneus and in the hallux with contact geometries ($w_P = 70\%$ and $w_M = 30\%$); Light Blue: *1M* – Mean kinematics computed with one marker in the head of the second metatarsal with contact geometries ($w_P = 80\%$ and $w_M = 20\%$). All the reduced combinations maintain four markers in the tibia. Full line – Mean of the four trials and both feet (8 different trials). . . 127

List of Tables

3.1	Anatomical landmarks, selected on the bones mesh, used to compute the joint axes and segments origin.	30
3.2	Ligaments geometrical path description. The Resting Length is presented for the generic model, before scaling.	33
4.1	Markers anatomical position and associated <i>OpenSim</i> tracking weight (w). (*) Markers used only for the static acquisitions.	45
4.2	Total number of trials used for the inverse kinematics and dynamics simulations for each subject and each condition, Left and Right leg added together.	47
5.1	Absolute mean and peak kinematics differences, and percentage of within standard deviation between the kinematics means of 1) <i>MO</i> vs. <i>AMP</i> ; 2) <i>AMP</i> vs. <i>PiG</i> ; 3) <i>AMP</i> vs. <i>PiGe</i> ; 4) <i>AMP</i> vs. <i>2M</i> ; 5) <i>AMP</i> vs. <i>1M</i> . For all 8 DOF.	71
5.2	Mean distance between the position of the measured markers and the position of the virtual marker computed using the different modeling approaches: 1) <i>MO</i> ; 2) <i>AMP</i> ; 3) <i>PiG</i> ; 4) <i>PiGe</i> ; 5) <i>2M</i> ; 6) <i>1M</i> . (*) – Tracked Marker. (#) – The means were computed excluding the CMTI marker. The high distances verified for this marker in all the approaches are probably related to a modeling error.	72

D.1	Midtarsal Eversion/Inversion kinematics (joint angles) for Phase 1 of stance. Each cell contains the mean difference in relative orientation over all subjects, all trials and both legs between the barefoot and insole condition.	129
D.2	Midtarsal Eversion/Inversion kinematics (joint angles) for Phase 2 of stance. Each cell contains the mean difference in relative orientation over all subjects, all trials and both legs between the barefoot and insole condition.	129
D.3	Midtarsal Eversion/Inversion kinematics (joint angles) for Phase 3 of stance. Each cell contains the mean difference in relative orientation over all subjects, all trials and both legs between the barefoot and insole condition.	130
D.4	Midtarsal Plantarflexion/Dorsiflexion kinematics (joint angles) for Phase 1 of stance. Each cell contains the mean difference in relative orientation over all subjects, all trials and both legs between the barefoot and insole condition.	130
D.5	Midtarsal Plantarflexion/Dorsiflexion kinematics (joint angles) for Phase 2 of stance. Each cell contains the mean difference in relative orientation over all subjects, all trials and both legs between the barefoot and insole condition.	130
D.6	Midtarsal Plantarflexion/Dorsiflexion kinematics (joint angles) for Phase 3 of stance. Each cell contains the mean difference in relative orientation over all subjects, all trials and both legs between the barefoot and insole condition.	131
D.7	Midtarsal Abduction/Adduction kinematics (joint angles) for Phase 1 of stance. Each cell contains the mean difference in relative orientation over all subjects, all trials and both legs between the barefoot and insole condition.	131
D.8	Midtarsal Abduction/Adduction kinematics (joint angles) for Phase 2 of stance. Each cell contains the mean difference in relative orientation over all subjects, all trials and both legs between the barefoot and insole condition.	131
D.9	Midtarsal Abduction/Adduction kinematics (joint angles) for Phase 3 of stance. Each cell contains the mean difference in relative orientation over all subjects, all trials and both legs between the barefoot and insole condition.	132

D.10 Tarsometatarsal Eversion/Inversion kinematics (joint angles) for Phase 1 of stance. Each cell contains the mean difference in relative orientation over all subjects, all trials and both legs between the barefoot and insole condition.	132
D.11 Tarsometatarsal Eversion/Inversion kinematics (joint angles) for Phase 2 of stance. Each cell contains the mean difference in relative orientation over all subjects, all trials and both legs between the barefoot and insole condition.	132
D.12 Tarsometatarsal Eversion/Inversion kinematics (joint angles) for Phase 3 of stance. Each cell contains the mean difference in relative orientation over all subjects, all trials and both legs between the barefoot and insole condition.	133
D.13 Tarsometatarsal Plantarflexion/Dorsiflexion kinematics (joint angles) for Phase 1 of stance. Each cell contains the mean difference in relative orientation over all subjects, all trials and both legs between the barefoot and insole condition.	133
D.14 Tarsometatarsal Plantarflexion/Dorsiflexion kinematics (joint angles) for Phase 2 of stance. Each cell contains the mean difference in relative orientation over all subjects, all trials and both legs between the barefoot and insole condition.	133
D.15 Tarsometatarsal Plantarflexion/Dorsiflexion kinematics (joint angles) for Phase 3 of stance. Each cell contains the mean difference in relative orientation over all subjects, all trials and both legs between the barefoot and insole condition.	134
D.16 Tarsometatarsal Abduction/Adduction kinematics (joint angles) for Phase 1 of stance. Each cell contains the mean difference in relative orientation over all subjects, all trials and both legs between the barefoot and insole condition.	134
D.17 Tarsometatarsal Abduction/Adduction kinematics (joint angles) for Phase 2 of stance. Each cell contains the mean difference in relative orientation over all subjects, all trials and both legs between the barefoot and insole condition.	134
D.18 Tarsometatarsal Abduction/Adduction kinematics (joint angles) for Phase 3 of stance. Each cell contains the mean difference in relative orientation over all subjects, all trials and both legs between the barefoot and insole condition.	135

Chapter 1

General Introduction

In Europe, over 200 million people suffer from disabling foot and ankle pain caused by a variety of pathologies as overloading injuries, degenerative joint disorders and systemic diseases (*e.g.* diabetes). Foot orthoses (FOs) or insoles have been vastly used as a conservative treatment to reduce injuries, provide comfort, relieve pathological symptoms and enhance performance [182, 139, 262]. E. and D. Janisse [124, 125] defined eight comprehensive purposes for the use of insoles: (1) impact reduction; (2) cushion the foot plantar surface; (3) redistribute plantar pressure, reducing high-pressure areas; (4) support and protect healed fracture sites; (5) reduce shear within the plantar tissues; (6) limit the motion of joints; (7) control, stabilize, support or correct flexible foot deformities (foot pathologies that may be corrected by passive or active intervention) and (8) accommodate resistant foot deformities (foot pathologies requiring surgical intervention).

The use of insoles as a conservative treatment for foot pathologies has been an area of continued research for over a century [137].

However, the current process of patient assessment for custom FOs design and manufacturing is handicraft work that fully relies on the experience of the clinician. It is often performed using stationary measurements, related only to the geometry of the foot, therefore neglecting the fact that most of the functional problems are related to the foot motion, see Figure 1.1.A.

The most common technique of patient assessment for custom FOs design and manufacturing is plaster casting [148, 122, 268, 201, 25], initially described by Merton L. Root, in 1981 [171], see Figure 1.1.A.3. A neutral suspension plaster

cast (negative impression) of each foot is taken in a non-weight bearing condition with the subtalar joint in the neutral position [122]. Other options like foam boxes are also used to create a negative impression of the foot shape. A positive mold is formed from the negative impression; a thermoplastic material is later applied to the positive mold to fabricate the total contact insole via vacuum suction [64, 235]. Recently, 3D digital scans [236, 237] are also becoming a valuable tool to facilitate and improve the digital design and molding of custom FOs.

It is crucial to develop an integrated workflow combining state-of-the-art methodologies to lift the design and manufacturing of insoles to an evidence-based level while increasing the objectivity in both patient assessment and treatment evaluation. This integrated workflow takes advantage of state-of-the-art methodologies that can be related to the following three main knowledge domains:

1. Foot orthosis manufacturing usually requires the manual or digital imprint of the foot plantar surface to create a mold of the foot. A broad range of thermoplastic materials can then be applied to this mold to fabrication custom FOs. 3D-printing is already being used as an alternative method to produce insoles, see Figure 1.1.B.5. Using this manufacturing procedure, it is possible to digitally design and efficiently produce customized insoles adapted to each subject. However, the production of this type of subject-specific insoles is still based on subjective decision making rather than on objective evidence.
2. Dynamic measurement systems are usually composed of 3D stereophotogrammetric systems, plantar pressure and force plates, see Figure 1.1.B.3 These systems are fundamental to measure kinematic parameters like joint angles, velocities and acceleration or kinetic parameters like ground reaction forces and plantar pressure distribution.
3. Musculoskeletal models are of great importance to augment the knowledge coming from the dynamic measurements by providing additional parameters, see Figure 1.1.B.4. These models are typically used in inverse motion simulations to estimate for example the internal loading of the musculoskeletal system (*i.e.* joint moments). However, in combination with a forward simulation formulation, these musculoskeletal models also allow to predict the biomechanical effects of interventions (*e.g.* insoles) – Forward predictive simulations.

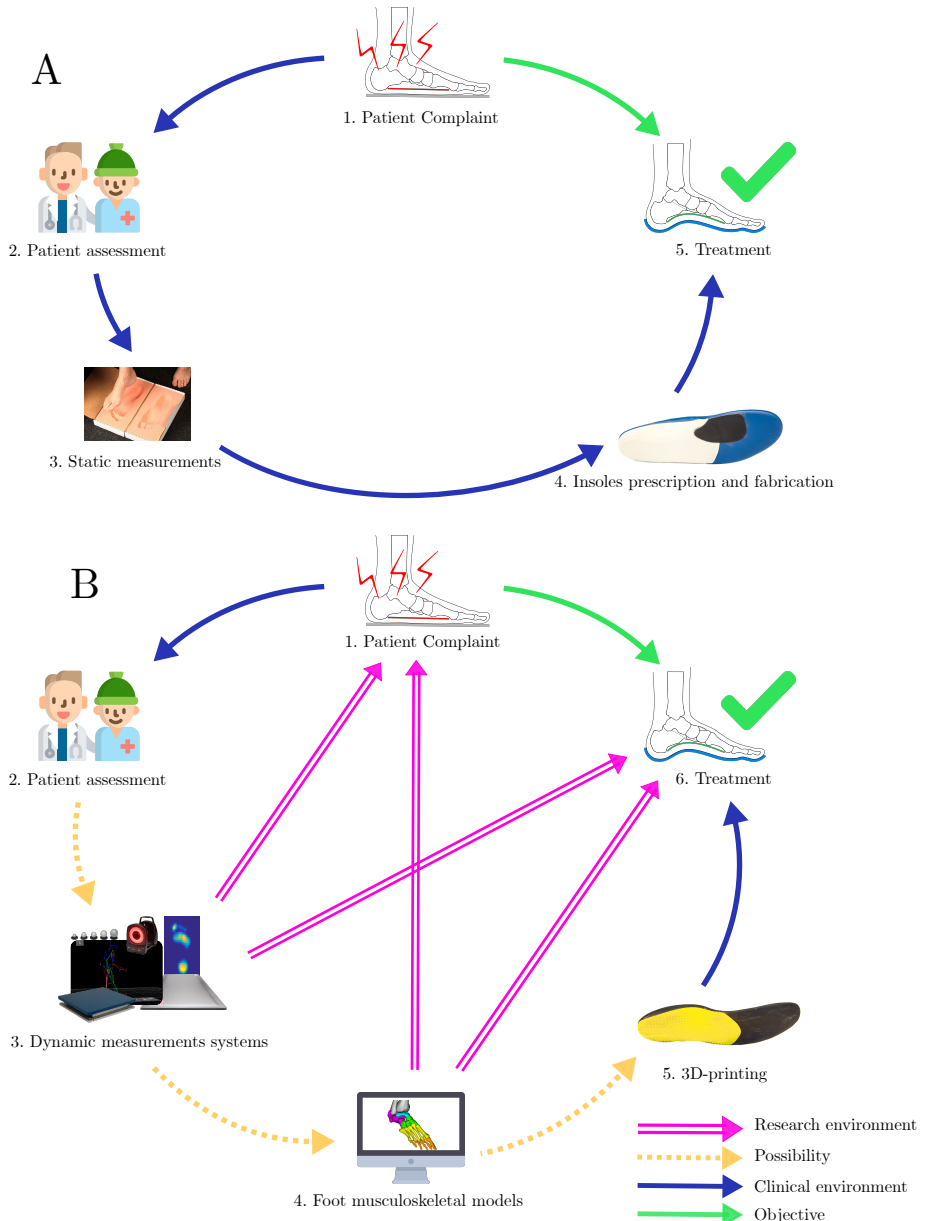


Figure 1.1: (A: Standard clinical procedure from patient assessment of foot pathologies to conservative treatment using insoles (A.1, A.2, A.3, A.4 and A.5). B: Envisioned clinical procedure from patient assessment of foot pathologies to conservative treatment using insoles (B.1, B.2, B.3, B.4, B.5 and B.6). Purple double lined arrows: Methodologies used in research environments to evaluate foot pathologies and insoles effectiveness. Yellow dashed arrows: Possibility of bringing research methodologies into clinical care.

Despite the wide use of different dynamic measurement systems and musculoskeletal models in research environments (Figure 1.1.B), the use of these methodologies in standard clinical care remains, in general, scarce [260], with the exception of plantar pressure systems, that are a well-established tool in clinical environments [87].

With the combination of these three knowledge domains, it is possible to envision a fully objective and automated digital framework that goes from the clinical assessment of foot biomechanics to the production of subject-specific 3D-printed insoles, see Figure 1.1.B. Therefore, dynamic measurement systems and musculoskeletal models will be fundamental clinical tools to quantify biomechanical parameters (*e.g.* joint angles, plantar pressure and joint moments) that are then used for the design of the subject-specific foot orthoses. Furthermore, the use of forward predictive simulations together with musculoskeletal models within the workflow will also enable the estimation of the optimal mechanical properties of the insole to support and correct the kinematics of the foot.

However, to achieve such an integrated framework, each of the three knowledge domains needs to be furthered beyond the current state-of-the-art. The following sections will discuss the state of the art of specific aspects of the different knowledge domain used in the current thesis (Figure 1.1). It will focus on the following topics:

1. Foot orthoses (Section 1.1): This section starts with a brief historical overview, followed by a description of the different types of foot orthoses, followed by a description of the materials and mechanical properties of foot orthoses.
2. Dynamic measurement systems (Section 1.2): This section contains a literature review of the different dynamic measurement systems used to evaluate foot related pathologies and the corrective effect of foot orthoses.
3. Foot musculoskeletal models (Section 1.3): This section covers different studies using the two most common types of foot musculoskeletal models: finite elements and multibody.

1.1 Foot Orthoses

The first reported studies on FOs focused on the conservative treatment of *pes valgus* (pronated foot). In 1845, Durlacher described a leather foot brace, and in 1874 Hugh Owen Thomas described a leather sole to treat pronated foot. In 1912, P. W. Roberts developed metal foot braces with an inverted heel cup and medial and lateral projections to invert foot motion (Figure 1.2.A). Royal Whitman, in 1913, published a similar metal foot brace designed to produce an inversion motion once the patient made full contact with the ground, thus causing a decrease in foot pronation. In 1920, Otto F. Schuster combined Whitman's and Roberts designs (Figure 1.2.B). Ben Levy, in 1950, described a technique to produce insoles with arch and toes support to control excessive pronation, made of a latex mixture bottom layer and a thick leather top layer (Figure 1.2.C). Merton L. Root, in 1958, improved Levy's insole durability with a thermoplastic polymer (mouldable at high temperatures and hard when cool), creating what is now known as the Root Functional Orthosis (Figure 1.2.D). In 1967, W. H. Henderson and J. W. Campbell developed a polypropylene FO, the University of California Biomechanics Laboratory shoe insert (U.C.B.L.), with high heel cup and medial and lateral projections to treat paediatric pes valgus deformity (Figure 1.2.E) [137].

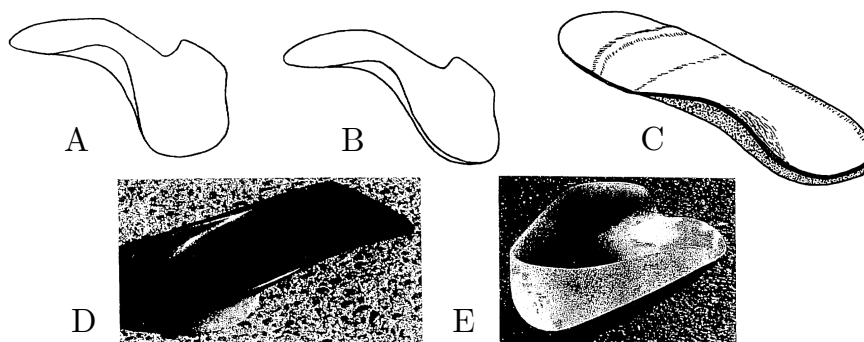


Figure 1.2: (A) Whitman's FO; (B) Robert-Whitman's FO; (C) Levy's FO; (D) Root's FO and (E) U.C.B.L. FO. Figure adapted from Kirby, K. and Green, D., 1992 [137].

The Root Functional Orthosis (Figure 1.2.D), along with its many design variations, has since become the most popular type of foot orthosis prescribed by clinicians. A more comprehensive and descriptive denomination as functional foot orthoses (FFOs) is used to group the design variations made on Root's

design [137]. In the early 1980s, Richard Blake developed a modified version of the FFOs to gain more control of foot pronation in runners. The resulting orthosis, the Blake Inverted Orthosis (BIO), is very similar in shape to an FFO. Even though the BIO was initially designed for runners, it has presently been successfully used to treat excessive pronation in children [137].

Due to the large variety of available FOs designs, a broader and more inclusive classification has been widely accepted by the clinical community [262].

1.1.1 Types of foot orthoses

Different types of FOs can be roughly classified as prefabricated, semi-custom or custom. Prefabricated FOs are used for comfort purposes, widely available and define the 'off-the-shelf', ready to use type [262]. These insoles have a lower cost and require less input from a clinician. Therefore, the use of prefabricated FOs is associated with disadvantages like inadequate foot posture correction due to their flat configuration and reduced longevity [124]. Another cost-effective type of insoles is the semi-custom, usually manufactured by adapting a prefabricated insole to the patient's feet with some subject-specific metrics (*e.g.* tibia-to-calcaneus angle) for foot pose correction [262, 126, 248].

Custom FOs require the manual or digital imprint of the foot plantar surface [262, 153, 208, 53]. They are usually prescribed when actual foot cushion, protection, support, pressure distribution or posture correction are required. There are three main types of custom FOs: soft, rigid and semi-rigid [124]. Soft custom FOs are primarily designed to cushion and protect the foot. Due to their less stiff material composition, they offer shock absorption and appropriate padding. This comfort type of insoles is suitable for a patient who has little or no deformity [123, 35]. Rigid FOs offer robust arch support, control and weight re-distribution for flexible foot deformities. However, they can only provide minimal cushion, shock absorption, and protection [125]. Semi-rigid FOs combine the support, control, and weight re-distribution of rigid orthoses with the cushion and protection of accommodative foot orthoses. A semi-rigid FO often consists of a soft, cushioned top layer with a firm, supportive base material [123, 250]. The difference between from soft and rigid custom FOs depends on the thickness, stiffness, layering and form of the fabrication material [52], described in Section 1.1.2.

1.1.2 Materials used for foot orthoses fabrication

A broad range of thermoplastic materials are currently used in the fabrication of custom FOs [107]. Polypropylene [201, 171] and Polyethylene [64, 235, 170] are most common due to their adequate mechanical properties, *i.e.* stiffness and flexibility with excellent dimensional stability, lightweight, and favorable weight/strength ratios. These ethylene-based polymers can be modified into other polymers that are also commonly used for insole fabrication like ethylene-vinyl (EVA) [126, 170, 207] and a variety of acrylates [52].

Polylactide (PLA), another thermoplastic polymer, is gaining importance due to its use in additive manufacturing (AM, 3D-printing). FOs fabricated using 3D-printing technology show similar flexibility to equivalent polypropylene devices as reflected in similar arch deflection under a standard load [236]. Moreover, dynamic insole structures can be fabricated using cellular structures. The mechanical properties of the cellular structures can vary locally, so that the 3D-printed insole at least in theory can be perfectly designed to optimally guide foot motion and therefore the other joints of the lower limb [262, 246].

The selection of materials for manufacturing FOs is subjective and depends exclusively on the experience of the clinician [82].

1.1.3 Foot orthoses mechanical properties assessment

Recently, research on the mechanical properties of materials used in the fabrication of FOs has highlighted six important properties that should be considered: 1) density, 2) resilience, 3) stiffness, 4) coefficient of friction and shear, 5) durability and 6) compression set [188].

- Density is a quantity that measures the amount of matter contained within a specific volume. Low-density FOs may be preferable to maintain gait efficiency.
- Resilience is the amount of energy returned during unloading as a percentage of the amount of energy absorbed during loading. For a higher damping or shock attenuation capacity of the FO, a lower resilience is necessary and vice versa.
- Stiffness is the material resistance to deformation. When studying FOs, stiffer materials may be useful to achieve motion control, support, and stability. Low stiffness FOs may be required for a better redistribution of plantar pressure.

- Friction can be defined as the force resisting the relative motion of objects. Shear can be described as opposing forces in a tissue that tend to push both parts of an object in an opposing direction. Shear forces occurring within the foot plantar tissue can potentially lead to the development of plantar ulceration. The preferred top layer of an insole should be designed to minimize shear forces, which requires a relatively low static coefficient of friction.
- Durability is the ability to resist wear, pressure, or damage. This property is determined by the number of gait cycles needed for loss of performance.
- Compression set is defined as the residual deformation (*i.e.* reduction in thickness) after it has been compressed [206]. Corrective insoles should ideally have a high compression set to avoid thickness reduction.

Research using mechanical bench tests is essential to establish objective criteria to select materials for insoles manufacturing. Different bench tests have been used to determine the above mentioned insoles' mechanical properties: compression tests for the stiffness [34, 206, 45, 82, 35, 76, 85, 90, 117], for the resilience [35, 90], for the compression set [82, 35, 85], for the durability [82, 35, 117]; tensiometers [206] for the stiffness and shear [34]; hardness meters [82] or durometers [206] for the hardness and modified Schob pendulum [82] for the resilience. Another approach is using custom developed equipment to study the different mechanical properties [209, 188].

It is recognized that bench tests provide important material property information for insoles manufacturing. However, if isolated they only allow for speculation on how the materials would perform in a dynamic situation when placed in footwear [107].

1.2 Dynamic measurement systems

The successful prescription of custom FOs has been studied using different dynamic measurement systems, like 3D stereophotogrammetry (Sub-Section 1.2.1) or plantar pressure (Sub-Section 1.2.3).

1.2.1 3D Stereophotogrammetry

Presently, 3D stereophotogrammetric systems or motion acquisition systems are being used in motion laboratories to measure precise kinematic information of movement, *i.e.* joint angles, velocities and accelerations [73]. Kinematic measures are crucial document the movement abnormalities and compare it to control in order to provide an objective basis for planning and follow-up of treatment. The standard passive approach is based on a procedure using skin-mounted, reflective marker and infrared cameras [73]. In the last decades, researchers and clinicians have used this method to quantify the effect of FOs on foot kinematics. These studies showed that insoles can correct and therefore limit progression of flexible postural foot deformities.

Custom FOs have proven to reduce excessive rearfoot pronation during walking in patients with flat foot deformity [126, 235, 227, 236, 170, 179, 162, 200, 146, 19, 74] and during running [20]. Insoles have also shown a potential to decrease internal tibia rotation [146, 65, 173]. However, this corrective effect is not consistent across literature; different studies presented no significant improvement in subjects with excessive rearfoot pronation when using custom FOs [268, 25, 64, 19, 36].

Foot orthoses have also shown potential to decrease internal tibia rotation [65, 173] and to reduce knee osteoarthritis progression [110]. Insoles with lateral wedges have been prescribed for medial compartment and medial wedges for lateral compartment osteoarthritis. Due to the prevalence of medial tibiofemoral osteoarthritis, lateral wedges have been widely researched and have proven their potential to reduce the adduction knee moment during walking [112, 110, 111]. Research on medial-wedged insoles for lateral compartment knee osteoarthritis is scarce. Nonetheless, recent studies support the use of medial wedges for the treatment of predominant lateral compartment osteoarthritis at an early stage but further research is needed to validate these findings. [110, 216].

The combination of 3D stereophotogrammetric analysis with force plates allows the computation of kinetics, more specific joint moments. Yet, the insoles' influence on joint moments is controversial, and the number of studies is limited. Some studies proved the insoles efficacy in reducing ankle inversion joint moment

both in subjects with no history of foot pathologies [170] and in subjects with excessively pronated foot [236, 227] while others failed to report significant changes [25, 57, 121].

Multiple studies have used isolated force plates to measure peak forces to test the effect of different FOs properties. High-density insoles have shown potential to significantly decrease vertical ground reaction forces (GRF) loading rate [6], while low density reduces plantar shear forces [66]; and lower FOs' stiffness led to a higher ability to reduce impact [76, 84].

The lack of consistent kinematic and kinetic results may be attributed to the variability introduced by subject-specific adaptations to the insoles (inter and intra-subjects' variability), by different insole types and/or manufacturing materials in different study. The lack of proper understanding of the biomechanics of the underlying foot pathologies (*e.g. planovalgus*) may also affect the subjects classification and thereby contribute to the results' variability across different studies [200, 74]. Lastly, the already mentioned subjective process of custom insole design and manufacturing based on static measurements also contributes to the reported variability of the treatment effectiveness.

Without a consistent level of evidence to support the corrective effects of FOs for different pathologies, clinicians are balancing evidence-based practice with potentially conflicting clinical experience [19]. Furthermore, insoles studies are often limited to a kinematics-based evaluation of the ankle joint, not capturing the full three-dimensional, multi-segmental correction induced by the FOs.

The use of extended 3D multi-segment foot models segments (3D multisegment foot models - 3DMFMs) [73, 18] could bring more insights into the corrective capacities of insoles [266]. The list of published 3DMFMs is currently very extensive. Nonetheless, two models stand out due to the number of clinical studies applying them. The first is known as the Milwaukee Foot Model (MFM) developed by Kidder *et al.* (1996) [73, 136]. It is designed to track the motion of the leg (tibia and fibula), hindfoot (calcaneus, talus, and navicular), forefoot (cuneiforms, cuboid, and metatarsals), and toes (phalanges and hallux) using a total of twelve markers (9 markers and a triad), as depicted in Figure 1.3. The MFM is widely used in kinematic clinical studies such as: ankle arthrosis [134, 135], hallux *rigidus* [46, 47], posterior tibial tendon dysfunction [158, 177], and to describe pediatric gait [172].

The second, the Oxford Foot Model (OFM) was established by Carson *et al.* (2001) [50]. The authors used a four-segment foot model: leg (tibia and fibula), hindfoot (calcaneus and talus), forefoot (five metatarsals) and hallux described by seventeen markers, see Figure 1.3. This model is commonly used

in the clinical analysis in studies like congenital *talipes equinovarus* [239] and rheumatoid *arthritis* [243, 244, 259].

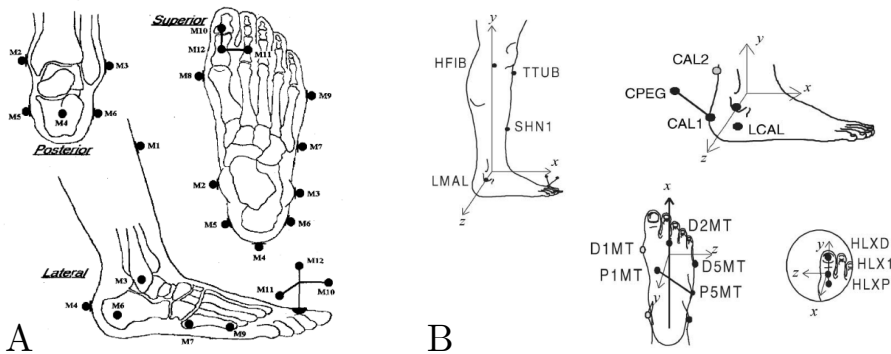


Figure 1.3: Most used 3D multisegment foot models - 3DMFMs: (A) Milwaukee Foot Model (MFM) adapted from Kidder *et al.* (1996) [73, 136]; (B) Oxford Foot Model (OFM) adapted from Carson *et al.* (2001) [50].

Other relevant 3DMFMs have been established using different number of segments and markers' protocols: five segments with five clusters of four-markers [141], nine segments with nineteen markers [154], four segments with fourteen [140] or sixteen markers [37].

A different approach to describe lower leg kinematics is using invasive bone anchored external marker triads[152, 17, 254]. This approach was developed to avoid problems arising from skin movement artifacts, rigid segment assumptions that state that individual foot bones do not move relative to each other and result in incomplete descriptions of foot and ankle kinematics as the movement of individual bones within one segment is not assessed because not all foot bones were included in the measurements [254].

Despite the proven benefit of using kinematics measurements systems to optimize the care of patients with ankle-foot problems, the acceptance of these systems in clinical care remains controversial. These systems are typically expensive, time-consuming and lack portability, complicating their extensive implementation in a clinical environment [260].

With the advancement of technology new acquisition methods like inertial measurement units (IMUs) can overcome the difficulty of measuring kinematics in a clinical environment.

1.2.2 Inertial measurement units

IMUs systems are a low-cost solution that has been tested to measure human motion dynamically. Usually, they are small, lightweight and low power measurement devices that can estimate sagittal plane ankle, knee, and hip kinematics during walking using 3D angular velocity and linear acceleration data from real motion sensors mounted on the foot and shank [83]. IMUs have already been used to quantify the reduction of impact transmitted from the ground to the tibia and forehead under different insoles' stiffnesses [84] and materials [196, 101].

The use of IMUs has grown during the past decade; however, widespread clinical use of this promising technology has yet to be realized. The use of IMUs for orthopaedic evaluation and rehabilitation practice requires further development and validation [216].

1.2.3 Plantar pressure

Ankle-foot specialists tend to rely on plantar pressure data to evaluate foot pathologies [87], due to the low economic cost and short preparation times compared to other approaches [183]. Pedobarography is the study of pressure distribution acting between the plantar surface of the foot and a supporting surface. Plantar distribution is relevant to study dynamic parameters like peak and mean pressure peak force, center of pressure, stance period or foot symmetry [169, 21, 187, 214, 79, 127, 130, 251, 113, 197, 167, 95]. It is accepted that the use of custom foot orthoses can significantly reduce local peak pressure and increase the contact area, thereby redistributing plantar pressure in pathologies such as *diabetes mellitus* [242, 43] (including the associated Charcot arthropathy) [123], *pes cavus* (high arch feet) [41], *hallux limitus* (stiff big toe) [215], metatarsalgia [118] and *pes planus* (flat feet) [230].

Furthermore, some studies confirmed peak plantar pressure reduction for specific FOs' mechanical properties like density [24], hardness [40], stiffness [55] and durability [117]. These studies used different insoles and materials, making it difficult to draw generalized conclusions. Nevertheless it is suggested that multi-density [40] and medium-hardness [24] insoles, with optimized stiffness (according to body mass) [55] reduced peak pressure. Additionally, mechanical material degradation did not reduce the FOs' ability to decrease peak pressures [117]. Other studies evaluated the effect of different insole fabrication materials to reduce peak pressure [166, 205, 240, 256]. These studies used different materials and did not specify the insoles mechanical properties, so it is again

difficult to compare and draw generalized conclusions on the corrective effect of the studied insoles.

A disadvantage of using plantar pressure is that it cannot be used to estimate ankle-foot kinematics, failing to describe the full biomechanical effect of pathologies and insole prescription on foot function.

1.3 Foot musculoskeletal models

Dynamic measurement systems alone cannot fully characterize the biomechanics effects provided by the insoles. These methods are limited because important variables, like internal joint stresses and moments, and muscle forces are not measurable. Musculoskeletal models are of great importance to complement and enhance the dynamic measurements on the effect of custom FOs by allowing the computation of these parameters. Musculoskeletal models can be divided in two main categories: finite elements (FE) models and multibody models.

1.3.1 Finite elements musculoskeletal models

FE modeling is a complementary tool to enhance our knowledge of foot biomechanics. FE analyses can predict the load distribution between the foot and supporting structures (*e.g.* soles or insoles) and provide information on the internal stress and strain states of the ankle-foot complex. These analyses enable efficient parametric evaluations on the effects of insole geometry and materials, without needing to fabricate and test FOs in a series of patient trials [58].

Simple foot FE models have been developed to study the stress distribution within the foot at different time points during stance phase [92] or to evaluate stress distributions in the plantar soft tissue [91]. These models described the foot as a unique segment and often used rough geometries of the bones. Other simple models were used to determine the stress distribution in the foot plantar soft tissue when using insoles [62, 232, 56, 145]. These static or *quasi*-static studies have shown the potential of custom FOs to reduce high pressures at the heel and metatarsal heads and to redistribute the pressure in the midfoot region when compared to flat insoles [56]; and that insoles with higher thickness were more effective in reducing peak plantar pressure [145].

Detailed models of the human foot and ankle, incorporating realistic geometric and material properties of both bone and soft tissue have been recently developed to study internal stresses at the foot joints [213, 151, 60, 44]. Cheung and Zhang 2005 [58] used a complex FE foot model to study the effect of both the material stiffness and the shape (flat and custom-molded) of insoles on plantar pressure and stress distribution in the bone and ligaments during balanced standing. The authors found that the use of low stiffness custom-molded insoles is the best combination for redistributing the plantar foot pressure.

FE analysis has provided valid insights into different aspects of lower limb musculoskeletal biomechanics, *e.g.* foot joints stress distribution and plantar distribution on the foot soft tissue.

However, FE musculoskeletal studies are limited to static or quasi-static evaluations due to the required demanding computational power.

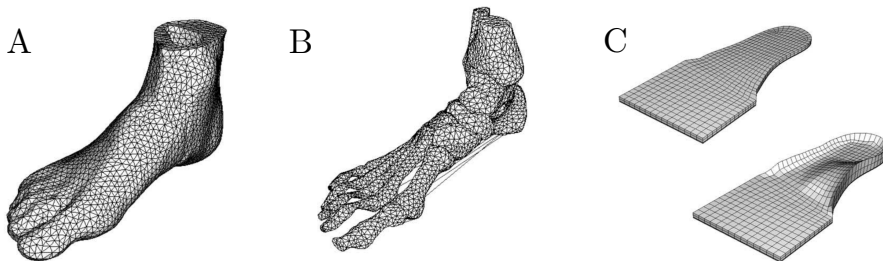


Figure 1.4: Finite Element (FE) model described in Cheung and Zhang 2005 adapted from [58]: (A) soft tissues; (B) bony and ligamentous structures and (C) flat and custom-molded insoles.

It is necessary to further develop methods to determine the dynamic biomechanical effect (kinematics and kinetics) of FOs [230]. Detailed or extended foot musculoskeletal multibody models (FMMM) allow an objective and quantitative evaluation (kinematically and kinetically) of the patients' dynamic behavior.

1.3.2 Foot musculoskeletal multibody models

Musculoskeletal multibody models are described by rigid segments (bones) connected through joints actuated by muscle tendon actuators. Dynamic simulations of human movement use these models to determine how different elements of the musculoskeletal system interact to produce movement. These dynamic simulations complement experimental approaches and can provide estimates of important variables, such as muscle and joint forces, which are difficult to measure experimentally. Dynamic simulations can be divided in two main topics, inverse and forward dynamics. Inverse dynamics and forward dynamics. The inverse dynamics (ID) tool is used to determine the generalized forces (*e.g.* net forces and torques) at each joint responsible given the kinematics and external forces. Forward dynamics is computes the model kinematics given all forces acting on the system (*e.g.* muscle excitations or joint torques) [71, 220].

The commonly used human multibody musculoskeletal models describe the foot using three or fewer segments. A small number of segments is generally insufficient to capture the detail of human 3D foot motion and joint loading [175] at the level required for the analysis of the corrective effect of insoles on foot kinematics. Studies comprehending musculoskeletal multibody modeling emerged in the 1970s with Chow and Jacobson [61] where a dynamic optimization procedure was applied to synthesize the observed pattern of normal gait describing the foot as a unique segment with one degree of freedom (DOF), the ankle, see Figure 1.5.A. Hatze [104] in the same decade simulated the behavior of the human right leg through a time optimization problem. In this study, a combined model of the lower leg and foot was used, see Figure 1.5.B.

Nowadays, a broad range of musculoskeletal modeling systems using different foot models is available. A simple division of these foot models, *i.e.* simple and extended, is presented in the next sections.

Simple foot models

The majority of studies described the foot as a unique segment with one degree of freedom (ankle) to study different aspects of human locomotion (walking or running) such as kinematics and kinetics [48, 181, 184, 159, 174, 7, 224, 258, 190, 203, 204, 202] or muscle activation and forces [218, 191, 69, 261, 185, 233, 14, 3]. Other movements and activities were studied using a similar simplified model of the foot complex, paraplegic standing [133], vertical jump [219, 28, 226, 247], trampoline planar somersaults [27], long jump [105] or cycling [128, 89, 198]. Some authors extended the ankle joint formulation to distinguish two [2, 252] or three DOFs [131, 103, 189, 138, 80, 9] to evaluate different aspects of human walking, *i.e.* metabolic cost, joint moments and muscle forces. Other authors modeled the foot as two segments, hindfoot (calcaneus, cuboid, navicular, cuneiforms, and metatarsals) and toes connected with two DOFs (ankle and metatarsophalangeal joints) [147, 265, 97, 96, 164, 234] or three DOFs defining the subtalar joint [11, 12]. These models were used to extend the kinematic and kinetic knowledge on foot function during human walking or vertical jumping [11]

Delp *et al.* (1990) [72] developed a three segments (talus, hindfoot and toes) and three DOFs model (ankle, subtalar and metatarsophalangeal) of the human lower extremity to study how surgical changes in musculoskeletal geometry and musculotendon parameters affect muscle force and their moments around the joints. This model is one of the most used musculoskeletal multibody models available in an open source software, *OpenSim* [71, 220], see Figure 1.5.C.

Extended foot models

Complex models are becoming more popular, allowing a detailed assessment of the complex foot motion and joint loading. Neptune *et al.* (2000) [175] developed a 3D foot model comprehending four segments (talus, rearfoot, midfoot and toes), with five degrees of freedom (ankle, subtalar, metatarsophalangeal and two at the midtarsal) and seventeen muscles to study lower extremity loading during dynamic activities, like heel-toe running.

Bruening *et al.* (2012) [38] tested a three segment foot model (hindfoot, forefoot, and hallux) with three degrees of freedom (ankle, midtarsal and 1st metatarsophalangeal) on pediatric subjects during normal gait, see Figure 1.5.F.

Morlock and Nigg (1991) [168] considered a complex foot model to study the bone-to-bone contact forces during a lateral side shuffle movement executed with two different shoes, see Figure 1.5.E. This model comprehended six segments (talus, calcaneus, navicular and cuneiforms plus 1st to 3rd metatarsals, cuboid and 4th and 5th metatarsals, 1st to 3rd phalanges, 4th and 5th phalanges with eighteen degrees of freedom (six at the metatarsophalangeal, three at the talonavicular, three at the calcaneocuboid, three at the subtalar and three at the ankle) and ten muscles.

Scott and Winter (1993) [217] developed a biomechanical model of the human foot to study kinematics and kinetics during the stance phase of walking. The foot model had eight segment foot model (talus, calcaneus, 1st metatarsal, 3rd metatarsal, 4th metatarsal, 5th metatarsal, 2nd metatarsal plus midfoot and hallux) with eight DOFs (ankle, subtalar, midtarsal, 1st tarsometatarsal, 3rd tarsometatarsal, 4th tarsometatarsal, 5th tarsometatarsal, 1st metatarsophalangeal), see Figure 1.5.D.

Despite the recognized value of integrating extended foot multibody models in dynamic simulations of movement as described in the following paragraph, the availability of these models bewteen research groups is still limited.

In summary, the number of available extended FMMM is limited. This is a major limitation to reproduce results or to use these models in different studies [71]. Furthermore, to the best of our knowledge, extended FMMM to date have not been used to evaluate the effect of insoles on foot kinematics or kinetics.

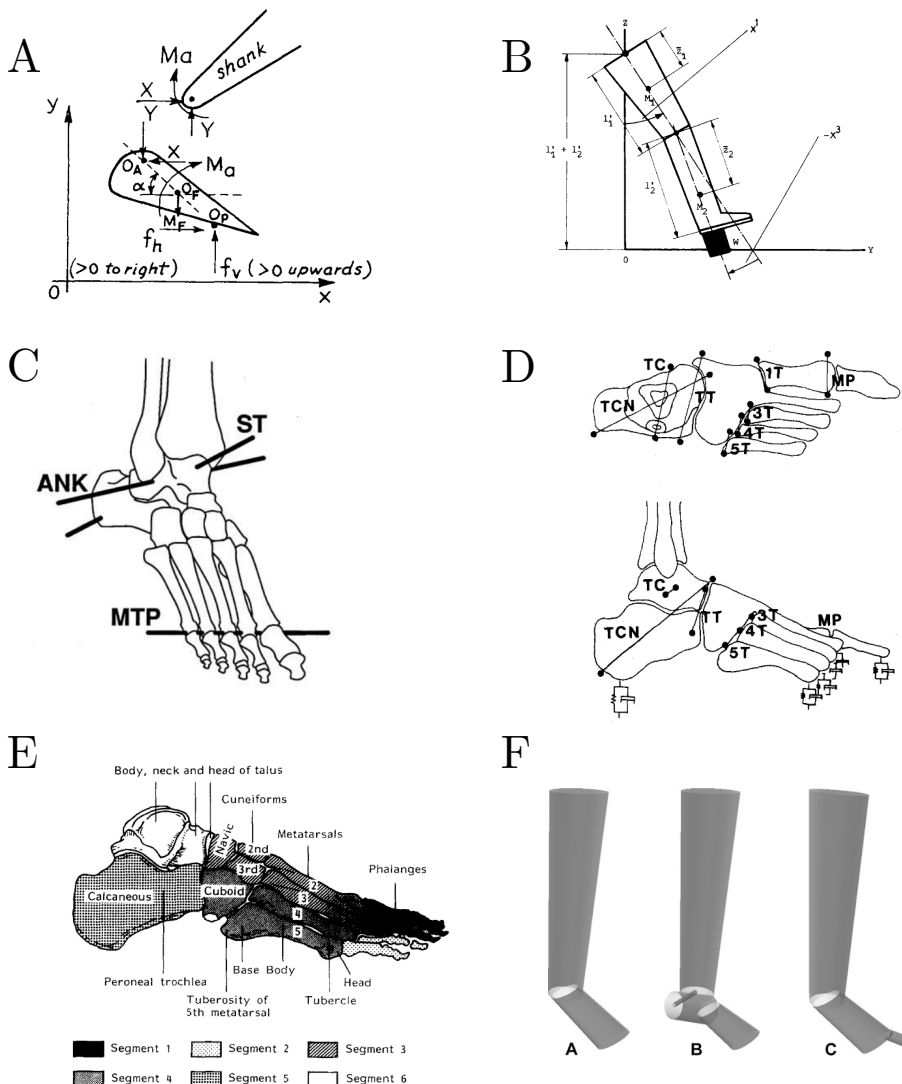


Figure 1.5: Different foot musculoskeletal multibody models (FMMM). (A) Chow and Jacobson (1971) adapted from [188]; (B) Hatze (1976) adapted from [104]; (C) Delp *et al.* (1990) adapted from [72]; (D) Scott and Winter (1993) adapted from [217]; (E) Morlock and Nigg (1991) adapted from [168] and (F) Bruening *et al.* (2012) adapted from [38].

1.3.3 Forward predictive simulations

Forward dynamic simulations allow the study of individual muscle function [176, 13, 150, 174, 163] or the simulation of experimentally measured kinematic and kinetic patterns [190, 202, 238]. These simulations can predict how the muscle forces or joint moments adapt for example to the application of external forces [263, 264]. Forward dynamic simulations are of great clinical relevance for predicting the kinematic and kinetic effect of treatments, *i.e.* insoles [5, 4]. Different approaches to apply external forces to forward dynamic simulations are possible, for example measured forces and center-of-pressure data can be applied to specified bodies, with the force and point of application vectors prescribed as functions of time. In the absence of experimental data, or to try to predict new motions, contact models (*e.g.* foot interaction with the ground) must be combined with the musculoskeletal models.

However, to the authors' knowledge, none of the existing FMMM, in combination with a contact model, was used in the context of a forward predictive simulation.

Several approaches for applying external forces are possible, for example measured forces can be applied to specified bodies. However, forward simulations can lead to altered kinematics thus changing the GRFs. Therefore, to have consistent GRF with the altered kinematics, the contact forces need to be computed as part of the simulation workflow.

Contact descriptive foot models

Contact force formulations like the Hertz theory and elastic foundation modeling (EFM) have been used to describe the interaction between the foot and the ground, see Figure 1.6. The popularity of these methods is related to their dynamic applicability [192, 220, 221]. The analytical method described by Hertz assumes that the size of the contact area is small when compared to the curvature radii of the surfaces in the initial contact point. It is a good approximation for small strains and non-conforming solids but is limited to simple geometric objects like spheres or cylinders [192]. Alternatively, EFM assumes that contacting solids may be considered rigid bodies but with a thin layer of elastic material at the surfaces. The geometry of each surface, which can be arbitrarily complex, is approximated with a triangular mesh. A spring is placed at the centroid of each triangle, discretizing the contact areas and enabling the computation of contact forces for each discrete element, independent of each other [220, 5, 221, 88, 32]. The force in each element is proportional to its penetration on the opposing surface.

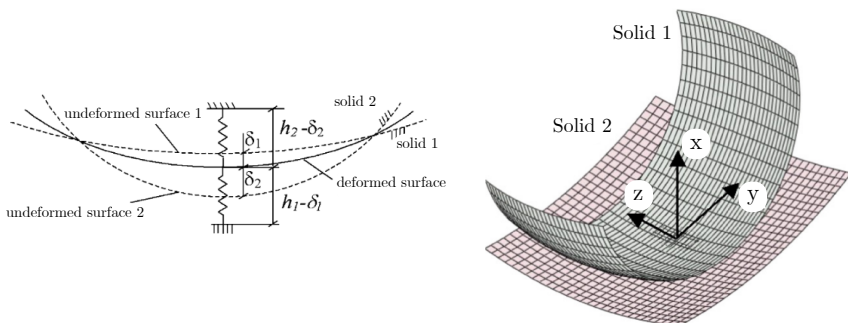


Figure 1.6: Elastic Foundation method formulation adapted from A. Pérez-González *et al.* (2008) [192].

1.4 Summary of the state-of-the-art limitations

In this section, a resume of the main state-of-the art-limitations detailed during the previous sections is presented.

1. The current process of patient assessment for custom foot orthoses design and manufacturing is handicraft work that fully relies on the experience of the clinician. It is often performed using static measurements, therefore neglecting the fact that most of the functional problems are related to the foot motion. This subjective process is one of the main causes for inconsistency in the corrective effects of insoles for different foot pathologies.
2. Dynamic measurements systems, *i.e.* 3D stereophotogrammetry, are crucial to describe the full biomechanical effect of pathologies and to establish a quantitative scientific basis for treatment planning (*e.g.* insole prescription). However, these systems are typically expensive, time-consuming and lack portability, complicating their extensive implementation in a clinical environment.
3. IMUs can overcome the difficulty of measuring kinematics in a clinical environment; however, widespread clinical use of this promising technology has yet to be realized. The use of IMUs for orthopaedic evaluation and rehabilitation practice requires further development and validation.
4. Plantar pressure systems are well-established in clinical care to evaluate foot pathologies, due to the low economic cost and short preparation times compared to the other measurement systems. A disadvantage of using plantar pressure is that it cannot be used to estimate ankle-foot kinematics, failing to describe the full biomechanical effect of pathologies and insole characteristics on foot function.
5. Musculoskeletal multibody models can be used in motion simulations to estimate for example the internal loading of the musculoskeletal system (*e.g.* joint stresses) and to predict the biomechanical effects of treatments. However, the number of accessible extended foot musculoskeletal multibody models is limited, this is a major limitation to reproduce results or to use these models in different studies. Furthermore, to the best of our knowledge, extended foot musculoskeletal multibody models including a contact model to date have not been used in a forward formulation to evaluate the effect of insoles on foot kinematics or kinetics.

Chapter 2

General Aim

Orthotic insoles are used for a variety of applications. During sports activities, the aim of insoles is to improve the biomechanical function of the foot and lower limb in order to reduce sports-related injuries and boost performance. In the presence of pathology, the goal is to optimize a patient's function during gait by relieving symptoms and slow down or even arrest the progression of the pathology. However, up till now, the process of patient assessment for insole design and manufacturing relies mainly on subjective decision making and time-consuming handicraft work by the orthotic technician.

Currently, 3D-printed insoles that reduce the manufacturing time of the insoles to a minimum are already being produced. However, an objective and scientific-based digital workflow linking patient assessment to subject-specific insoles production needs to be extended beyond the currently used static methods (*i.e.* 3D foot scans). This procedure neglects the fact that most foot related mechanical problems are of a dynamic nature. Due to the low economical cost and short preparation time, assessment of foot pathologies mainly relies on plantar pressure despite the availability of technologies, like 3D marker based stereophotogrammetric analysis, that allow accurate description of foot kinematics and kinetics but are time intensive.

The main goal of this thesis is to develop a simulation-based framework to estimate and predict the corrective effect of foot orthoses using an extended foot musculoskeletal multibody model and plantar pressure information.

To this end *in-vivo* gait analysis data, specifically plantar pressure, will be combined with an extended foot-ankle musculoskeletal multibody model that describes the interaction of the foot with the ground and with an insole.

2.1 Research Objective

Computational musculoskeletal multibody models provide the opportunity to develop evidence-based dynamic algorithms for the construction of optimal insoles for each specific patient. Despite the popularity of musculoskeletal multibody models, the availability of these models between research groups is still limited. Consequently, the number of available extended FMMM is limited, this being a major limitation to reproduce results or to use the reported models in different studies. To fill this gap:

Objective 1: It is crucial to increase the level of detail within currently available 3D multibody foot-ankle models.

The level of detail required for these models will be dictated by the functional units of the foot (*i.e.* foot bones moving together around the same axis throughout the stance phase of gait), as defined based on Hicks, 1953 [108].

Dynamic measurements, namely 3D stereophotogrammetry, together with validated extended foot and ankle musculoskeletal multibody models can bring new insights on pathological foot kinematics and kinetics (*e.g.* flat feet). This information can be used to investigate the influence of the currently produced 3D-printed insoles on the measured kinematics and kinetics of flat feet subjects and to compare their influence with the ones provided by standard manufactured insoles and shoes.

Objective 2: Thus, it is important to apply the developed musculoskeletal model to analyse dynamic gait measurements of flat feet patients to identify the influence of 3D-printed insoles on ankle-foot kinematics and kinetics.

The use of plantar pressure measurement systems to evaluate foot and ankle pathologies is well established in clinical practice. Although relevant to detect local tissue overloading, to date, plantar pressure data cannot be used to evaluate ankle-foot kinematics. Musculoskeletal multibody models that integrate a

contact model describing the foot-ground interaction can be used to extrapolate complex foot kinematic data from plantar pressure profiles. In order to develop a model-based relation between plantar pressure profile and foot and lower limb kinematics, it is necessary to firstly :

Objective 3: Implement an elastic foundation contact model to describe the interaction between the foot and the ground.

and secondly:

Objective 4: To evaluate the applicability of plantar pressure measurements to compute detailed ankle-foot kinematics.

Enhancing the use of plantar pressure information to evaluate ankle-foot kinematics will allow a more accurate and objective clinical measurement of foot pathologies.

To objectively improve the link between patient assessment and subject-specific insoles engineering, considering different insoles' combinations of structural and material design factors, it is essential to predict the biomechanical effect of insoles on the foot and ankle kinematics and kinetics. Developing computational tools able to objectively predict the biomechanical effect of insoles would allow a fully informed prescription of these orthoses. Multibody-based algorithms can relate the medical requirements and the required manufacturing parameters, for example stiffness, highlighted as being one of the most important insoles' design factors. To achieve such relation:

Objective 5: It is necessary to develop a predictive simulation framework to evaluate the differences in foot kinematics under the effect of different 3D-printed insoles' stiffnesses.

This PhD thesis was partially developed within *Aladyn*, a collaborative (KU Leuven, *RSScan*, *Materialise* and *RS Print*) and multidisciplinary project. The *Aladyn* project aimed at developing a fully automated, digital workflow from patient assessment to production of subject-specific 3D-printed orthotic insoles that is based on objective evidence rather than subjective decision making.

2.2 Thesis Outline

This thesis is divided in four core chapters that address the five objectives of this thesis. In Chapter 3 a simple, reproducible and efficient semi-automatic tool to compute multi-segment foot models based on computed tomography (CT) scans was developed, providing a more detailed representation of the ankle-foot complex with eight and fifteen degrees of freedom (DOFs). Due to the more accurate representation of the DOFs in the foot, these models have the potential to offer new insights in pathological foot kinematics and dynamics.

The eight DOFs foot model was applied in Chapter 4 using *in-vivo* gait analysis measurements of flat feet and control subjects using different footwear while walking. The kinematic and kinetic differences between control subjects and the flat feet subjects in barefoot and shoed walking were estimated, as well as to the influence of subject specific 3D-printed insoles on the kinematics and kinetics of flat feet subjects and control subjects.

The enhancement of the eight DOFs foot model with foot-ground contact structures thereby allowing the estimation of plantar pressure from foot kinematics is described in Chapter 5. Moreover, Chapter 5 also describes an optimization algorithm that allows the estimation of foot kinematics based on plantar pressure information and the coordinates of a limited set of markers. The set-up simplicity has significant research and clinical implications on both the preparation time of 3D motion capture of foot kinematics as well as on its access and evaluation.

Finally, Chapter 6 describes a torque driven forward dynamic algorithm able to exhaustively predict foot kinematics under the effect of different combinations of directional insoles stiffness. This computational workflow is a step towards developing an evidence-based algorithm for the construction of optimal orthoses in therapeutic shoe design.

Chapter 3

Extended foot-ankle musculoskeletal models for application in movement analysis

Tiago de Melo Malaquias^a, Carolina Silveira^b, Wouter Aerts^a, Friedl De Groote^c, Greta Dereymaeker^a, Jos Vander Sloten^a, Ilse Jonkers^c

^a Biomechanics Section, Mechanical Engineering Department, KU Leuven, Leuven, Belgium

^b Department of Physics, University of Coimbra, Portugal

^c Human Movement Biomechanics Research Group, Department of Movement Sciences, KU Leuven, Belgium

Adapted from:

Tiago M. Malaquias, Carolina Silveira, Wouter Aerts, Friedl De Groote, Greta Dereymaeker, Jos Vander Sloten and Ilse Jonkers (2016). Extended foot-ankle musculoskeletal models for application in movement analysis. *Computer Methods in Biomechanics and Biomedical Engineering*, 20:2, 153-159. The publication is available in Taylor & Francis Online via <http://dx.doi.org/10.1080/10255842.2016.1206533>

3.1 Abstract

Multibody simulations of human motion require representative models of the anatomical structures. An available model that captures the complexity of the foot is still lacking. In the present work, two detailed 3D multibody foot-ankle models generated based on CT scans using a semi-automatic framework are described. The proposed models consists of five rigid segments (talus, calcaneus, midfoot, forefoot and toes), connected by five joints (ankle, subtalar, midtarsal, tarsometatarsal and metatarsophalangeal), one with fifteen DOFs and the other with eight DOFs. The calculated kinematics of both models were evaluated using gait trials and compared against literature, both presenting realistic results. An inverse dynamic analysis was performed for the eight DOFs model, again presenting feasible dynamic results.

3.2 Introduction

The foot is a highly complex structure. Nevertheless, musculoskeletal models commonly describe it by simplified kinematic and dynamic models with three or fewer segments [12, 38]. Being an intricate structure, a small number of segments is generally insufficient to capture the detail of human foot motion and joint loading [175].

In the present work, two extended multibody foot-ankle models that capture important foot movements at the midtarsal and tarsometatarsal (mentioned in Hicks (1953) [108]) were developed. A framework to construct 3D multibody foot-ankle models for use in *OpenSim* [71] based on CT scans was created. This tool defines the body reference frames and joint axes based on anatomical reference points in the CT images as well as the body inertial properties based on the grey scale and volume. Both models consisted of five rigid segments (talus, calcaneus, midfoot, forefoot and toes) with five anatomical joints (ankle, subtalar, midtarsal, tarsometatarsal and metatarsophalangeal) with fifteen and eight DOFs respectively. The first model has three DOFs at each joint, the DOFs of the second model were based on the work of Hicks (1953) [108]. In addition, the geometry of the intrinsic and extrinsic muscles were included as well as the major ligaments. Both models were validated by comparing inverse kinematics for gait with joint kinematics published in literature (Lundgren *et al.* (2008) [152]). Furthermore, the eight DOFs model was used to evaluate inverse dynamics and ligament strain during gait.

3.3 Methods

The following workflow describes the methodology applied to develop both models.

3.3.1 Surfaces and volume meshes generation

CT scan foot data from one healthy subject (age: 34 years and gender: Female) was segmented using *Mimics® Innovation Suite* (*Materialise NV*, Leuven, Belgium). The same software was used to create the surfaces and volume meshes of the bones and the soft tissues. The soft tissue meshes were only used for the computation of the segments' mass and inertia tensor. The bone segments were generated through the union of the corresponding bones: midfoot (navicular, cuboid and cuneiforms), forefoot (metatarsals) and toes (phalanges). Each segment was exported as a surface mesh (triangles) and as a volume mesh (tetrahedrons) separately. The soft tissue was divided in four different regions (calcaneus, midfoot, forefoot and toes) using cutting planes. Each plane was defined using three anatomical landmarks, see Figure 3.1.

- Midtarsal Plane - Central point of the lateral side of the cuboid at the level of the calcaneal-cuboid joint line, central point of the medial side and central point of the dorsal side of the navicular bone at the level of the talus-navicular joint line;
- Tarsometatarsal Plane - Central point of the medial side of the 1st metatarsal bone at the level of the metatarsal-cuneiform joint line, central point of the lateral side of the 5th metatarsal bone at the level of metatarsal-cuboid joint line and the highest central point of the dorsal side of the 2nd metatarsal bone;
- Metatarsophalangeal Plane – Lowest central point at the plantar side of the 1st proximal phalanx, highest central point of the 1st proximal phalanx and central point of the lateral side of the 5th proximal phalanx.

3.3.2 Computation of the local coordinate systems

An Euclidean transform in 3D space, based on single value decomposition [23], was used to transform the foot segment meshes from the CT scan coordinate system to *OpenSim* based on four corresponding points in both feet (CT scan and *OpenSim* – Model Gait 2392). A reference frame with origin at the joint center

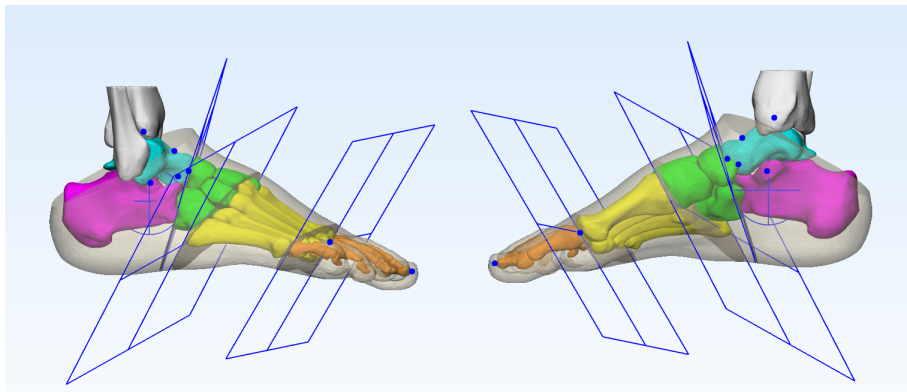


Figure 3.1: Cutting planes used to divide the soft tissue and anatomical landmarks selected in *Mimics® Innovation Suite*.

Table 3.1: Anatomical landmarks, selected on the bones mesh, used to compute the joint axes and segments origin.

Bones	Landmarks
Talus	Supero-medial aspect of the neck of the talus Tip of the lateral process Center of the ankle joint (medium point)
Calcaneus	<i>Sustentaculum Tali</i> Postero-lateral ‘corner’ of the calcaneus Center of the calcaneus/cuboid joint Center of the subtalar joint (Center of the sphere defined by four points)
Midfoot	Supero medial aspect of the head of the talus Tip of the lateral process of the calcaneus Center of the midtarsal joint (medium point)
Forefoot	Mid-dorsum of the foot over the base of the 3 rd metatarsal Tuberosity of the Navicular Center of the Tarsometatarsal joint (medium point)
Toes	Tip of the 1 st distal phalanx Center of the metatarsophalangeal joint (medium point)
	Tip of the medial malleolus Tip of the lateral malleolus
	Center of the posterior articular surface Center of the middle articular surface Center of the anterior articular surface Tip of the trochlear process
	Medial medium point of the talo-navicular joint Lateral medium point of the calcaneo-cuboid joint
	Lateral tuberosity of the 5 th metatarsal Medial medium point of the cuneiform-1 st metatarsal articular surface
	Medial medium point of the 1 st metatarsal-1 st proximal phalanx articular surface Lateral medium point of the 5 th metatarsal-5 th proximal phalanx articular surface

was computed for each segment based on reproducible anatomical landmarks (Table 3.1 and Figure 3.1), selected on the bones mesh using *Mimics® Innovation Suite*.

3.3.3 Anthropometric properties computation

The segments properties (volume, mass and center of mass) were computed using the volume mesh information and the CT scan's greyscale of each element. The inertia tensor was computed based on the density information using explicit formulas for the moments of inertia of 3D tetrahedrons as polynomials of their vertex coordinates [241].

Mimics® Innovation Suite allowed to assign a density value (ρ) to each volume mesh element (n) based on a linear relation between the CT scan's greyscale (Hounsfield units - HU) and the correspondent density value (Equation 3.1). In total, ten different densities were assigned to each segment (i), with each density value correlating to an equally spaced set of HU measures.

$$\rho_{n,i} = b_i + a_i \cdot HU_n \quad (3.1)$$

The line's slope (a) and the y-intersect (b) for each segment resulted from the following system of equations:

$$\begin{cases} \rho_{Trabecular} = b_i + a_i \cdot HU_{min_i} \\ \rho_{Cortical} = b_i + a_i \cdot HU_{max_i} \end{cases} \quad (3.2)$$

where HU_{min_i} and HU_{max_i} are the minimum and maximum greyscale value for each segment, and represent the trabecular and cortical bone. The density values used in (Equation) for the trabecular and cortical bone were 0.05×10^3 and 1.75×10^3 kg/m³ respectively, based on femur bone density values, which were assumed to have similar densities to foot bones [26]. For the soft tissue a uniform density ($\rho_{ST}=1.0158 \times 10^3$ kg/m³) was used by averaging muscle [253] and fat density [81].

A lower limit of 0.001 kg·m² was established for the principal direction of the inertia tensor to avoid problems during the dynamic simulation.

3.3.4 Model creation

Using all the information previously described both models were automatically generated using the *Matlab-OpenSim* interface (see Figure 3.2).

The fifteen DOFs model has three DOFs at each joint (Plantarflexion/Dorsiflexion, Abduction/Adduction, and Eversion/Inversion). The eight DOFs model is based on the work of Hicks, 1953 [108] and has

- one DOF at the ankle joint - plantarflexion/dorsiflexion;
- one DOF at the subtalar joint - defined by an oblique axis, combining eversion-abduction-extension/inversion-adduction-flexion;
- two DOF at the midtarsal joint - defined by two axes, an oblique and an anterior-posterior axis. Both allowing a combination of eversion-abduction-extension/inversion-adduction-flexion;
- two DOF at the tarsometatarsal joint - defined by two axes, the 1st ray axis and the 5th ray axis, both allowing flexion-eversion/extension-eversion;
- two DOF at the metatarsophalangeal joint - plantarflexion/dorsiflexion and abduction/adduction.

Thirty-six ligaments that span at least two of the defined segments were included in our model (Table 3.2). The implementation of these structures required a geometrical path, described by an anatomical based point set (origin, insertion and optional via points). The geometrical path was defined based on *Sarrafian's Anatomy of the Foot and Ankle* [129].

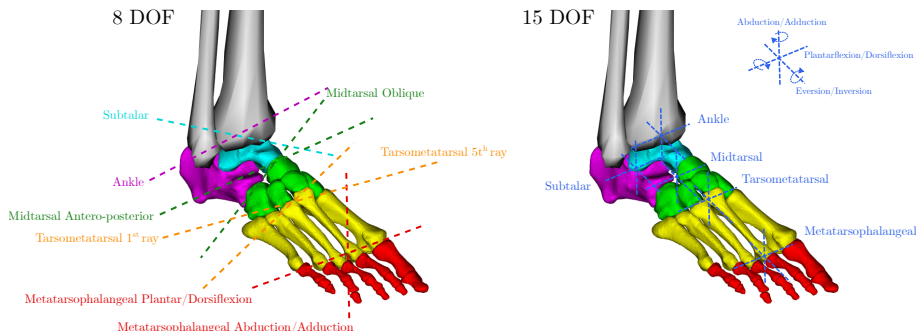


Figure 3.2: Extended foot models (*OpenSim*). Left) 8 DOF model and Right) 15 DOF model. Depicted segments: Cyan - Talus; Purple - Calcaneus; Green - Midfoot; Yellow - Forefoot; Red – Toes. The dashed lines depict the joint axes.

3.3.5 Marker set protocol and Acquisition

Experimental data was collected in five healthy subjects (two males and three females, 53.8 ± 6.5 years, BMI: 23.0 ± 2.9) walking barefoot at self-selected speed (1.15 ± 0.13 m/s) over a 10 m walkway. Four stance phase trials per subject and foot were collected, resulting in a total of forty trials. Motion

Table 3.2: Ligaments geometrical path description. The Resting Length is presented for the generic model, before scaling.

Ligament	Origin	Via Points	Insertion	Resting Length (m)
Tibio-Talar Posterior	Tibia	-	Talus	0.01982
Tibio-Talar Anterior	Tibia	-	Talus	0.02534
Tibio-Calcaneal	Tibia	-	Calcaneus	0.03015
Tibio-Navicular	Tibia	-	Navicular	0.04080
Talo-Fibular Posterior	Tibia	-	Talus	0.03009
Talo-Fibular Anterior	Tibia	-	Talus	0.03016
Calcaneo-Fibular	Tibia	-	Calcaneus	0.03571
Plantar Fascia	Calcaneus	1 st Metatarsal	1 st Prox. Phalange	0.14290
Plantar Fascia	Calcaneus	2 nd Metatarsal	2 nd Prox. Phalange	0.14404
Plantar Fascia	Calcaneus	3 rd Metatarsal	3 rd Prox. Phalange	0.14335
Plantar Fascia	Calcaneus	4 th Metatarsal	4 th Prox. Phalange	0.13612
Plantar Fascia	Calcaneus	5 th Metatarsal	5 th Prox. Phalange	0.12815
Longitudinal Plantar	Calcaneus	Cuboid	2 nd Metatarsal	0.08037
Longitudinal Plantar	Calcaneus	Cuboid	3 rd Metatarsal	0.07665
Longitudinal Plantar	Calcaneus	Cuboid	4 th Metatarsal	0.07153
Longitudinal Plantar	Calcaneus	Cuboid	5 th Metatarsal	0.06389
Calcaneo-Navicular Plantar	Calcaneus	-	Navicular	0.01968
Calcaneo-Navicular Plantar	Calcaneus	-	Navicular	0.01214
Calcaneo-Navicular Plantar	Calcaneus	-	Navicular	0.01041
Calcaneo-Cuboid Plantar	Calcaneus	-	Cuboid	0.01767
Calcaneo-Cuboid Plantar	Calcaneus	-	Cuboid	0.02296
Calcaneo-Cuboid Dorsal	Calcaneus	-	Cuboid	0.02543
Talo-Navicular Dorsal	Talus	-	Navicular	0.01164
Talo-Navicular Dorsal	Talus	-	Navicular	0.01164
Calcaneo-Navicular Bifurcate	Calcaneus	-	Navicular	0.01659
Calcaneo-Cuboid Bifurcate	Calcaneus	-	Cuboid	0.01422
Tarsometatarsal Dorsal	Medial Cuneiform	-	1 st Metatarsal	0.01271
Tarsometatarsal Dorsal	Inter. Cuneiform	-	2 nd Metatarsal	0.00963
Tarsometatarsal Dorsal	Lateral Cuneiform	-	3 rd Metatarsal	0.00684
Tarsometatarsal Dorsal	Cuboid	-	4 th Metatarsal	0.00852
Tarsometatarsal Dorsal	Cuboid	-	5 th Metatarsal	0.00733
Tarsometatarsal Plantar	Medial Cuneiform	-	1 st Metatarsal	0.00903
Tarsometatarsal Plantar	Inter. Cuneiform	-	2 nd Metatarsal	0.00745
Tarsometatarsal Plantar	Lateral Cuneiform	-	3 rd Metatarsal	0.00697
Tarsometatarsal Plantar	Cuboid	-	4 th Metatarsal	0.00767
Tarsometatarsal Plantar	Cuboid	-	5 th Metatarsal	0.00897

capture data was collected using ten infrared *Vicon* cameras (*Vicon*, Oxford Metrics, UK) to track the motion of sixty-five skin-mounted markers (eighteen positioned on each foot) at a sampling rate of 200 Hz [78]. Synchronized ground reaction forces (GRF) and plantar pressure data were collected. Consistency of the normal force computed from the pressure data with the vertical component of the GRF was verified and confirmed in all trials. Force data was collected at 1000 Hz using two *AMTI* force plates (Advanced Medical Technology, Watertown, Massachusetts) embedded in the walkway. Dynamic plantar pressure data were obtained using two *footscan*® pressure plates (RSscan International, Paal, Belgium) positioned on top of the force plates and recorded data at a sampling rate of 500 Hz. The study was approved by the local ethical committee and all participants provided written informed consent.

3.3.6 Decomposition of ground reaction forces

At each time frame, the magnitude of the GRF was decomposed proportional to the measured plantar pressure magnitude under each foot segment. The plantar pressure under the foot was divided into four zones (calcaneus, midfoot, forefoot and toes) using manually defined masks over all time steps. The ratio of the three components of each resultant GRF vector applied to each segment was the same as for the initial GRF vector. The decomposed GRF components were applied to the calcaneus, midfoot, forefoot and toes respectively and using the inverse dynamics tool in *OpenSim*.

3.3.7 Validation

A total of 40 trials was used. The model was scaled in *OpenSim* for each subject using a static measurement. Joint kinematics were estimated for both models (eight DOFs and fifteen DOFs) using a Kalman smoothing algorithm for inverse kinematics [70]. Seven trials for the fifteen DOFs model and four for the eight DOFs model were left out because the outputted kinematic solution presented a physiologically unrealistic movement due to an inaccurate marker data. The rotation of the foot segments around the joints (*i.e.* joint kinematics) was estimated using the inverse kinematics algorithm, based on which the orientation of the segments relative to each other was computed.

Using the computed kinematics the elongation of the ligaments was calculated as a percentage of their resting length during the stance phase of gait. The joint moments of the eight DOFs model were calculated using an inverse dynamics analysis.

3.4 Results

The mean relative motion between segments, mean joint moments and mean ligament elongation, and their correspondent standard deviation (SD) are displayed in Figure 3.3. The kinematic results are compared against the *in-vivo* foot kinematics data of Lundgren *et al.* (2008) [152]. In this work they used bone anchored external markers to describe the kinematics, a more direct measurement of skeletal kinematics than skin mounted markers which are prone to soft tissue artefacts.

The kinematics computed with the fifteen DOFs model presents more inter-subject variability when comparing to the eight DOFs model (*i.e.* maximal

$SD_{Tibia-Talus}^{15DOF} = 8.3^\circ$ against maximal $SD_{Tibia-Talus}^{8DOF} = 6.3^\circ$). The mean kinematics comparison between both models and literature, using the root mean square (RMS), are generally consistent (*i.e.* $RMS_{Tibia-Talus}^{8DOF} = 2.0^\circ$ and $RMS_{Calcaneus-Midfoot}^{8DOF} = 1.7^\circ$, $RMS_{Tibia-Talus}^{15DOF} = 2.0^\circ$ and $RMS_{Calcaneus-Midfoot}^{15DOF} = 2.7^\circ$,). The largest differences are observed in the motion between the talus and midfoot ($RMS_{Talus-Midfoot}^{8DOF} = 8.8^\circ$ and $RMS_{Talus-Midfoot}^{15DOF} = 9.3^\circ$).

Since kinematics computed with the eight DOFs model was less variable (smaller SD) and to some extent more in accordance with literature (smaller RMS) than kinematics computed with the fifteen DOFs model, the dynamics analysis was only performed for the eight DOFs model. The SD of the joint torques (Figure 3.3B) is small (*i.e.* maximal $SD_{Subtalar}^{8DOF} = 0.13 \text{ Nm/kg}$ and maximal $SD_{Tarsometatarsal\ 5^{\text{th}}\ Ray}^{8DOF} = 0.087 \text{ Nm/kg}$), indicating a high inter-subject consistency. Furthermore, the definition of the ligaments' geometry allowed the assessment of their elongation during gait compared to their length in anatomical position, presenting an average maximum elongation for the ankle ligaments of 5.3% (Figure 3.3C).

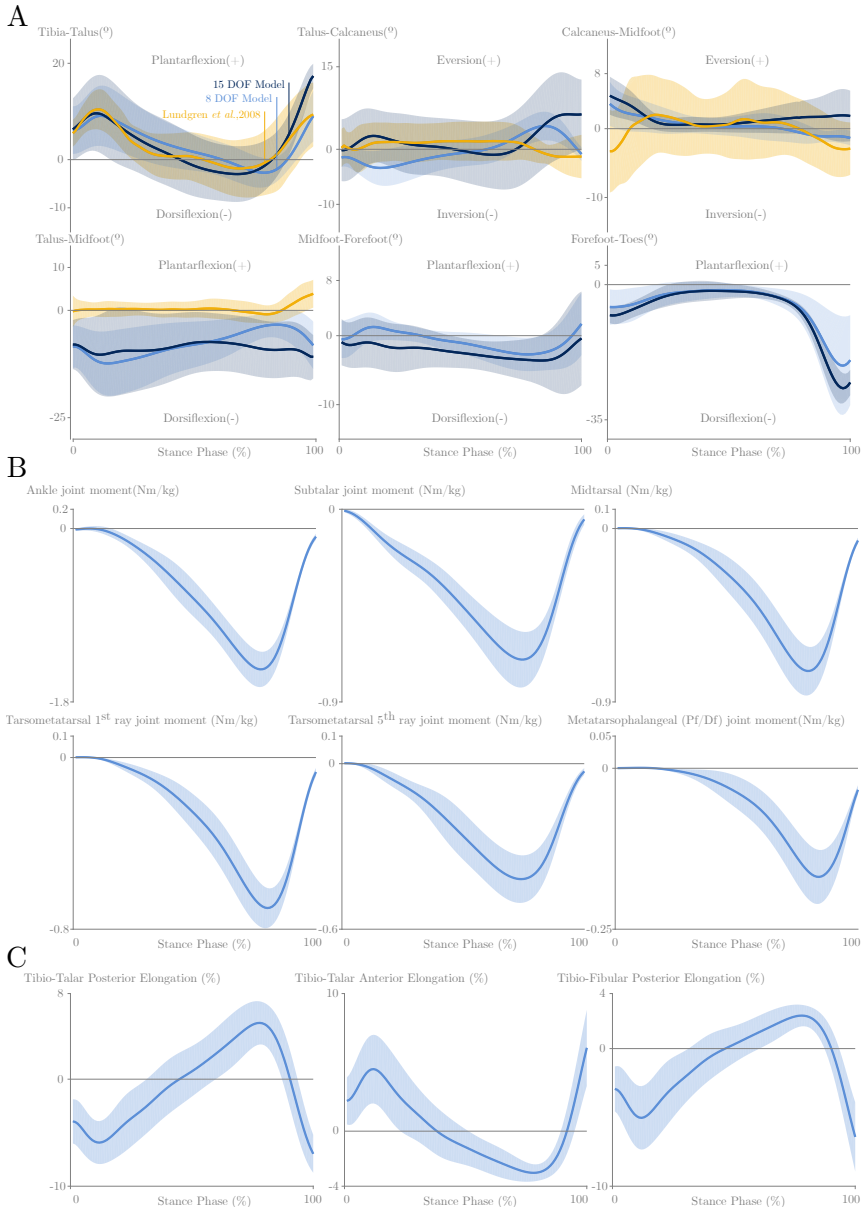


Figure 3.3: Results: (A) Kinematic results - Angles (degrees) between the two specified bodies for the 8 DOF model (green), 15 DOF model (red) and Lundgren *et al.* (2008) [152] (blue) during the stance phase of gait; (B) Inverse Dynamics results - Joint normalised moments (Nm/Kg) obtained for the 8 DOF model during the stance phase of gait; (C) Ligaments - Elongation of the right foot ligaments (% of their resting length) during the stance phase of gait. The solid lines represent the mean of the trials and the dashed lines $\pm 1\text{SD}$.

3.5 Discussion

The eight DOFs model resulted in kinematics with less inter-subject variability. The fifteen DOFs model, has more freedom to solve the inverse kinematics problem due to the three rotational DOFs in each joint and is thus more prone to measurement errors, which might explain the higher standard deviations. However, the authors acknowledge that inter-subject variability might be an imprecise criterion to choose the best model. Di Marco *et al.* (2006) [75] reported high foot and ankle kinematics variability between different subjects using four different experimental marker set-ups similar to the one used in this study. Di Marco *et al.* (2016) [75] highlighted some critical issues concerning the clinical meaningfulness of normative bands specially when handling for example hindfoot-tibia angles with a maximal standard deviation of 3°. In this study the less variable model (8 DOF) presented a standard deviation of 6.3° for an equivalent angle, this presents a high inter-subject variability. In the future, criteria related to intra-subject variability may be considered *e.g.* using a linear fit method [75].

Nonetheless, the eight DOFs model also better resembled literature than the fifteen DOFs model. The main differences, when comparing to Lundgren *et al.* (2008) [152] are observed in the movements between talus and midfoot (*i.e.* navicular, cuboid and cuneiforms). However, this difference might be explained by the fact that both studies consider slightly different kinematics. The model evaluates the movement between segments (talus and midfoot) whereas Lundgren *et al.* measured the movement between talus and the navicular bone individually, which moves with respect to the other bones in the midfoot [152]. Since the work of Lundgren *et al.* (2008) [152] did not include bone pins in the phalanges, it was not possible to compare the metatarsophalangeal joint kinematics. Likewise, no reference data for the relative movement of the midfoot-forefoot was available.

To date, only a limited number of foot models provide dynamic joint information for other joints than the ankle, making the comparison of our results challenging. Nevertheless, the presented results are consistent with the available literature for the joint moments at the ankle, subtalar, midtarsal, and metatarsophalangeal joints [217, 38, 155].

The ankle ligaments average maximum elongation showed a physiological acceptable value, since ligament rupture occurs above 8% [178]. However, for the smaller foot ligaments, further refinement is needed.

A limitation of this study may be the limited number of subjects ($n = 5$). Furthermore, the variability in the bone pin data is large and this is a confounding factor that complicates the statistical comparison. Therefore, to improve the kinematic comparison between the newly developed models

against the study of Lundgren *et al.* (2008) [152], in the future we would need to increase the number of subjects, use the same marker positioning and similar demographics (the group age of the evaluated subjects is higher in this study).

3.6 Conclusion

A simple, reproducible and efficient semi-automatic framework to compute multi-segment foot models based on CT scans was developed, allowing a more detailed representation of the ankle-foot complex with eight DOFs and fifteen DOFs. A total of 36 ligaments were included in both models to allow evaluating their elongation. The eight DOFs model-based inverse kinematic and inverse dynamic analysis of gait resulted in realistic kinematics and dynamics. Due to the more accurate representation of the degrees of freedom in the foot, this model has the potential to offer new insights in pathological foot kinematics and dynamics.

Future research should concentrate on quantifying the specific dynamic parameters of the intrinsic muscles and ligaments (*e.g.* ligament resting length, stiffness, muscle's optimal fiber length and tendon slack length), allowing the study of muscle and ligament forces.

3.7 Supplementary material

The model is made available in: simtk.org/home/kul_footmodel.

3.8 Acknowledgements

This work was funded by the Berghmans - Dereymaeker research chair on Foot and Ankle Biomechanics and the Aladyn Project (IWT, Flanders).

Authors' Contributions

Tiago de Melo Malaquias focused on the skeletal model creation, the kinematics and kinetics simulations, and writing.

Carolina Silveira focused on the ligaments implementation and the kinematics and kinetics simulations.

Wouter Aerts supervised the kinematics and kinetics simulations and revised the manuscript.

Greta Dereymaeker supervised the research.

Friedl De Groote supervised the research and revised the manuscript.

Jos Vander Sloten supervised the research and revised the manuscript.

Ilse Jonkers supervised the research and revised the manuscript.

The experimental data was available from the work of Fien Burg [39] performed in the Movements & posture Analysis Laboratory Leuven.

Chapter 4

A multi-segment foot-model based kinematics and kinetics analysis on the influence of 3D-printed insoles in flat feet subjects

Tiago de Melo Malaquias^{a*}, Tuur van der Have^{b*}, Wouter Aerts^a, Jos Vander Sloten^a, Ilse Jonkers^b

^a Biomechanics Section, Mechanical Engineering Department, KU Leuven, Leuven, Belgium

^b Human Movement Biomechanics Research Group, Department of Movement Sciences, KU Leuven, Belgium

* These authors have contributed equally to this work.

4.1 Abstract

Flat feet (*pes planus*) is a postural mal-alignment characterized by the collapse of the medial longitudinal foot arch, thereby increasing the foot-ground contact area. Custom foot orthoses (FOs) or insoles have been used as initial conservative therapy in *pes planus*, due to their potential to correct altered foot position and movement. The current manufacturing process of customized insoles relies on subjective decision making and time-consuming handicraft work. Hence, improved manufacturing of FOs, namely using 3D-printing technology is currently on the rise allowing a patient-specific, pathology-driven design of subject-specific insoles. Furthermore, 3D-printing may guarantee a more efficient production and the use of more durable materials.

This work quantified differences in foot and ankle kinematics and kinetics between control and flat feet subjects during barefoot walking. In parallel, the influence of subject-specific 3D-printed insoles on kinematics and kinetics of flat feet subjects was compared to the influence of a subject-specific Ethylene-Vinyl Acetate (EVA) molded insole. Eighteen participants were grouped by a two-step method, using the *RSscan footscan D3DTM* software and divided into control subjects (n= 11) or flat feet subjects (n= 7). 3D Motion, ground reaction forces, and plantar pressure distributions were recorded in at least four different conditions: barefoot, minimalist shoe and minimalist shoe with EVA molded and 3D-printed insoles. An *OpenSim* full-body model with an eight degrees of freedom (DOF) foot model calculated the motion of the tibia, calcaneus, and forefoot during the stance phase of gait. Flat feet subjects presented elevated forefoot dorsiflexion and abduction during barefoot walking. The use of EVA and 3D-printed insoles corrected the aberrant flat feet-related kinematics and kinetics presented during the minimalist shoe condition: arch height increased, as reflected by the decreased forefoot dorsiflexion and abduction. Both insoles provided similar correction, thereby confirming the suitability of 3D-printed insoles in the correction of flat feet kinematics and kinetics.

4.2 Introduction

Pes planus (flat feet) is characterized by the collapse of the medial longitudinal foot arch, leading to an increased foot contact area with the ground [146, 228]. It is characterized by eversion of the rearfoot with respect to the tibia [15, 22, 33, 49, 86, 146, 157, 161, 222, 228], combined with abduction and dorsiflexion of the midfoot and forefoot (metatarsals) with respect to the rearfoot [15, 33, 49, 86, 146, 148, 157, 161]. Whereas the kinematics of flat feet subjects is well described in literature, detailed studies on flat feet kinetics (*i.e.*

joint moments) are still scarce and mostly limited to the ankle and subtalar joint (tibial-calcaneal and calcaneal-talar joints) [25, 121, 195, 210, 227]. The few studies quantifying moments acting on the joints forming the medial longitudinal arch (*i.e.* midtarsal and tarsometatarsal) present conflicting results [195, 210]. Further kinetics studies on the medial longitudinal arch joints are needed to extend our knowledge on flat feet and assist in the selection of treatments.

Custom foot orthoses (FOs) or subject-specific insoles are frequently used as conservative therapy in *pes planus* treatment, to relieve symptoms, to slow down the progression and ultimately to avoid early foot surgery [19, 160, 262]. Custom FOs require the manual or digital imprint of the foot plantar surface, which can be obtained using plaster casting or foam impression or digitally using a 3D scanner [53, 153, 262]. Custom insoles have a high potential to correct foot posture, adapting the skeletal alignment, lowering limb muscular activity and impact forces and to redistribute weight [54, 59, 146, 211, 231, 236, 267]. However, instrumented gait analysis studies using multi-segment foot models have presented conflicting results on the effect of custom insoles. A number of studies showed reduced excessive rearfoot eversion in flat feet subjects when using custom foot orthoses [74] while others presented no significant improvement [19]. Furthermore, custom insoles have no proven significant effect on excessive forefoot dorsiflexion [74]. The insoles' influence on joint moments is also controversial, some studies proved the insoles efficacy in reducing ankle inversion joint moment [227, 236] while others failed to report significant changes [25, 57, 121].

Without a consistent level of evidence to support the corrective effects of FOs to treat flat feet, clinicians are balancing evidence-based practice with potentially conflicting clinical experience [19]. Furthermore, insoles studies are often limited to the kinematics and kinetics evaluation of the ankle joint, not capturing the full three-dimensional, multi-segmental correction induced by the FOs.

The current design and manufacturing of customized FOs through molding thermoplastics like EVA [262] relies on subjective decision making and time-consuming handicraft work. Currently, 3D-printed insoles are being fabricated allowing efficient and objective production of subject-specific insoles. Moreover, 3D-printing technology allows full production control over several insole properties like thickness [211], stiffness [54, 59], heel and arch height [267] and wedges [114, 201]. However, studies about the corrective effect of these new custom foot orthoses are to the authors' knowledge still non-existent.

This work aims to use a complex foot multibody musculoskeletal model [156] to quantify flat feet foot kinematics and kinetics. Secondly, to evaluate the influence of 3D-printed subject specific insoles on the kinematics and kinetics and to compare this influence to EVA subject specifics insoles in minimalistic

shoes.

4.3 Methods

Eighteen participants (age: 40.2 ± 11.4 years and weight: 74.9 ± 13 kg) were recruited for this study. Categorization by arch height into flat feet subjects (seven) and controls (eleven) was performed based on dynamic plantar pressure measurements using a protocol during walking and running at self-selected speed [87]. Seven categories ranging from flat (category one) to high (category seven) arched feet were defined using dynamic plantar pressure data obtained using two *footscan*® pressure plates (RSscan International, Belgium). The categorization was performed automatically by the *footscan*® software (RSscan International, Belgium): the ratio of the pressure area under the midfoot compared to the total area of the foot without the toes (in %) is used to classify the patient into one of the seven arch height categories. Participants in category one or two were grouped as flat feet subjects.

Gait analysis was performed using sixteen infrared cameras (8 MX T40-S, 8 Bonita 10, *Vicon*, Oxford Metrics, UK, 200 Hz) and a marker model with fifty-eight markers for static calibration (thirty for the foot-ankle complex, eighteen individual markers and four triad clusters), see Table 4.1. Thirteen anatomical foot-ankle markers were removed during the gait evaluation, keeping the triad clusters on the calcaneus, midfoot and two on the forefoot and an individual marker in the hallux base. Ground reaction forces (GRF) (2 *AMTI* force plates, Advanced Medical Technology, Watertown, Massachusetts, 1000 Hz and 1 *IBV Dinascan*, *Vicon*, Oxford Metrics, UK, 1000 Hz) and dynamic plantar pressure (*footscan*® 0.5 m high-end, 500 Hz, and *footscan*® 1 m high-end, 250Hz, *RSscan* International, Paal, Belgium) were collected. The plantar pressure plates were positioned on top of the ground-embedded force plates to allow dynamic calibration of the pressure plates.

Table 4.1: Markers anatomical position and associated *OpenSim* tracking weight (w). (*) Markers used only for the static acquisitions.

Head		Foot (left and right)	
RHV	Right head ventral (w = 1)	CDL*	Tuberculum peronealis
LHV	Left head ventral (w = 1)	CDM*	Sustentaculum tali
RHD	Right head dorsal (w = 1)	CPL*	Proximal lateral aspect of calcaneus
LHD	Left head dorsal (w = 1)	CPM*	Proximal medial aspect of calcaneus
Trunk		Cu*	Cuboid bone
CTO	Cervicothoracal transition (w = 1)	Na*	Navicular bone
T10	Processus spinosus 10	CM*	Medial cuneiform bone
ACR	Acromion (w = 100)	BMTI*	Metatarsal base I
STER	Sternum (w = 1)	BMTII*	Metatarsal base II
CLAV	Manubrium sterni (w = 1)	BMTIII*	Metatarsal base III
Pelvis		BMTV*	Metatarsal base V
SIAS	Spina illiaca anterior superior (w = 100)	CMTI*	Metatarsal head I
SIPS	Spina illiaca posterior superior (w = 100)	CMTII*	Metatarsal head II
Upper leg (left and right)		CMTIII*	Metatarsal head III
EPILB	Epicondylus lateralis leg (w = 1)	CMTV*	Metatarsal head V
EPIMB	Epicondylus medialis leg (w = 1)	HAL	Base distal phalanx (w = 100)
CrVBB	Cranial ventral upper leg cluster (w = 10)	CalCa	Calcaneus cluster: caudal marker (w = 100)
CrDBB	Cranial dorsal upper leg cluster (w = 10)	CalCrL	Calcaneus cluster: cranial lateral marker (w = 100)
CaVBB	Caudal ventral upper leg cluster (w = 10)	CalCrM	Calcaneus cluster: cranial medial marker (w = 100)
CaDBB	Caudal dorsal upper leg cluster (w = 10)	MFD	Midfoot cluster: distal marker (w = 10)
Lower leg (left and right)		MFPM	Midfoot cluster: proximal medial marker (w = 10)
ML*	Maleolus lateralis (w = 1)	MFPL	Midfoot cluster: proximal lateral marker (w = 10)
MM*	Maleolus medialis (w = 1)	FFMCr	Forefoot Med cluster: cranial marker (w = 100)
FC	Caput fibulae (w = 1)	FFMCaP	Forefoot Med cluster: caudal proximal marker (w = 100)
TT	Tuberositas tibiae (w = 1)	FFMCaD	Forefoot Med cluster: caudal distal marker (w = 100)
CrMOB	Cranial medial lower leg cluster (w = 100)	FFFLCr	Forefoot Lat cluster: cranial marker (w = 100)
CrLOB	Cranial lateral lower leg cluster (w = 100)	FFFLCaP	Forefoot Lat cluster: caudal proximal marker (w = 100)
CaMOB	Caudal medial lower leg cluster (w = 100)	FFFLCaD	Forefoot Lat cluster: caudal distal marker (w = 100)
CaLOB	Caudal lateral lower leg cluster (w = 100)		

Each participant was sequentially measured barefoot, with minimalist shoes (*Labshoe*) without and with *EVA Molded* and *3D-printed* insoles from *Phits* (*RS Print*, Paal, Belgium powered by *Materialise NV*, Leuven, Belgium), see Figure 4.1. In all four conditions (barefoot, *Labshoes*, *EVA Molded*, *3D-printed*) one static and ten walking trials per foot (full gait cycle) were acquired.

A full-body model with eight degrees of freedom (DOF) foot model [156] was scaled to each participant based on the static measurement in *OpenSim* [71]. Joint kinematics were estimated using the inverse kinematics algorithm, based on it, the relative orientation of the segments was computed (in this work only tibia – calcaneus and calcaneus-forefoot were evaluated).

At each time frame, the magnitude of the GRF was decomposed proportional to the measured plantar pressure magnitude under each foot segment. The plantar pressure under the foot was divided into four zones (calcaneus, midfoot, forefoot and toes) using automatically defined masks based on the sum of plantar pressure map over all time steps. The automated masks were computed using the convex Hull algorithm available in *Matlab*. The ratio of the three components of each resultant GRF vector applied to each segment was the same as for the initial GRF vector. The decomposed GRF components were applied to the calcaneus, midfoot, forefoot and toes respectively and using the inverse



Figure 4.1: A) Minimalistic shoes (*Labshoe*), B) *EVA Molded* insoles and C) *3D-printed* insoles.

dynamics tool in *OpenSim*. Joint moments were then estimated and normalized to the body weight of the participant.

The 3D joint angles and moments were time normalized over stance. Each stance phase was divided into four phases (P1, P2, P3 and P4) accordingly from initial contact (0%) – foot flat (16%) – midstance (42%) - heel off (66%) to toe off (100%). For each condition, an average value over each phase per trial and per leg was taken. Swing phase was not analyzed during this project. The number of measurements per subject and per condition is summarized in Table 4.2.

Statistical tests were performed to evaluate the biomechanical differences between flat feet and control subjects, and the biomechanical influence of the Labshoes and both insoles (*EVA Molded* and *3D-printed*). A Linear Mixed Model (LMM) was used to determine if there were significant differences in tibia-calcaneus and calcaneus-forefoot angles or ankle, midtarsal and tarsometatarsal joint moments (1) Barefoot Control vs. Barefoot Flat Feet; (2) Barefoot Control vs. *Labshoe* Control; (3) Barefoot Flat Feet vs. *Labshoe* Flat Feet; (4) *Labshoe* Control vs. *Labshoe* Flat Feet; (5) *Labshoe* Flat Feet vs. *3D-printed* Insole Flat Feet; (6) *Labshoe* Flat Feet vs. *EVA Molded* Insole Flat Feet; (7) *Labshoe* Control vs. *3D-printed* Insole Control and (8) *Labshoe* Control vs. *EVA Molded* Insole Control.

The LMM computed for each phase is described, using Wilkinson's notation, as:

$$X_{Phase} \sim 1 + Condition + Side + (1 | Subject) \quad (4.1)$$

Where X_{Phase} was the dependent variable both for the 3D joint angles and the joint moments, and we evaluated this dependency for each of the three phases of stance. *Condition* (different insole stiffnesses) and *Side* (Left or Right) were the fixed effects and *Subject* was the random effect. All statistics were calculated using *Matlab* (Statistics Toolbox Release 2016b, The MathWorks, Inc., Natick, Massachusetts, United States.). The results were found significant if the $p - value$ was lower than 0.05/8, applying the Bonferroni correction for multiple comparisons.

An overview of the number of trials per subject is presented in Table 4.2. Motion trials were excluded if there was missing or inaccurate marker data complicating kinematic reconstruction as well as technical issues with the pressure plate data at the time of the collection.

Table 4.2: Total number of trials used for the inverse kinematics and dynamics simulations for each subject and each condition, Left and Right leg added together.

		Controls											
		S1	S2	S3	S4	S5	S6	S7	S8	S9	S10	S11	Total
Barefoot	Kinematics	12	10	7	11	6	15	14	13	12	12	13	125
	Inverse Dynamics	12	4	6	10	-	14	9	8	10	9	11	93
<i>Labshoe</i>	Kinematics	12	11	7	12	8	12	13	12	9	8	10	114
	Inverse Dynamics	12	5	6	9	5	4	4	1	7	3	9	65
<i>3D-printed</i>	Kinematics	12	15	11	14	10	15	12	12	11	11	10	133
	Inverse Dynamics	6	4	6	10	7	2	-	8	5	7	2	57
<i>EVA Molded</i>	Kinematics	-	14	11	15	11	-	-	-	-	4	-	55
	Inverse Dynamics	-	8	6	12	7	-	-	-	-	1	-	34
Flat Feet													
		S12	S13	S14	S15	S16	S17	S18	Total				
Barefoot	Kinematics	8	11	9	10	8	-	12	58				
	Inverse Dynamics	8	2	4	10	6	-	8	38				
<i>Labshoe</i>	Kinematics	14	13	11	11	10	11	9	79				
	Inverse Dynamics	4	9	10	8	10	7	2	50				
<i>3D-printed</i>	Kinematics	15	10	9	10	12	12	9	77				
	Inverse Dynamics	13	-	3	8	11	10	2	47				
<i>EVA Molded</i>	Kinematics	11	13	2	11	10	12	14	73				
	Inverse Dynamics	3	4	2	8	6	12	3	38				

4.4 Results

4.4.1 Kinematics

Forefoot dorsiflexion and abduction were significantly increased in the flat feet group during barefoot walking compared to the control group during most of the stance phase, see Figure 4.2.

The use of *Labshoes* significantly increased forefoot dorsiflexion and abduction for the entire stance phase, indicative of arch flattening in the control subjects. For the flat feet subjects, dorsiflexion increased at P1 and P2, but decreased for P3 and P4, whereas abduction increased in P1 but decreased during the remainder of stance, see Figure 4.2. As a result, no significant differences between control subjects and flat feet subjects were observed during *Labshoe* condition.

The *EVA Molded* insoles decreased both forefoot dorsiflexion and abduction during the entire stance phase in the flat feet subjects. For the control group, there was a small ($< 1^\circ$) significant increase in forefoot dorsiflexion and decrease in abduction during most of the stance phase, see Figure 4.3 and 4.4. The *3D-printed* insoles significantly decreased forefoot dorsiflexion and abduction in both groups, most pronounced in the flat feet subjects, see Figure 4.3 and 4.4.

Flat feet tibia-calcaneus angle was not significantly different from the control group and the effect of the *Labshoe* and both insoles was in general small ($< 1^\circ$). Except for the significant increase of calcaneus dorsiflexion in the control subjects using both insoles. Because of the little added value of these results, the joint angle between tibia and calcaneus is not presented in this work.

4.4.2 Kinetics

Compared to control subjects, flat feet subjects presented lower midtarsal and tarsometatarsal joint moments throughout most of the stance phase (except P1), see Figure 4.5. Using *Labshoes*, the joint moments of the control group decreased throughout most of the stance phase, up to the levels of the joint moments in the flat feet subjects, see Figure 4.5. Both insoles further reduced the tarsometatarsal joint moment in P2 and P3 in the flat feet subjects, see Figure 4.6. For the control subjects, only the *EVA Molded* insole significantly reduced the tarsometatarsal joint moment throughout most of the stance phase, see Figure 4.7.

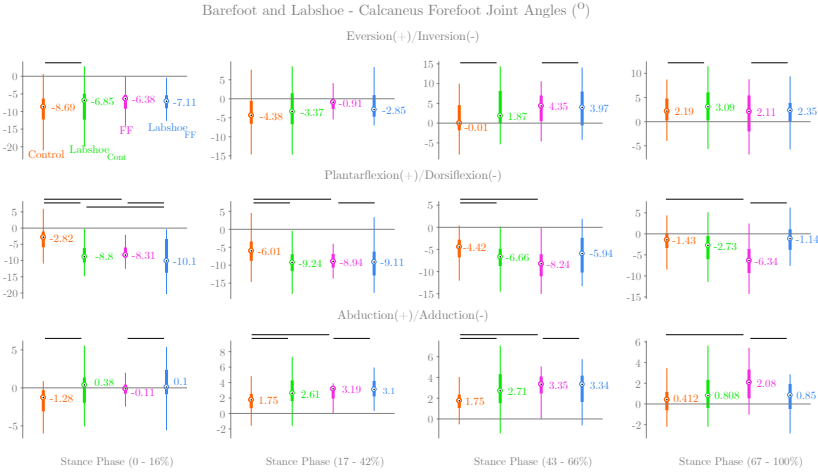


Figure 4.2: Mean joint angles between calcaneus and forefoot for each phase of the stance phase for the barefoot and *Labshoe* condition. Orange – Control barefoot; Light Green – Control *Labshoe*; Pink – Flat Feet barefoot; Light Blue – Flat Feet *Labshoe*. The black lines represent significant difference (p – value < 0.05/8). The box plots do not depict eventual outliers.

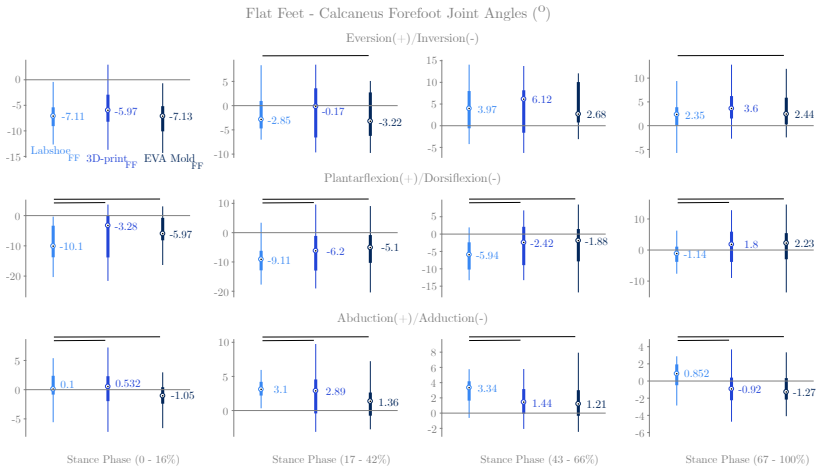


Figure 4.3: Mean joint angles between calcaneus and forefoot for each phase of the stance phase for the different conditions of the flat feet group. Light Blue – Flat Feet *Labshoe*; Blue – Flat Feet *3D-printed*; Dark Blue – Flat Feet *EVA Molded*. The black lines represent significant difference (p – value < 0.05/8). The box plots do not depict eventual outliers.

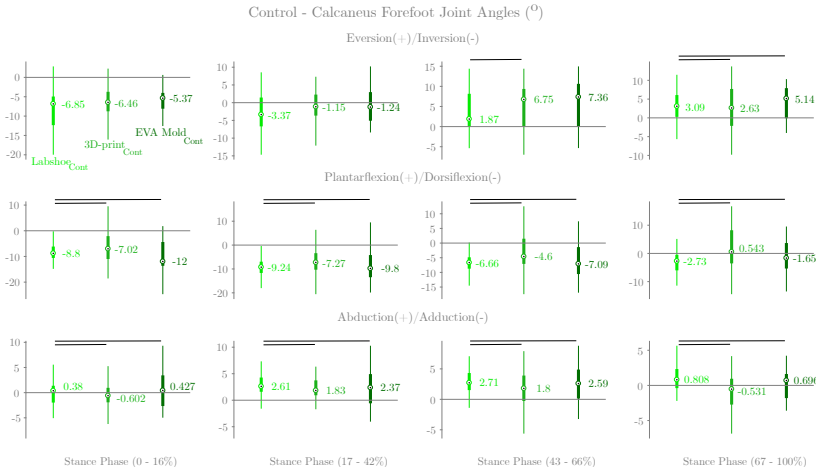


Figure 4.4: Mean joint angles between calcaneus and forefoot for each phase of the stance phase for the different conditions of the control group. Light Green – Flat Feet *Labshoe*; Green – Flat Feet *3D-printed*; Dark Green – Flat Feet *EVA Molded*. The black lines represent significant difference ($p - value < 0.05/8$). The box plots do not depict eventual outliers.

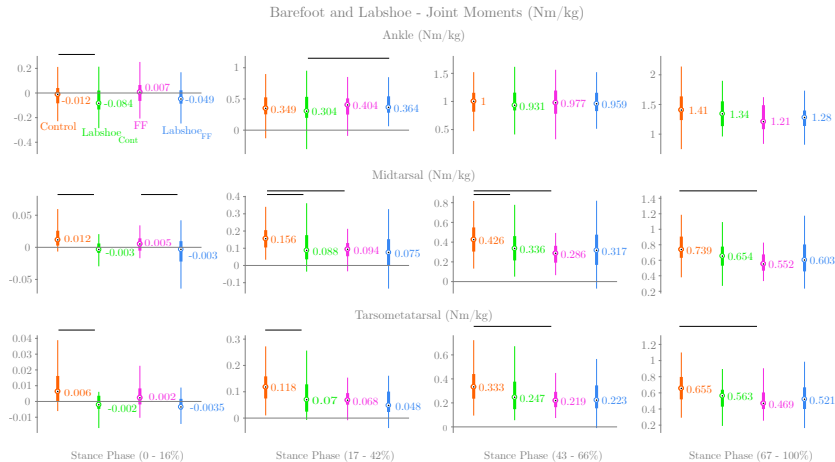


Figure 4.5: Mean joint moments (ankle, midtarsal and tarsometatarsal) for each phase of the stance phase for the barefoot and *Labshoe* condition. Orange – Control barefoot; Light Green – Control *Labshoe*; Pink – Flat Feet barefoot; Light Blue – Flat Feet *Labshoe*. The black lines represent significant difference ($p - value < 0.05/8$). The box plots do not depict eventual outliers.

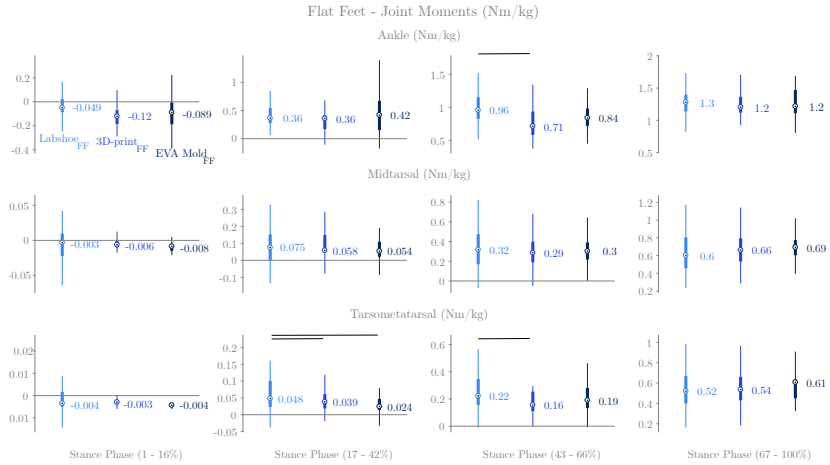


Figure 4.6: Mean joint moments (ankle, midtarsal and tarsometatarsal) for each phase of the stance phase for the different conditions of the flat feet group. Light Blue – Flat Feet *Labshoe*; Blue – Flat Feet *3D-printed*; Dark Blue – Flat Feet *EVA Molded*. The black lines represent significant difference (p – value < 0.05/8). The box plots do not depict eventual outliers.

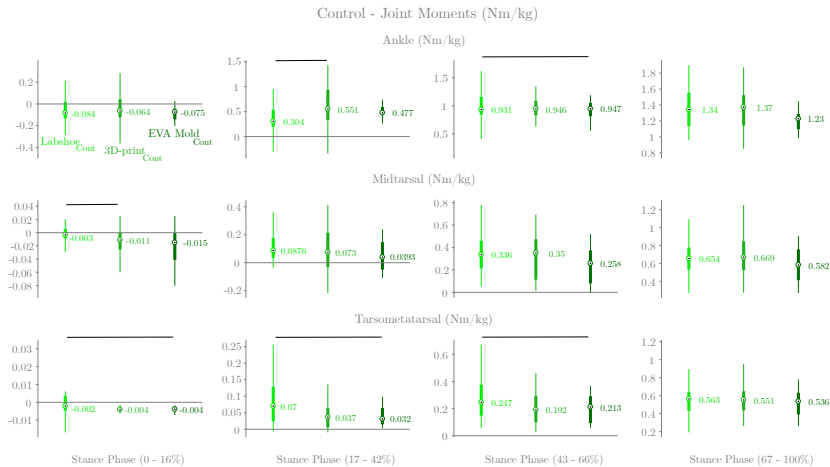


Figure 4.7: Mean joint moments (ankle, midtarsal and tarsometatarsal) for each phase of the stance phase for the different conditions of the control group. Light Green – Control *Labshoe*; Green – Control *3D-printed*; Dark Green – Control *EVA Molded*. The black lines represent significant difference (p – value < 0.05/8). The box plots do not depict eventual outliers.

4.5 Discussion

In this study we evaluated kinematic and kinetic characteristics of flat feet subjects and evaluated the corrective potential of two different insoles using a complex multi-segment foot model. The flat feet subjects were characterized by increased forefoot dorsiflexion and abduction throughout the entire stance phase of gait (Figure 4.2), characterizing a low medial longitudinal arch [15, 33, 86, 119, 146, 148, 157, 161, 210, 245]. Excessive rearfoot pronation (*i.e.* calcaneus eversion in relation to the tibia) was not confirmed in this study, despite often being the focus of intervention in *pes planus* [15, 22, 33, 86, 146, 157, 161, 228]. Other authors have also concluded that excessive rearfoot pronation is not always as prominent as expected [99, 119, 144, 245]. It is possible that the procedure used to differentiate flat feet subjects based on plantar pressure was too inclusive, including erroneously some control subjects, neutralizing the expected kinematics differences. In the future, a stricter selection of flat feet subjects could be considered, including not only the pressure measurements but also radiographic and morphological features of the foot (*i.e.* medial longitudinal arch height and static calcaneus alignment in relation to the tibia).

The kinematics influence of a minimalistic shoe should be negligible in order to isolate the corrective effect of the insoles. However, the use of minimalistic shoes had an effect on the foot kinematics, introducing arch flattening most pronounced in the control subjects. This kinematics effect is possibly related to the lack of adaptation time provided to the subjects during the acquisition sessions [68, 186]. Considering the influence of the minimalistic shoes it was possible to understand the isolated effect of the insoles.

Both insoles (*EVA Molded* and *3D-printed*) decreased forefoot dorsiflexion and abduction in flat feet subjects (Figure 4.3). The insoles increase the medial longitudinal arch height by providing increased stiffness and cushioning to the arch. As such, the insoles can provide the desired effect and correct the low medial longitudinal arch. The effect of both insoles in the control group, although significant, was in general not meaningful (Figure 4.4). This small effect is expected, as in the control subjects insoles are not expected not to impose kinematic corrections but only provide comfort.

The available literature on the kinetics evaluation of the midtarsal and tarsometatarsal joints in flat feet subjects is scarce and incoherent [195, 210]. So, the clinical kinetic description of these joints in flat feet subjects is not clear [210]. The current study showed that midtarsal and tarsometatarsal moments were lower for flat feet subjects compared to control subjects (Figure 4.5). These results are in agreement with the study of P. Saraswat *et al.* (2014) [210]. During the midstance of gait, flat feet subjects bear weight in the midfoot as

well as in the calcaneus and forefoot, thereby altering the weight distribution over the different segments, affecting both the force magnitude and points of force application, depicted in Figure 4.8.A and B. So, the decreased force vectors magnitude and force application points closer to the joint axes, will decrease the midfoot and forefoot moments.

Insoles increase the plantar support under the midfoot leading to a reduction in the magnitudes and force application points in the calcaneus and forefoot during the midstance of gait, see Figure 4.8.C. This was demonstrated by a small reduction in the midtarsal and more significantly in the tarsometatarsal joint moments for both groups, see Figure 4.6 and 4.7. The insoles, by reducing the moment in the foot joints, are decreasing the joint effort required to counteract the GRF, translated by a smaller effort on the passive and active soft tissue structures (*i.e.* muscle and ligaments). These results showed that insoles have a beneficial functional advantage for both the flat feet and control subjects.

When analyzing the results, it should be considered that the subtalar joint was indirectly estimated through markers placed on the foot and calcaneus and tibia as no markers could be placed on the talus. Therefore, a clamping constraint (Range: [−20° to 20°]) was imposed to guide the inverse kinematics estimation. The current protocol only placed one marker on the hallux and therefore toes' motion was not analyzed. Additionally, the different phases of stance were assumed to have a constant duration in all subjects based on the stance phase division established by the Rancho Los Amigos National Rehabilitation Centre [1]. The authors believe that the assumption of this fixed percentage will not significant impact the results because the inter-subject variability of the different phases in the gait cycle was reported to be smaller than 3% for an adult population by Hollman *et al.* (2011) [115] and therefore a minimal impact on the average angle during the phases is expected. Nonetheless, in principle, the duration of the different stance phases for each gait trial could be determined to verify the influence of this assumption for future research.

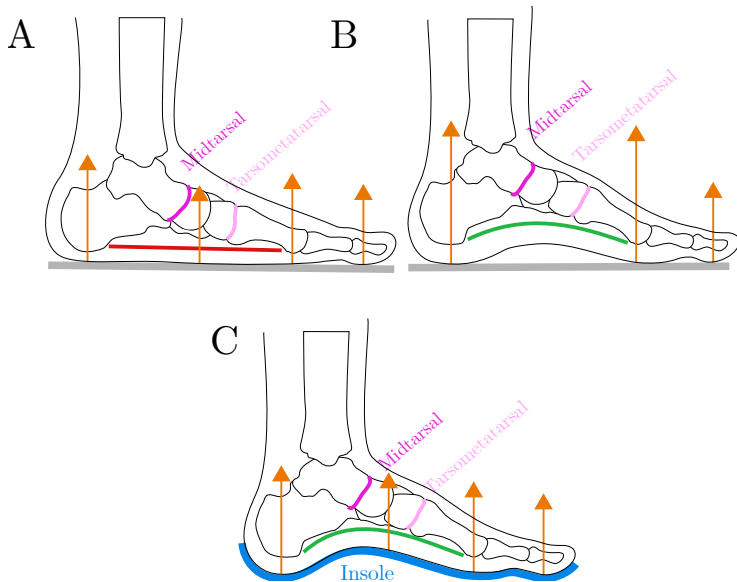


Figure 4.8: Representation of the foot weigh bearing mechanism during the midstance of gait. A) Flat feet subjects bear weight in the midfoot as well as in the calcaneus, forefoot and toes. B) Control subjects bear weight do not bear weigh in the midfoot. C) Both flat feet and control subjects bear weigh in the midfoot when using insoles.

Lastly, the data collected in this sample of patients allowed detecting small but significant differences between insole conditions (up to 1°) using a multilevel statistic model and a conservative correction for multiple comparisons, *i.e.* linear mixed model with a Bonferroni correction. Nonetheless, a larger sample size should be considered in order to verify potential significances of differences currently not confirmed as statistically significant (*e.g.* calcaneus eversion/inversion in relation to the tibia). A power analysis based on this work could serve as a basis for a sample size calculation of future studies.

4.6 Conclusion

This study assessed the kinematic and kinetic differences between control participants and flat feet subjects using a multi-segment foot model in combination with 3D motion capture, force plate and plantar pressure data.

Flat feet subjects presented an expected increased forefoot dorsiflexion and abduction compared to controls while walking barefoot.

Use of insoles corrected the dynamic foot posture by supporting the arch in flat feet subjects, decreasing forefoot dorsiflexion and abduction, thereby increasing arch height. The insoles also demonstrated a beneficial kinetic advantage for both the flat feet and control subjects by reducing the tarsometatarsal joint moment.

Finally, the corrective performance of the EVA molded insoles can be achieved using 3D-printing technology. In the future this can offer an opportunity towards more efficient production, the use of better more materials less prone to wear and an objective pathology-oriented design of subject-specific insoles.

4.7 Acknowledgements

This work was funded by the Berghmans - Dereymaeker research chair on Foot and Ankle Biomechanics and the Aladyn Project (IWT, Flanders).

Authors' Contributions

Tiago de Melo Malaquias focused on the kinematics and kinetics simulations, the statistical evaluation, and writing.

Tuur van der Have focused on the kinematics and kinetics simulations.
Wouter Aerts helped in the development of auxiliary code.

Ilse Jonkers supervised the research and revised the manuscript.

Jos Vander Sloten supervised the research and revised the manuscript.
The experimental data was collected by the RSscan research team.

Chapter 5

Plantar pressure based estimates of foot kinematics during gait – a least squares optimization approach

Tiago de Melo Malaquias^a, Wouter Aerts^a, Ilse Jonkers^b, Jos Vander Sloten^a, Friedl De Groot^b

^a Biomechanics Section, Mechanical Engineering Department, KU Leuven, Leuven, Belgium

^b Human Movement Biomechanics Research Group, Department of Movement Sciences, KU Leuven, Belgium

5.1 Abstract

The use of plantar pressure measurement systems to evaluate foot and ankle pathologies is well established in clinical practice. Although relevant to detect local tissue (over) loading, to date, plantar pressure data is not used to evaluate ankle-foot kinematics. Here, we present a multibody model-based algorithm to estimate ankle-foot kinematics based on plantar pressure data and the trajectories of a limited number of markers.

The method is based on a least squares optimization algorithm that minimizes the weighted difference between simulated and measured plantar pressure and different marker combinations data. Both marker positions and plantar pressures are simulated in *OpenSim* using an extended musculoskeletal shank and foot model with six rigid bodies and fourteen degrees of freedom coupled with an ellipsoid-based elastic foundation contact model (EFM).

To validate the method, a two-step approach was used: (1) the influence of including plantar pressure data in the kinematics estimation was quantified when tracking sixteen markers (twelve foot + four tibia markers). (2) the influence of reducing the number of tracked markers on the plantar pressure-based kinematics estimation was evaluated. The inclusion of plantar pressure data had a limited effect in the kinematics estimation, presenting similar results to the full markers only approach (within standard deviation $\geq 75\%$, mean absolute difference $\leq 3^\circ$ and peak absolute difference $\leq 5^\circ$).

The reduction of the number of markers showed that in combination with the pressure data, a minimum of four-foot markers is needed to estimate kinematics with accuracy comparable to the full marker approach (within standard deviation $\geq 75\%$, mean absolute difference $\leq 3^\circ$ and peak absolute difference $\leq 5^\circ$).

The ability of estimating full foot kinematics using a simplified set-up that relies on a limited number of reflective markers combined with plantar pressure measurements has significant time and economic implications for both research and clinical applications. It will allow a more accessible and objective clinical evaluation of foot pathologies.

5.2 Introduction

Clinicians treating foot pathologies, tend to rely mainly on plantar pressure data to evaluate foot functional deficits. This despite the availability of technologies that allow accurate description of foot kinematics using camera-based systems combined with reflective skin markers. Foot kinematics and kinetics are

important biomechanical variables to evaluate pathologies affecting the foot [73, 255, 8, 199, 63, 106, 212, 10, 134, 47, 94, 239, 135]. The main reason for using plantar pressure systems is their low economic cost and short preparation time compared to marker-based technologies [183].

Plantar pressure systems have been used extensively to study parameters like peak pressure, mean pressure, peak force, the center of pressure, stance period or symmetry. Multiple studies have been conducted using these parameters to analyze: ankle instability [169], patellofemoral pain syndrome [21], anthropology [113], balance control [251], gout and the associated antalgic gait [229], neuropathic diabetic foot [16, 42, 123, 187], rheumatoid arthritis [149], obesity [109], injuries [214], surgeries [79], footwear [197], amputees [130], postmenopausal woman [167], pregnancy [127], among others [93].

To the authors' knowledge, only one study simulated heel motion from pressure plate measurements [102]. The heel motion was simulated as a rolling spherical rigid body and compared to the center of pressure available from measured plantar pressure data.

Musculoskeletal models that include foot-ground contact structures are already used to estimate plantar pressure from foot kinematics [5]. However, estimation of kinematics from plantar pressure is more challenging. Within this work, we propose and evaluate a musculoskeletal model-based algorithm to estimate ankle-foot kinematics based on plantar pressure data and the trajectories of a limited number of markers. This method has the potential of increasing the applicability of plantar pressure data to evaluate foot kinematics. Therefore the economic cost and the preparation time needed for evaluation of foot kinematics, currently typically done using camera-based systems, can be strongly reduced.

5.3 Methods

5.3.1 Marker set protocol and acquisition

Experimental data was collected in five healthy subjects (two males and three females, 53.8 ± 6.5 years, BMI: 23.0 ± 2.9) walking barefoot at self-selected speed (1.15 ± 0.13 m/s) over a 10 m walkway. Four stance phase trials per subject and foot were collected, resulting in a total of forty trials. Motion capture data was collected using ten infrared *Vicon* cameras (*Vicon*, Oxford Metrics, UK) that tracked the motion of a multi-segment foot models composed of sixteen skin-mounted markers (twelve positioned on each foot and four on the tibia, see Figure 5.4 and Table 5.2 at a sampling rate of 200 Hz [78]. Synchronized ground reaction forces (GRF) and plantar pressures were collected. Force data

were recorded at 1000 Hz using two *AMTI* force plates (Advanced Medical Technology, Watertown, Massachusetts) embedded in the walkway. Dynamic plantar pressure data were obtained using two *footscan®* pressure plates (*RScan* International, Paal, Belgium), each covering a measuring area of 488 mm by 325 mm. Each plate contained 4096 (64 x 64 sensors) individual pressure sensors of size 7.62 mm by 5.08 mm. The pressure plates' sampling frequency was set to 500 Hz. The study was approved by the local ethical committee of KU Leuven, and all participants provided written informed consent.

5.3.2 Foot musculoskeletal model

The extended *OpenSim* [71, 220] musculoskeletal lower leg model consisted of six rigid bodies: shank (tibia and fibula), talus, calcaneus, midfoot (cuboid, navicular and cuneiforms), forefoot (metatarsals) and toes, interconnected by eight degrees of freedom (DOF): ankle_{plantarflexion/dorsiflexion}, subtalar_{inversion/eversion}, midtarsal_{antero-posterior}, midtarsal_{oblique}, tarsometatarsal_{1st ray}, tarsometatarsal_{5th ray}, metatarsophalangeal_{plantarflexion/dorsiflexion} and metatarsophalangeal_{abduction/adduction}. Six additional DOFs described the position and orientation of the shank relative to the ground, see Figure 5.1, [156]. The model was scaled in *OpenSim* [71, 220] for each subject using a static trial.

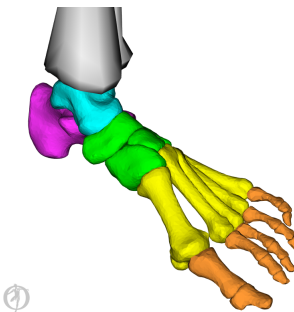


Figure 5.1: Musculoskeletal lower leg model (*OpenSim*). Depicted segments: Cyan – talus; Purple – calcaneus; Green – midfoot; Yellow – forefoot; Orange – toes.

5.3.3 Contact Model

Human-environment interaction is usually simulated using finite element modeling (FEM), Hertz theory and elastic foundation modeling (EFM) [221]. However, the use of FEM is limited to static or *quasi*-static situations due to the

large computational cost. The analytical method with Hertz theory is limited to simple geometries like spheres or cylinders. Alternatively, EFM assumes that the objects in contact are rigid bodies with only a thin layer of elastic material at the surfaces. A triangular mesh approximates the geometry of each surface. A spring-damper system is placed at the centroid of each triangle of the mesh. The normal force acting on each mesh element is a function of the indentation and indentation speed [120].

In order to simulate the dynamic plantar pressure using EFM, it is necessary to compute a foot plantar surface model that captures the variability within each subject's steps. An EFM anatomical-based contact model (*e.g.* using a 3D scan) would not be able to simulate the foot plantar surface adaptation of each step because EFM does not allow for deformation of the contact geometry. Computing a different EFM contact model for each step is crucial to represent the functional behaviour of the plantar surface of the foot. As no information on the geometry of the foot during dynamic loading was available, we assumed that the locations of high pressure corresponded to the most protruding parts of the foot sole. So, a contact model was computed for each individual trial and for each leg based on the plantar pressure distribution of each trial. These models were then added to the subject-specific scaled musculoskeletal model.

To create a trial-specific contact model, a 3D cloud of virtual points corresponding to each of the 64×64 pressure sensors (pp_{norm}) was defined based on the sum of the plantar pressure over the stance phase, normalized to the maximum value over all sensors:

$$\frac{\sum_{i=1}^{nT} \hat{pp}_i}{\max(\sum_{i=1}^{nT} \hat{pp}_i)} = pp_{norm} \quad (5.1)$$

with \hat{pp}_i the matrix (64×64) of measured plantar pressure at time step i and nT the number of time steps. The horizontal coordinates (x, y) of the virtual points were the position of the sensor and the, vertical coordinate (z) was a virtual distance obtained by multiplying pp_{norm} with a scaling factor ($s = 2$ cm) and dividing by the maximum of the summed normalized plantar pressure ($\max(pp_{norm})$). The scaling factor was selected based on a sensitivity analysis over all trials, based on: 1) a qualitative evaluation of the foot kinematics and 2) mean optimization function value over each trial (f) computed using the kinematics estimation method detailed in Section 5.3.4, for more information consult Appendix B. Points were only used for fitting if the summed force on the corresponding sensor was above 5 N ($\sum_{i=1}^{nT} \hat{pp}_i \cdot A_s > 5$ N), with A_s the area of the sensors.

Four different ellipsoids were fitted to the cloud of virtual points to model the contact of the different regions of the foot sole (calcaneus, midfoot, forefoot, and toes). These regions were delimited by a manually defined mask (guided by the *RSscan* automatic mask) [5] and a three-step approach was used, see Figure 5.2:

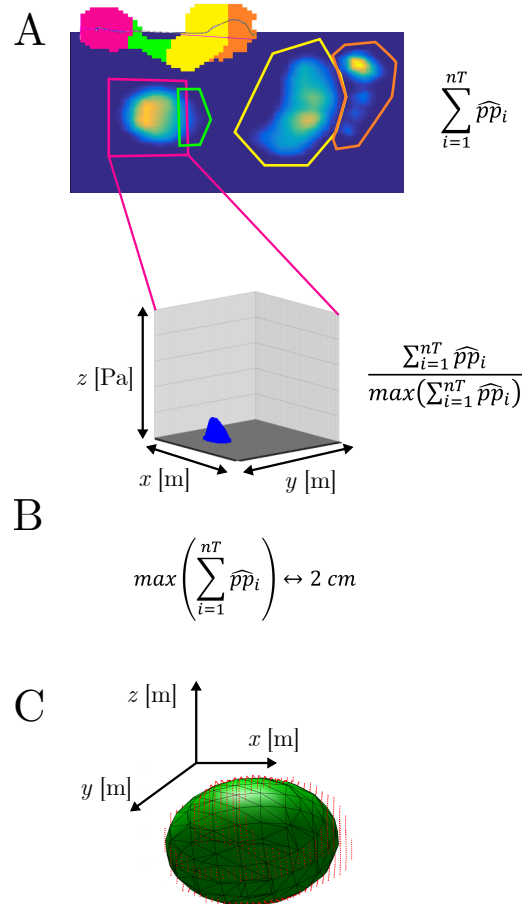


Figure 5.2: Ellipsoid contact geometry computation. Step A - Selection of different pressure areas (3D clouds of virtual points) and scaling of pressure; Step B – Conversion of scaled pressures to clouds of virtual points; Step C – Ellipsoid fit: Least squares optimization.

First, a linear least-squares algorithm [194] was used to fit the ellipsoids according to a ten-parameter ($A, B, C, D, E, F, G, H, I, J$) conic algebraic equation:

$$Ax^2 + By^2 + Cz^2 + 2Dxy + 2Exz + 2Fyz + 2Gx + 2Hy + 2Iz + J = 1 \quad (5.2)$$

Next, the position of the ellipsoids relative the foot segments and relative to the ground surface was estimated. The fitted ellipsoids (four in total, one for each contact region, see example in Figure 5.3 and Figure 5.2) were initially positioned on the foot using an empirical anatomical approach, *i.e.* at the center of the calcaneus, center of the midfoot, head of the third metatarsal and center of the hallux. The ellipsoids centre position and the vertical position of the ground surface relative to the musculoskeletal model were then optimized by minimizing the difference between the computed (using the EFM contact model described above) and the measured sum of the plantar pressure over the stance phase, normalized to the maximum value over all sensors (Equation 5.6). The positioning optimization was solved using the *fmincon* function with the *Interior-Point* algorithm, *Matlab* and *Optimization Toolbox R2015b* (The MathWorks, Inc., Natick, Massachusetts, United States).

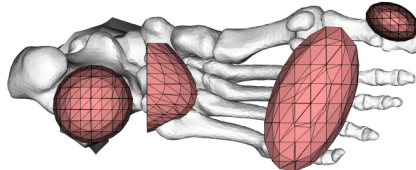


Figure 5.3: Example of the foot model with the optimized location of the ellipsoid contact geometries.

5.3.4 Estimation of kinematics

The optimal foot kinematics for each time step (i) was computed using an algorithm that minimized the weighted difference between measured and simulated marker positions and plantar pressure, using a *Matlab-OpenSim* interface:

$$f_i = w_P \cdot f_{pp_i} + w_M \cdot f_{M_i} \quad (5.3)$$

The kinematics (q_i) was input to compute the plantar pressure and the virtual marker positions. Where, f_{pp_i} was the pressure error computed as the sum

of the squared difference of the simulated (\hat{pp}_i) and measured pressures (\hat{pp}_i) normalized to the maximum pressure of that time step.

$$f_{pp_i} = \sum \left\| \frac{\hat{pp}_i}{\max(\hat{pp}_i)} - \frac{pp_i(q_i)}{\max(pp_i(q_i))} \right\| \quad (5.4)$$

f_{M_i} was the marker error computed as the sum of the scaled squared distance between the virtual (M_i) and measured marker (\hat{M}_i) positions over all markers. The marker error was scaled (s_M) such that the pressure and marker errors had the same order of magnitude.

$$f_{M_i} = \sum s_M \cdot \left\| \hat{M}_i - M_i(q_i) \right\| \quad (5.5)$$

w_P and w_M were respectively the pressure error and the markers error weight. The optimization was solved using the *fmincon* function with the *Interior-Point* algorithm, *Matlab* and *Optimization Toolbox R2015b* (The MathWorks, Inc., Natick, Massachusetts, United States). The optimized kinematics for one-time step were used as an initial guess for the next time step. The kinematics for the first time step were computed with the Inverse Kinematics analysis of *OpenSim* [71, 220] using the full marker set [156].

5.3.5 Validation

A two-step approach was used to test the application of plantar pressure distribution to estimate kinematics. First, we evaluated the influence of using plantar pressure along with the EFM on the estimated kinematics to evaluate the influence of the contact model on the kinematics estimation. The kinematics computed using the multibody model-based algorithm coupled with plantar pressure data and the trajectories of the full markers set [78] (All Markers + Pressure – AMP, $w_P = 60\%$ and $w_M = 40\%$) were compared with the kinematics computed using the same algorithm but with the pressure weight set to zero (Markers Optimization – MO, $w_P = 0\%$ and $w_M = 100\%$), see Table 5.1 and Figure 5.4. This approach is identical to using the Inverse Kinematics Tool in *OpenSim* [71, 220]. Mean absolute kinematics difference over the stance phase (*meanabsdiff*), the peak absolute kinematics difference (*peakabsdiff*) and the total percentage of stance phase, in which the AMP was within the standard deviation (*withinstd*) of the MO were evaluated.

Differences in kinematics between different approaches were considered relevant if $withinstd \geq 75\%$, $meanabsdiff \leq 3^\circ$ and $peakabsdiff \leq 5^\circ$. This cut off value of *meanabsdiff*, and the *peakabsdiff* values were chosen based on the

reported difference in kinematics between a full skin markers set-up and bone pins (from 1.9° to 5.1°) [152], while the cut off value of $withinstd$ was based on empirical evaluation of the data sets.

Second, we evaluated if the marker set could be simplified by quantifying the effect of reducing the number of markers on the plantar pressure-based kinematics estimation. To this end, the kinematics computed using the *AMP* was compared to the kinematics computed using the same approach but by varying the tracked markers (see Table 5.1 and Figure 5.2) and weight distribution (w_P and w_M) in the cost function. A sensitivity analysis was performed to determine the best weight distribution for each marker combination, in one representative trial.

The different makers combinations were chosen due to their simplicity and inspired by the *PiG* set-up [249]. A widely accepted marker set-up for a simple full-body kinematics estimation due to its time-saving assembly. All the markers combinations used consisted of four tibia markers (lateral epicondyle knee marker, an upper posterior marker of the tibia cluster, a lower anterior marker of the tibia cluster and a lower posterior marker of the tibia cluster) and the following foot markers (Figure 5.4):

- *Plug in Gait (PiG)* [249] - lateral malleoli marker, upper posterior marker of the calcaneus cluster and caput metatarsal II marker ($w_P = 80\%$ and $w_M = 20\%$);
- *PiG extended (PiGe)* - lateral malleoli marker, an upper posterior marker of the calcaneus cluster, caput metatarsal II marker and distal phalanx I marker ($w_P = 80\%$ and $w_M = 20\%$);
- *2 Markers (2M)* - an upper posterior marker of the calcaneus cluster and distal phalanx I marker ($w_P = 70\%$ and $w_M = 30\%$);
- *1 Marker (1M)* - caput metatarsal II marker ($w_P = 80\%$ and $w_M = 20\%$).

Differences in kinematics between the different marker combinations and the *AMP* were considered relevant if $withinstd \geq 75\%$, $meanabsdiff \leq 3^\circ$ and $peakabsdiff \leq 5^\circ$. Despite only tracking the markers mentioned above, the entire marker set was still present in the model. Allowing to compare the distances between all the measured and the correspondent virtual markers in each model. The mean distance between the measured and simulated marker (ϵ_{marker} , see Equation 5.6) computed for each one separately and the mean plantar pressure error (f_{pp} , see Equation 5.7), are used as an extra outcome variable to evaluate the different markers combinations.

$$\epsilon_{marker} = \frac{\sum_{nS} \frac{\sum_{nR} \frac{\sum_{nT} d_{marker_{i,r,s}}}{n_T}}{n_R}}{n_S} \quad (5.6)$$

$$f_{pp} = \frac{\sum_{nS} \frac{\sum_{nR} \frac{\sum_{nT} f_{pp_{i,r,s}}}{n_T}}{n_R}}{n_S} \quad (5.7)$$

Where r is the trial, nR is the number of trials, s is the subjects, nS is the number of subjects, d_{marker_i} is the distance between measured and the simulated marker and f_{pp_i} is already described in Section 5.3.4. The overall mean markers' distance ($\sum \epsilon_{marker}/nM$, where nM is the number of markers) was computed excluding the CMTI marker given the high distances obtained for this marker in all the approaches, most likely due to modeling simplification.

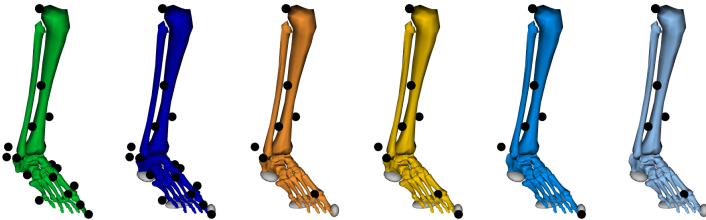


Figure 5.4: Musculoskeletal model with the different markers combinations used to quantify: 1) the influence of pressure as an input for the kinematics estimation and 2) the influence of the number of markers on the plantar pressure-based kinematics estimation. Green: Markers Optimization (MO) - Entire marker set (Table 5.2) without contact geometries ($w_P = 0\%$ and $w_M = 100\%$); Dark Blue: All Markers + Pressure (AMP) - Entire marker set with contact geometries ($w_P = 60\%$ and $w_M = 40\%$); Orange: PiG - PiG marker set with contact geometries ($w_P = 80\%$ and $w_M = 20\%$); Yellow: PiG extended (PiGe) - PiG marker set plus one marker in the hallux with contact geometries ($w_P = 80\%$ and $w_M = 20\%$); Blue: 2 Markers (2M) – One marker in the calcaneus and in the hallux with contact geometries ($w_P = 70\%$ and $w_M = 30\%$); Light Blue: 1 Marker (1M) – One marker in the head of the second metatarsal with contact geometries ($w_P = 80\%$ and $w_M = 20\%$). All the reduced combinations maintain four markers in the tibia.

5.4 Results

The inclusion of pressure in the kinematics estimation (*AMP*) presented a noteworthy decrease in the mean pressure error (*MO* $f_{pp} = 22.78$, *AMP* $f_{pp} = 12.29$, Table 5.1), while inducing a slight increase in mean distance between the measured and the virtual markers position (*MO* 3.98 mm, *AMP* 7.76 mm, Table 5.2). Compared to the standard approach (*MO*), the inclusion of plantar pressure data in the kinematics estimation (*AMP*) presented similar ($withinstd \geq 75\%$, $meanabsdiff \leq 3^\circ$ and $peakabsdiff \leq 5^\circ$) kinematics, for most of the degrees of freedom with the exception of the midtarsal_{oblique} and metatarsophalangeal_{abduction/adduction} degrees of freedom ($withinstd < 75\%$, $meanabsdiff > 3^\circ$ and $peakabsdiff > 5^\circ$), see Figure 5.5 and Figure 5.7, and Table 5.1.

All the different combinations of markers (*PiG*, *PiGe*, *2M*, and *1M*) presented good estimates for the ankle, subtalar and tarsometatarsal_{5th ray} kinematics ($withinstd \geq 75\%$, $meanabsdiff \leq 3^\circ$ and $peakabsdiff \leq 5^\circ$), see Figure 5.6 and Table 5.1.

A good kinematics estimation for the midtarsal_{antero/posterior} motion required the combination of the contact geometries with at least one marker in the forefoot (*PiG*, *PiGe* and *1M*). The only markers combination (*2M*) without forefoot markers showed a noticeable deviation from the *AMP*, see Figure 5.6 and Table 5.1.

For accurate kinematics estimation of the tarsometatarsal_{1st ray} ray the use of both the forefoot contact geometry with one marker in the distal part of the forefoot and one in the calcaneus (*PiG* and *PiGe*), proved to be the most similar to the standard marker approach (*AMP*), see Figure 5.6 and Table 5.1.

The metatarsophalangeal_{plantarflexion/dorsiflexion} kinematics estimation required a marker in the toes (*PiGe*) in order to be comparable to the *AMP* solution. Despite the totaled deviation presented by the *2M*, this approach showed a similar motion pattern for most of the stance phase, see Figure 5.6 and Table 5.1.

The *PiGe* was the only approach that showed similar kinematics to all the degrees of freedom, see Figure 5.6 and 5.8 and Table 5.1.

The distances between each model virtual markers and the measured markers were in general small (< 1.5 cm) for all the markers combinations (*PiG* 1.08 cm, *PiGe* 0.91 cm, *2M* 0.68 cm, *1M* 1.48 cm), see Table 5.2. Furthermore, all the approaches presented a similar mean pressure errors to the *AMP* (*PiG* $f_{pp} = 11.19$, *PiGe* $f_{pp} = 11.29$, *2M* $f_{pp} = 15.9$, *1M* $f_{pp} = 13.01$, see Table 5.1).

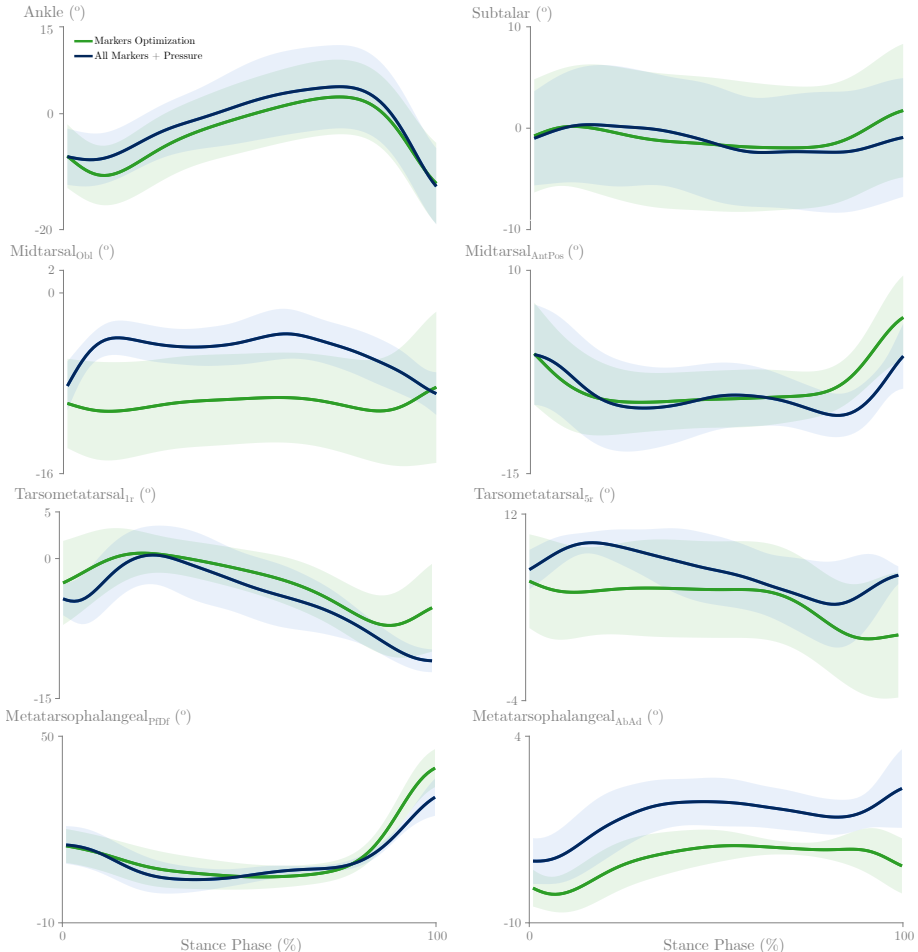


Figure 5.5: Kinematics results for the 8 DOF. Green: *MO* – Mean kinematics computed with the entire marker set without contact geometries ($w_P = 0\%$ and $w_M = 100\%$) with standard deviation; Dark Blue: *AMP* – Mean kinematics computed with the entire marker set with contact geometries ($w_P = 60\%$ and $w_M = 40\%$) with standard deviation. Full line – Mean of the five subjects, four trials and both feet (40 different trials).

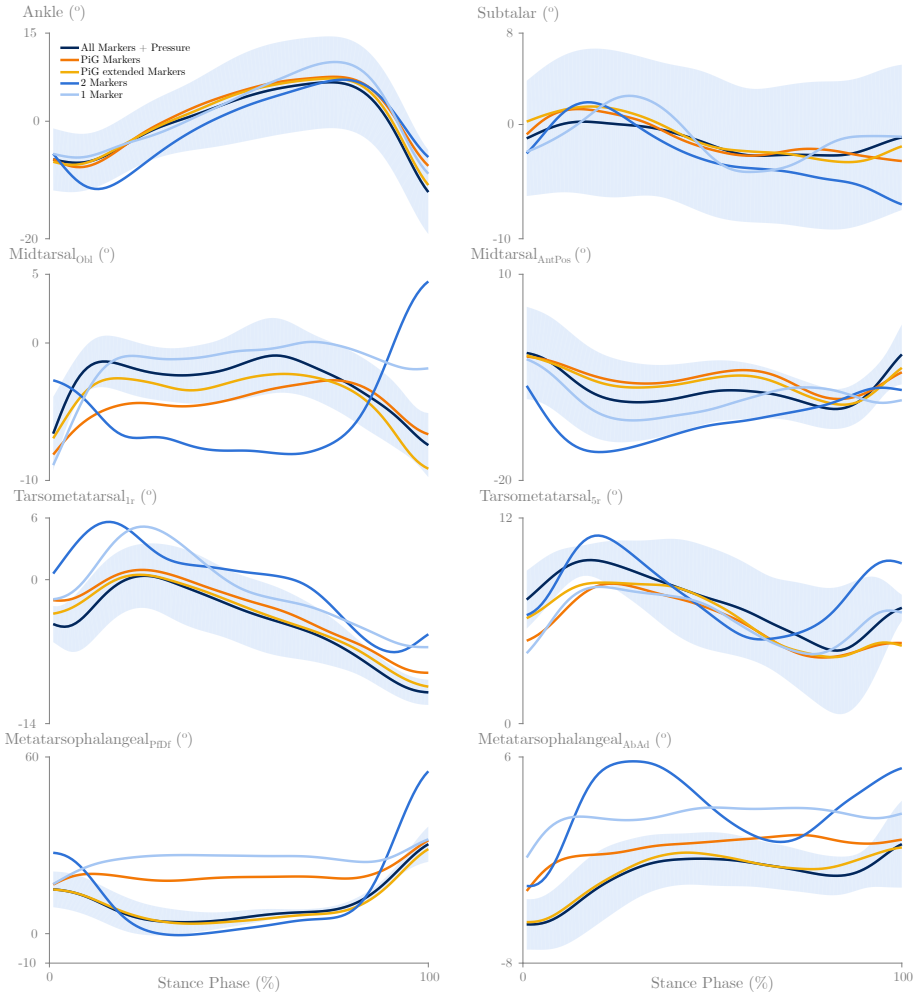


Figure 5.6: Kinematics results for the 8 DOF. Dark Blue: AMP – Mean kinematics computed with the entire marker set with contact geometries ($w_P = 60\%$ and $w_M = 40\%$) with standard deviation; Orange: PiG – Mean kinematics computed with the PiG marker set with contact geometries ($w_P = 60\%$ and $w_M = 40\%$); Yellow: PiGe - Mean kinematics computed with the PiG marker set plus one marker in the hallux with contact geometries ($w_P = 80\%$ and $w_M = 20\%$); Blue: 2M – Mean kinematics computed with one marker in the calcaneus and in the hallux with contact geometries ($w_P = 70\%$ and $w_M = 30\%$); Light Blue: 1M – Mean kinematics computed with one marker in the head of the second metatarsal with contact geometries ($w_P = 80\%$ and $w_M = 20\%$). All the reduced combinations maintain four markers in the tibia. Full line – Mean of the five subjects, four trials and both feet (40 different trials).

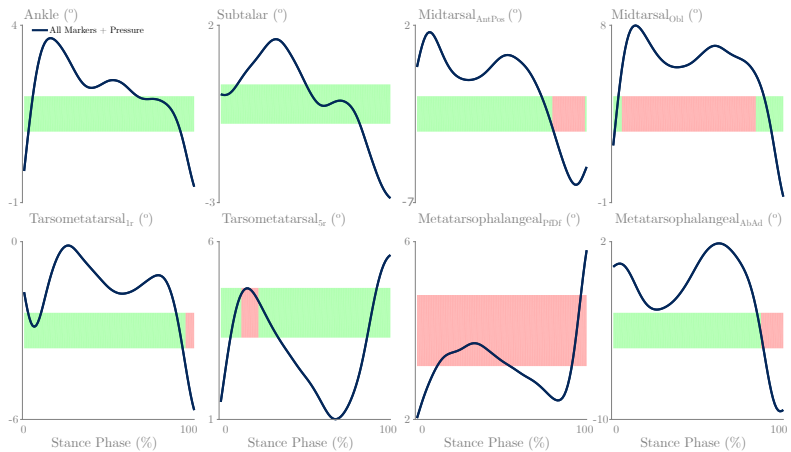


Figure 5.7: Dark Blue line – Kinematics differences between the means of the *MO* and the *AMP* approaches for the 8 DOF. Green Bar – The mean kinematics of the *AMP* approach is within the standard deviation of the *MO* approach. Red Bar – The mean kinematics of the *AMP* is not within the standard deviation of the *MO* approach.

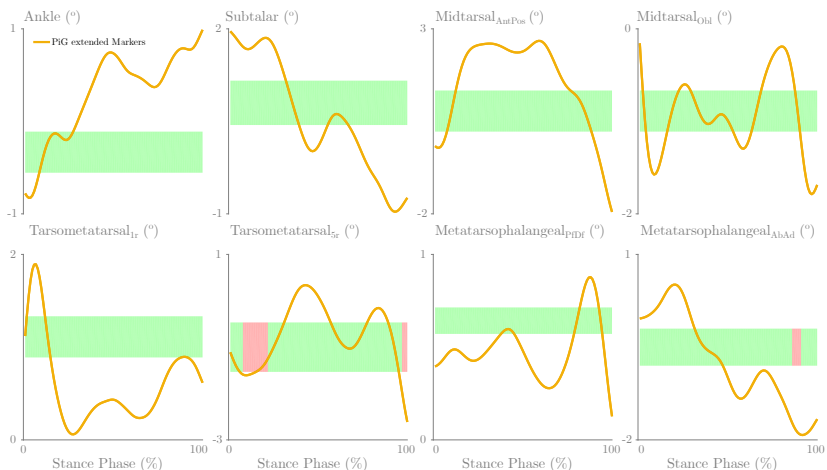


Figure 5.8: Yellow line - Kinematics differences between the means of the *AMP* and the *PiGe* approaches for the 8 DOF. Green bar – If the mean kinematics of the *PiGe* approach is within the standard deviation of the *AMP* approach. Red bar – If the mean kinematics of the *PiGe* approach is not within the standard deviation of the *AMP* approach.

Table 5.1: Absolute mean and peak kinematics differences, and percentage of within standard deviation between the kinematics means of 1) *MO vs. AMP*; 2) *AMP vs. PiG*; 3) *AMP vs. PiGe*; 4) *AMP vs. 2M*; 5) *AMP vs. 1M*. For all 8 DOF.

		<i>MO</i>	<i>AMP</i>	<i>PiG</i>	<i>PiGe</i>	<i>2M</i>	<i>1M</i>
Ankle	Within std (%)	.	100	100	100	86	100
	Mean abs diff (°)	.	2.14	1.02	0.56	1.24	1.29
	Peak abs diff (°)	.	3.64	4.46	1.19	5.96	3.55
Subtalar	Within std (%)	.	100	100	100	100	100
	Mean abs diff (°)	.	0.29	0.15	0.29	1.17	0.23
	Peak abs diff (°)	.	1.15	1.15	1.47	1.71	2.58
Midtarsal _{antero-posterior}	Within std (%)	.	81	100	100	40	94
	Mean abs diff (°)	.	1.2	1.75	1.17	4.37	1.29
	Peak abs diff (°)	.	1.65	3.04	2.21	1.48	2.8
Midtarsal _{oblique}	Within std (%)	.	22	58	100	13	69
	Mean abs diff (°)	.	5.78	1.67	1.05	2.79	1.26
	Peak abs diff (°)	.	7.99	0.79	0.34	11.91	5.59
Tarsometatarsal _{1st ray}	Within std (%)	.	96	80	100	23	36
	Mean abs diff (°)	.	1.66	1.24	0.54	4.06	3.29
	Peak abs diff (°)	.	0.13	2.58	1.7	7.96	4.79
Tarsometatarsal _{5th ray}	Within std (%)	.	90	75	83	81	76
	Mean abs diff (°)	.	2.5	1.15	0.81	0.57	0.89
	Peak abs diff (°)	.	5.12	0.32	0	3.62	0.79
Metatarsophalangeal _{abduction/adduction}	Within std (%)	.	0	51	100	0	4
	Mean abs diff (°)	.	3.24	1.9	0.28	4.57	4.02
	Peak abs diff (°)	.	5.81	3.77	0.83	7.81	6.46
Metatarsophalangeal _{plantarflexion/dorsiflexion}	Within std (%)	.	87	14	95	26	10
	Mean abs diff (°)	.	1.46	10.17	0.73	1.52	15.74
	Peak abs diff (°)	.	1.88	14.63	0.51	24.76	22.8
Cost Function Mean Marker Error (f_M)		18.9	14.97	25.05	25.3	17.34	17.25
Cost Function Mean Pressure Error (f_{pp})		22.78	12.29	11.19	11.29	15.9	13.01
Mean cost function (f)		18.9	12.52	13.96	14.09	16.34	13.86

Table 5.2: Mean distance between the position of the measured markers and the position of the virtual marker computed using the different modeling approaches: 1) *MO*; 2) *AMP*; 3) *PiG*; 4) *PiGe*; 5) *2M*; 6) *1M*. (*) – Tracked Marker. (#) – The means were computed excluding the CMTI marker. The high distances verified for this marker in all the approaches are probably related to a modeling error.

Markers	Marker Anatomical Position	<i>MO</i> (mm)	<i>AMP</i> (mm)	<i>PiG</i> (mm)	<i>PiGe</i>	<i>2M</i> (mm)	<i>1M</i> (mm)
EPILB	Lateral epicondyle Knee	8.61*	14.24*	15.74*	16.21*	11.86*	20.66*
CrDOB	Upper posterior marker of the Tibia cluster	2.89*	5.56*	8.01*	7.35*	1.61*	8.50*
CaVOB	Lower anterior marker of the Tibia cluster	4.41*	6.22*	8.14*	7.43*	2.74*	11.42*
CaDOB	Lower posterior of the Tibia cluster	2.68*	4.97*	6.58*	6.19*	2.42*	9.24*
LM	ILateral Malleoli	2.44*	4.85*	6.45*	6.22*	6.08	14.7
CCrD	Upper posterior marker of the Calcaneus cluster	2.48*	6.13*	8.81*	8.26*	1.59*	20.82
CCaD	Lower posterior marker of the Calcaneus cluster	3.60*	7.15*	9.79	9.34	3.41	20.61
Cu	Cuboid	3.08*	10.61*	10.93	11.57	9.96	16.09
Na	Navicular	4.75*	8.50*	8.96	9.12	9.49	14.44
CM	Medial Cuneiform	4.92*	8.75*	8.96	9.24	9.2	13.34
BMTII	Basis Metatarsal II	3.68*	8.06*	8.85	9.16	8.67	10.58
CMTII	Caput Metatarsal II	4.72*	5.92*	8.79*	7.62*	10.24	1.27*
CMTI	Caput Metatarsal I	34.61*	38.90*	38.89	39.92	44.03	38.41
CMTV	Caput Metatarsal V	4.42*	13.72*	13.81	14.43	16.63	17.95
LDFI	Lateral Phalanx I	4.10*	6.48*	16.36	7.56	1.19	17.05
DFI	Distal Phalanx I	2.93*	5.23*	21.43	6.58*	7.36*	25.87
	Mean	3.98#	7.76#	10.77#	9.09#	6.83#	14.84#

For more detailed figures comparing the kinematics of the different approaches for each subject individually see Appendix C.

5.5 Discussion

We presented an optimization method to compute ankle-foot kinematics based on plantar pressure and a limited set of markers using a least-squares optimization approach. Marker positions and plantar pressure were simulated in *OpenSim* [71, 220] using an extended musculoskeletal shank and foot model coupled with an elastic foundation contact model (EFM).

Adding plantar pressure data to the trajectories of a full marker set had a limited effect on the estimation of ankle-foot kinematics. The kinematics computed using the multibody model-based algorithm coupled with plantar pressure data (*AMP*) and the trajectories of the full markers set (*MO*) presented similar kinematics results. Though, there was a slight increase in the distances between the measured and the virtual markers for the *AMP* approach. These distances

are, however, well within *OpenSim*'s [71, 220] recommended range (maximum marker error should generally be less than 2-4 cm).

The increased markers distances (Table 5.2) is possibly related to contact modeling errors. The optimization algorithm minimized the difference between the measured pressure and simulated pressure, computed using a contact model that was not a perfect representation of the plantar surface of the foot. Consequently, there was a difference (error) between simulated and measured pressure, so the kinematics solution of *MO* and *AMP* had to be necessarily different. Nevertheless, the inclusion of plantar pressure provided extra valuable information to the kinematics estimation. Modeling the interaction of the foot with the ground led to a better simulation of plantar pressure, shown by a smaller mean pressure error (f_{pp}) in the *AMP* approach compared to the *MO*.

The reduction of the number of markers showed that a minimum of four-foot markers is needed when using pressure data to estimate kinematics comparable to the full marker approach with pressure (*AMP*) for all the degrees of freedom. The presented algorithm was tested with different markers combinations and compared against the *AMP* approach to evaluate the influence of the number of markers on the different degrees of freedom. The ankle, subtalar and tarsometatarsal_{5th} ray motions were well-defined in the optimization problem with both the contact geometries underneath the associated segments (calcaneus and forefoot) as with the number of markers coupled with its movement for all the approaches.

The difficulty of estimating the midtarsal_{antero/posterior} motion with a reduced marker can be explained by the lack of contact between the midfoot and the ground because of the foot curvature. Since there is no pressure and marker data information for the midfoot, its position is estimated indirectly through the position and orientation of the neighboring segments, which already have an associated uncertainty.

A reliable estimation of tarsometatarsal_{1st} ray motion required the combination of the forefoot contact geometry with one marker in the forefoot and one in the calcaneus (*PiG* and *PiGe*). If there is only plantar pressure information in the forefoot region (*2M*), or even if the forefoot marker is present (*1M*), there is not enough information to solve the redundant kinematics for all the foot joints during the initial contact phase (0-16% of stance phase). So, the calcaneus marker is essential to solve the kinematics redundancy.

A good kinematics estimation of the metatarsophalangeal_{plantarflexion/dorsiflexion} kinematics required the use of a marker in the toes (*PiGe*). Its absence (*PiG* and *1M*) together with the lack of pressure information underneath the toes until the heel off phase of the gait cycle (80-100% of stance phase) cannot

provide enough information to solve the optimization gradient problem. So, the toes will be kept in a relatively constant position until the heel off phase, where the pressure will provide the required input. The *2M* approach also showed a noticeable deviation, however Figure 5.6 shows a similar motion pattern for this marker combination compared to the *AMP*. The difference can be justified by a small standard deviation and a high range of motion for this degree of freedom present in the *AMP*.

The markers distance for the different markers combinations despite being larger than the *AMP* approach are, as well, within *OpenSim*'s [71, 220] recommended range (maximum marker error should generally be less than 2-4 cm). Therefore, the reduction of the number of tracked markers in the plantar pressure-based estimation of foot kinematics has a minor influence in the global virtual markers position.

In summary, the *PiGe* approach was the only approach that did not present a significant difference from the *AMP* approach. Therefore, a reduction from twelve-foot markers to four, using the plantar pressure-based estimation of foot kinematics presents acceptable kinematics for most of the foot degrees of freedom. The ability to estimate foot kinematics with a reduced set-up is an excellent development for clinical evaluation of foot kinematics.

A limitation to this approach is that it still requires some marker information. Without markers information, the gradient-based optimization approach does not converge due to the lack of gradient information when the foot is not in contact with the ground, and the simulated plantar pressures are zero. Moreover, the kinematics used for the first-time step was computed using the full marker set, other approaches could have been implemented like the kinematics mean of a representative group for that instance of time (initial contact).

Also, plantar pressure does not uniquely define foot kinematics, so a kinematics estimation algorithm exclusively based on plantar pressure would be infeasible and inaccurate. Moreover, to accurately simulate plantar pressure, a reliable representation of the feet plantar surface is needed, so the contact geometries shapes should be physiological as similar as possible to the feet sole. In this study, a combination of four ellipsoids, based on the dynamic evolution of plantar pressure, was used to represent the feet sole. These contact geometries do not hold the ground truth; other contact formulations could be used to maximize the accuracy of plantar pressure simulation, like statistical shape models or 3D scanners for unloaded foot shape.

For the described algorithm the stiffness and damping values of each element are not relevant since we are only comparing normalized pressure distributions and all the elements have the same stiffness and damping.

As a final remark, only five subjects were used to test the methodology. The variability in the *MO* approach is large and this is a confounding factor that complicates the statistical comparison. For this reason, we decided to perform a more qualitative analysis. In the future, a power analysis based on this study should be considered to further validate this method.

5.6 Conclusion

The presented optimization algorithm allows the estimation of foot kinematics based on plantar pressure information and the coordinates of a limited set of markers. The set-up simplicity has significant research and clinical implications on both the preparation time of 3D motion capture of foot kinematics as well as on its assessment and evaluation. It will allow a more accurate and objective clinical interpretation of foot pathologies.

In the future inertial measurement units (IMUs) in combination with 3D scanning information will be tested and validated to verify the possibility of using this data together with plantar pressure data to provide foot and ankle kinematics to further simplify the acquisition set-up.

5.7 Acknowledgements

This work was funded by the Berghmans - Dereymaeker research chair on Foot and Ankle Biomechanics and the Aladyn Project (IWT, Flanders).

Authors' Contributions

Tiago de Melo Malaquias focused on the development of the pressure based optimization algorithm, and writing.

Wouter Aerts helped in the development of the pressure based optimization algorithm.

Ilse Jonkers supervised the research and revised the manuscript.

Jos Vander Sloten supervised the research and revised the manuscript.

Friedl De Groote supervised the research and revised the manuscript.

The experimental data was available from the work of Fien Burg [39] performed in the Movements & posture Analysis Laboratory Leuven.

Chapter 6

Predictive simulations of the corrective effect of controlled stiffness 3D-printed insoles during the stance phase of gait

Tiago de Melo Malaquias^a, Friedl De Groote^b, Wouter Aerts^a, Ilse Jonkers^b, Jos Vander Sloten^a

^a Biomechanics Section, Mechanical Engineering Department, KU Leuven, Leuven, Belgium

^b Human Movement Biomechanics Research Group, Department of Movement Sciences, KU Leuven, Belgium

6.1 Abstract

With the introduction of 3D-printing came the ability to manufacture insoles with mechanical properties that are tailored to specific subjects in a time efficient manner. However, our understanding of how mechanical insole properties influence the dynamic behavior of the foot during movement is limited. This study, therefore, aims to develop a torque driven forward simulation framework to evaluate the effect of insole properties on the kinematics of an extended musculoskeletal multibody foot model. With this framework the authors want to evaluate the effect of different insole stiffnesses on foot kinematics during walking, specifically on the ankle and subtalar (tibia-calcaneus), midtarsal (calcaneus-midfoot) and tarsometatarsal (midfoot-forefoot) joints.

The torque driven forward simulations were computed in *OpenSim* using a musculoskeletal shank and foot model with six segments (shank, talus, calcaneus, midfoot, forefoot, and toes), fourteen degrees of freedom, and thirty-six ligaments. The model was coupled with an elastic foundation foot-ground contact model. The insoles were modeled using bushing forces connecting the calcaneus to the forefoot. We computed reference kinematics and joint torques by tracking marker trajectories and pressure data measured during barefoot walking of four healthy individuals. The reference torques and kinematics were then used to guide forward simulation to study the effect of different insole stiffness profiles on walking kinematics. We evaluated (A) bending stiffnesses (around the mediolateral axis) between 10 – 90 Nm/rad; (B) torsional stiffnesses (around the anteroposterior axis) between 1 - 6 Nm/rad; and (C) a combination of (A) and (B).

The results showed that increased bending stiffness, mostly independent from torsional stiffness, led to increased midfoot dorsiflexion and forefoot dorsiflexion and adduction. The increase in forefoot adduction is a kinematic adaptation needed to partially correct flat feet deformity, as seen in a previous *in-vivo* study using arch supportive semi-rigid 3D-printed insoles.

The proposed framework was able to exhaustively estimate foot kinematics under the effect of 69 different combinations of directional flat insoles stiffness. This work is a step towards establishing a scientific-based approach for the construction of optimal orthoses in therapeutic shoe design.

6.2 Introduction

Foot orthoses (FOs) or insoles are used to reduce sports injuries, provide comfort or to relieve symptoms in the presence of pathologies. Custom FOs are mostly prescribed for individuals with flat feet or *pes planus*, which affects up to 23% of the adult population, to correct excessive rearfoot pronation and medial longitudinal arch collapse [19, 98]. Nowadays, insoles are typically designed using static measurements of the foot, thereby neglecting that most foot related mechanical problems are of a dynamic nature [25, 122, 148, 171, 201, 236, 237, 268]. Furthermore, the conventional process of insole design and manufacturing relies on subjective decisions and time-consuming handicraft work and is often limited to capturing the foot shape using traditional techniques such as plaster casting. This leads to subjectivity in the prescription of insoles and restricts the design to simple parameters such as cushioning and support [182].

Newly developed 3D-printed insoles have the potential to allow a more efficient and objective production of subject-specific insoles by enabling the definition of topological variation in structural and material design factors (*i.e.* arch support, thickness, and stiffness). However, the flexibility with which these can be combined has further increased the need for guidelines that inform foot healthcare professionals about the effect of the insole on foot kinematics and kinetics [54, 59].

Models of the musculoskeletal structures, *i.e.* finite element (FE) or multibody, have the potential to evaluate how different biomechanical parameters (*i.e.* plantar pressure, joint stress, kinematics, and kinetics) are altered under the influence of insoles with different mechanical properties [67, 100].

Musculoskeletal multibody simulations have great potential to complement *in-vivo* gait analysis, since experimental data alone cannot measure important variables, such as joint moments or muscle forces. Currently, complex musculoskeletal multibody models of the foot are being integrated in dynamic simulations of movement [38, 156]. This methodology can bring new insights into the manufacturing of scientific-based subject specific insoles. Forward simulations can compute the kinematics solution given the controls, *i.e.* muscle excitations or joint actuators, by solving the differential equations that define the dynamics of a musculoskeletal or skeletal model [71].

We aim to develop a torque driven forward simulation framework to evaluate the effect of insole properties on the kinematics of an extended musculoskeletal multibody foot model. With this framework, we want to evaluate the effect of different insole stiffnesses on foot kinematics during walking, specifically on the ankle and subtalar (tibia-calcaneus), midtarsal (calcaneus-midfoot) and tarsometatarsal (midfoot-forefoot) joints [19, 74]. We assume that insoles

introduce the same changes in kinematics in healthy and flat feet individuals. So, in order to correct flat feet, insoles must increase forefoot adduction and decrease excessive forefoot dorsiflexion as described previously in a gait analysis study using arch supportive semi-rigid 3D-printed insoles (Chapter 4).

6.3 Methods

Figure 6.1 gives a schematic representation of the framework to simulate ankle-foot kinematics under the effect of different insole stiffness that is described in detail in the following sections.

6.3.1 Marker set protocol and acquisition

Experimental data were collected in four healthy subjects (one male and three females, 56.5 ± 4.0 years, BMI: 22.1 ± 2.5) walking barefoot at self-selected speed (1.11 ± 0.12 m/s) over a 10 m walkway. One static trial per subject and four stance phase trials per subject and foot were collected, resulting in a total of thirty-two trials. Motion capture data was collected using ten infrared Vicon cameras (Vicon, Oxford Metrics, UK) to track the motion of sixty-five skin-mounted markers (twelve positioned on each foot) at a sampling rate of 200 Hz [78]. Force data was recorded at 1000 Hz using two AMTI force plates (Advanced Medical Technology, Watertown, Massachusetts) embedded in the walkway. Dynamic plantar pressure data was obtained using two *footscan*® pressure plates (RSscan International Belgium), each covering a measuring area of 488 mm by 325 mm. Each plate contained 4096 (64 by 64 sensors) individual pressure sensors of 7.62 mm by 5.08 mm. The pressure plates' sampling frequency was set at 500 Hz. The study was approved by the local ethical committee of KU Leuven, and all participants provided written informed consent.

6.3.2 Insoles mechanical testing

To determine the range of bending and torsional stiffness characteristics of 3D-printed insoles from *Phits* (RS Print, Paal, Belgium powered by Materialise NV, Leuven, Belgium), three-point bending, and torsional tests were performed on an Instron Electropuls™ E10000 testing machine in TECHSPERT BVBA, Ghent University Spin-off — Mechanics of Materials and Structures Research Group. A total of eighteen insoles were tested (both for torsional and bending tests), consisting of six different 3D-printing insoles design with three samples

per design. The stiffness of each sample was calculated based on the slope of the experimental force-displacement curve. The obtained stiffness was averaged over the three samples available for each design. Bending stiffness values of the 3D-printed insoles ranged from 10 to 90 Nm/rad and torsional stiffness ranged from 1 to 6 Nm/rad.

6.3.3 Foot musculoskeletal model

The extended *OpenSim* [71, 220] musculoskeletal lower leg model consisted of six rigid bodies: shank (tibia and fibula), talus, calcaneus, midfoot (cuboid, navicular and cuneiforms), forefoot (metatarsals) and toes, interconnected by eight degrees of freedom (DOF): ankle_{plantarflexion/dorsiflexion}, subtalar_{inversion/eversion}, midtarsal_{antero-posterior}, midtarsal_{oblique}, tarsometatarsal_{1st} ray, tarsometatarsal_{5th} ray, metatarsophalangeal_{plantarflexion/dorsiflexion} and metatarsophalangeal_{abduction/adduction}. Six additional DOFs describe the position and orientation of the shank with respect to the ground, see Figure 6.1 [156]. The model was scaled in *OpenSim* [71, 220] for each subject using a static measurement.

6.3.4 Ligaments

Thirty-six-foot ligaments were implemented in the model according to Malaquias *et al.* (2016) [156]. A frequently used ligaments' strain-stress curve was applied [32, 29, 30, 257]

$$f = \begin{cases} \frac{k\varepsilon^2}{4\varepsilon_l} & 0 \leq \varepsilon \leq 2\varepsilon_l \\ k(\varepsilon - \varepsilon_p) & \varepsilon_p > \varepsilon > 2\varepsilon_l \\ k\varepsilon_p & \varepsilon \geq \varepsilon_p \\ 0 & \varepsilon < 0 \end{cases} \quad (6.1)$$

Generic parameters were defined based on literature: The initial strain (ε_l) was assumed to be 0.03 for all ligaments [30, 223]. The yield strain ($\varepsilon_p = 0.16$) was the mean of the *in-vivo* data reported by Siegler *et al.* (1988) [223]. k is the ligament stiffness computed by fitting C. Mkandawire *et al.* (2005) [165] foot ligament data using non-linear regression ($R^2 = 0.73$):

$$p_1 \cdot \left(\frac{a}{L_0} \right) + p_2 \quad (6.2)$$

$$p_1 = 4.06 \times 10^7, p_2 = 9.187 \times 10^4 \quad (6.3)$$

Where a is the ligament's cross-sectional area, defined using *in-vivo* data [143] for the following ligaments: Tibio-talar posterior, Tibio-talar anterior, Tibio-calcaneal, Talo-fibular posterior, Talo-fibular anterior, Calcaneo-fibular, Calcaneo-navicular plantar, Tarsometatarsal dorsal and Tarsometatarsal plantar. The mean of the *in-vivo* data from C. Mkandawire *et al.* (2005) [165] was used for the remaining ligaments. L_0 is the ligament zero load length, in this study it was assumed to equal the ligament anatomical reference length. L_0 was computed based on the geometry of the musculoskeletal foot model in the reference position used in the static trial.

6.3.5 Contact model

An ellipsoid shaped elastic foundation contact model (EFM) was generated based on four high-pressure regions (calcaneus, midfoot, forefoot, and toes), see Figure 6.1. As no information on the geometry of the loaded foot was available, we assumed that the foot surface geometry was related to the observed plantar pressure map and that the locations of high pressure corresponded to the most protruding parts of the foot sole. Each contact model was added to the corresponding subject's scaled musculoskeletal model in order to simulate dynamic plantar pressure. Computational details for the contact model can be found in Appendix A.

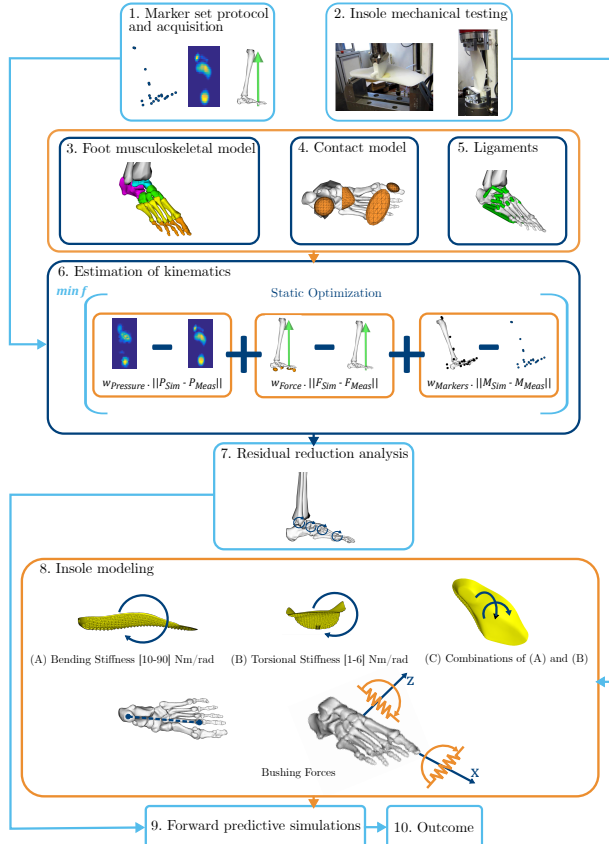


Figure 6.1: Descriptive framework used to predict ankle-foot kinematics under the effect of different insole stiffness using torque driven forward dynamic simulations. (1) Marker set protocol, pressure and ground reaction forces (GRF) acquisition. (2) Insoles mechanical tests: Left – Three-point bending test, Right – Torsional test. (3) Musculoskeletal lower leg model (*OpenSim*). Depicted segments: Cyan – talus; Purple – calcaneus; Green – midfoot; Yellow – forefoot; Orange – toes. (4) Foot model with the ellipsoid based contact geometries. (5) Ligaments visualization. (6) Visual summary of the optimization algorithm used to compute the kinematics. (7) A simple representation of the RRA algorithm. (8) Insoles model: Top - The different types of insoles: A) Pure torsional (Stiffnesses: 1 to 6 Nm/rad); B) Pure bending (Stiffnesses: 10 to 90 Nm/rad) and C) Combination of both. Bottom - Bushing forces representation: Left) Connection between the calcaneus and the forefoot; Right) Springs representation resisting relative rotation.

6.3.6 Estimation of Kinematics

Foot kinematics for each time frame (i) were computed by minimizing the weighted difference between measured and simulated marker positions, plantar pressure and vertical ground reaction force (GRF), using a *Matlab-OpenSim* interface:

$$f_i = w_P \cdot f_{pp_i} + w_M \cdot f_{M_i} + w_F \cdot f_{F_i} + w_K \cdot f_{K_i} \quad (6.4)$$

The kinematics (q_i) was input to compute the plantar pressure, the virtual marker positions and the vertical GRF. Where, f_{pp_i} was the pressure error computed as the sum of the squared difference of the simulated (pp_i) and measured pressures (\hat{pp}_i) normalized to the maximum pressure of that time step.

$$f_{pp_i} = \sum \left\| \frac{\hat{pp}_i}{\max(\hat{pp}_i)} - \frac{pp_i(q_i)}{\max(pp_i(q_i))} \right\| \quad (6.5)$$

f_{M_i} was the marker error computed as the sum of the scaled squared distance between the simulated (M_i) and measured marker (\hat{M}_i) positions over all markers. The marker error was scaled (s_M) such that the pressure and marker errors had the same order of magnitude.

$$f_{M_i} = \sum s_M \cdot \left\| \hat{M}_i - M_i(q_i) \right\| \quad (6.6)$$

f_{F_i} was the vertical GRF error computed as the squared difference between the simulated (F_i) and measured (\hat{F}_i) vertical ground reaction force using the pressure plate.

$$f_{F_i} = (\hat{F}_i - F_i(q_i))^2 \quad (6.7)$$

f_{K_i} was a penalization that favored kinematic solutions with limited ranges of motion as seen physiologically. This penalty was computed as the sum of the squared ratios between the joint angles (q_i) and the range of motion of the corresponding DOF.

$$f_{K_i} = \sum \left(\frac{q_i}{|ROM_i|} \right)^2 \quad (6.8)$$

The different weights ($w_P = 1\%$, $w_M = 94\%$ and $w_F = 5\%$) were selected such that the pressure, vertical GRF and marker errors had the same order of magnitude. The optimization was solved using the *fmincon* function with the *Interior-Point* algorithm, *Matlab* and *Optimization Toolbox R2015b* (The MathWorks, Inc., Natick, Massachusetts, United States). The optimized kinematics for one-time step were used as an initial guess for the next time step. The kinematics for the first time step were computed with the Inverse Kinematics analysis of *OpenSim* [71, 220] using the full marker set [156].

6.3.7 Residual Reduction Analysis

Reference actuator joint torques (*i.e.* control signals needed to generate joint actuator forces and torques) that generated walking kinematics (see Section 6.3.6) were computed using the residual reduction analysis (RRA) in *OpenSim* [71].

6.3.8 Insoles Modeling

The evaluated FOs were composed of two layers: a highly flexible top layer intended to provide comfort covering the entire foot plantar surface; and a bottom rigid 3D-printed layer to support and correct foot posture partly covering the foot plantar surface (calcaneus to metatarsals heads). The top flexible layer was not modeled, and the bottom 3D-printed layer was modeled as a bushing force connecting the calcaneus to the metatarsals heads, with torsional stiffness resisting relative rotation around the anteroposterior axis and bending stiffness resisting relative rotation around the mediolateral axis, see Figure 1. Due to the simple representation of the insoles, where geometry (*i.e.* arch support) was not considered, the modeling is more representative of flat insole [59, 60]. The bushing force reference frame attached to calcaneus coincided with the body reference frame and the bushing force reference frame of the forefoot was aligned with the bushing force reference frame of the calcaneus in the first time-step of each trial (heel strike). Three different types of insoles were modeled with different stiffnesses: pure torsion ($T=1$ to 6 Nm/rad), pure bending ($B=10$ to 90 Nm/rad) or a combination of both, in total 69 types of insoles.

6.3.9 Forward Simulations

The forward simulations were performed using *OpenSim*'s Forward Dynamics tools with the reference actuator joint torques and kinematics as input. When

using *OpenSim*'s Forward Dynamics tool, additional correction controllers are automatically added to each DOF. These are feedback controllers that track the reference kinematics. To evaluate the insoles' effect on the kinematics, the simulation must be allowed to deviate from the reference. So, the correction controllers must be set to a minimum, *i.e.* by setting low error gains (position error gain: $kp = 0.01$, velocity error gain: $kv = 0.2$); A total of 2033 simulations were successfully computed accounting for, subjects, feet, trials (the simulations failed to run for three trials), different insole stiffnesses and barefoot. The computational resources and services used in this work were provided by the VSC (Flemish Supercomputer Center), funded by the Research Foundation - Flanders (FWO) and the Flemish Government – department EWI.

6.3.10 Outcome Variables

The kinematic (joint angles computed with the relative orientations between segments in the three planes of motion) results for each stance phase of each leg were normalized to 100 data points. Each stance phase was divided into four phases (P1, P2, P3, and P4) respectively from initial contact (0%) – foot flat (16%) – midstance (42%) - heel off (66%) to toe off (100%). Swing phase and P4 were not analyzed during this project because the effect of the evaluated FOs was not aimed at these phases. For each leg and trial, joint angles were averaged over each phase. The results were grouped based on insole properties. This study focusses only on predicting the stiffness effect on the kinematics in the three planes of motion (sagittal: dorsiflexion/plantarflexion; coronal: inversion/eversion; transverse: abduction/adduction) of the ankle and subtalar (tibia-calcaneus), midtarsal (calcaneus-midfoot) and tarsometatarsal (midfoot-forefoot) joints.

A Linear Mixed Model was used to determine significant differences in kinematics and kinetics between insoles with different stiffnesses and barefoot walking for each type of forward simulation:

$$X_{Phase} \sim 1 + Condition + Side + (1 | Subject) \quad (6.9)$$

Where X_{Phase} was the dependent variable for the 3D joint angles, and we evaluated this dependency for each of the three phases of stance. *Condition* (different insole stiffnesses) and *Side* (Left or Right) were the fixed effects and *Subject* was the random effect. All statistics were calculated using *Matlab* (Statistics Toolbox Release 2016b, The MathWorks, Inc., Natick, Massachusetts, United States.). The results were found significant if the p – value was lower than 0.05/69, applying the Bonferroni correction for multiple comparisons.

6.4 Results

Increasing the insoles' bending stiffness led to significant kinematic changes mostly independent from torsional stiffness. Combined bending and torsional stiffness resulted in very similar ($< 1^\circ$) kinematic differences for most of the evaluated movements (*i.e.* calcaneus-midfoot and midfoot-forefoot) compared to pure bending insoles ($B=10$ to 90 Nm/rad , $T=0 \text{ Nm/rad}$) (Figure 6.2 and 6.3).

Small bending stiffnesses already introduced large changes in kinematics. For bending stiffnesses lower or equal than 40 Nm/rad there was already an increase of 3° in midfoot dorsiflexion and inversion with respect to calcaneus (Figure 6.2 and Appendix D). Additional changes with increased bending stiffness ($> 40 \text{ Nm/rad}$) were relatively smaller. Forefoot dorsiflexion and adduction with respect to midfoot increased linearly with bending stiffness over the entire range (Figure 6.3 and Appendix D). The imposed stiffness mimicking the effect of the insoles had little kinematic influence on the midfoot abduction/adduction with respect to the calcaneus, the forefoot inversion/eversion with respect to midfoot and no significant effect on the relative movement of calcaneus and tibia (*i.e.* ankle and subtalar joints).

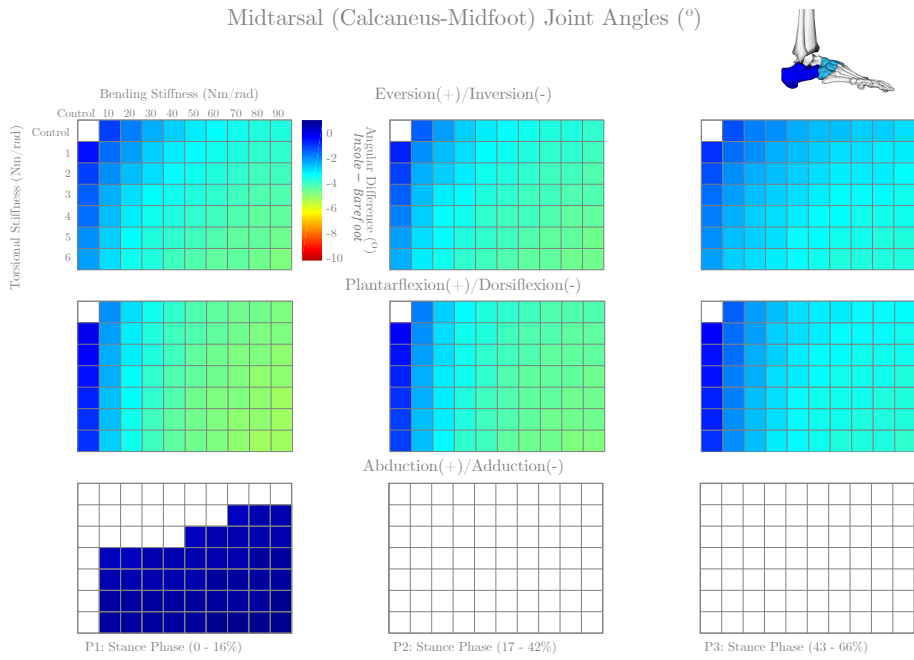


Figure 6.2: Calcaneus-Midfoot (Midtarsal) kinematics (joint angles). Each square represents the mean angular difference between the barefoot and insole condition, over all subjects, all trials and both legs per phase of stance. The white squares represent insoles that did not cause a significant difference ($p - \text{value} < 0.05/69$). For the exact means and standard deviation values consult and Appendix D.

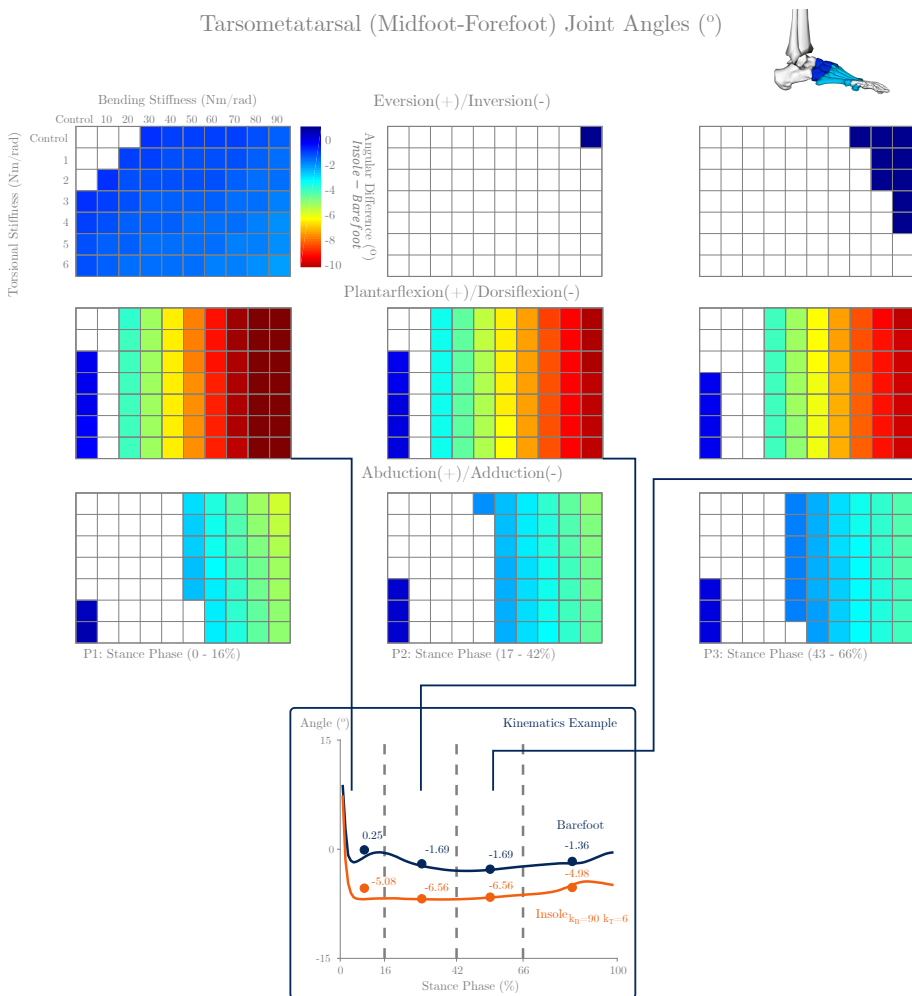


Figure 6.3: Midfoot-Forefoot (Tarsometatarsal) kinematics (joint angles). Each square represents the mean angular difference between the barefoot and insole condition, over all subjects, all trials and both legs per phase of stance. The white squares represent insoles that did not cause a significant difference ($p - \text{value} < 0.05/69$). For the exact means and standard deviation values consult and Appendix D. The highlighted square depicts an example of the mean kinematics of the barefoot and the insole with the highest combined values of bending and torsional stiffness ($T=6$ Nm/rad, $B=90$ Nm/rad) during the entire stance phase. The dots represent the mean of each phase (P1, P2, P3 and P4).

6.5 Discussion

The present work describes a torque driven forward simulation framework to simulate the effect of insole mechanical properties on foot kinematics using an extended musculoskeletal multibody foot model. With this framework we evaluated how insole stiffness affected foot kinematics during walking, specifically, the effect on the ankle and subtalar (tibia-calcaneus), midtarsal (calcaneus-midfoot) and tarsometatarsal (midfoot-forefoot) joints [19, 74]. Insoles are mostly prescribed as a conservative therapy to correct flat feet by reducing excessive rear-foot pronation (reduce ankle eversion) and correct the drop of the foot medial longitudinal arch by reducing excessive midfoot and forefoot dorsiflexion and abduction [19, 49, 74, 116, 132, 210].

In this study, we showed the isolated effect of insole directional stiffness on foot kinematics throughout the stance phase. Increased bending stiffness mostly independent from torsional stiffness, led to increased midfoot dorsiflexion and forefoot dorsiflexion and adduction. These results were partially verified in a previous gait analysis study, where arch supportive semi-rigid 3D-printed insoles showed high potential to counteract flat foot by increasing forefoot adduction (Chapter 4). However, increasing stiffness also led to an increase in forefoot dorsiflexion, the opposite of what was verified in the same study (Chapter 4). The insoles used in the referred study had increased arch support which was not modeled in this work. The authors believe that the combination of increased arch support with increased stiffness is responsible for the measured reduced forefoot dorsiflexion verified in the *in-vivo* study (Chapter 4).

The increased tarsometatarsal dorsiflexion ($< 10^\circ$) resulting from the increase in bending stiffness appears disproportionate compared to the normal range of motion of this joint ($\sim [-6^\circ \text{ to } 6^\circ]$) [156] and compared to the decrease in forefoot dorsiflexion ($< 6^\circ$) imposed by the insoles evaluated in Chapter 4. A detailed *in-vivo* motion acquisition study, under different flat insoles stiffnesses, would be necessary to further validate this framework and to evaluate the kinematics correction limits provided by the insoles. Nevertheless, to the authors' knowledge the present work is a first attempt to simulate insoles' influence on gait kinematics, complementing the plantar pressure results commonly presented in static or *quasi-static* FE approaches.

The foot contact geometry in the model should be physiologically as similar as possible to the foot sole. In this study, a combination of four ellipsoids, based on the dynamic change in plantar pressure, was used to represent the foot sole. Other contact formulations could be used to maximize the accuracy of plantar pressure simulation, like statistical shape models or 3D scanners for unloaded foot shape. Moreover, forward simulations are constrained by the

modeled ligaments which in most implemented cases have not been validated *in-vivo*. The assumption that the ligament zero load length is equal to the ligament anatomical reference length has already been disproven [31]. Still, there is insufficient experimental data to model all the 36 ligaments.

The different phases of stance were assumed to have a constant duration in all subjects based on the stance phase division established by the Rancho Los Amigos National Rehabilitation Centre [1]. The authors believe that the assumption of this fixed percentage will not significant impact the results because the inter-subject variability of the different phases in the gait cycle was reported to be smaller than 3% for an adult population by Hollman *et al.* (2011) [115] and therefore a minimal impact on the average angle during the phases is expected. Nonetheless, in principle, the duration of the different stance phases for each gait trial could be determined to verify the influence of this assumption for future research.

Despite the presented limitations, the proposed evidence-based predictive framework has great potential and a vast number of possible applications. To exemplify, we used this framework to simulate the insoles' effect under a different assumption on how humans adapt. We hypothesized that given the kinematic redundancy of the skeletal system, the subjects could try to counteract the kinematics influence of the insoles by changing their control (joint moments). This was simulated by imposing high correction controllers, *i.e.* high error gains (position error gain: $kp = 100$, velocity error gain: $kv = 20$) [71, 220]. The results showed that it was not possible to counteract the insoles' influence for bending stiffnesses higher than 70 Nm/rad when the foot was in full contact with the ground (P2 and P3); leading to an increase in forefoot dorsiflexion with respect to midfoot, see Figure 6.4. This test showed that relatively high joint moments (>10 Nm) are needed to counteract the FOs' influence on the kinematics. Therefore, it is unlikely that subjects will adapt their control to an extent that the control adaptations will counteract changes in kinematics.

The proposed torque driven framework could also have been used to evaluate the effect of other insole properties on foot kinematics, for example, damping, by just adapting the bushing forces mechanical parameters. To further evaluate the insoles' corrective potential using the presented forward dynamic methodology, the effect of geometric corrections (*i.e.* increased arch support) should be implemented. Additionally, the kinematics of the knee and hip joints should be evaluated for a complete understanding of the insoles' effect on the lower limbs. For a future application, the bushing forces used in this framework could be repositioned to mimic the effect of synthetic ligaments or tendons on foot kinematics. This possibility is of great value to anticipate the result of reconstructive surgical interventions.

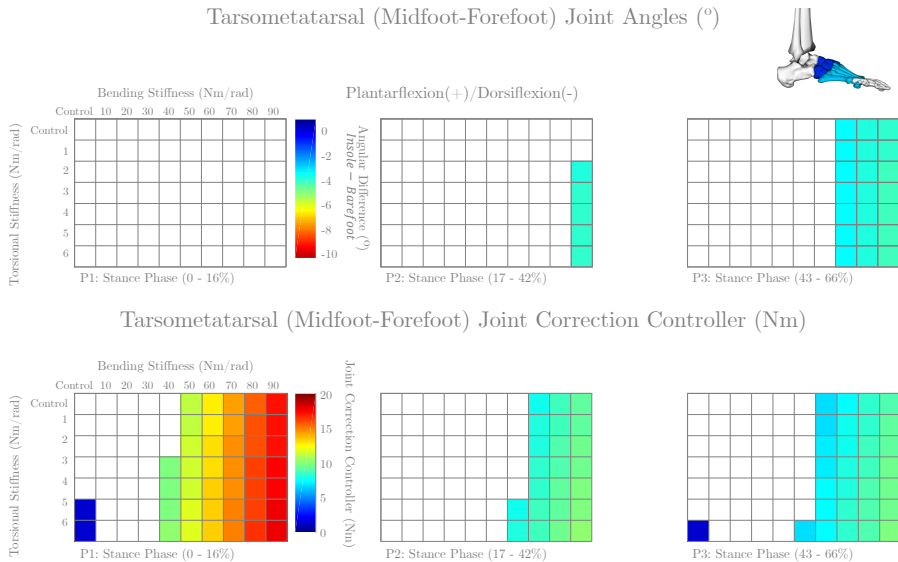


Figure 6.4: Example of control adaptation. Top) Tarsometatarsal kinematics (joint angles). Each square represents the mean angular difference between the barefoot and insole condition, over all subjects, all trials and both legs per phase of stance; Bottom) Tarsometatarsal correction controllers. Each square represents the mean joint correction controller computed for each insole condition, over all subjects, all trials and both legs per phase of stance. The white squares represent insoles with no significant difference ($p - value < 0.05/69$).

6.6 Conclusion

The proposed framework was able to exhaustively estimate foot kinematics under the effect of 69 different combinations of directional flat insoles stiffness. This work is a step towards establishing a scientific-based approach for the construction of optimal orthoses in therapeutic shoe design.

Our simulations demonstrated that increased bending stiffness, mostly independent from torsional stiffness, led to a kinematic adaptation that has the potential to partially correct flat feet by increasing forefoot adduction.

A detailed, *in-vivo* 3D motion analysis study, under different insole stiffnesses, is still required to further validate this framework. Additionally, to have a better representation of the insoles, the geometric information (*i.e.* increased arch support) should be modeled.

6.7 Acknowledgements

This work was funded by the Berghmans - Dereymaeker research chair on Foot and Ankle Biomechanics and the Aladyn Project (IWT, Flanders).

Authors' Contributions

Tiago de Melo Malaquias focused on the development of the predictive framework, and writing.

Friedl De Groote supervised the research and revised the manuscript. Wouter Aerts helped in the development of code for the VSC (Flemish Supercomputer Center).

Ilse Jonkers supervised the research and revised the manuscript.

Jos Vander Sloten supervised the research and revised the manuscript.

The experimental data was available from the work of Fien Burg [39] performed in the Movements & posture Analysis Laboratory Leuven.

Chapter 7

General conclusion and Future work

In this chapter, the objectives formulated in Chapter 1 are restated together with the conclusion and contributions of each study (Chapter 3 – 6) in Section 7.1. Additionally, the studies are related and discussed together in Section 7.2. Finally, the future developments are presented in Section 7.3.

7.1 Individual contributions

7.1.1 Study 1: Extended foot-ankle musculoskeletal models for application in movement analysis - Chapter 3

Despite the popularity of musculoskeletal multibody models, the number of accessible extended FMMM is limited. This is a major limitation to reproduce published model outcomes or to use the published models with other data sets. Furthermore, it is crucial to increase the level of detail within the current available musculoskeletal 3D multibody foot-ankle models.

We developed two multibody foot-ankle models with different DOFs that capture the most critical functional foot movements.

These models were made fully available in *OpenSim*, an open-source and free platform that lets users develop models of musculoskeletal structures and create dynamic simulations of a wide variety of movements. Both models consisted of five rigid segments (talus, calcaneus, midfoot, forefoot, and toes), connected through five anatomical joints (ankle, subtalar, midtarsal, tarsometatarsal and metatarsophalangeal). One model featured fifteen degrees of freedom and the other eight. The geometry of the most important ligaments ($n=36$) were included.

Using 3D motion capture collected during gait, the 8 DOF model calculated joint angles and moments consistent with the available literature. In contrast, the 15 DOF model, due to the larger freedom to solve the inverse kinematics problem, was more prone to computational errors. Due to the more accurate representation of the degrees of freedom in the foot, the 8 DOF model has the potential to offer new insights in pathological foot kinematics and dynamics than more simple musculoskeletal foot models currently used.

7.1.2 Study 2: Multi-Segment foot kinematics and kinetics analysis on the influence of 3D-printed insoles on flat feet subjects - Chapter 4

Gait analysis together with validated extended FMMMs can be used to investigate the influence of the currently produced 3D-printed insoles on the measured kinematics and kinetics of flat feet subjects and to compare their influence with standard manufactured insoles and shoes.

The authors applied a newly developed musculoskeletal model to *in-vivo* gait analysis measurements in subjects with flat feet to assess the influence of 3D-printed and EVA molded insoles on ankle-foot kinematics and kinetics.

This study showed that the main kinematic differences between the control and the flat feet subjects were increased forefoot dorsiflexion and abduction, throughout the entire stance phase of gait, which characterizes a low medial longitudinal arch. Inverse dynamics during the barefoot trials showed decreased midtarsal and tarsometatarsal joint moments for the flat feet subjects.

The two custom insoles (EVA Molded and 3D-printed) provided increased stiffness and support to the medial longitudinal arch of the foot, decreasing forefoot dorsiflexion and abduction in the flat feet subjects. The FOs further reduced the midtarsal and tarsometatarsal joints' moments due to a higher

redistribution of the ground reaction forces induced by the increased contact of the insole with the foot.

The corrections provided by commonly used insoles (EVA molded) can be equally achieved using 3D-printing technology. This can offer an opportunity towards more efficient production, the use of better more durable and less prone to wear materials and an objective pathology-oriented design of subject-specific insoles.

7.1.3 Study 3: Plantar pressure based estimates of foot kinematics during gait – a least squares optimization approach - Chapter 5

The use of plantar pressure measurement systems to evaluate foot and ankle pathologies is well established in clinical practice. Although relevant to detect local tissue overloading, to date plantar pressure data cannot be used to evaluate ankle-foot kinematics. Musculoskeletal multibody models that integrate a contact model describing the foot-ground interaction can be used to extrapolate complex foot kinematic data from plantar pressure profiles. So, the third objective of this thesis was to implement an elastic foundation contact model to describe the interaction between the foot and the ground, whereas in the fourth objective was to evaluate the applicability of plantar pressure measurements to compute ankle-foot kinematics.

The authors proposed and evaluated a musculoskeletal model-based optimization algorithm to estimate ankle-foot kinematics based on plantar pressure data and the trajectories of a limited number of markers.

Marker positions and plantar pressure were simulated in *OpenSim* using the newly developed extended FMMM coupled with an elastic foundation contact model (EFM).

Four ellipsoids were implemented to approximate the geometry of the plantar surface of the foot.

The presented optimization algorithm allows the estimation of foot kinematics based on plantar pressure information and the coordinates of a limited set of four markers. The set-ups simplicity has significant research and clinical implications on both the preparation time of 3D motion capture of foot kinematics as well

as on its assessment and evaluation potential. It will allow a more accurate and objective clinical interpretation of foot pathologies, otherwise typically evaluated using plantar pressure systems alone.

7.1.4 Study 4: Predictive simulations of the corrective effect of controlled stiffness 3D-printed insoles during the stance phase of gait - Chapter 6

To objectively improve the link between patient assessment and subject-specific insoles engineering, considering different insoles' combinations of structural and material design factors, it is essential to predict the biomechanical effect of insoles on the foot and ankle kinematics and kinetics during gait. Thus, the fifth objective of this thesis was to develop a predictive simulation framework to evaluate the effect of different 3D-printed insoles' stiffnesses on the foot kinematics under, specifically on the ankle and subtalar (tibia-calcaneus), midtarsal (calcaneus-midfoot) and tarsometatarsal (midfoot-forefoot) joints.

A framework was developed to predict foot kinematics under the effect of different 3D-printed insoles stiffnesses using torque driven forward dynamic simulations.

Three different types of insoles were tested with different stiffnesses: pure torsional, pure bending or a combination of both. Therefore, a total of 69 insoles were tested *in-silico*.

The results showed that increased bending stiffness, mostly independent from torsional stiffness, led to increased midfoot dorsiflexion and forefoot dorsiflexion and adduction. The increase in forefoot adduction is a kinematic adaptation needed to partially correct flat feet deformity, as seen in a previous *in-vivo* study using arch supportive semi-rigid 3D-printed insoles (Chapter 4).

This work is a step towards establishing a scientific-based approach for the construction of optimal orthoses in therapeutic shoe design.

7.2 General discussion

During this thesis, we implemented the building blocks underlying a future predictive simulation framework required to evaluate the differences in foot kinematics under the effect of different 3D-printed insoles' stiffnesses.

This methodology is a pioneer in approaching the influence of insoles' stiffness on gait kinematics based on a minimal data set of plantar pressure data and motion data using a complex musculoskeletal model.

Within this work, the isolated effect of insole directional stiffness on foot kinematics throughout the stance phase was predicted in Chapter 6. The simulation results showed that increased stiffness led to increased midfoot dorsiflexion and forefoot dorsiflexion and abduction. The validity of this effect can be evaluated against the experimentally observed effect of insoles in Chapter 4. The model results are only in partial agreement with the results of Chapter 4, semi-rigid 3D-printed insoles with arch support showed high potential to counteract flat foot by increasing forefoot adduction. In contrast, the model was unable to confirm the decreased forefoot dorsiflexion observed in Chapter 4. It is important to note that this may be due to the simple representation of the modeled insoles, where the arch geometry (*i.e.* arch support) was not considered. Therefore, this implementation is more representative of flat insoles [59, 60]. It should, therefore, be questioned if this discrepancy may be attributed to the absence of the corrective effect of the arch support that was not modeled in Chapter 6, but that was one of the main corrective characteristics of the insoles tested in Chapter 4.

Nevertheless, the comparison of the findings of both chapters allows to conclude that morphological problems like a flat foot (*i.e.* increased forefoot dorsiflexion and abduction) cannot be tackled by only increasing flat insoles' stiffness. Geometrical correction (*e.g.* increased arch support) must be therefore considered and combined with increased stiffness so that insoles can provide sufficient support to achieve the required correction to reduce forefoot dorsiflexion and abduction as documented experimentally in Chapter 4. In order to verify this finding, the predictive tool should be extended to include the effect of the geometric support and further validated based on patient-specific kinematics reported in Chapter 4.

The magnitude of the predicted correction in Chapter 6 needs to be evaluated with care: with increasing stiffness, forefoot dorsiflexion increases ($< 10^\circ$). This is disproportionate compared to the normal range of motion of the tarsometatarsal joint ($\sim [-6^\circ \text{ to } 6^\circ]$) observed in Chapter 3 and compared to the decrease in forefoot dorsiflexion ($< 6^\circ$) imposed by the insoles evaluated in Chapter 4. Inadequate parameters or inappropriate modeling of the foot ligaments [32] will result in inadequate restraint to the joint during a forward simulation, therefore inducing joint movement outside the physiological range of motion of the joint. As indicated, there is a lack of validated

mechanical properties for all the thirty-six ligaments, *e.g.* resting length and stiffness. Experimentally measuring these properties on the small foot ligaments is challenging, and the available studies are scarce. Uni-axial or bi-axial extension tests should be considered in future studies to accurately evaluate the muscles' and ligaments' mechanical properties. Dynamic foot motion simulators (*i.e.* *in-vitro* gait simulators) can then be used to evaluate the functional behavior of ligaments in a cadaveric foot-ankle specimen during an imposed movement comparable to physiological gait, thereby taking advantage of the high repeatability of *in-vitro* protocols that reduce intra-specimen variability.

The predictive simulation in Chapter 6 evaluated the isolated effect of insoles' stiffness on foot kinematics using torque-driven forward simulation. This strategy may be too permissive, as in reality subjects may adapt their muscle activation in response to the insole, thereby modifying the predicted response. The current predictive framework already allows to incorporate this effect on the simulation, as the inclusion of this effect would rely on adequate tuning of the correction controllers present at each DOF. These feedback controllers control the extent to which the simulated kinematics deviate from the reference kinematics. In the current implementation, the effect of the correction controllers (*i.e.* error gains) was set to a minimal value, allowing the simulated kinematics to deviate from the reference kinematics significantly. To accommodate for the subject's response to the insoles, the correction controllers' gains values could be adjusted to closer track the reference kinematics, thereby balancing the effect of the insole stiffness and the subject's response. Although increasing the biofidelity of this approach would require extensive experimental data on the immediate and long-term adaptive response of the ankle and foot muscles in order to optimize the control gains.

In future applications, the predictive framework developed in Chapter 6 will rely on a minimal data set and therefore needs to be combined with the pressure-based kinematics estimation framework developed in Chapter 5, so that the corrective effect of the insoles on the patient's kinematics can be evaluated. To do so, there is an important aspect that needs further validation, *i.e.* the representation of the feet plantar surface implemented in Chapter 5. The contact geometries should be physiological as similar as possible to the foot sole. In this study, a combination of four ellipsoids, based on the dynamic evolution of plantar pressure, was used to represent the feet sole geometry. Most likely more detailed contact formulations could be used to maximize the accuracy and representativeness of plantar pressure simulation. In particular, the use of statistical shape models based on 3D surface scanning of the unloaded foot may provide an interesting alternative. In addition, the predictive framework proposed in Chapter 6 could not be validated. In the future, a detailed *in-vivo* 3D motion analysis study, under different flat insoles stiffnesses, should be

performed and compared with the results obtained in this thesis.

In the current work, the pressure-based estimation of kinematics frameworks (Chapter 5) and the insoles predictive framework (Chapter 6) were tested for applications in a healthy population with normal pressure distribution and assuming a purely passive corrective effect of the insole. Therefore, the use of the methodology in more pathological subjects may be challenging especially when they interfere with the underlying assumptions that the detail of the foot sole geometry adequately couples the plantar pressure profile to the foot segment kinematics, that the ligaments adequately constrain the different DOFs in the model and that no corrective controllers are needed to reflect the subject's response to the orthosis. This dictates the need to incorporate more representative contact geometries, optimized pathology-specific strategies as well as adapted ligaments' properties for different target populations. Nonetheless, based on the results in Chapter 3, the appropriateness of the extended musculoskeletal foot model (8 DOF FMMM) to accurately evaluate kinematics (joint angles) and kinetics (joint moments) in flat feet subjects (Chapter 4) could be confirmed.

The use of skin mounted markers is an inherent limitation of the four different studies presented in this thesis. Soft tissue motion can limit the validity with which the skin-markers reflect the underlying bone kinematics [78, 180, 142]. Peters *et al.* (2010) [193] reported kinematic errors on the foot and ankle due to skin-motion artefacts between 2° and 6° . The authors recognize that an accurate estimation of foot kinematics using skin-markers measurements may be difficult. Due to this limitation, the repeatability and reliability of the skin-markers protocol used within this thesis was studied as part of another doctoral thesis [77]. This study was performed on 20 healthy subjects (age: 27 ± 3 years and weight: 72.92 ± 11.01 kg) and reported high intra-rater reliability (Intraclass correlation or $ICC \geq 0.700$) for motion of the hip, knee, ankle, midfoot and hallux, and low ($ICC < 0.500$) forefoot intra-rater reliability. Inter-rater reliability was comparable to those results; however, reliability was found to be moderate ($0.500 \leqslant ICC < 0.700$) for the calculated midfoot motion. Similar intra-reliability results were found for similar marker protocols [225, 51]. So, the kinematic comparisons between different conditions tested with the same subjects, using the presented skin-marker set-up, placed by the same rater, are still expected to present enough accuracy to draw meaningful conclusions. Furthermore, in our studies marker placement was not altered between different conditions, therefore limiting strongly the influence of measurement variability observed in studies considering inter- and intra-observer variability.

Lastly, a limitation of this study may be the limited number of subjects ($n = 5$) used in Chapter 3 and 5. The variability in data is large and this is a confounding factor that complicates the statistical comparison. For this reason,

we decided to do more qualitative analyses. Therefore, to improve the kinematic comparison between the different models developed in Chapter 3 and between the different marker set-ups used in Chapter 3, in the future we would need to increase the number of subjects. The sample size used in Chapter 4 ($n = 17$) and 6 ($n = 4$), although different for both studies, allowed detecting small but significant differences between insole conditions (up to 1°) using a multilevel statistic model and a conservative correction for multiple comparisons, *i.e.* linear mixed model with a Bonferroni correction. Nonetheless, a larger sample size should be considered in order to verify potential significances of differences currently not confirmed as statistically significant (*e.g.* calcaneus eversion/inversion in relation to the tibia). A power analysis based on these works could serve as a basis for a sample size calculation of future studies.

7.3 Future perspectives

The framework developed in this thesis can: **1) estimate ankle-foot kinematics using a simplified set-up based on plantar pressure information and the coordinates of a limited set of markers and 2) predict the influence of mechanical parameters (*e.g.* stiffness) for the design of foot orthoses using dynamic information.** The framework developed in this work therefore provides a solid proof of concept for the different building blocks required to introduce computer-aided design of insoles based on a minimal data set of plantar pressure data in clinics. As such, the developments presented in this thesis can objectively improve insoles' computer-assisted design and rapid manufacturing, specifically 3D-printing insoles. In addition, these advancements have the potential to simplify motor evaluation of the musculoskeletal system and to predict its response to dedicated interventions, thereby improving orthopedic patient care and reducing long term treatment costs for the patient and the healthcare provider.

7.3.1 Simulation-based insole design, the route to application

To objectively improve the link between patient assessment and subject-specific insoles engineering, considering different insoles' combinations of structural and material design factors, it is essential to develop computational tools able to predict the biomechanical effect of insoles objectively. Therefore, the authors developed a predictive simulation framework to evaluate the differences in foot kinematics under the effect of different 3D-printed insoles' stiffnesses during gait. The proposed torque driven framework could also have been used to evaluate the effect of other insole properties on foot kinematics, for example damping,

by just adapting the bushing forces mechanical parameters. Furthermore, it could be used for other movements besides gait, *e.g.* running, squatting, high and long jump. It could also be applied at sports performance, adapting the insoles' mechanical properties so that subjects can optimize their movement (as discussed in the general discussion). In the future the framework could also be extended, for example, to simulate different mechanical parameters of sports shoes in order to estimate the best combination for different sports and athletes. In particular, the customization of the mechanical properties of a foot-ankle insole to the subject's need seems to hold great potential. Furthermore, the external forces used in this predictive framework (*i.e.* bushing forces) could be repositioned in the foot to mimic the effect of synthetic ligaments or tendons on foot kinematics. This possibility is of great value to anticipate the result of reconstructive surgical interventions.

The proposed predictive framework must achieve some milestones before its application becomes a reality. Software like *footscan®* (*RSScan International, Paal, Belgium*) allows the design of 3D-printed insoles using subject-specific plantar pressure information. This software proposes insoles specifications (*e.g.* arch support, heel height, and metatarsal support) based on the plantar pressure distribution, which can be adapted by the clinician using their insights. However, this software cannot estimate or predict the kinematics influence of the insole. Combining the previously described simplified kinematics acquisition set-up (Chapter 6) and the prediction framework into software like *footscan®* would provide objective biomechanical knowledge that will increase the clinician's confidence for prescribing the computed insole. Outputting barefoot kinematics information and allowing the clinician to virtually impose different insoles mechanical parameters (*e.g.* stiffness and damping) or even to impose some geometrical specification (*e.g.* arch support) and visualizing its corrective effect would be a great advance for insoles prescription. However, this would require, in a first instance, the extension of the predictive framework to receive other mechanical parameters (*e.g.* damping) and geometry information.

Nevertheless, the proposed framework to estimate ankle-foot kinematics based on plantar pressure data and the trajectories of a limited number of markers must overcome some specific limitations before its broad application becomes a reality. The presented framework still requires reflective markers to provide 3D coordinates of points positioned in different parts of the foot segments. Plantar pressure does not uniquely define foot kinematics, so the kinematics estimation algorithm exclusively based on plantar pressure would be infeasible and inaccurate. In the future, inertial measurement units (IMUs) should be tested and validated to verify the possibility of using this data together with plantar pressure data to provide foot and ankle kinematics to simplify the acquisition set-up further.

Furthermore, to integrate this framework in clinical practise, clinicians need to be educated in the objective evaluation of dynamic foot function and the corrective effect of insoles' mechanical properties *e.g.* stiffness and damping. Clinicians, in general, are not familiar with kinematic evaluation of dynamic foot function and only a limited number of them use plantar pressure information for insole prescription. Therefore, the use of the predictive workflow to optimize the gait kinematics and kinetics patterns in individual patients will require a dedicated training. Of concern is the requirement of substantial computational power that is not commonly available in a clinical environment. The framework would have to be connected to a dedicated server that allows reasonable computational time and parallelization.

Finally, the translation of the insole idealized mechanical properties determined on the predictive simulation flow would need to be translated into an effective 3D-printing production line. To the authors' knowledge, the current 3D-printing technology does not allow perfect control of the printed structure mechanical parameters. To overcome this challenge, companies like *Materialise NV* (Leuven, Belgium) are improving the printing process of 'cellular structures' that allow local geometric variations within the final product. These variations will influence the mechanical properties of the insole and allow for manufacturing a product that has a dynamic corrective behavior tailored to everyone.

7.3.2 Pressure-based kinematic simulations for broader biomechanics applications

To the extent of our knowledge, plantar pressure measurement systems, to date, cannot be used to evaluate ankle-foot kinematics. To overcome this limitation, the authors developed a musculoskeletal model-based optimization algorithm to estimate ankle-foot kinematics based on plantar pressure data and the trajectories of a limited number of markers. The set-up simplicity has significant research and clinical implications on both the preparation time of 3D motion capture of foot kinematics as well as on its evaluation. It will allow a more standardized, accurate and objective clinical interpretation of foot pathologies.

The application of a simplified motion estimation, using pressure data and a limited number of tracking markers, could be extended beyond gait analysis and the ankle-foot complex. This approach seems highly powerful in the field of lower limb prosthetics where the kinematics of an amputated segments within a socket of the prosthesis could be estimated based on the pressure measurement inside the socket. This is highly relevant to optimize prosthesis socket design and avoid pistonning, as it is more difficult to place tracking markers inside the

prosthesis compared to intra-socket pressure sensors. Ergonomics is another field where the pressure-based estimations of kinematics could be applied. The framework could be used to facilitate the kinematics evaluation of individuals in long periods of immobilization like bed rest or wheelchairs. Using pressure data from the contact surface (being either a bed or cushion) has potential to simplify the procedure of vertebral kinematics acquisition bringing new insights to improve the design of back supports to reduce bad seating posture.

Appendix A

Contact model computation

This appendix reviews the methodology to compute the ellipsoid shaped elastic foundation contact model (EFM) based on high pressure regions (Section A.1). It also describes the stiffness optimization algorithm implemented to assure the dynamic consistency between kinematics and the vertical ground reaction force measured with the pressure plates (Section A.2).

A.1 Geometry and position

Human-environment interaction is usually simulated using finite element modeling (FEM), Hertz theory and elastic foundation modeling (EFM) [5]. However, the use of FEM is limited to static or *quasi*-static situations due to the large computational cost. The analytical method with Hertz theory is limited to simple geometries like spheres or cylinders. Alternatively, EFM assumes that the objects in contact are rigid bodies with only a thin layer of elastic material at the surfaces. A triangular mesh approximates the geometry of each surface. A spring-damper system is placed at the centroid of each triangle of the mesh. The normal force acting on each mesh element is a function of the indentation and indentation speed [120].

An elastic foundation contact model [221] was defined and -given the lack of loaded foot geometrical information (*i.e.* 3D scan) - tuned for each stance phase trial. The contact model was then added to the subject-specific scaled musculoskeletal model in order to simulate the plantar pressure. As no information on the geometry of the loaded foot was available, we assumed

that the locations of high pressure corresponded to the most protruding parts of the foot sole. Therefore, a 3D cloud of virtual points corresponding to each of the 64×64 pressure sensors (pp_{norm}) was defined based on the sum of the plantar pressure over the stance phase, normalized to the maximum value over all sensors:

$$\frac{\sum_{i=1}^{nT} \hat{pp}_i}{\max(\sum_{i=1}^{nT} \hat{pp}_i)} = pp_{norm} \quad (\text{A.1})$$

with \hat{pp}_i the matrix (64×64) of measured plantar pressure at time step i and nT the number of time steps. The horizontal coordinates (x, y) of the virtual points were the position of the sensor and the, vertical coordinate (z) was a virtual distance obtained by multiplying pp_{norm} with a scaling factor ($s = 2\text{cm}$) and dividing by the maximum of the summed normalized plantar pressure ($\max(pp_{norm})$). The scaling factor was selected based on a sensitivity analysis over all trials based on the marker and plantar pressure error, detailed in Section 5.3.4. Points were only used for fitting if the summed force on the corresponding sensor was above 5 N ($(\sum_{i=1}^{nT} \hat{pp}_i \cdot A_s > 5N)$, with A_s the area of the sensors.

Four different ellipsoids were fitted to the cloud of virtual points to model the contact of the different regions of the foot sole (calcaneus, midfoot, forefoot, and toes). These regions were delimited by a manually defined mask (guided by the *RSscan* automatic mask) [5], see Figure A.1 Step A, and a three-step approach was used:

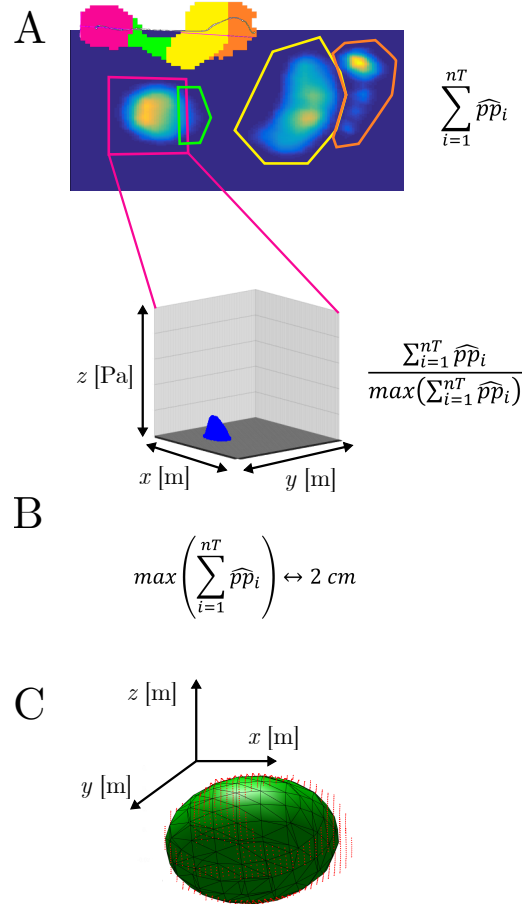


Figure A.1: Ellipsoid contact geometry computation. Step A - Selection of different pressure areas (3D clouds of virtual points) and scaling of pressure; Step B – Conversion of scaled pressures to clouds of virtual points; Step C – Ellipsoid fit: Least squares optimization.

First, a linear least-squares algorithm [194] was used to fit the ellipsoids according to a ten-parameter ($A, B, C, D, E, F, G, H, I, J$) conic algebraic equation:

$$Ax^2 + By^2 + Cz^2 + 2Dxy + 2Exz + 2Fyz + 2Gx + 2Hy + 2Iz + J = 1 \quad (\text{A.2})$$

Next, the position of the ellipsoids relative the foot segments and relative to

the ground surface was estimated. The fitted ellipsoids (four in total, one for each contact region, see example in Figure 5.3 and Figure A.1) were initially positioned on the foot using an empirical anatomical approach: *i.e.* at the center of the calcaneus, center of the midfoot, head of the third metatarsal and center of the hallux. The ellipsoids center position and the vertical position of the ground surface relative to the musculoskeletal model were then optimized by minimizing the difference between the computed (using the EFM contact model described above) and measured plantar pressure at 50% of the stance phase. This instant was chosen to assure full contact between the foot and the ground. The vertical position of the ellipsoids center and the ground surface was optimized to assure contact between the foot contact geometries and the ground. The positioning optimization was solved using the *fmincon* function with the *Interior-Point* algorithm, *Matlab* and *Optimization Toolbox R2015b* (The MathWorks, Inc., Natick, Massachusetts, United States).

A.2 Stiffness optimization

To assure the dynamic consistency between kinematics and the vertical GRF measured with the pressure plates. The stiffness optimization algorithm estimates the global optimal foot kinematics (fourteen DOF) for ten equally distant time steps of the stance phase (I) and the stiffness constants for the four ellipsoids, using a *Matlab-OpenSim* interface. The kinematics (q_t) is the input to compute the vertical ground reaction force (GRF), the virtual marker positions and the four stiffnesses parameters. The algorithm minimizes the global difference between measured and simulated marker positions and vertical ground reaction force:

$$f = \sum_{i \in I} f_i \quad (\text{A.3})$$

$$f_i = w_M \cdot f_{M_i} + w_F \cdot f_{F_i} \quad (\text{A.4})$$

Where, f_{M_i} is the marker error computed as the sum of the scaled squared distance between the simulated (M_i) and measured marker (\hat{M}_i) positions over all markers. The marker error was scaled (s_M) such that the pressure and marker errors had the same order of magnitude.

$$f_{M_t} = \sum s_M \cdot \left\| \hat{M}_i - M_i(q_i) \right\| \quad (\text{A.5})$$

f_{F_t} is the vertical GRF error computed as the squared difference between the simulated (F_t) and measured (\hat{F}_t) vertical ground reaction force.

$$f_{F_i} = (\hat{F}_i - F_i(q_i))^2 \quad (\text{A.6})$$

The positioning and stiffness optimization were solved using the *fmincon* function with the *Interior-Point* algorithm, *Matlab* and *Optimization Toolbox R2015b* (The MathWorks, Inc., Natick, Massachusetts, United States).

Appendix B

Sensitivity analysis: ellipsoids scaling factor

This appendix details the sensitivity analysis performed in Chapter 5 to select the factor used to scale the ellipsoids contact geometries.

The scaling factor is important to have contact geometries that can penetrate the ground during the walking trial. The contact geometries are a representation of the plantar surface of the foot during ground contact. The factor was selected based on a sensitivity analysis over all trials based: 1) a qualitative evaluation of the foot kinematics and 2) mean optimization function value over each trial (f) computed using the kinematics estimation method detailed in Section 5.3.3.

Figure B.1 compares the joint angles for the ankle, subtalar and metatarsophalangeal plantarflexion/dorsiflexion degrees of freedom during the stance phase of gait computed with contact geometries with different scaling factors (2 cm , 2.5 cm and 3 cm) with the same angles computed with a standard approach (without contact geometries). The kinematics for the three joint angles is similar for the different scaling factors and similar to the standard approach.

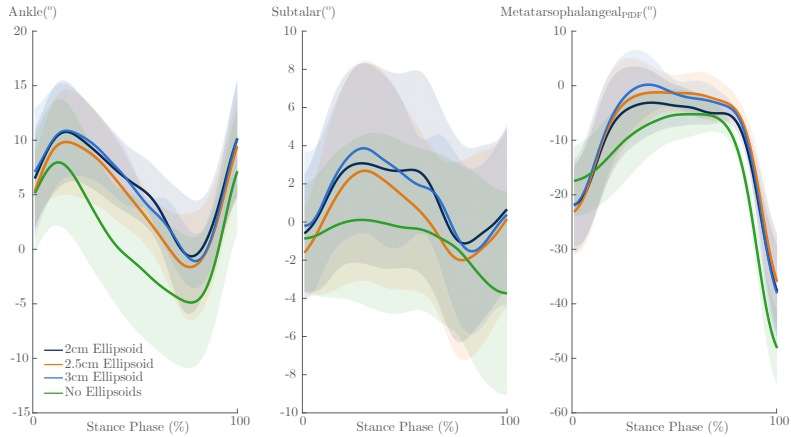


Figure B.1: Joint angles for the ankle, subtalar and metatarsophalangeal plantarflexion/dorsiflexion degrees of freedom during the stance phase of gait for different scaling factors. Dark Blue – 2cm scaling factor; Orange – 2.5cm scaling factor; Blue - 3cm scaling factor; Green – No contact geometries.

The comparison between the three different mean optimization function values over each trial (f), computed using the kinematics estimation method detailed in Section 5.3.3, shows that the 2 cm scaling factor presents in general a smaller f mean value.

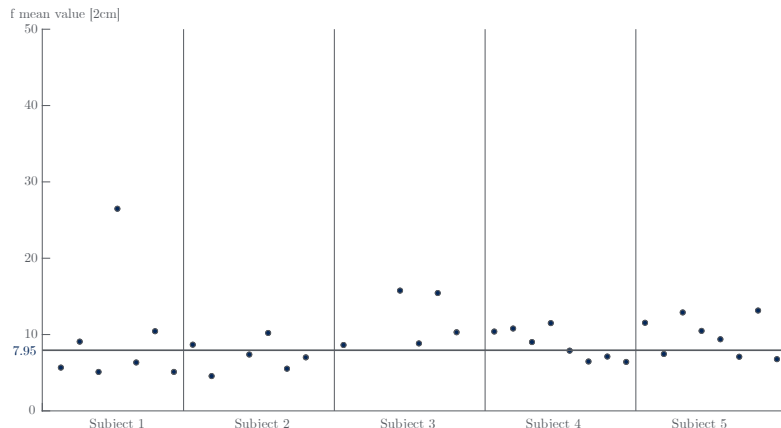


Figure B.2: Mean optimization function value (f) computed using the kinematics estimation method detailed in Section 5.3.3 for each trial and leg. These values were obtained using ellipsoid contact geometries generated with the 2 cm scaling factor.

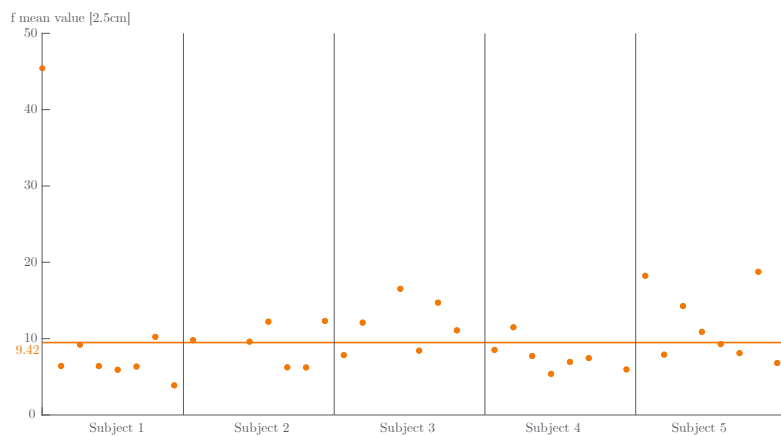


Figure B.3: Mean optimization function value (f) computed using the kinematics estimation method detailed in Section 5.3.3 for each trial and leg. These values were obtained using ellipsoid contact geometries generated with the 2.5 cm scaling factor.

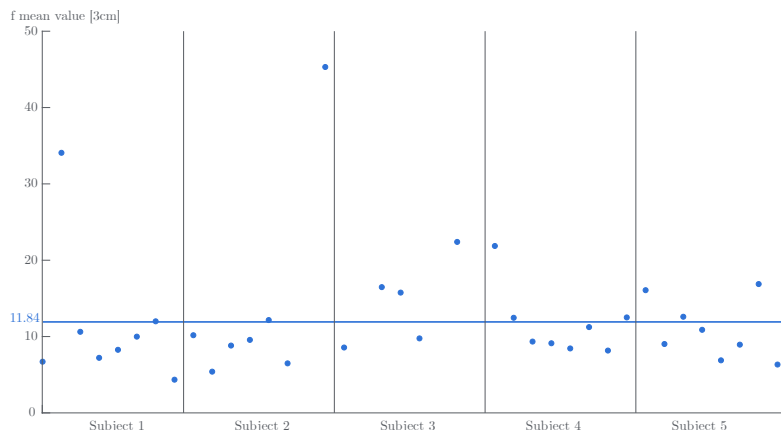


Figure B.4: Mean optimization function value (f) computed using the kinematics estimation method detailed in Section 5.3.3 for each trial and leg. These values were obtained using ellipsoid contact geometries generated with the 3 cm scaling factor.

Appendix C

Extended results of Chapter 5

This appendix details the kinematics results for each subject using the six different kinematic estimation approaches presented in Chapter 5: Markers Optimization (*MO*), All Markers + Pressure (*AMP*), *PiG*, *PiG* extended (*PiGe*), 2 Markers (*2M*) and 1 Marker (*1M*).

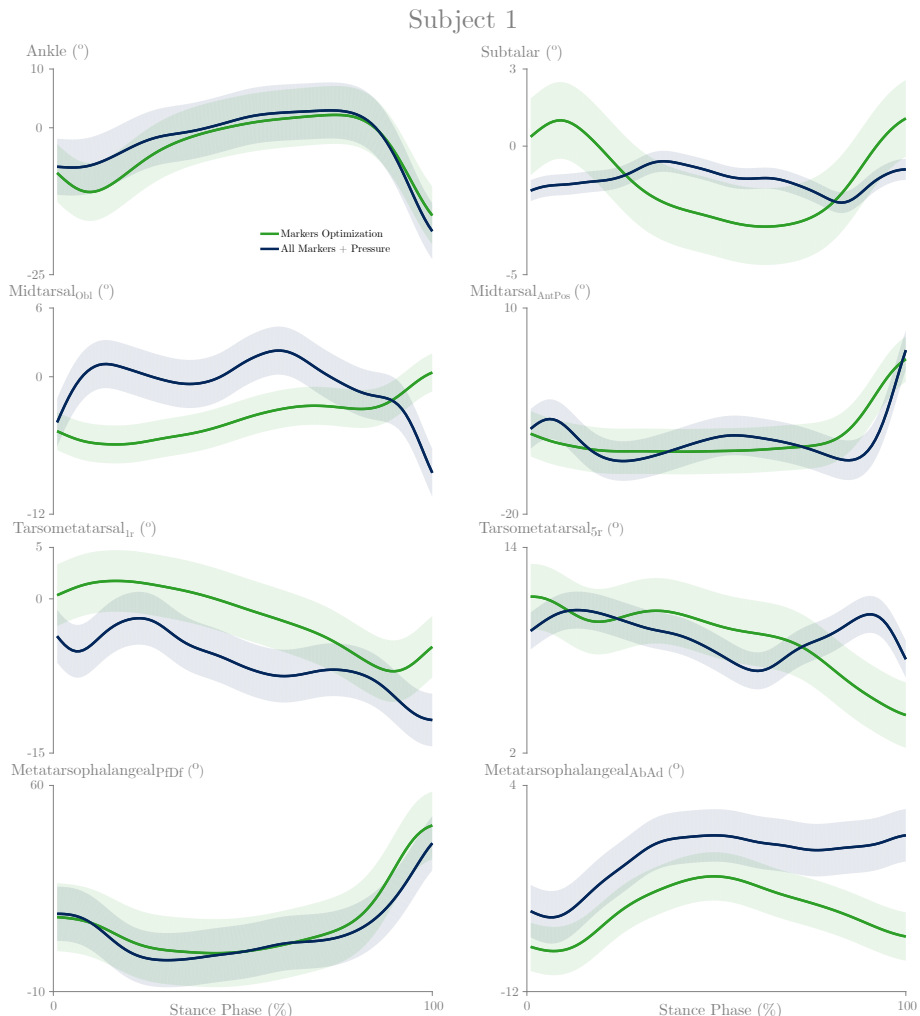


Figure C.1: Kinematics results for the 8 DOF for Subject 1. Green: *MO* – Mean kinematics computed with the entire marker set without contact geometries ($w_P = 0\%$ and $w_M = 100\%$); Dark Blue: *AMP* – Mean kinematics computed with the entire marker set with contact geometries ($w_P = 60\%$ and $w_M = 40\%$). Full line – Mean of the four trials and both feet (8 different trials).

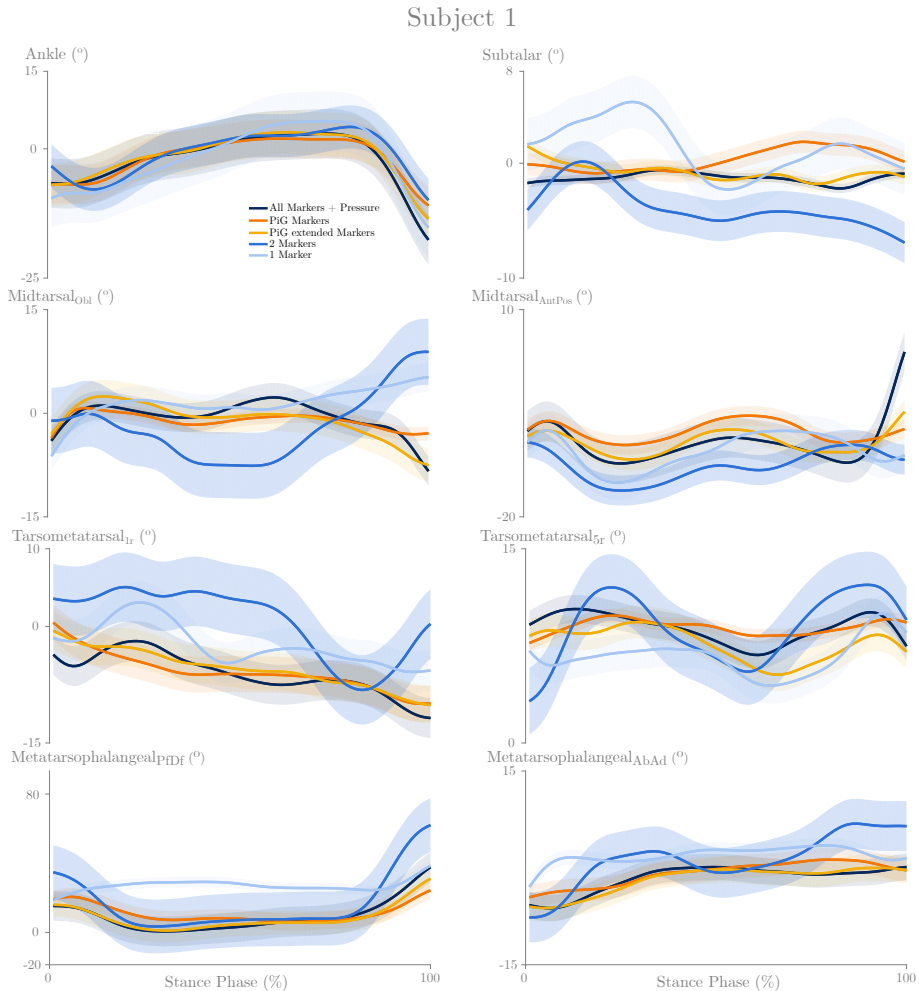


Figure C.2: Kinematics results for the 8 DOF for Subject 1. Dark Blue: *AMP* – Mean kinematics computed with the entire marker set with contact geometries ($w_P = 60\%$ and $w_M = 40\%$); Orange: *PiG* – Mean kinematics computed with the *PiG* marker set with contact geometries ($w_P = 60\%$ and $w_M = 40\%$); Yellow: *PiGe* - Mean kinematics computed with the *PiG* marker set plus one marker in the hallux with contact geometries ($w_P = 80\%$ and $w_M = 20\%$); Blue: *2M* – Mean kinematics computed with one marker in the calcaneus and in the hallux with contact geometries ($w_P = 70\%$ and $w_M = 30\%$); Light Blue: *1M* – Mean kinematics computed with one marker in the head of the second metatarsal with contact geometries ($w_P = 80\%$ and $w_M = 20\%$). All the reduced combinations maintain four markers in the tibia. Full line – Mean of the four trials and both feet (8 different trials).

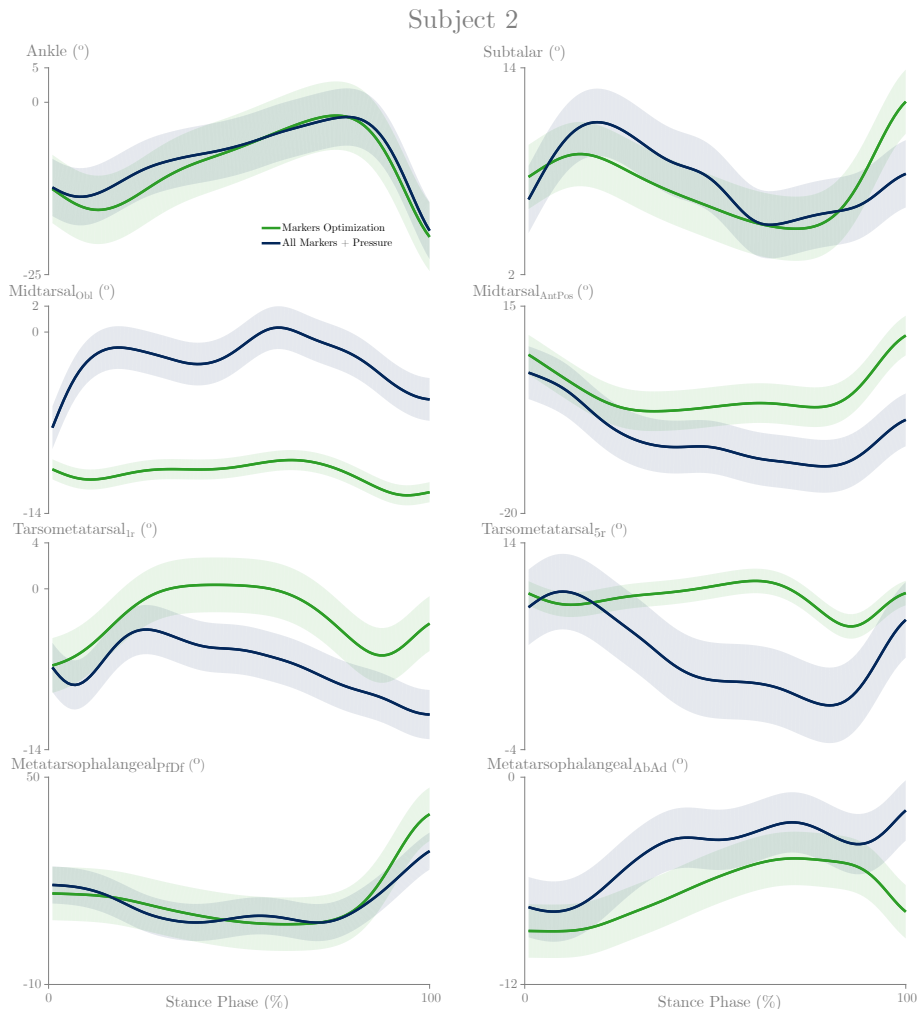


Figure C.3: Kinematics results for the 8 DOF for Subject 2. Green: *MO* – Mean kinematics computed with the entire marker set without contact geometries ($w_P = 0\%$ and $w_M = 100\%$); Dark Blue: *AMP* – Mean kinematics computed with the entire marker set with contact geometries ($w_P = 60\%$ and $w_M = 40\%$). Full line – Mean of the four trials and both feet (8 different trials).

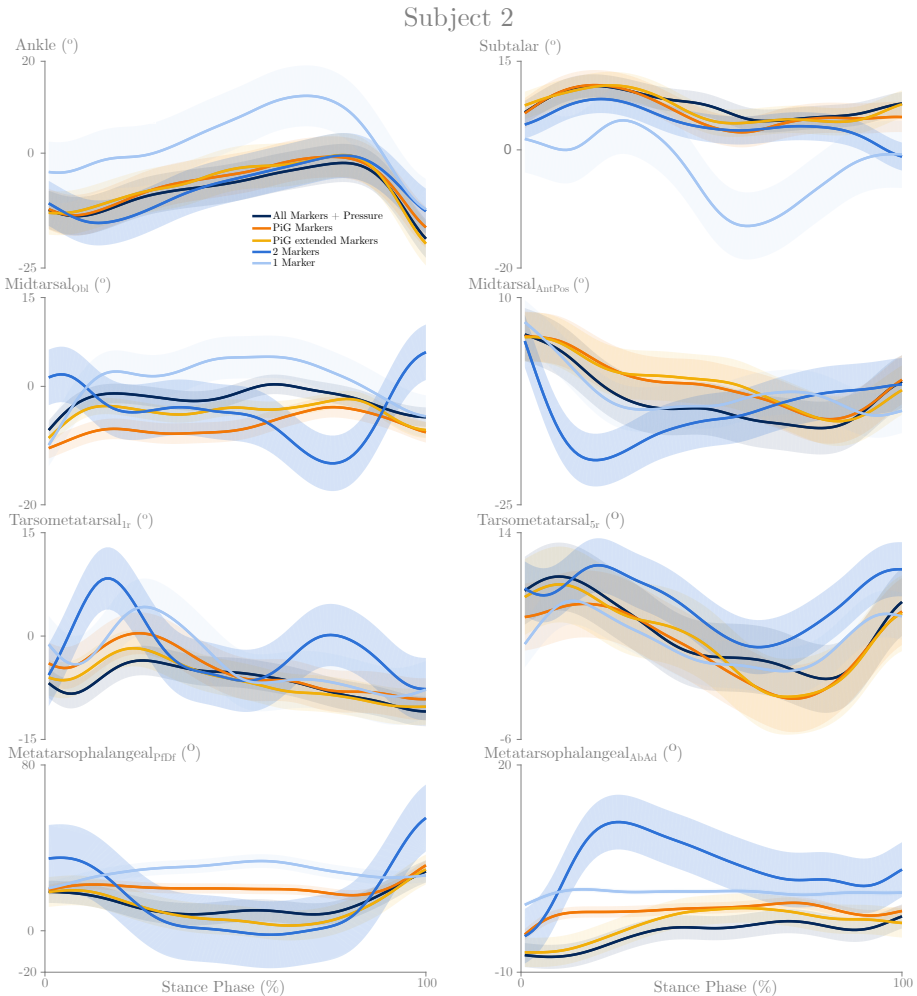


Figure C.4: Kinematics results for the 8 DOF for Subject 2. Dark Blue: *AMP* – Mean kinematics computed with the entire marker set with contact geometries ($w_P = 60\%$ and $w_M = 40\%$); Orange: *PiG* – Mean kinematics computed with the *PiG* marker set with contact geometries ($w_P = 60\%$ and $w_M = 40\%$); Yellow: *PiGe* - Mean kinematics computed with the *PiG* marker set plus one marker in the hallux with contact geometries ($w_P = 80\%$ and $w_M = 20\%$); Blue: *2M* – Mean kinematics computed with one marker in the calcaneus and in the hallux with contact geometries ($w_P = 70\%$ and $w_M = 30\%$); Light Blue: *1M* – Mean kinematics computed with one marker in the head of the second metatarsal with contact geometries ($w_P = 80\%$ and $w_M = 20\%$). All the reduced combinations maintain four markers in the tibia. Full line – Mean of the four trials and both feet (8 different trials).

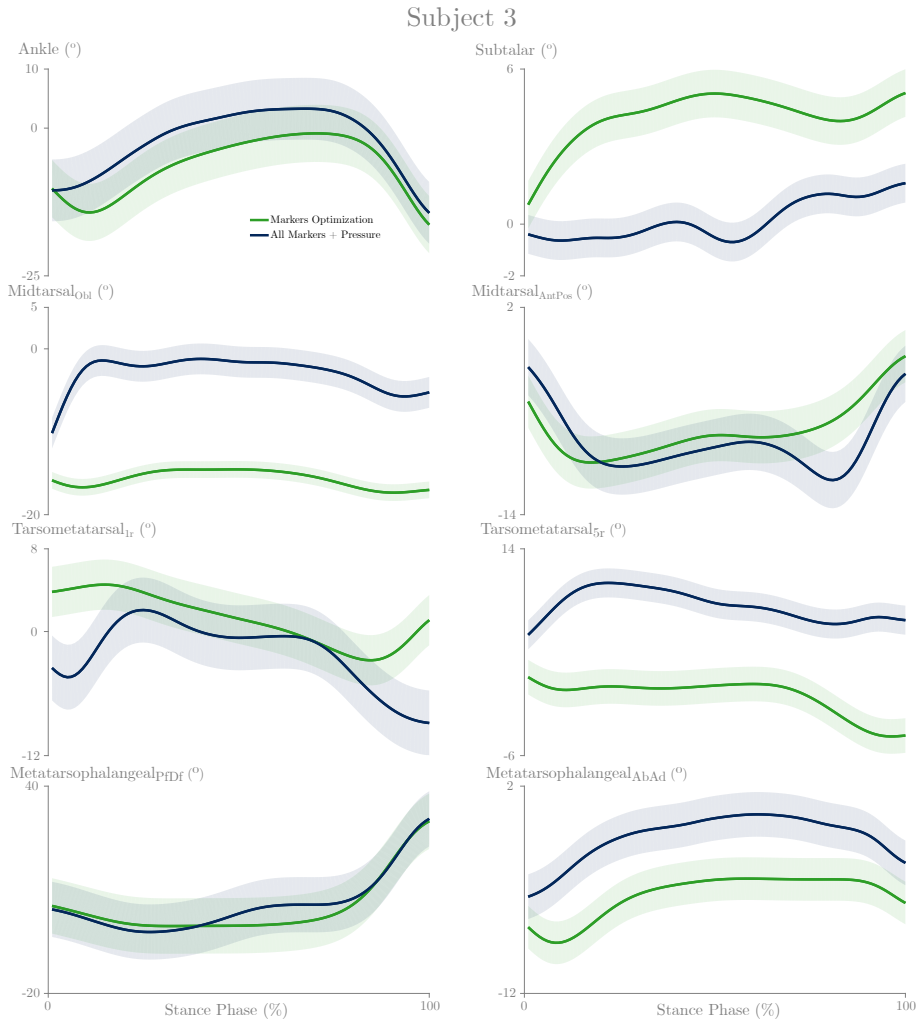


Figure C.5: Kinematics results for the 8 DOF for Subject 3. Green: *MO* – Mean kinematics computed with the entire marker set without contact geometries ($w_P = 0\%$ and $w_M = 100\%$); Dark Blue: *AMP* – Mean kinematics computed with the entire marker set with contact geometries ($w_P = 60\%$ and $w_M = 40\%$). Full line – Mean of the four trials and both feet (8 different trials).

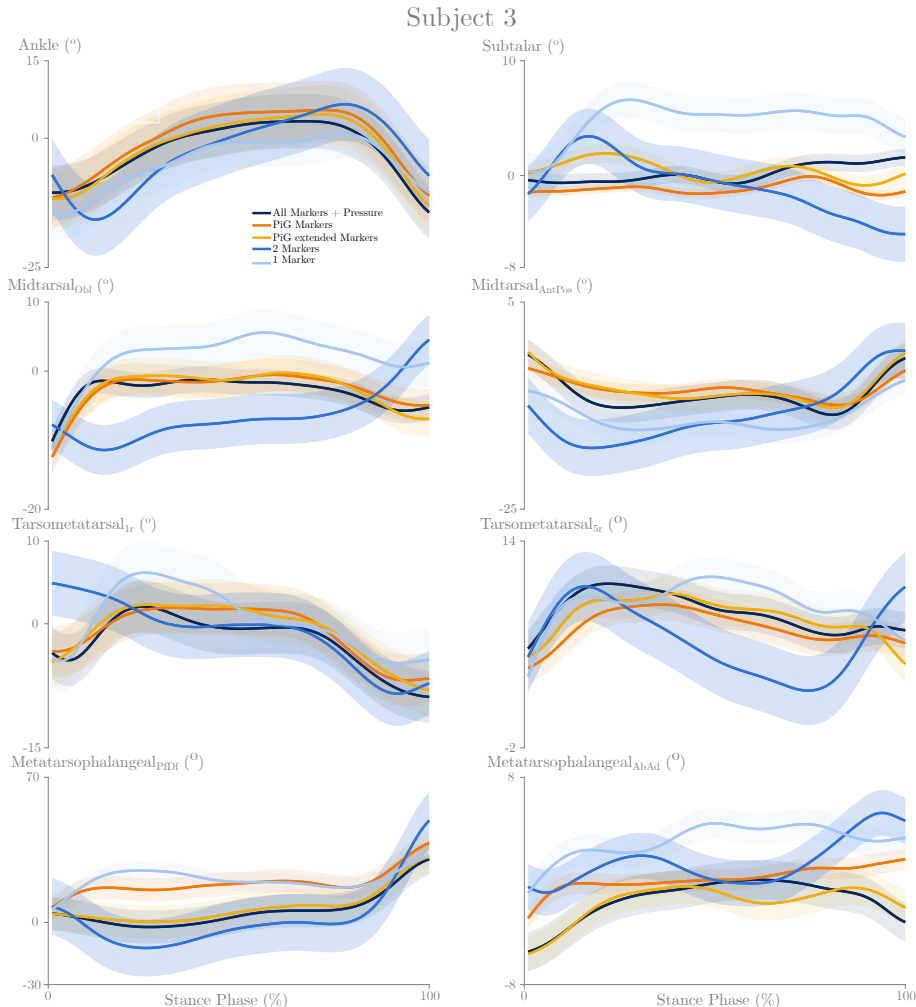


Figure C.6: Kinematics results for the 8 DOF for Subject 3. Dark Blue: AMP – Mean kinematics computed with the entire marker set with contact geometries ($w_P = 60\%$ and $w_M = 40\%$); Orange: PiG – Mean kinematics computed with the PiG marker set with contact geometries ($w_P = 60\%$ and $w_M = 40\%$); Yellow: PiGe - Mean kinematics computed with the PiG marker set plus one marker in the hallux with contact geometries ($w_P = 80\%$ and $w_M = 20\%$); Blue: 2M – Mean kinematics computed with one marker in the calcaneus and in the hallux with contact geometries ($w_P = 70\%$ and $w_M = 30\%$); Light Blue: 1M – Mean kinematics computed with one marker in the head of the second metatarsal with contact geometries ($w_P = 80\%$ and $w_M = 20\%$). All the reduced combinations maintain four markers in the tibia. Full line – Mean of the four trials and both feet (8 different trials).

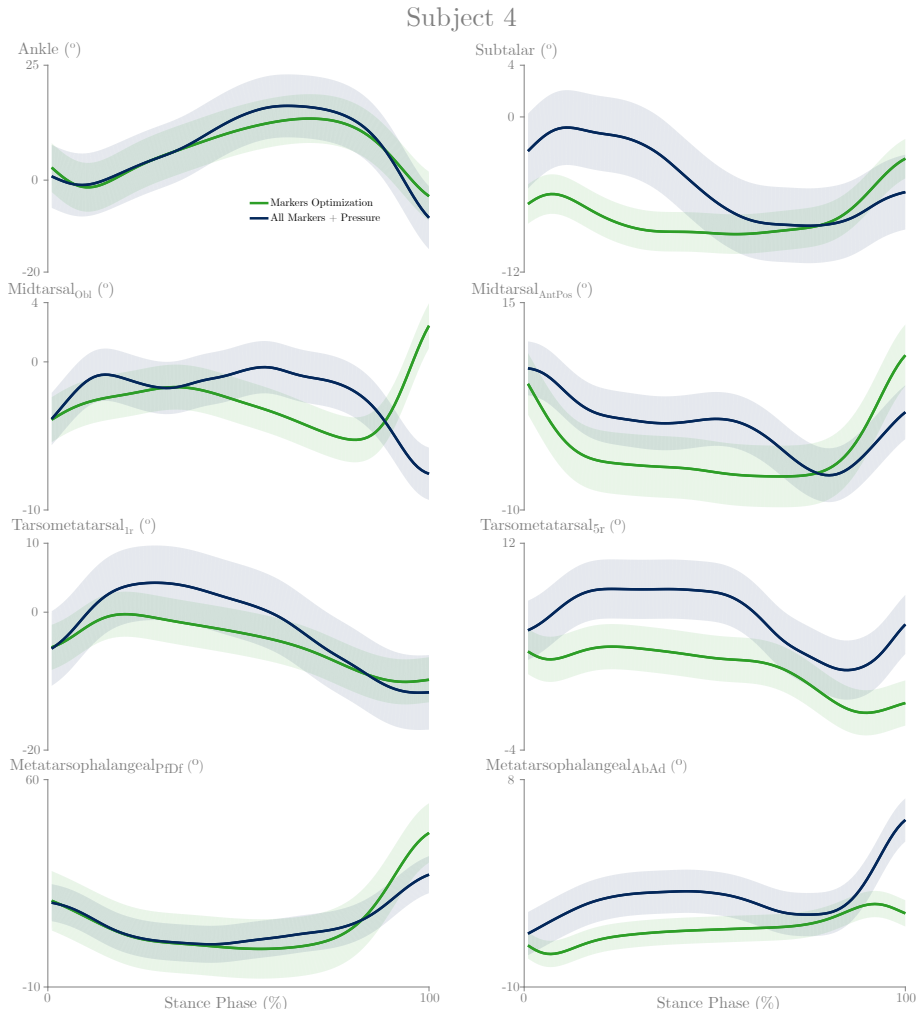


Figure C.7: Kinematics results for the 8 DOF for Subject 4. Green: *MO* – Mean kinematics computed with the entire marker set without contact geometries ($w_P = 0\%$ and $w_M = 100\%$); Dark Blue: *AMP* – Mean kinematics computed with the entire marker set with contact geometries ($w_P = 60\%$ and $w_M = 40\%$). Full line – Mean of the four trials and both feet (8 different trials).

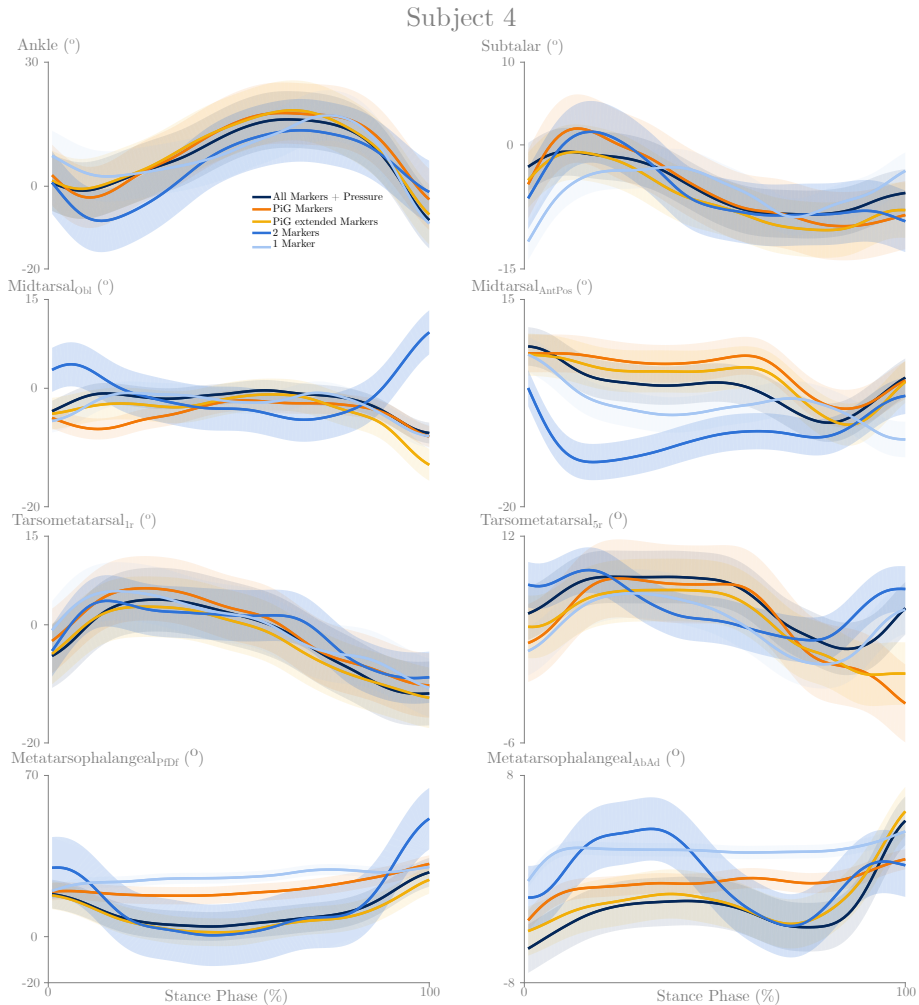


Figure C.8: Kinematics results for the 8 DOF for Subject 4. Dark Blue: *AMP* – Mean kinematics computed with the entire marker set with contact geometries ($w_P = 60\%$ and $w_M = 40\%$); Orange: *PiG* – Mean kinematics computed with the *PiG* marker set with contact geometries ($w_P = 60\%$ and $w_M = 40\%$); Yellow: *PiGe* - Mean kinematics computed with the *PiG* marker set plus one marker in the hallux with contact geometries ($w_P = 80\%$ and $w_M = 20\%$); Blue: *2M* – Mean kinematics computed with one marker in the calcaneus and in the hallux with contact geometries ($w_P = 70\%$ and $w_M = 30\%$); Light Blue: *1M* – Mean kinematics computed with one marker in the head of the second metatarsal with contact geometries ($w_P = 80\%$ and $w_M = 20\%$). All the reduced combinations maintain four markers in the tibia. Full line – Mean of the four trials and both feet (8 different trials).

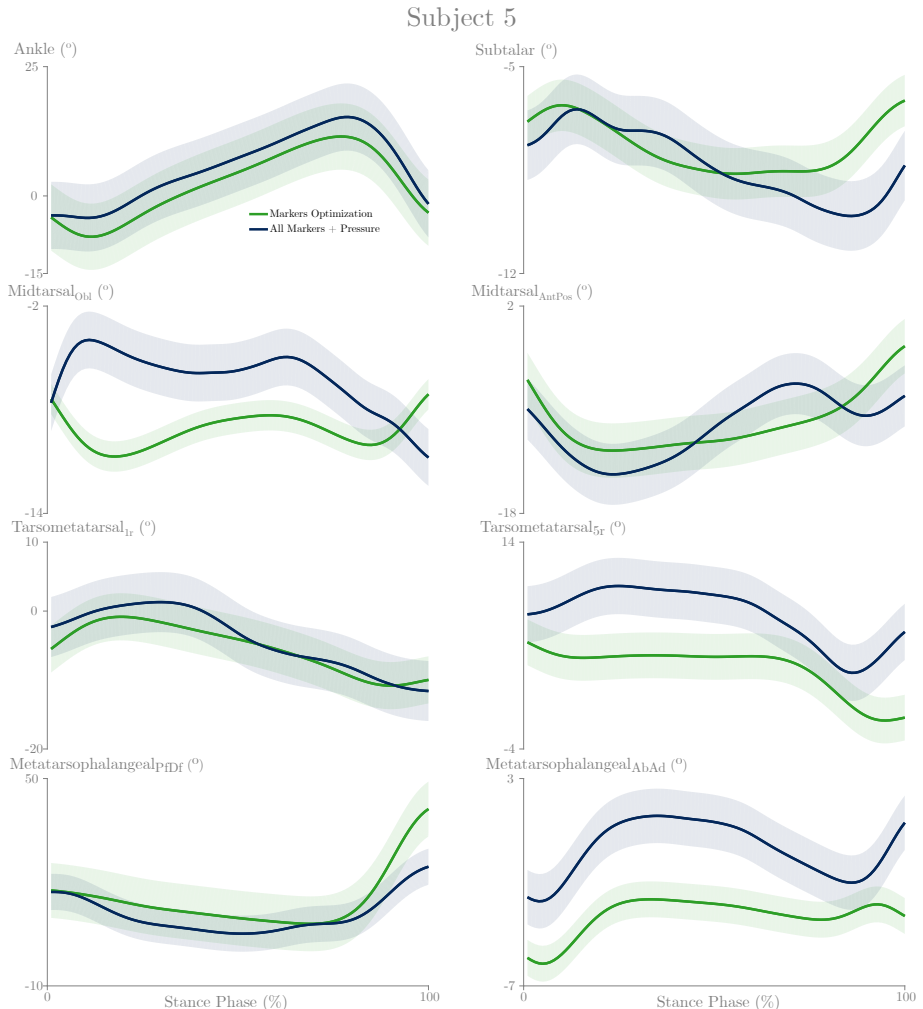


Figure C.9: Kinematics results for the 8 DOF for Subject 5. Green: *MO* – Mean kinematics computed with the entire marker set without contact geometries ($w_P = 0\%$ and $w_M = 100\%$); Dark Blue: *AMP* – Mean kinematics computed with the entire marker set with contact geometries ($w_P = 60\%$ and $w_M = 40\%$). Full line – Mean of the four trials and both feet (8 different trials).

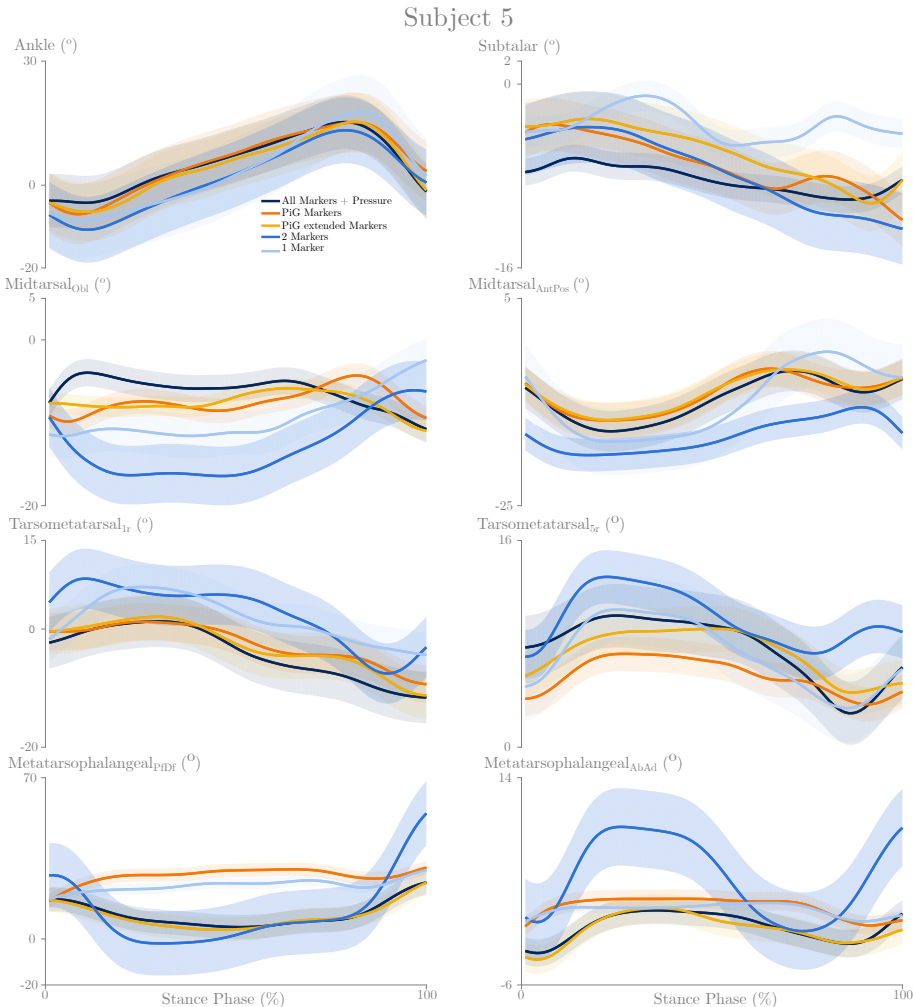


Figure C.10: Kinematics results for the 8 DOF for Subject 5. Dark Blue: *AMP* – Mean kinematics computed with the entire marker set with contact geometries ($w_P = 60\%$ and $w_M = 40\%$); Orange: *PiG* – Mean kinematics computed with the *PiG* marker set with contact geometries ($w_P = 60\%$ and $w_M = 40\%$); Yellow: *PiGe* - Mean kinematics computed with the *PiG* marker set plus one marker in the hallux with contact geometries ($w_P = 80\%$ and $w_M = 20\%$); Blue: *2M* – Mean kinematics computed with one marker in the calcaneus and in the hallux with contact geometries ($w_P = 70\%$ and $w_M = 30\%$); Light Blue: *1M* – Mean kinematics computed with one marker in the head of the second metatarsal with contact geometries ($w_P = 80\%$ and $w_M = 20\%$). All the reduced combinations maintain four markers in the tibia. Full line – Mean of the four trials and both feet (8 different trials).

Appendix D

Extended results of Chapter 6

The following tables detail the means and standard deviation values for Figure 6.2 and 6.3.

Table D.1: Midtarsal Eversion/Inversion kinematics (joint angles) for Phase 1 of stance. Each cell contains the mean difference in relative orientation over all subjects, all trials and both legs between the barefoot and insole condition.

Midtarsal Eversion(+) / Inversion(-) for P1: Stance phase (0-16%)											
Mean joint angles \pm Standard Deviations											
Bending Stiffness (Nm/rad)											
	10	20	30	40	50	60	70	80	90		
Torsional Stiffness (Nm/rad)	1	-0.59 \pm 0	-1.68 \pm 1.08	-1.93 \pm 1.16	-2.47 \pm 1.32	-2.85 \pm 1.44	-3.15 \pm 1.52	-3.37 \pm 1.58	-3.56 \pm 1.62	-3.7 \pm 1.66	-3.81 \pm 1.68
	2	-1.08 \pm 0	-2.09 \pm 1.25	-2.68 \pm 1.43	-3.09 \pm 1.54	-3.4 \pm 1.62	-3.65 \pm 1.69	-3.83 \pm 1.73	-3.99 \pm 1.77	-4.13 \pm 1.81	-4.23 \pm 1.83
	3	-1.46 \pm 0	-2.42 \pm 1.41	-2.95 \pm 1.57	-3.32 \pm 1.66	-3.61 \pm 1.72	-3.84 \pm 1.77	-4.02 \pm 1.82	-4.17 \pm 1.84	-4.3 \pm 1.89	-4.39 \pm 1.9
	4	-1.79 \pm 0	-2.69 \pm 1.55	-3.18 \pm 1.68	-3.52 \pm 1.76	-3.79 \pm 1.81	-4.01 \pm 1.86	-4.18 \pm 1.9	-4.32 \pm 1.92	-4.46 \pm 1.97	-4.55 \pm 1.98
	5	-2.06 \pm 0	-2.91 \pm 1.68	-3.37 \pm 1.79	-3.69 \pm 1.85	-3.96 \pm 1.9	-4.16 \pm 1.94	-4.34 \pm 1.98	-4.47 \pm 2	-4.6 \pm 2.04	-4.75 \pm 2.05
	6	-2.29 \pm 0	-3.11 \pm 1.79	-3.54 \pm 1.89	-3.85 \pm 1.93	-4.09 \pm 1.97	-4.3 \pm 2.01	-4.47 \pm 2.05	-4.61 \pm 2.07	-4.73 \pm 2.11	-4.83 \pm 2.12

Table D.2: Midtarsal Eversion/Inversion kinematics (joint angles) for Phase 2 of stance. Each cell contains the mean difference in relative orientation over all subjects, all trials and both legs between the barefoot and insole condition.

Midtarsal Eversion(+) / Inversion(-) for P2: Stance phase (17-42%)											
Mean joint angles \pm Standard Deviations											
Bending Stiffness (Nm/rad)											
	10	20	30	40	50	60	70	80	90		
Torsional Stiffness (Nm/rad)	1	-0.7 \pm 0	-2.06 \pm 1.31	-2.68 \pm 1.42	-3.07 \pm 1.51	-3.37 \pm 1.59	-3.61 \pm 1.67	-3.79 \pm 1.74	-3.92 \pm 1.8	-4.03 \pm 1.84	-4.12 \pm 1.88
	2	-1.23 \pm 0	-2.4 \pm 1.58	-2.94 \pm 1.65	-3.29 \pm 1.72	-3.56 \pm 1.78	-3.79 \pm 1.84	-3.96 \pm 1.9	-4.09 \pm 1.95	-4.19 \pm 1.99	-4.28 \pm 2.02
	3	-1.61 \pm 0	-2.67 \pm 1.82	-3.14 \pm 1.86	-3.47 \pm 1.91	-3.73 \pm 1.95	-3.94 \pm 2	-4.11 \pm 2.05	-4.23 \pm 2.09	-4.34 \pm 2.13	-4.42 \pm 2.16
	4	-1.93 \pm 0	-2.89 \pm 2.03	-3.32 \pm 2.06	-3.63 \pm 2.09	-3.88 \pm 2.11	-4.08 \pm 2.15	-4.24 \pm 2.19	-4.37 \pm 2.23	-4.47 \pm 2.26	-4.55 \pm 2.28
	5	-2.2 \pm 0	-3.08 \pm 2.21	-3.49 \pm 2.23	-3.77 \pm 2.25	-4.01 \pm 2.26	-4.21 \pm 2.29	-4.37 \pm 2.33	-4.49 \pm 2.36	-4.59 \pm 2.38	-4.67 \pm 2.4
	6	-2.43 \pm 0	-3.25 \pm 2.37	-3.63 \pm 2.37	-3.91 \pm 2.39	-4.14 \pm 2.4	-4.34 \pm 2.42	-4.49 \pm 2.45	-4.61 \pm 2.47	-4.71 \pm 2.5	-4.79 \pm 2.51

Table D.3: Midtarsal Eversion/Inversion kinematics (joint angles) for Phase 3 of stance. Each cell contains the mean difference in relative orientation over all subjects, all trials and both legs between the barefoot and insole condition.

Midtarsal Eversion(+) / Inversion(-) for P3: Stance phase (43-66%)											
Mean joint angles \pm Standard Deviations											
Bending Stiffness (Nm/rad)											
	10	20	30	40	50	60	70	80	90		
Torsional Stiffness (Nm/rad)	1	-0.9±0	-1.73±1.11	-2.14±1.32	-2.44±1.46	-2.68±1.57	-2.85±1.65	-2.97±1.71	-3.07±1.75	-3.13±1.78	-3.19±1.79
	2	-1.34±0	-2.05±1.31	-2.4±1.48	-2.67±1.59	-2.89±1.68	-3.05±1.76	-3.16±1.82	-3.25±1.86	-3.31±1.88	-3.36±1.89
	3	-1.65±0	-2.28±1.52	-2.6±1.64	-2.85±1.73	-3.06±1.81	-3.21±1.87	-3.32±1.93	-3.4±1.97	-3.46±1.98	-3.51±2
	4	-1.87±0	-2.46±1.74	-2.76±1.81	-2.99±1.88	-3.2±1.94	-3.35±1.99	-3.45±2.05	-3.53±2.08	-3.59±2.1	-3.64±2.1
	5	-2.07±0	-2.62±1.94	-2.9±1.98	-3.12±2.02	-3.32±2.07	-3.47±2.11	-3.58±2.15	-3.65±2.19	-3.71±2.2	-3.76±2.2
	6	-2.24±0	-2.75±2.11	-3.03±2.13	-3.24±2.15	-3.44±2.18	-3.59±2.22	-3.69±2.26	-3.76±2.29	-3.83±2.3	-3.87±2.3

Table D.4: Midtarsal Plantarflexion/Dorsiflexion kinematics (joint angles) for Phase 1 of stance. Each cell contains the mean difference in relative orientation over all subjects, all trials and both legs between the barefoot and insole condition.

Midtarsal Plantarflexion(+) / Dorsiflexion(-) for P1: Stance phase (0-16%)											
Mean joint angles \pm Standard Deviations											
Bending Stiffness (Nm/rad)											
	10	20	30	40	50	60	70	80	90		
Torsional Stiffness (Nm/rad)	1	-0.27±0	-2.23±0.94	-3.13±1.28	-3.73±1.5	-4.13±1.63	-4.41±1.69	-4.59±1.71	-4.75±1.72	-4.87±1.73	-4.97±1.75
	2	-0.47±0	-2.39±1.02	-3.26±1.32	-3.85±1.53	-4.24±1.66	-4.51±1.73	-4.68±1.75	-4.83±1.76	-4.96±1.78	-5.06±1.79
	3	-0.64±0	-2.54±1.07	-3.36±1.37	-3.94±1.56	-4.32±1.69	-4.6±1.77	-4.78±1.79	-4.91±1.79	-5.04±1.82	-5.14±1.83
	4	-0.78±0	-2.63±1.11	-3.45±1.4	-4.02±1.6	-4.4±1.73	-4.67±1.81	-4.84±1.82	-4.99±1.84	-5.11±1.86	-5.22±1.87
	5	-0.89±0	-2.73±1.16	-3.53±1.43	-4.09±1.62	-4.48±1.77	-4.74±1.84	-4.92±1.87	-5.05±1.87	-5.18±1.89	-5.28±1.91
	6	-0.99±0	-2.81±1.2	-3.6±1.46	-4.15±1.65	-4.53±1.78	-4.8±1.87	-4.98±1.9	-5.1±1.9	-5.23±1.92	-5.33±1.93

Table D.5: Midtarsal Plantarflexion/Dorsiflexion kinematics (joint angles) for Phase 2 of stance. Each cell contains the mean difference in relative orientation over all subjects, all trials and both legs between the barefoot and insole condition.

Plantarflexion(+) / Dorsiflexion(-) for P2: Stance phase (17-42%)											
Mean joint angles \pm Standard Deviations											
Bending Stiffness (Nm/rad)											
	10	20	30	40	50	60	70	80	90		
Torsional Stiffness (Nm/rad)	1	-1.94±0.93	-2.81±1.23	-3.39±1.43	-3.77±1.57	-4.02±1.67	-4.18±1.72	-4.27±1.75	-4.35±1.78	-4.41±1.82	
	2	-0.66±0	-2.3±1.1	-3.07±1.33	-3.6±1.51	-3.96±1.65	-4.21±1.76	-4.37±1.82	-4.47±1.85	-4.54±1.88	-4.59±1.91
	3	-0.85±0	-2.41±1.16	-3.16±1.37	-3.69±1.55	-4.04±1.69	-4.29±1.8	-4.45±1.86	-4.55±1.9	-4.62±1.92	-4.67±1.95
	4	-1.01±0	-2.51±1.2	-3.24±1.41	-3.76±1.58	-4.11±1.72	-4.36±1.83	-4.52±1.9	-4.62±1.94	-4.69±1.96	-4.74±1.98
	5	-1.14±0	-2.59±1.25	-3.31±1.45	-3.82±1.61	-4.17±1.75	-4.42±1.87	-4.59±1.94	-4.69±1.98	-4.76±2	-4.81±2.02
	6	-1.25±0	-2.66±1.29	-3.37±1.48	-3.88±1.64	-4.23±1.79	-4.48±1.9	-4.65±1.97	-4.75±2.01	-4.82±2.03	-4.87±2.05

Table D.6: Midtarsal Plantarflexion/Dorsiflexion kinematics (joint angles) for Phase 3 of stance. Each cell contains the mean difference in relative orientation over all subjects, all trials and both legs between the barefoot and insole condition.

Midtarsal Plantarflexion(+) / Dorsiflexion(-) for P3: Stance phase (43-66%)									
Mean joint angles \pm Standard Deviations									
Bending Stiffness (Nm/rad)									
	10	20	30	40	50	60	70	80	90
Torsional Stiffness (Nm/rad)	-1.51 \pm 0.93	-2.22 \pm 1.19	-2.7 \pm 1.35	-3 \pm 1.43	-3.17 \pm 1.46	-3.26 \pm 1.47	-3.33 \pm 1.47	-3.38 \pm 1.48	-3.43 \pm 1.48
	-1.66 \pm 0.96	-2.33 \pm 1.2	-2.81 \pm 1.37	-3.11 \pm 1.45	-3.27 \pm 1.49	-3.37 \pm 1.5	-3.44 \pm 1.51	-3.48 \pm 1.51	-3.53 \pm 1.52
	-0.54 \pm 0	-1.77 \pm 0.98	-2.43 \pm 1.22	-2.9 \pm 1.39	-3.19 \pm 1.47	-3.37 \pm 1.51	-3.46 \pm 1.53	-3.53 \pm 1.54	-3.57 \pm 1.54
	-0.66 \pm 0	-1.86 \pm 1	-2.51 \pm 1.24	-2.98 \pm 1.41	-3.27 \pm 1.5	-3.45 \pm 1.54	-3.54 \pm 1.56	-3.61 \pm 1.57	-3.65 \pm 1.58
	-0.77 \pm 0	-1.94 \pm 1.02	-2.59 \pm 1.25	-3.05 \pm 1.42	-3.34 \pm 1.51	-3.52 \pm 1.56	-3.62 \pm 1.59	-3.68 \pm 1.6	-3.73 \pm 1.6
	-0.85 \pm 0	-2.01 \pm 1.05	-2.65 \pm 1.27	-3.11 \pm 1.44	-3.4 \pm 1.53	-3.58 \pm 1.58	-3.69 \pm 1.61	-3.75 \pm 1.62	-3.79 \pm 1.63
	-0.93 \pm 0	-2.07 \pm 1.07	-2.71 \pm 1.29	-3.17 \pm 1.45	-3.46 \pm 1.55	-3.64 \pm 1.6	-3.74 \pm 1.64	-3.81 \pm 1.65	-3.85 \pm 1.65

Table D.7: Midtarsal Abduction/Adduction kinematics (joint angles) for Phase 1 of stance. Each cell contains the mean difference in relative orientation over all subjects, all trials and both legs between the barefoot and insole condition.

Midtarsal Abduction(+) / Adduction(-) for P1: Stance phase (0-16%)									
Mean joint angles \pm Standard Deviations									
Bending Stiffness (Nm/rad)									
	10	20	30	40	50	60	70	80	90
Torsional Stiffness (Nm/rad)	-0.06 \pm 0.34	0.04 \pm 0.45	0.11 \pm 0.53	0.18 \pm 0.58	0.24 \pm 0.63	0.3 \pm 0.69	0.35 \pm 0.75	0.38 \pm 0.79	0.41 \pm 0.82
	0.25 \pm 0	0.15 \pm 0.45	0.21 \pm 0.54	0.26 \pm 0.6	0.31 \pm 0.64	0.36 \pm 0.69	0.42 \pm 0.75	0.46 \pm 0.8	0.5 \pm 0.84
	0.43 \pm 0	0.32 \pm 0.54	0.35 \pm 0.62	0.38 \pm 0.67	0.43 \pm 0.7	0.47 \pm 0.74	0.52 \pm 0.79	0.56 \pm 0.85	0.59 \pm 0.88
	0.58 \pm 0	0.45 \pm 0.62	0.47 \pm 0.69	0.49 \pm 0.73	0.52 \pm 0.76	0.56 \pm 0.79	0.61 \pm 0.84	0.64 \pm 0.89	0.68 \pm 0.93
	0.7 \pm 0	0.58 \pm 0.69	0.58 \pm 0.75	0.58 \pm 0.79	0.61 \pm 0.81	0.64 \pm 0.84	0.69 \pm 0.89	0.72 \pm 0.93	0.76 \pm 0.97
	0.82 \pm 0	0.68 \pm 0.74	0.67 \pm 0.8	0.67 \pm 0.84	0.69 \pm 0.86	0.72 \pm 0.88	0.76 \pm 0.93	0.79 \pm 0.98	0.83 \pm 1.01
	0.92 \pm 0	0.77 \pm 0.8	0.75 \pm 0.85	0.74 \pm 0.89	0.76 \pm 0.9	0.79 \pm 0.92	0.83 \pm 0.97	0.87 \pm 1.02	0.9 \pm 1.06

Table D.8: Midtarsal Abduction/Adduction kinematics (joint angles) for Phase 2 of stance. Each cell contains the mean difference in relative orientation over all subjects, all trials and both legs between the barefoot and insole condition.

Midtarsal Abduction(+) / Adduction(-) for P2: Stance phase (17-42%)									
Mean joint angles \pm Standard Deviations									
Bending Stiffness (Nm/rad)									
	10	20	30	40	50	60	70	80	90
Torsional Stiffness (Nm/rad)	-0.15 \pm 0.32	-0.21 \pm 0.47	-0.27 \pm 0.56	-0.3 \pm 0.6	-0.33 \pm 0.63	-0.34 \pm 0.66	-0.35 \pm 0.7	-0.37 \pm 0.72	-0.38 \pm 0.75
	0.11 \pm 0	-0.05 \pm 0.45	-0.14 \pm 0.56	-0.21 \pm 0.63	-0.25 \pm 0.67	-0.28 \pm 0.7	-0.3 \pm 0.72	-0.32 \pm 0.75	-0.33 \pm 0.78
	0.19 \pm 0	0.01 \pm 0.55	-0.08 \pm 0.63	-0.16 \pm 0.69	-0.21 \pm 0.73	-0.25 \pm 0.75	-0.27 \pm 0.77	-0.29 \pm 0.8	-0.3 \pm 0.82
	0.25 \pm 0	0.07 \pm 0.62	-0.04 \pm 0.69	-0.12 \pm 0.75	-0.17 \pm 0.77	-0.21 \pm 0.8	-0.24 \pm 0.82	-0.26 \pm 0.84	-0.27 \pm 0.87
	0.31 \pm 0	0.11 \pm 0.68	0.2 \pm 0.75	-0.09 \pm 0.8	-0.14 \pm 0.82	-0.18 \pm 0.84	-0.21 \pm 0.86	-0.23 \pm 0.88	-0.24 \pm 0.91
	0.35 \pm 0	0.16 \pm 0.73	0.04 \pm 0.79	-0.05 \pm 0.84	-0.11 \pm 0.86	-0.15 \pm 0.88	-0.18 \pm 0.9	-0.2 \pm 0.92	-0.22 \pm 0.94
	0.4 \pm 0	0.19 \pm 0.78	0.07 \pm 0.83	-0.02 \pm 0.88	-0.08 \pm 0.9	-0.12 \pm 0.91	-0.16 \pm 0.93	-0.18 \pm 0.95	-0.2 \pm 0.97

Table D.9: Midtarsal Abduction/Adduction kinematics (joint angles) for Phase 3 of stance. Each cell contains the mean difference in relative orientation over all subjects, all trials and both legs between the barefoot and insole condition.

Midtarsal Abduction(+) /Adduction(-) for P3: Stance phase (43-66%)										
Mean joint angles ± Standard Deviations										
Bending Stiffness (Nm/rad)										
	10	20	30	40	50	60	70	80	90	
Torsional Stiffness (Nm/rad)	1 -0.04±0	-0.3±0.71	-0.49±0.93	-0.63±1.08	-0.73±1.05	-0.82±1.15	-0.89±1.24	-0.95±1.29	-1.01±1.35	-1.07±1.41
	2 -0.05±0	-0.3±0.9	-0.49±1.08	-0.63±1.21	-0.74±1.31	-0.83±1.4	-0.9±1.47	-0.97±1.52	-1.03±1.58	-1.09±1.62
	3 -0.06±0	-0.31±1.04	-0.49±1.2	-0.63±1.33	-0.74±1.42	-0.83±1.49	-0.91±1.56	-0.98±1.61	-1.04±1.66	-1.1±1.7
	4 -0.07±0	-0.32±1.16	-0.5±1.31	-0.64±1.42	-0.74±1.5	-0.84±1.58	-0.92±1.64	-0.99±1.69	-1.05±1.73	-1.11±1.78
	5 -0.07±0	-0.32±1.26	-0.5±1.39	-0.64±1.51	-0.75±1.58	-0.84±1.65	-0.92±1.71	-0.99±1.75	-1.05±1.8	-1.11±1.84
	6 -0.07±0	-0.33±1.35	-0.51±1.48	-0.64±1.57	-0.75±1.64	-0.85±1.72	-0.93±1.77	-1±1.81	-1.06±1.85	-1.12±1.9

Table D.10: Tarsometatarsal Eversion/Inversion kinematics (joint angles) for Phase 1 of stance. Each cell contains the mean difference in relative orientation over all subjects, all trials and both legs between the barefoot and insole condition.

Tarsometatarsal Eversion(+) /Inversion(-) for P1: Stance phase (0-16%)										
Mean joint angles ± Standard Deviations										
Bending Stiffness (Nm/rad)										
	10	20	30	40	50	60	70	80	90	
Torsional Stiffness (Nm/rad)	1 -0.29±0	-0.66±0.88	-0.93±0.9	-1.06±1.01	-1.07±1.15	-1.07±1.26	-1.09±1.32	-1.17±1.41	-1.29±1.56	-1.42±1.81
	2 -0.58±0	-0.88±0.97	-1.09±0.97	-1.19±1.06	-1.2±1.19	-1.21±1.3	-1.23±1.36	-1.31±1.44	-1.42±1.6	-1.55±1.83
	3 -0.8±0	-1.04±1.05	-1.21±1.03	-1.3±1.11	-1.31±1.24	-1.32±1.34	-1.35±1.4	-1.42±1.49	-1.54±1.63	-1.67±1.85
	4 -0.98±0	-1.16±1.12	-1.31±1.08	-1.39±1.16	-1.4±1.28	-1.41±1.37	-1.45±1.44	-1.52±1.52	-1.64±1.66	-1.77±1.87
	5 -1.11±0	-1.25±1.18	-1.39±1.13	-1.47±1.2	-1.48±1.31	-1.49±1.41	-1.54±1.47	-1.61±1.56	-1.73±1.69	-1.87±1.9
	6 -1.21±0	-1.33±1.22	-1.46±1.17	-1.54±1.23	-1.54±1.35	-1.56±1.44	-1.61±1.51	-1.7±1.59	-1.81±1.73	-1.96±1.93

Table D.11: Tarsometatarsal Eversion/Inversion kinematics (joint angles) for Phase 2 of stance. Each cell contains the mean difference in relative orientation over all subjects, all trials and both legs between the barefoot and insole condition.

Tarsometatarsal Eversion(+) /Inversion(-) for P2: Stance phase (17-42%)										
Mean joint angles ± Standard Deviations										
Bending Stiffness (Nm/rad)										
	10	20	30	40	50	60	70	80	90	
Torsional Stiffness (Nm/rad)	1 -0.24±0	-0.3±0.49	-0.24±0.64	-0.16±0.86	-0.06±1.36	0.32±1.88	0.61±2.32	0.89±2.69	1.13±3	1.32±3.27
	2 -0.45±0	-0.41±0.57	-0.34±0.7	-0.25±0.9	-0.04±1.37	0.21±1.87	0.48±2.31	0.75±2.66	0.98±2.96	1.16±3.22
	3 -0.58±0	-0.49±0.64	-0.41±0.76	-0.33±0.94	-0.12±1.38	0.12±1.87	0.37±2.29	0.63±2.64	0.84±2.93	1.02±3.18
	4 -0.66±0	-0.56±0.69	-0.48±0.8	-0.39±0.97	-0.19±1.4	0.04±1.86	0.28±2.28	0.52±2.62	0.72±2.89	0.89±3.14
	5 -0.73±0	-0.61±0.75	-0.53±0.85	-0.45±1	-0.25±1.41	-0.02±1.86	0.2±2.27	0.42±2.6	0.62±2.87	0.78±3.11
	6 -0.77±0	-0.66±0.8	-0.58±0.89	-0.49±1.03	-0.31±1.43	-0.08±1.86	0.13±2.25	0.34±2.58	0.52±2.84	0.67±3.08

Table D.12: Tarsometatarsal Eversion/Inversion kinematics (joint angles) for Phase 3 of stance. Each cell contains the mean difference in relative orientation over all subjects, all trials and both legs between the barefoot and insole condition.

Tarsometatarsal Eversion(+) / Inversion(-) for P3: Stance phase (43-66%)										
Mean joint angles \pm Standard Deviations										
Bending Stiffness (Nm/rad)										
	10	20	30	40	50	60	70	80	90	
Torsional Stiffness (Nm/rad)	0.04 \pm 0.41	0.2 \pm 0.64	0.45 \pm 1.16	0.92 \pm 2.13	1.47 \pm 3.05	2.03 \pm 3.87	2.56 \pm 4.57	2.99 \pm 5.04	3.35 \pm 5.36	
	-0.3 \pm 0	-0.11 \pm 0.46	0.06 \pm 0.69	0.32 \pm 1.16	0.77 \pm 2.09	1.29 \pm 3	1.84 \pm 3.8	2.36 \pm 4.5	2.78 \pm 4.95	3.14 \pm 5.28
	-0.44 \pm 0	-0.22 \pm 0.53	-0.04 \pm 0.73	0.21 \pm 1.16	0.65 \pm 2.06	1.15 \pm 2.96	1.67 \pm 3.75	2.18 \pm 4.43	2.59 \pm 4.88	2.94 \pm 5.2
	-0.53 \pm 0	-0.3 \pm 0.59	-0.12 \pm 0.77	0.12 \pm 1.17	0.55 \pm 2.04	1.03 \pm 2.92	1.53 \pm 3.7	2.02 \pm 4.36	2.42 \pm 4.82	2.76 \pm 5.13
	-0.61 \pm 0	-0.37 \pm 0.64	-0.2 \pm 0.81	0.04 \pm 1.18	0.47 \pm 2.02	0.92 \pm 2.89	1.4 \pm 3.66	1.87 \pm 4.3	2.26 \pm 4.76	2.59 \pm 5.07
	-0.67 \pm 0	-0.43 \pm 0.68	-0.26 \pm 0.84	-0.03 \pm 1.19	0.39 \pm 1.99	0.83 \pm 2.85	1.29 \pm 3.62	1.73 \pm 4.25	2.12 \pm 4.71	2.44 \pm 5.01
	-0.72 \pm 0	-0.48 \pm 0.72	-0.31 \pm 0.87	-0.09 \pm 1.2	0.32 \pm 1.97	0.76 \pm 2.82	1.2 \pm 3.58	1.62 \pm 4.2	1.99 \pm 4.66	2.3 \pm 4.96

Table D.13: Tarsometatarsal Plantarflexion/Dorsiflexion kinematics (joint angles) for Phase 1 of stance. Each cell contains the mean difference in relative orientation over all subjects, all trials and both legs between the barefoot and insole condition.

Tarsometatarsal Plantarflexion(+) / Dorsiflexion(-) for P1: Stance phase (0-16%)										
Mean joint angles \pm Standard Deviations										
Bending Stiffness (Nm/rad)										
	10	20	30	40	50	60	70	80	90	
Torsional Stiffness (Nm/rad)	-2.16 \pm 0.95	-3.63 \pm 1.37	-4.79 \pm 1.9	-5.94 \pm 2.74	-7.12 \pm 3.77	-8.34 \pm 4.9	-9.52 \pm 5.94	-10.52 \pm 6.73	-11.47 \pm 7.52	
	-0.08 \pm 0	-2.24 \pm 0.94	-3.68 \pm 1.36	-4.82 \pm 1.89	-5.94 \pm 2.71	-7.1 \pm 3.72	-8.31 \pm 4.85	-9.5 \pm 5.9	-10.48 \pm 6.69	-11.43 \pm 7.48
	-0.12 \pm 0	-2.3 \pm 0.94	-3.71 \pm 1.36	-4.83 \pm 1.88	-5.93 \pm 2.69	-7.09 \pm 3.7	-8.29 \pm 4.81	-9.46 \pm 5.86	-10.44 \pm 6.65	-11.39 \pm 7.43
	-0.16 \pm 0	-2.32 \pm 0.94	-3.72 \pm 1.36	-4.83 \pm 1.87	-5.94 \pm 2.68	-7.07 \pm 3.67	-8.26 \pm 4.77	-9.41 \pm 5.8	-10.41 \pm 6.61	-11.35 \pm 7.38
	-0.2 \pm 0	-2.33 \pm 0.93	-3.72 \pm 1.35	-4.84 \pm 1.87	-5.93 \pm 2.66	-7.06 \pm 3.64	-8.23 \pm 4.73	-9.38 \pm 5.76	-10.38 \pm 6.58	-11.31 \pm 7.34
	-0.22 \pm 0	-2.33 \pm 0.93	-3.72 \pm 1.35	-4.84 \pm 1.87	-5.93 \pm 2.66	-7.04 \pm 3.62	-8.21 \pm 4.7	-9.35 \pm 5.72	-10.35 \pm 6.53	-11.28 \pm 7.3
	-0.23 \pm 0	-2.32 \pm 0.93	-3.71 \pm 1.34	-4.83 \pm 1.87	-5.92 \pm 2.64	-7.02 \pm 3.6	-8.18 \pm 4.66	-9.31 \pm 5.67	-10.32 \pm 6.5	-11.25 \pm 7.26

Table D.14: Tarsometatarsal Plantarflexion/Dorsiflexion kinematics (joint angles) for Phase 2 of stance. Each cell contains the mean difference in relative orientation over all subjects, all trials and both legs between the barefoot and insole condition.

Plantarflexion(+) / Dorsiflexion(-) for P2: Stance phase (17-42%)										
Mean joint angles \pm Standard Deviations										
Bending Stiffness (Nm/rad)										
	10	20	30	40	50	60	70	80	90	
Torsional Stiffness (Nm/rad)	-2.16 \pm 0.95	-3.63 \pm 1.37	-4.79 \pm 1.9	-5.94 \pm 2.74	-7.12 \pm 3.77	-8.34 \pm 4.9	-9.52 \pm 5.94	-10.52 \pm 6.73	-11.47 \pm 7.52	
	-0.08 \pm 0	-2.24 \pm 0.94	-3.68 \pm 1.36	-4.82 \pm 1.89	-5.94 \pm 2.71	-7.1 \pm 3.72	-8.31 \pm 4.85	-9.5 \pm 5.9	-10.48 \pm 6.69	-11.43 \pm 7.48
	-0.12 \pm 0	-2.3 \pm 0.94	-3.71 \pm 1.36	-4.83 \pm 1.88	-5.93 \pm 2.69	-7.09 \pm 3.7	-8.29 \pm 4.81	-9.46 \pm 5.86	-10.44 \pm 6.65	-11.39 \pm 7.43
	-0.16 \pm 0	-2.32 \pm 0.94	-3.72 \pm 1.36	-4.83 \pm 1.87	-5.94 \pm 2.68	-7.07 \pm 3.67	-8.26 \pm 4.77	-9.41 \pm 5.8	-10.41 \pm 6.61	-11.35 \pm 7.38
	-0.2 \pm 0	-2.33 \pm 0.93	-3.72 \pm 1.35	-4.84 \pm 1.87	-5.93 \pm 2.66	-7.06 \pm 3.64	-8.23 \pm 4.73	-9.38 \pm 5.76	-10.38 \pm 6.58	-11.31 \pm 7.34
	-0.22 \pm 0	-2.33 \pm 0.93	-3.72 \pm 1.35	-4.84 \pm 1.87	-5.93 \pm 2.66	-7.04 \pm 3.62	-8.21 \pm 4.7	-9.35 \pm 5.72	-10.35 \pm 6.53	-11.28 \pm 7.3
	-0.23 \pm 0	-2.32 \pm 0.93	-3.71 \pm 1.34	-4.83 \pm 1.87	-5.92 \pm 2.64	-7.02 \pm 3.6	-8.18 \pm 4.66	-9.31 \pm 5.67	-10.32 \pm 6.5	-11.25 \pm 7.26

Table D.15: Tarsometatarsal Plantarflexion/Dorsiflexion kinematics (joint angles) for Phase 3 of stance. Each cell contains the mean difference in relative orientation over all subjects, all trials and both legs between the barefoot and insole condition.

Tarsometatarsal Plantarflexion(+) / Dorsiflexion(-) for P3: Stance phase (43-66%)								
Mean joint angles \pm Standard Deviations								
Bending Stiffness (Nm/rad)								
	10	20	30	40	50	60	70	80
Torsional Stiffness (Nm/rad)	-1.69 \pm 0.77	-2.76 \pm 1.2	-3.71 \pm 1.75	-4.73 \pm 2.66	-5.77 \pm 3.65	-6.78 \pm 4.56	-7.7 \pm 5.35	-8.49 \pm 5.95
1	-0.13 \pm 0	-1.71 \pm 0.76	-2.77 \pm 1.19	-3.71 \pm 1.75	-4.72 \pm 2.63	-5.75 \pm 3.61	-6.74 \pm 4.52	-7.65 \pm 5.31
2	-0.13 \pm 0	-1.72 \pm 0.76	-2.77 \pm 1.19	-3.7 \pm 1.71	-4.7 \pm 2.61	-5.72 \pm 3.58	-6.71 \pm 4.48	-7.61 \pm 5.26
3	-0.12 \pm 0	-1.72 \pm 0.76	-2.77 \pm 1.19	-3.7 \pm 1.7	-4.69 \pm 2.59	-5.7 \pm 3.55	-6.67 \pm 4.45	-7.58 \pm 5.23
4	-0.11 \pm 0	-1.71 \pm 0.76	-2.77 \pm 1.19	-3.69 \pm 1.69	-4.68 \pm 2.57	-5.67 \pm 3.53	-6.64 \pm 4.43	-7.55 \pm 5.2
5	-0.09 \pm 0	-1.71 \pm 0.76	-2.77 \pm 1.19	-3.69 \pm 1.68	-4.67 \pm 2.56	-5.65 \pm 3.5	-6.62 \pm 4.4	-7.52 \pm 5.18
6	-0.07 \pm 0	-1.7 \pm 0.76	-2.76 \pm 1.18	-3.68 \pm 1.68	-4.65 \pm 2.54	-5.63 \pm 3.48	-6.6 \pm 4.38	-7.5 \pm 5.15

Table D.16: Tarsometatarsal Abduction/Adduction kinematics (joint angles) for Phase 1 of stance. Each cell contains the mean difference in relative orientation over all subjects, all trials and both legs between the barefoot and insole condition.

Tarsometatarsal Abduction(+) / Adduction(-) for P1: Stance phase (0-16%)								
Mean joint angles \pm Standard Deviations								
Bending Stiffness (Nm/rad)								
	10	20	30	40	50	60	70	80
Torsional Stiffness (Nm/rad)	-0.62 \pm 0.34	-1.04 \pm 0.54	-1.47 \pm 0.91	-2.02 \pm 1.54	-2.68 \pm 2.3	-3.42 \pm 3.12	-4.13 \pm 3.82	-4.69 \pm 4.29
1	0.1 \pm 0	-0.49 \pm 0.39	-0.94 \pm 0.58	-1.37 \pm 0.92	-1.91 \pm 1.54	-2.56 \pm 2.28	-3.28 \pm 3.08	-3.98 \pm 3.76
2	0.23 \pm 0	-0.39 \pm 0.44	-0.85 \pm 0.61	-1.29 \pm 0.94	-1.83 \pm 1.53	-2.45 \pm 2.26	-3.16 \pm 3.03	-3.86 \pm 3.71
3	0.33 \pm 0	-0.31 \pm 0.48	-0.78 \pm 0.64	-1.22 \pm 0.95	-1.75 \pm 1.54	-2.36 \pm 2.24	-3.05 \pm 3	-3.73 \pm 3.66
4	0.41 \pm 0	-0.24 \pm 0.51	-0.71 \pm 0.66	-1.16 \pm 0.97	-1.68 \pm 1.53	-2.28 \pm 2.24	-2.95 \pm 2.97	-3.63 \pm 3.62
5	0.48 \pm 0	-0.18 \pm 0.54	-0.66 \pm 0.68	-1.11 \pm 0.98	-1.63 \pm 1.53	-2.21 \pm 2.21	-2.87 \pm 2.94	-3.54 \pm 3.58
6	0.53 \pm 0	-0.12 \pm 0.57	-0.61 \pm 0.7	-1.05 \pm 0.99	-1.57 \pm 1.53	-2.15 \pm 2.2	-2.8 \pm 2.91	-3.44 \pm 3.54

Table D.17: Tarsometatarsal Abduction/Adduction kinematics (joint angles) for Phase 2 of stance. Each cell contains the mean difference in relative orientation over all subjects, all trials and both legs between the barefoot and insole condition.

Tarsometatarsal Abduction(+) / Adduction(-) for P2: Stance phase (17-42%)								
Mean joint angles \pm Standard Deviations								
Bending Stiffness (Nm/rad)								
	10	20	30	40	50	60	70	80
Torsional Stiffness (Nm/rad)	-0.64 \pm 0.26	-1.06 \pm 0.46	-1.42 \pm 0.68	-1.88 \pm 1.23	-2.38 \pm 1.85	-2.94 \pm 2.49	-3.5 \pm 3.09	-4.02 \pm 3.63
1	0.05 \pm 0	-0.59 \pm 0.28	-1.01 \pm 0.47	-1.38 \pm 0.69	-1.83 \pm 1.22	-2.32 \pm 1.84	-2.86 \pm 2.46	-3.42 \pm 3.06
2	0.12 \pm 0	-0.55 \pm 0.31	-0.98 \pm 0.48	-1.34 \pm 0.7	-1.79 \pm 1.22	-2.27 \pm 1.83	-2.8 \pm 2.44	-3.35 \pm 3.03
3	0.17 \pm 0	-0.52 \pm 0.33	-0.95 \pm 0.5	-1.31 \pm 0.7	-1.76 \pm 1.21	-2.23 \pm 1.81	-2.74 \pm 2.42	-3.28 \pm 3
4	0.21 \pm 0	-0.49 \pm 0.34	-0.92 \pm 0.51	-1.29 \pm 0.71	-1.73 \pm 1.2	-2.19 \pm 1.8	-2.7 \pm 2.4	-3.22 \pm 2.98
5	0.24 \pm 0	-0.47 \pm 0.36	-0.94 \pm 0.52	-1.26 \pm 0.72	-1.7 \pm 1.2	-2.16 \pm 1.79	-2.66 \pm 2.39	-3.17 \pm 2.96
6	0.27 \pm 0	-0.45 \pm 0.38	-0.88 \pm 0.53	-1.24 \pm 0.72	-1.67 \pm 1.2	-2.13 \pm 1.78	-2.62 \pm 2.37	-3.12 \pm 2.93

Table D.18: Tarsometatarsal Abduction/Adduction kinematics (joint angles) for Phase 3 of stance. Each cell contains the mean difference in relative orientation over all subjects, all trials and both legs between the barefoot and insole condition.

Tarsometatarsal Abduction(+) /Adduction(-) for P3: Stance phase (43-66%)								
Mean joint angles \pm Standard Deviations								
Bending Stiffness (Nm/rad)								
	10	20	30	40	50	60	70	80
	-0.55 \pm 0.26	-0.94 \pm 0.44	-1.31 \pm 0.67	-1.74 \pm 1.12	-2.22 \pm 1.63	-2.71 \pm 2.14	-3.17 \pm 2.65	-3.58 \pm 3.09
Torsional Stiffness (Nm/rad)	1 -0.04 \pm 0	-0.55 \pm 0.32	-0.93 \pm 0.47	-1.3 \pm 0.69	-1.72 \pm 1.13	-2.18 \pm 1.62	-2.67 \pm 2.12	-3.13 \pm 2.62
	2 -0.04 \pm 0	-0.55 \pm 0.39	-0.93 \pm 0.52	-1.28 \pm 0.71	-1.7 \pm 1.14	-2.16 \pm 1.62	-2.64 \pm 2.11	-3.1 \pm 2.6
	3 -0.03 \pm 0	-0.54 \pm 0.45	-0.92 \pm 0.55	-1.27 \pm 0.73	-1.69 \pm 1.15	-2.13 \pm 1.62	-2.6 \pm 2.1	-3.06 \pm 2.58
	4 -0.02 \pm 0	-0.54 \pm 0.5	-0.91 \pm 0.59	-1.26 \pm 0.75	-1.67 \pm 1.16	-2.11 \pm 1.62	-2.57 \pm 2.09	-3.03 \pm 2.56
	5 -0.01 \pm 0	-0.53 \pm 0.54	-0.91 \pm 0.62	-1.25 \pm 0.77	-1.66 \pm 1.17	-2.09 \pm 1.62	-2.55 \pm 2.09	-3 \pm 2.55
	6 0 \pm 0	-0.52 \pm 0.57	-0.9 \pm 0.64	-1.24 \pm 0.79	-1.65 \pm 1.17	-2.07 \pm 1.62	-2.53 \pm 2.09	-2.97 \pm 2.54
								-3.39 \pm 2.96
								-3.75 \pm 3.3

Bibliography

- [1] *Observational Gait Analysis Handbook*. Pathokinesiology Department & the Physical Therapy Department, Rancho Los Amigos Medical Center, 1989.
- [2] ACKERMANN, M., AND SCHIEHLEN, W. Dynamic analysis of human gait disorder and metabolical cost estimation. *Archive of Applied Mechanics* 75 (2006), 569–594.
- [3] ACKERMANN, M., AND VAN DEN BOGERT, A. J. Optimality principles for model-based prediction of human gait. *Journal of Biomechanics* 43, 6 (apr 2010), 1055–1060.
- [4] ACKERMANN, M., AND VAN DEN BOGERT, A. J. Predictive simulation of gait in rehabilitation. *2010 Annual International Conference of the IEEE Engineering in Medicine and Biology Society, EMBC'10*, 3 (2010), 5444–5447.
- [5] AERTS, W., DE GROOTE, F., VANDER SLOTHEN, J., AND JONKERS, I. Modeling foot-ground interaction with foot surface contour and elastic foundation modeling. In *International Symposium on Computer Methods in Biomechanics and Biomedical Engineering* (Salt Lake City, Utah, US, 2013).
- [6] ALIREZAEI NOGHONDAR, F., AND BRESSEL, E. Effect of shoe insole density on impact characteristics and performance during a jump-landing task. *Footwear Science* 9, 2 (2017), 95–101.
- [7] ALKJAER, T., SIMONSEN, E. B., AND DYHRE-POULSEN, P. Comparison of inverse dynamics calculated by two- and three-dimensional models during walking. *Gait & Posture* 13, 2 (apr 2001), 73–7.
- [8] ALONSO-VÁZQUEZ, A., VILLARROYA, M. A., FRANCO, M. A., ASÍ, J., AND CALVO, B. Kinematic assessment of paediatric forefoot varus. *Gait & Posture* 29, 2 (2009), 214–219.

- [9] AMIROUCHE, F. M., IDER, S. K., AND TRIMBLE, J. Analytical method for the analysis and simulation of human locomotion. *Journal of Biomechanical Engineering* 112, November 1990 (1990), 379–386.
- [10] ANDERSEN, H., GADEBERG, P. C., BROCK, B., AND JAKOBSEN, J. Muscular atrophy in diabetic neuropathy : a stereological magnetic resonance imaging study. *Diabetologia* 40 (1997), 1062–1069.
- [11] ANDERSON, F. C., AND PANDY, M. G. A Dynamic Optimization Solution for Vertical Jumping in Three Dimensions. *Computer Methods in Biomechanics and Biomedical Engineering* 2, 3 (1999), 201–231.
- [12] ANDERSON, F. C., AND PANDY, M. G. Dynamic Optimization of Human Walking. *Journal of Biomechanical Engineering* 123, 5 (2001), 381–90.
- [13] ANDERSON, F. C., AND PANDY, M. G. Individual muscle contributions to support in normal walking. *Gait & Posture* 17 (2003), 159–169.
- [14] AOI, S., OGIHARA, N., SUGIMOTO, Y., AND TSUCHIYA, K. Simulating Adaptive Human Bipedal Locomotion Based on Phase Resetting Using Foot-Contact Information. *Advanced Robotics* 22 (2008), 1697–1713.
- [15] ARANGIO, G. A., REINERT, K. L., AND SALATHE, E. P. A biomechanical model of the effect of subtalar arthroereisis on the adult flexible flat foot. *Clinical Biomechanics* 19 (2004), 847–852.
- [16] ARMSTRONG, D. G., PETERS, E. J., ATHANASIOU, K. A., AND LAVERY, L. A. Is there a critical level of plantar foot pressure to identify patients at risk for neuropathic foot ulceration? *Journal of Foot and Ankle Surgery* 37, 4 (1998), 303–307.
- [17] ARNDT, A., WOLF, P., LIU, A., NESTER, C., STACOFF, A., JONES, R., LUNDGREN, P., AND LUNDBERG, A. Intrinsic foot kinematics measured in vivo during the stance phase of slow running. *Journal of Biomechanics* 40, 12 (2007), 2672–2678.
- [18] BAKER, R., AND ROBB, J. Foot models for clinical gait analysis. *Gait & Posture* 23 (2006), 399–400.
- [19] BANWELL, H. A., MACKINTOSH, S., AND THEWLIS, D. Foot orthoses for adults with flexible pes planus: a systematic review. *Journal of Foot and Ankle Research* 7, 23 (2014).
- [20] BATES, B. T., OSTERNIG, L. R., MASON, B., AND JAMES, L. S. Foot orthotic devices to modify selected aspects of lower extremity mechanics. *The American Journal of Sports Medicine* 7, 6 (1979), 338–342.

- [21] BEK, N., KINIKLI, G. I., CALLAGHAN, M. J., AND ATAY, O. A. Foot biomechanics and initial effects of infrapatellar strap on gait parameters in patients with unilateral patellofemoral pain syndrome. *The Foot* 21 (2011), 114–118.
- [22] BERTANI, A., CAPPELLO, A., BENEDETTI, M. G., SIMONCINI, L., AND CATANI, F. Flat foot functional evaluation using pattern recognition of ground reaction data. *Clinical Biomechanics* 14 (1999), 484–493.
- [23] BESL, P., AND MCKAY, N. A Method for Registration of 3-D Shapes, 1992.
- [24] BIRKE, J. A., FOTO, J. G., AND PFIEFER, L. A. Effect of orthosis material hardness on walking pressure in high-risk diabetes patients. *Journal of Prosthetics and Orthotics* 11, 2 (1999), 43–46.
- [25] BISHOP, C., ARNOLD, J. B., AND MAY, T. Effects of taping and orthoses on foot biomechanics in adults with flat-arched feet. *Medicine & Science in Sports & Exercise* 48, 4 (2016), 689–696.
- [26] BITSAKOS, C., KERNER, J., FISHER, I., AND AMIS, A. A. The effect of muscle loading on the simulation of bone remodelling in the proximal femur. *Journal of Biomechanics* 38 (2005), 133–139.
- [27] BLAJER, W., AND CZAPLICKI, A. Contact Modeling and Identification of Planar Somersaults on the Trampoline. *Multibody System Dynamics* 10 (2003), 289–312.
- [28] BLAJER, W., DZIEWIECKI, K., AND MAZUR, Z. Multibody modeling of human body for the inverse dynamics analysis of sagittal plane movements. *Multibody System Dynamics* 18, 2 (2007), 217–232.
- [29] BLANKEVOORT, L., AND HUISKES, H. W. J. Ligament-bone interaction in a three-dimensional model of the knee. *Journal of Biomechanical Engineering: Transactions of the ASME* 113, 3 (1991), 263–269.
- [30] BLANKEVOORT, L., AND HUISKES, R. Validation of a three-dimensional model of the knee. *Journal of Biomechanics* 29, 7 (1996), 955–961.
- [31] BLANKEVOORT, L., HUISKES, R., AND LANGE, A. The envelope of passive knee joint motion. *Journal of Biomechanics* 21, 9 (1988), 705–720.
- [32] BLANKEVOORT, L., KUIPER, J. H., HUISKES, R., AND GROOTENBOER, H. J. Articular contact in a three-dimensional model of the knee. *Journal of Biomechanics* 24, 11 (1991), 1019–1031.

- [33] BOERUM, D. H. V., AND SANGEORZAN, B. J. Biomechanics and pathophysiology of flat foot. *Foot and Ankle Clinics of North America* 8 (2003), 419–430.
- [34] BRODSKY, J. W., KOUROSH, S., STILLS, M., AND MOONEY, V. Objective Evaluation of Insert Material for Diabetic and Athletic Footwear. *Foot & Ankle International* 9, 3 (1988), 111–116.
- [35] BRODSKY, J. W., POLLO, F. E., CHELEUITTE, D., AND BAUM, B. S. Physical Properties, Durability, and Energy-Dissipation Function of Dual-Density Orthotic Materials Used in Insoles for Diabetic Patients. *Foot & Ankle International* 21, 6 (2009), 238.
- [36] BROWN, G. P., DONATELLI, R., CATLIN, P. A., AND WOODEN, M. J. The effect of two types of foot orthoses on rearfoot mechanics. *The Journal of Orthopaedic & Sports Physical Therapyorthopaedic* 21, 5 (1995), 258–267.
- [37] BRUENING, D. A., COONEY, K. M., AND BUCZEK, F. L. Analysis of a kinetic multi-segment foot model part I: Model repeatability and kinematic validity. *Gait & Posture* 35, 4 (2012), 529–34.
- [38] BRUENING, D. A., COONEY, K. M., AND BUCZEK, F. L. Analysis of a kinetic multi-segment foot model part II: kinetics and clinical implications. *Gait & Posture* 35, 4 (2012), 535–540.
- [39] BURG, J. *Biomechanics of the foot-ankle complex before and after total ankle arthroplasty: An in vivo and in vitro analysis*. Ph.d. thesis, KU Leuven, 2014.
- [40] BURNS, J., BEGG, L., AND VICARETTI, M. Comparison of Orthotic Materials on Foot Pain, Comfort, and Plantar Pressure in the Neuroischemic Diabetic Foot. *Journal of the American Podiatric Medical Association* 98, 2 (2008), 143–148.
- [41] BURNS, J., CROSBIE, J., OUVRIER, R., AND HUNT, A. Effective Orthotic Therapy for the Painful Cavus Foot. *Journal of the American Podiatric Medical Association* 96, 3 (2006), 205–211.
- [42] BUS, S. A., HASPELS, R., AND BUSCH-WESTBROEK, T. E. Evaluation and optimization of therapeutic footwear for neuropathic diabetic foot patients using in-shoe plantar pressure analysis. *Diabetes Care* 34, 7 (2011), 1595–1600.
- [43] BUS, S. A., VALK, G. D., VAN DEURSEN, R. W., ARMSTRONG, D. G., CARAVAGGI, C. P., HLAVACEK, P., BAKKER, K., CAVANAGH,

- P. R., AND 1DEPARTMENT. The effectiveness of footwear and offloading interventions to prevent and heal foot ulcers and reduce plantar pressure in diabetes: a systematic review. *Diabetes/Metabolism Research and Reviews* 24, 1 (2008), 162–180.
- [44] CAMACHO, D. L., LEDOUX, W. R., ROHR, E. S., SANGEORZAN, B. J., AND CHING, R. P. A three-dimensional, anatomically detailed foot model: a foundation for a finite element simulation and means of quantifying foot-bone position. *Journal of Rehabilitation Research and Development* 39, 3 (2002), 401–410.
- [45] CAMPBELL, G., NEWELL, E., AND MCLURE, M. Compression testing of foamed plastics and rubbers for use as orthotic shoe insoles. *Prosthetics and Orthotics International* 6, 1 (1982), 48–52.
- [46] CANSECO, K., LONG, J., MARKS, R., KHAZZAM, M., AND HARRIS, G. Quantitative characterization of gait kinematics in patients with hallux rigidus using the Milwaukee foot model. *Journal of Orthopaedic Research* 26, 4 (2008), 419–27.
- [47] CANSECO, K., LONG, J., MARKS, R., KHAZZAM, M., AND HARRIS, G. Quantitative motion analysis in patients with hallux rigidus before and after cheilectomy. *Journal of Orthopaedic Research* 27, 1 (2009), 128–34.
- [48] CAPPOZZO, A., LEO, T., AND PEDOTTI, A. A general computing method for the analysis of human locomotion. *Journal of Biomechanics* 8 (1975), 307–320.
- [49] CARAVAGGI, P., SFORZA, C., LEARDINI, A., PORTINARO, N., AND PANOU, A. Effect of plano-valgus foot posture on midfoot kinematics during barefoot walking in an adolescent population. *Journal of Foot and Ankle Research* 11, 1 (2018), 1–9.
- [50] CARSON, M. C., HARRINGTON, M. E., THOMPSON, N., O'CONNOR, J. J., AND THEOLOGIS, T. N. Kinematic analysis of a multi-segment foot model for research and clinical applications: a repeatability analysis. *Journal of Biomechanics* 34, 10 (2001), 1299–307.
- [51] CARSON, M. C., HARRINGTON, M. E., THOMPSON, N., O'CONNOR, J. J., AND THEOLOGIS, T. N. Kinematic analysis of a multi-segment foot model for research and clinical applications: a repeatability analysis. *Journal of biomechanics* 34, 10 (2001), 1299–307.
- [52] CASELLI, M. A. Orthoses, materials, and foot function. *Podiatry Management* 23, September (2004), 131–138.

- [53] CASTRO-MÉNDEZ, A., MUNUERA, P. V., AND ALBORNOZ-CABELLO, M. The short-term effect of custom-made foot orthoses in subjects with excessive foot pronation and lower back pain: A randomized, double-blinded, clinical trial. *Prosthetics and Orthotics International* 37, 5 (2013), 384–390.
- [54] CHATZISTERGOS, P. E., NAEMI, R., AND CHOOCKALINGAM, N. A method for subject-specific modelling and optimisation of the cushioning properties of insole materials used in diabetic footwear. *Medical Engineering and Physics* 37, 6 (2015), 531–538.
- [55] CHATZISTERGOS, P. E., NAEMI, R., HEALY, A., GERTH, P., AND CHOOCKALINGAM, N. Subject Specific Optimisation of the Stiffness of Footwear Material for Maximum Plantar Pressure Reduction. *Annals of Biomedical Engineering* 45, 8 (2017), 1929–1940.
- [56] CHEN, W. P., JU, C. W., AND TANG, F. T. Effects of total contact insoles on the plantar stress redistribution: A finite element analysis. *Clinical Biomechanics* 18, 6 (2003), 17–24.
- [57] CHEN, Y. C., LOU, S. Z., HUANG, C. Y., AND SU, F. C. Effects of foot orthoses on gait patterns of flat feet patients. *Clinical Biomechanics* 25, 3 (2010), 265–270.
- [58] CHEUNG, J. T. M., AND ZHANG, M. A 3-dimensional finite element model of the human foot and ankle for insole design. *Archives of Physical Medicine and Rehabilitation* 86, February (2005), 353–358.
- [59] CHEUNG, J. T. M., AND ZHANG, M. Parametric design of pressure-relieving foot orthosis using statistics-based finite element method. *Medical Engineering and Physics* 30, 3 (2008), 269–277.
- [60] CHEUNG, J. T. M., ZHANG, M., LEUNG, A. K. L., AND FAN, Y. B. Three-dimensional finite element analysis of the foot during standing - A material sensitivity study. *Journal of Biomechanics* 38 (2005), 1045–1054.
- [61] CHOW, C., AND JACOBSON, D. Studies of human locomotion via optimal programming. *Mathematical Biosciences* 10 (1971), 239–306.
- [62] CHU, T.-M., AND REDDY, N. P. Stress distribution in the ankle-foot orthosis used to correct pathological gait. *Journal of Rehabilitation Research and Development* 32, 4 (1995), 349–360.
- [63] COBB, S. C., TIS, L. L., JOHNSON, J. T., TAI, Y., GEIL, M. D., AND MCCARTY, F. A. The effect of low-mobile foot posture on multi-segment medial foot model gait kinematics. *Gait & Posture* 30 (2009), 334–339.

- [64] COBB, S. C., TIS, L. L., JOHNSON, J. T., WANG, Y. T., AND GEIL, M. D. Custom-molded foot-orthosis intervention and multisegment medial foot kinematics during walking. *Journal of Athletic Training* 46, 4 (2011), 358–365.
- [65] CORNWALL, M. W., AND MCPHAIL, T. G. Footwear and Foot Orthotic Effectiveness Research: A New Approach. *Journal of Orthopaedic & Sports Physical Therapy* 21, 6 (1995), 337–344.
- [66] CURRYER, M., AND LEMAIRE, E. D. Effectiveness of various materials in reducing plantar shear forces. A pilot study. *Journal of the American Podiatric Medical Association* 90, 7 (2000), 346–353.
- [67] DAHMEN, R., HASPELS, R., KOOMEN, B., AND HOEKSMA, A. Therapeutic Footwear for the Neuropathic Foot: An Algorithm. *Diabetes Care* 24, 4 (2016), 705–709.
- [68] DAVIS, I. S. The Re-emergence of the Minimal Running Shoe. *Journal of Orthopaedic & Sports Physical Therapy* 44, 10 (2014), 775–784.
- [69] DAVY, D. T., AND AUDU, M. L. A dynamic optimization technique for predicting muscle forces in the swing phase of gait. *Journal of Biomechanics* 20, 2 (1987), 187–201.
- [70] DE GROOTE, F., DE LAET, T., JONKERS, I., AND DE SCHUTTER, J. Kalman smoothing improves the estimation of joint kinematics and kinetics in marker-based human gait analysis. *Journal of Biomechanics* 41 (2008), 3390–3398.
- [71] DELP, S. L., ANDERSON, F. C., ARNOLD, A. S., LOAN, P., HABIB, A., JOHN, C. T., GUENDELMAN, E., AND THELEN, D. G. OpenSim: Open-source software to create and analyze dynamic simulations of movement. *IEEE Transactions on Biomedical Engineering* 54, 11 (2007), 1940–1950.
- [72] DELP, S. L., LOAN, J. P., HOY, M. G., AND ZAJAC, F. E. An interactive Graphics-Based Model of the Lower Extremity to Study Orthopaedic Surgical Procedures. *IEEE Transactions on Biomedical Engineering* 37, 8 (1990), 757 – 767.
- [73] DESCHAMPS, K., STAES, F., ROOSE, P., NOBELS, F., DESLOOVERE, K., BRUYNINCKX, H., AND MATRICALI, G. A. Body of evidence supporting the clinical use of 3D multisegment foot models: a systematic review. *Gait & Posture* 33, 3 (2011), 338–49.
- [74] DESMYTTERE, G., HAJIZADEH, M., BLEAU, J., AND BEGON, M. Effect of foot orthosis design on lower limb joint kinematics and kinetics during

- walking in flexible pes planovalgus: A systematic review and meta-analysis. *Clinical Biomechanics* 59, September (2018), 117–129.
- [75] DI MARCO, R., ROSSI, S., RACIC, V., CAPPA, P., AND MAZZÀ, C. Concurrent repeatability and reproducibility analyses of four marker placement protocols for the foot-ankle complex. *Journal of Biomechanics* 49, 14 (2016), 3168–3176.
- [76] DIXON, S. J., WATERWORTH, C., SMITH, C. V., AND HOUSE, C. M. Biomechanical analysis of running in military boots with new and degraded insoles. *Medicine and Science in Sports and Exercise* 35, 3 (2003), 472–479.
- [77] DUERINCK, S. *Biomechanics of the ankle-foot complex: Consequences of restricted gait*. Ph.d. thesis, Vrije Universiteit Brussel, 2015.
- [78] DUERINCK, S., HAGMAN, F., JONKERS, I., ROY, P. V., AND VAES, P. Forefoot deformation during stance : Does the forefoot collapse during loading? *Gait & Posture* 39, 1 (2014), 40–47.
- [79] ELLIS, S. J., YU, J. C., JOHNSON, A. H., ELLIOTT, A., MALLEY, M. O., AND DELAND, J. Plantar Pressures in Patients with and without Lateral Foot Pain After Lateral Column Lengthening. *The Journal of Bone & Joint Surgery* 92, 1 (2010), 81–91.
- [80] ENG, J. J., AND WINTER, D. A. Kinetic Analysis of the Lower Limbs During Walking : What Information can be gained from a Three-Dimensional Model? *Journal of Biomechanics* 28, 6 (1995).
- [81] FARVID, M. S., NG, T. W. K., CHAN, D. C., BARRETT, P. H. R., AND WATTS, G. F. Association of adiponectin and resistin with adipose tissue compartments, insulin resistance and dyslipidaemia. *Diabetes, Obesity and Metabolism* 7 (2005), 406–413.
- [82] FAULÍ, A. C., ANDRÉS, C. L., ROSAS, N. P., FERNÁNDEZ, M. J., PARREÑO, E. M., AND BARCELÓ, C. O. Physical evaluation of insole materials used to treat the diabetic foot. *Journal of the American Podiatric Medical Association* 98, 3 (2008), 229–38.
- [83] FINDLOW, A., GOULERMAS, J. Y., NESTER, C., HOWARD, D., AND KENNEY, L. P. J. Predicting lower limb joint kinematics using wearable motion sensors. *Gait & Posture* 28, 1 (2008), 120–126.
- [84] FORNER, A., GARCIA, A. C., ALCANTARA, E., RAMIRO, J., HOYOS, J. V., AND VERA, P. Properties of shoe insert materials related to shock wave transmission during gait. *Foot and Ankle International* 16, 12 (1995), 778–786.

- [85] FOTO, J. G., AND BIRKE, J. A. Evaluation of multidensity orthotic materials used in footwear for patients with diabetes. *Foot & Ankle International* 19, 12 (1998), 836–841.
- [86] FRANCO, A. H. Pes Cavus and Pes Planus Analyses and Treatment. *Physical Therapy* 67, 5 (1986), 688–694.
- [87] FRANKLYN-MILLER, A., BILZON, J., WILSON, C., AND MCCRORY, P. Can RSScan footscan D3D software predict injury in a military population following plantar pressure assessment ? A prospective cohort study. *The Foot* 24, 1 (2014), 6–10.
- [88] FREGLY, B. J., BEI, Y., AND SYLVESTER, M. E. Experimental evaluation of an elastic foundation model to predict contact pressures in knee replacements. *Journal of Biomechanics* 36 (2003), 1659–1668.
- [89] FREGLY, B. J., AND ZAJAC, F. E. A state-space analysis of mechanical energy generation, absorption, and transfer during pedaling. *Journal of Biomechanics* 29 (1996), 81–90.
- [90] GARCIA, A. C., DURA, J. V., RAMIRO, J., HOYOS, J. V., AND VERA, P. Dynamic study of insole materials simulating real loads. *Foot & Ankle International* 15, 6 (1994), 311–323.
- [91] GEFEN, A. Plantar soft tissue loading under the medial metatarsals in the standing diabetic foot. *Medical Engineering and Physics* 25, 6 (2003), 491–499.
- [92] GEFEN, A., MEGIDO-RAVID, M., ITZCHAK, Y., AND ARCAN, M. Biomechanical analysis of the three-dimensional foot structure during gait: a basic tool for clinical applications. *Journal of Biomechanical Engineering* 122, December 2000 (2000), 630–639.
- [93] GIACOMOZZI, C. Potentialities and Criticalities of Plantar Pressure Measurements in the Study of Foot Biomechanics : Devices , Methodologies and Applications. In *Biomechanics in Applications*, V. Klika, Ed. InTech, 2011, ch. 11.
- [94] GIACOMOZZI, C., BENEDETTI, M. G., LEARDINI, A., MACELLARI, V., AND GIANNINI, S. Gait Analysis with an Integrated System for Functional Assessment of Talocalcaneal Coalition. *Journal of the American Podiatric Medical Association* 96, 2 (2006), 107–115.
- [95] GIACOMOZZI, C., AND MACELLARI, V. Piezo-dynamometric platform for a more complete analysis of foot-to- floor interaction. *IEEE Transactions on Rehabilitation Engineering* 5, 4 (1997), 322–330.

- [96] GILCHRIST, L. A., AND WINTER, D. A. A two part, viscoelastic model for use in gait simulations. *Journal of Biomechanics* 29, 6 (1996), 795–798.
- [97] GILCHRIST, L. A., AND WINTER, D. A. A Multisegment Computer Simulation of Normal Human Gait. *IEEE Transactions on Rehabilitation Engineering* 5, 4 (1997), 290–299.
- [98] GOLIGHTLY, Y. M., HANNAN, M. T., DUFOUR, A. B., AND JORDAN, J. M. Racial differences in foot disorders and foot type. *Arthritis Care and Research* 64, 11 (2012), 1756–1759.
- [99] GOULD, N. Evaluation of Hyperpronation and Pes Planus in Adults. *Clinical Orthopaedics and Related Research* 181 (1983), 38–45.
- [100] GULDEMOND, N. A., LEFFERS, P., SCHAPER, N. C., SANDERS, A. P., NIEMAN, F., WILLEMS, P., AND WALENKAMP, G. H. I. M. The effects of insole configurations on forefoot plantar pressure and walking convenience in diabetic patients with neuropathic feet. *Clinical Biomechanics* 22, 1 (2007), 81–87.
- [101] GÜNER, S., ALSANCAK, S., ALTINKAYNAK, H., AND GÜVEN, E. Effects of Different Low-Density Insoles on Foot Activation Time at Different Walking Speeds in Young Females. *Physical Medicine and Rehabilitation - International* 5, 2 (2018).
- [102] HAGMAN, F. *Can plantar pressure predict foot motion?* Phd thesis, Technische Universiteit Eindhoven, 2005.
- [103] HARDT, D. E. Determining muscle forces in the leg during normal human walking - An application and evaluation of optimization methods. *Journal of Biomechanical Engineering* 100 (1978), 72–78.
- [104] HATZE, H. The complete optimization of a human motion. *Mathematical Biosciences* 28 (1976), 99–135.
- [105] HATZE, H. A comprehensive model for human motion simulation and its application to the take-off phase of the long jump. *Journal of Biomechanics* 14, 3 (1981), 135–142.
- [106] HAZARI, A., MAIYA, A. G., SHIVASHANKARA, K. N., AGOURIS, I., MONTEIRO, A., JADHAV, R., KUMAR, S., KUMAR, C. G. S., AND MAYYA, S. S. Kinetics and kinematics of diabetic foot in type 2 diabetes mellitus with and without peripheral neuropathy : a systematic review and meta - analysis. *SpringerPlus* 5, 1, 1819 (2016).
- [107] HEALY, A., DUNNING, D. N., AND CHOCKALINGAM, N. Materials used for footwear orthoses: A review. *Footwear Science* 2, 2 (2010), 93–110.

- [108] HICKS, J. H. The Mechanics of the Foot I-The Joints. *Journal of Anatomy* 87, 4 (1953), 345–357.
- [109] HILLS, A. P., HENNIG, E. M., McDONALD, M., AND BAR-OR, O. Plantar pressure differences between obese and non-obese adults: a biomechanical analysis. *International Journal of Obesity* 25 (2001), 1674–1679.
- [110] HINMAN, R. S., AND BENNELL, K. L. Advances in insoles and shoes for knee osteoarthritis. *Current Opinion in Rheumatology* 21, 2 (2009), 164–170.
- [111] HINMAN, R. S., BOWLES, K. A., PAYNE, C., AND BENNELL, K. L. Effect of length on laterally-wedged insoles in knee osteoarthritis. *Arthritis Care and Research* 59, 1 (2008), 144–147.
- [112] HINMAN, R. S., PAYNE, C., METCALF, B. R., WRIGLEY, T. V., AND BENNELL, K. L. Lateral wedges in knee osteoarthritis: What are their immediate clinical and biomechanical effects and can these predict a three-month clinical outcome? *Arthritis Care and Research* 59, 3 (2008), 408–415.
- [113] HIRASAKI, E., HIGURASHI, Y., AND KUMAKURA, H. Dynamic Plantar Pressure Distribution during Locomotion in Japanese Macaques (*Macaca fuscata*). *American Journal of Physical Anthropology* 142 (2010), 149–156.
- [114] HODGE, M. C., BACH, T. M., AND CARTER, G. M. Orthotic management of plantar pressure and pain in rheumatoid arthritis. *Clinical Biomechanics* 14, 8 (1999), 567–575.
- [115] HOLLMAN, J. H., McDADE, E. M., AND PETERSEN, R. C. Normative spatiotemporal gait parameters in older adults. *Gait & Posture* 34, 1 (2011), 111–118.
- [116] HÖSL, M., BÖHM, H., MULTERER, C., AND DÖDERLEIN, L. Does excessive flatfoot deformity affect function? A comparison between symptomatic and asymptomatic flatfeet using the Oxford Foot Model. *Gait & Posture* 39, 1 (2014), 23–28.
- [117] HOUSE, C. M., WATERWORTH, C., ALLSOPP, A. J., AND DIXON, S. J. The influence of simulated wear upon the ability of insoles to reduce peak pressures during running when wearing military boots. *Gait & Posture* 16, 3 (2002), 297–303.
- [118] HSI, W. L., KANG, J. H., AND LEE, X. X. Optimum position of metatarsal pad in metatarsalgia for pressure relief. *American Journal of Physical Medicine and Rehabilitation* 84, 7 (2005), 514–520.

- [119] HUNT, A. E., AND SMITH, R. M. Mechanics and control of the flat versus normal foot during the stance phase of walking. *Clinical Biomechanics* 19, 4 (2004), 391–397.
- [120] HUNT, K. H., AND CROSSLEY, F. R. E. Coefficient of Restitution Interpreted as Damping in Vibroimpact. *Journal of Applied Mechanics* 42, 2 (1975), 440–445.
- [121] HURD, W. J., KAVROS, S. J., AND KAUFMAN, K. R. Comparative biomechanical effectiveness of over-the-counter devices for individuals with a flexible flatfoot secondary to forefoot varus. *Clinical Journal of Sport Medicine* 20, 6 (2010), 428–435.
- [122] HUTCHISON, L., SCHARFBILLIG, R., UDEN, H., AND BISHOP, C. The effect of footwear and foot orthoses on transverse plane knee motion during running - A pilot study. *Journal of Science and Medicine in Sport* 18, 6 (2015), 748–752.
- [123] JANISSE, D. J. A scientific approach to insole design for the diabetic foot. *The Foot* 3, 3 (1993), 105–108.
- [124] JANISSE, D. J., AND JANISSE, E. Shoe modification and the use of orthoses in the treatment of foot and ankle pathology. *Journal of the American Academy of Orthopaedic Surgeons* 16, 3 (2008), 152–158.
- [125] JANISSE, D. J., AND JANISSE, E. J. Pedorthic and Orthotic Management of the Diabetic Foot. *Foot and Ankle Clinics* 11, 4 (2006), 717–734.
- [126] JOHANSON, M. A., DONATELLI, R., WOODEN, M. J., ANDREW, P. D., AND CUMMINGS, G. S. Effects of Three Different Posting Methods on Controlling Abnormal Subtalar Pronation. *Physical Therapy* 74, 2 (1994), 149–158.
- [127] KARADAG-SAYGI, E., UNLU-OZKAN, F., AND BASGUL, A. Plantar Pressure and Foot Pain in the Last Trimester of Pregnancy. *Foot & Ankle International* 31, 2 (2010), 153–157.
- [128] KAUTZ, S. A., AND HULL, M. L. Dynamic optimization analysis for equipment setup problems in endurance cycling. *Journal of Biomechanics* 28, Ii (1995), 1391–1401.
- [129] KELIKIAN, A. S., AND SARRAFIAN, S. K. *Sarrafian's Anatomy of the Foot and Ankle: Descriptive, Topographic, Functional*. M - Medicine Series. Lippincott Williams & Wilkins, Philadelphia, 1983.

- [130] KENDELL, C., LEMAIRE, E. D., DUDEK, N. L., AND KOFMAN, J. Indicators of dynamic stability in transtibial prosthesis users. *Gait & Posture* 31 (2010), 375–379.
- [131] KEPPEL, T. M., SIEGEL, K. L., AND STANHOPE, S. J. Relative contributions of the lower extremity joint moments to forward progression and support during gait. *Gait & Posture* 6 (1997), 1–8.
- [132] KERR, C. M., STEBBINS, J., THEOLOGIS, T., AND ZAVATSKY, A. B. Static postural differences between neutral and flat feet in children with and without symptoms. *Clinical Biomechanics* 30, 3 (2015), 314–317.
- [133] KHANG, G. O. N., AND ZAJAC, F. E. Paraplegic Standing Controlled by Functional Neuromuscular Stimulation: Part I - Computer Model and Control-System Design. *Ieee Transactions on Biomedical Engineering* 36, 9 (1989), 873–884.
- [134] KHAZZAM, M., LONG, J. T., MARKS, R. M., AND HARRIS, G. F. Preoperative gait characterization of patients with ankle arthrosis. *Gait & Posture* 24, 1 (aug 2006), 85–93.
- [135] KHAZZAM, M., LONG, J. T., MARKS, R. M., AND HARRIS, G. F. Kinematic Changes of the Foot and Ankle in Patients with Systemic Rheumatoid Arthritis and Forefoot Deformity. *Journal of Orthopaedic Research* 25, 3 (2007), 319–329.
- [136] KIDDER, S. M., ABUZZAHAB, F. S., HARRIS, G. F., AND JOHNSON, J. E. A System for the Analysis of Foot and Ankle Kinematics During Gait. *IEEE Transactions on Rehabilitation Engineering* 4, 1 (1996), 25–32.
- [137] KIRBY, K. A., AND GREEN, D. R. Evaluation and nonoperative management of pes valgus. *Foot and Ankle Disorders in Children*, July (1992), 295–327.
- [138] KOOPMAN, B., GROOTENBOER, H. J., AND DE JONGH, H. J. An inverse dynamics model for the analysis, reconstruction and prediction of bipedal walking. *Journal of Biomechanics* 28, 11 (1995), 1369–76.
- [139] LANDORF, K. B., AND KEENAN, A.-M. M. Efficacy of foot orthoses. What does the literature tell us? *Journal of the American Podiatric Medical Association* 90, 3 (2000), 149–158.
- [140] LEARDINI, A., BENEDETTI, M. G., BERTI, L., BETTINELLI, D., NATIVO, R., AND GIANNINI, S. Rear-foot, mid-foot and fore-foot motion during the stance phase of gait. *Gait & Posture* 25, 3 (2007), 453–62.

- [141] LEARDINI, A., BENEDETTI, M. G., CATANI, F., SIMONCINI, L., AND GIANNINI, S. An anatomically based protocol for the description of foot segment kinematics during gait. *Clinical Biomechanics* 14, 8 (1999), 528–536.
- [142] LEARDINI, A., CHIARI, L., DELLA CROCE, U., AND CAPPOZZO, A. Human movement analysis using stereophotogrammetry. *Gait & Posture* 21, 2 (2005), 226–237.
- [143] LEDOUX, W., CAMACHO, D., CHING, R., AND SANGEORZAN, B. The Development and Validation of a Computational Foot and Ankle Model. In *Proceedings of the 22nd Annual EMBS International Conference* (Chicago IL, 2000), pp. 2899–2902.
- [144] LEE, S. Y., AND HERTEL, J. Arch Height and Maximum Rearfoot Eversion During Jogging in 2 Static Neutral Positions. *Journal of Athletic Training* 47, 1 (2012), 83–90.
- [145] LEMMON, D., SHIANG, T. Y., HASHMI, A., ULBRECHT, J. S., AND CAVANAGH, P. R. The effect of insoles in therapeutic footwear - A finite element approach. *Journal of Biomechanics* 30, 6 (1997), 615–620.
- [146] LEUNG, A. K. L., MAK, A. F. T., AND EVANS, J. H. Biomechanical gait evaluation of the immediate effect of orthotic treatment for flexible flat foot. *Prosthetics and Orthotics International*, 852 (1998), 25–34.
- [147] LEVINE, W., ZAJAC, F., BELZER, M., AND ZOMLEFER, M. Ankle controls that produce a maximal vertical jump when other joints are locked. *IEEE Transactions on Automatic Control* 28, 1 (1983), 1008–1016.
- [148] LEVINGER, P., MURLEY, G. S., BARTON, C. J., COTCHETT, M. P., MCSWEENEY, S. R., AND MENZ, H. B. A comparison of foot kinematics in people with normal- and flat-arched feet using the Oxford Foot Model. *Gait & Posture* 32, 4 (2010), 519–523.
- [149] LI, C.-Y., IMAISHI, K., SHIBA, N., TAGAWA, Y., MAEDA, T., MATSUO, S., GOTO, T., AND YAMANAKA, K. Biomechanical Evaluation of Foot Pressure and Loading Force during Gait in Rheumatoid Arthritic Patients with and without Foot Orthosis. *The Kurume Medical Journal* 47, 3 (2011), 211–217.
- [150] LIU, M. Q., ANDERSON, F. C., PANDY, M. G., AND DELP, S. L. Muscles that support the body also modulate forward progression during walking. *Journal of Biomechanics* 39, 14 (2006), 2623–2630.

- [151] LUBOZ, V., PERRIER, A., STAVNESS, I., LLOYD, J. E., BUCKI, M., CANNARD, F., DIOT, B., VUILLERME, N., AND PAYAN, Y. Foot ulcer prevention using biomechanical modelling. *Computer Methods in Biomechanics and Biomedical Engineering: Imaging and Visualization* 2, 4 (2014), 189–196.
- [152] LUNDGREN, P., NESTER, C., LIU, A., ARNDT, A., JONES, R., STACOFF, A., WOLF, P., AND LUNDBERG, A. Invasive in vivo measurement of rear-, mid- and forefoot motion during walking. *Gait & Posture* 28, 1 (2008), 93–100.
- [153] MACLEAN, C., MCCLAY DAVIS, I., AND HAMILL, J. Influence of a custom foot orthotic intervention on lower extremity dynamics in healthy runners. *Clinical Biomechanics* 21, 6 (2006), 623–630.
- [154] MACWILLIAMS, B. A., COWLEY, M., AND NICHOLSON, D. E. Foot kinematics and kinetics during adolescent gait. *Gait & Posture* 17, 3 (2003), 214–24.
- [155] MALAQUIAS, T. M., GONÇALVES, S. B., AND DA SILVA, M. A Three-Dimensional Multibody Model of the Human Ankle-Foot Complex. In *New Trends in Mechanism and Machine Science SE - 47*, P. Flores and F. Viadero, Eds., vol. 24 of *Mechanisms and Machine Science*. Springer International Publishing, 2015, pp. 445–453.
- [156] MALAQUIAS, T. M., SILVEIRA, C., AERTS, W., DE GROOTE, F., DEREYMAEKER, G., VANDER SLOTHEN, J., AND JONKERS, I. Extended foot-ankle musculoskeletal models for application in movement analysis. *Computer Methods in Biomechanics and Biomedical Engineering*, July (2016), 1–7.
- [157] MANN, R. A. Acquired Flatfoot in Adults. *Clinical Orthopaedics and Related Research* 181 (1983), 46–51.
- [158] MARKS, R. M., LONG, J. T., NESS, M. E., KHAZZAM, M., AND HARRIS, G. F. Surgical reconstruction of posterior tibial tendon dysfunction: prospective comparison of flexor digitorum longus substitution combined with lateral column lengthening or medial displacement calcaneal osteotomy. *Gait & Posture* 29, 1 (2009), 17–22.
- [159] MARSHALL, R. N., WOOD, G. A., AND JENNINGS, L. S. Performance objectives in human movement: A review and application to the stance phase of normal walking. *Human Movement Science* 8, 80 (1989), 571–594.
- [160] MARZANO, R. Nonoperative management of adult flatfoot deformities. *Clinics in Podiatric Medicine and Surgery* 31, 3 (2014), 337–347.

- [161] MCCORMACK, A. P., CHING, R. P., AND SANGEORZAN, B. J. Biomechanics of procedures used in adults flatfoot deformity. *Foot and Ankle Clinics* 6, 1 (2001), 15–23.
- [162] MCCULLOCH, M. U., BRUNT, D., AND VANDER LINDEN, D. The effect of foot orthotics and gait velocity on lower limb kinematics and temporal events of stance. *The Journal of Orthopaedic & Sports Physical Therapy* 17, 1 (1993), 2–10.
- [163] MCGOWAN, C. P., KRAM, R., AND NEPTUNE, R. R. Modulation of leg muscle function in response to altered demand for body support and forward propulsion during walking. *Journal of Biomechanics* 42, 7 (2009), 850–856.
- [164] MILLARD, M., MCPHEE, J., AND KUBICA, E. Multi-step forward dynamic gait simulation. *Multibody Dynamics* (2008).
- [165] MKANDAWIRE, C., LEDOUX, W. R., SANGEORZAN, B. J., AND CHING, R. P. Foot and ankle ligament morphometry. *Journal of Rehabilitation Research and Development* 42, 6 (2005), 809–820.
- [166] MOHAMED, O., CERNY, K., ROJEK, L., HERBERT, K., TURNER, R., AND WAISTELL, S. The effects of plastazote® and aliplast®/plastazote® orthoses on plantar pressures in elderly persons with diabetic neuropathy. *Journal of Prosthetics and Orthotics* 16, 2 (2004), 55–63.
- [167] MONTEIRO, M. A., GABRIEL, R. E., AND MOREIRA, M. H. Exercise effects in plantar pressure of postmenopausal women. *Menopause* 17, 5 (2010), 1017–1025.
- [168] MORLOCK, M., AND NIGG, B. M. Theoretical considerations and practical results on the influence of the representation of the foot for the estimation of internal forces with models. *Clinical Biomechanics* 6 (1991), 3–13.
- [169] MORRISON, K. E., HUDSON, D. J., DAVIS, I. S., RICHARDS, J. G., ROYER, T. D., DIERKS, T. A., AND KAMINSKI, T. W. Plantar Pressure During Running in Subjects With Chronic Ankle Instability. *Foot & Ankle International* 31, 11 (2010), 994–1000.
- [170] MÜNDERMANN, A., NIGG, B. M., HUMBLE, R. N., AND STEFANYSHYN, D. J. Foot orthotics affect lower extremity kinematics and kinetics during running. *Clinical Biomechanics* 18, 3 (2003), 254–262.
- [171] MURLEY, G. S., LANDORF, K. B., AND MENZ, H. B. Do foot orthoses change lower limb muscle activity in flat-arched feet towards a pattern

- observed in normal-arched feet? *Clinical Biomechanics* 25, 7 (2010), 728–736.
- [172] MYERS, K. A., WANG, M., MARKS, R. M., AND HARRIS, G. F. Validation of a multi-segment foot and ankle kinematic model for pediatric gait. *IEEE Transactions on Neural Systems and Rehabilitation Engineering* 12, 1 (2004), 122 – 130.
- [173] NAWOCZENSKI, D. A., COOK, T. M., AND SALTZMAN, C. L. The Effect of Foot Orthotics on Three-Dimensional Kinematics of the Leg and Rearfoot During Running. *Journal of Orthopaedic & Sports Physical Therapy* 21, 6 (1995), 317–327.
- [174] NEPTUNE, R. R., KAUTZ, S., AND ZAJAC, F. E. Contributions of the individual ankle plantar flexors to support, forward progression and swing initiation during walking. *Journal of Biomechanics* 34, 11 (2001), 1387–98.
- [175] NEPTUNE, R. R., WRIGHT, I. C., AND VAN DEN BOGERT, A. J. A method for numerical simulation of single limb ground contact events: Application to Heel-Toe Running. *Computer Methods in Biomechanics and Biomedical Engineering* 3, 4 (2000), 321–334.
- [176] NEPTUNE, R. R., ZAJAC, F. E., AND KAUTZ, S. A. Muscle force redistributes segmental power for body progression during walking. *Gait & Posture* 19, 2 (2004), 194–205.
- [177] NESS, M. E., LONG, J., MARKS, R., AND HARRIS, G. Foot and ankle kinematics in patients with posterior tibial tendon dysfunction. *Gait & Posture* 27, 2 (2008), 331–9.
- [178] NORDIN, M., AND FRANKEL, V. H. *Basic Biomechanics of the Musculoskeletal System*, 3rd ed. Lippincott Williams & Wilkins Health, 2001.
- [179] NOVICK, A., AND KELLEY, D. L. Position and movement changes of the foot with orthotic intervention during the loading response of gait. *Journal of Orthopaedic & Sports Physical Therapy* 11, 7 (1990), 301–312.
- [180] OKITA, N., MEYERS, S. A., CHALLIS, J. H., AND SHARKEY, N. A. An objective evaluation of a segmented foot model. *Gait & Posture* 30, 1 (2009), 27–34.
- [181] ONYSHKO, S., AND WINTER, D. A. A mathematical model for the dynamics of human locomotion. *Journal of Biomechanics* 13 (1980), 361–368.

- [182] OOSTERWAAL, M., TELFER, S., TØRHOLM, S., CARBES, S., VAN RHIJN, L. W., MACDUFF, R., MEIJER, K., AND WOODBURN, J. Generation of subject-specific, dynamic, multisegment ankle and foot models to improve orthotic design: a feasibility study. *BMC Musculoskeletal Disorders* 12 (2011), 256.
- [183] ORLIN, M. M. N., AND MCPHIL, T. T. G. Plantar Pressure Assessment. *Physical Therapy* 80, 4 (2000), 399–409.
- [184] PANDY, M. G., AND BERME, N. Quantitative assessment of gait determinants during single stance via a three-dimensional model - Part 1. Normal Gait. *Journal of Biomechanics* 22, 6/7 (1989), 717–724.
- [185] PANDY, M. G., ZAJAC, F. E., SIM, E., AND LEVINE, W. S. An optimal control model for maximum-height human jumping. *Journal of Biomechanics* 23, 12 (1990), 1185–1198.
- [186] PAQUETTE, M. R., ZHANG, S., AND BAUMGARTNER, L. D. Acute effects of barefoot, minimal shoes and running shoes on lower limb mechanics in rear and forefoot strike runners. *Footwear Science* 5, 1 (2013), 9–18.
- [187] PATAKY, Z., DE LEÓN RODRIGUEZ, D., ALLET, L., GOLAY, A., ASSAL, M., ASSAL, J., AND HAUERT, C. Complications Biofeedback for foot offloading in diabetic patients with peripheral neuropathy. *Diabetic Medicine* 27 (2010), 61–64.
- [188] PATON, J., JONES, R. B., STENHOUSE, E., AND BRUCE, G. The Physical Characteristics of Materials Used in the Manufacture of Orthoses for Patients with Diabetes. *Foot & Ankle International* 28, 10 (2007), 1057–1063.
- [189] PATRIARCO, A. G., MANN, R. W., SIMON, S. R., AND MANSOUR, J. M. An evaluation of the approaches of optimization models in the prediction of muscle forces during human gait. *Journal of Biomechanics* 14 (1981), 513–525.
- [190] PEASGOOD, M., KUBICA, E., AND MCPHEE, J. Stabilization of a Dynamic Walking Gait Simulation. *Journal of Computational and Nonlinear Dynamics* 2, 1 (2007), 65–72.
- [191] PEDOTTI, A., KRISHNAN, V. V., AND STARK, L. Optimization of Muscle-Force Sequencing in Human locomotion. *Mathematical Biosciences* 38 (1978), 57–76.
- [192] PÉREZ-GONZÁLEZ, A., FENOLLOSA-ESTEVE, C., SANCHO-BRU, J. L., SÁNCHEZ-MARÍN, F. T., VERGARA, M., AND RODRÍGUEZ-CERVANTES,

- P. J. A modified elastic foundation contact model for application in 3D models of the prosthetic knee. *Medical Engineering & Physics* 30, 3 (2008), 387–398.
- [193] PETERS, A., GALNA, B., SANGEUX, M., MORRIS, M., AND BAKER, R. Quantification of soft tissue artifact in lower limb human motion analysis: A systematic review. *Gait and Posture* 31, 1 (2010), 1–8.
- [194] PETROV, Y. Ellipsoid fit, 2009.
- [195] PRACHGOSIN, T., Y.R. CHONG, D., LEELASAMRAN, W., AND CHATPUN, P. S. Medial longitudinal arch biomechanics evaluation during gait in subjects with flexible flatfoot. *Acta of Bioengineering and Biomechanics* 17, 4 (2015).
- [196] PRATT, D. J., REES, P. H., AND RODGERS, C. Assessment of some shock absorbing insoles. *Prosthetics and orthotics international* 10 (1986), 43–45.
- [197] QUEEN, R. M., ABBEY, A. N., WIEGERINCK, J. I., YODER, J. C., AND NUNLEY, J. A. Effect of shoe type on plantar pressure: A gender comparison. *Gait & Posture* 31 (2010), 18–22.
- [198] RAASCH, C. C., ZAJAC, F. E., MA, B., AND LEVINE, W. S. Muscle coordination of maximum-speed pedaling. *Journal of Biomechanics* 30, 96 (1997), 595–602.
- [199] RAO, S., BAUMHAUER, J. F., TOME, J., AND NAWOCZENSKI, D. A. Comparison of in vivo segmental foot motion during walking and step descent in patients with midfoot arthritis and matched asymptomatic control subjects. *Journal of Biomechanics* 42 (2009), 1054–1060.
- [200] RAZEGHI, M., AND BATT, M. E. Biomechanical Analysis of the Effect of Orthotic Shoe Inserts. *Sports Medicine* 29, 6 (2000), 425–438.
- [201] REDMOND, A., LUMB, P. S. B., AND LANDORF, K. Effect of Cast and Noncast Foot Orthoses on Plantar Pressure and Force During Normal Gait. *Journal of the American Podiatric Medical Association* 90, 9 (2000), 441–449.
- [202] REMY, C. D., AND THELEN, D. G. Optimal estimation of dynamically consistent kinematics and kinetics for forward dynamic simulation of gait. *Journal of Biomechanical Engineering* 131, March 2009 (2009), 031005.
- [203] REN, L., JONES, R. K., AND HOWARD, D. Predictive modelling of human walking over a complete gait cycle. *Journal of Biomechanics* 40 (2007), 1567–1574.

- [204] REN, L., JONES, R. K., AND HOWARD, D. Whole body inverse dynamics over a complete gait cycle based only on measured kinematics. *Journal of Biomechanics* 41 (2008), 2750–2759.
- [205] ROGERS, K., OTTER, S. J., AND BIRCH, I. The effect of Poron® and Plastazote® insoles on forefoot plantar pressures. *British Journal of Podiatry* 9, 4 (2006), 111–114.
- [206] ROME, K. A study of the properties of materials used in podiatry. *Journal of the American Podiatric Medical Association* 81, 2 (1991), 73–83.
- [207] ROME, K., AND BROWN, C. L. Randomized clinical trial into the impact of rigid foot orthoses on balance parameters in excessively pronated feet. *Clinical Rehabilitation* 18, 6 (2004), 624–630.
- [208] SALLES, A. S., AND GYI, D. E. The Specification and Evaluation of Personalised Footwear for Additive Manufacturing. *Work* 41 (2012), 1771–1774.
- [209] SANDERS, J. E., GREVE, J. M., MITCHELL, S. B., AND ZACHARIAH, S. G. Material properties of commonly-used interface materials and their static coefficients of friction with skin and socks. *Journal of Rehabilitation Research and Development* 35, 2 (1998), 161–176.
- [210] SARASWAT, P., MACWILLIAMS, B. A., DAVIS, R. B., AND D'ASTOUS, J. L. Kinematics and kinetics of normal and planovalgus feet during walking. *Gait & Posture* 39, 1 (2014), 339–345.
- [211] SARIKHANI, A., MOTALEBIZADEH, A., ASIAEI, S., AND KAMALI DOOST AZAD, B. Studying Maximum Plantar Stress per Insole Design Using Foot CT-Scan Images of Hyperelastic Soft Tissues. *Applied Bionics and Biomechanics* 2016 (2016).
- [212] SAWACHA, Z., CRISTOFERI, G., GUARNERI, G., CORAZZA, S., DONÀ, G., DENTI, P., FACCHINETTI, A., AVOGARO, A., AND COBELLI, C. Characterizing multisegment foot kinematics during gait in diabetic foot patients. *Journal of NeuroEngineering and Rehabilitation* 6, 37 (2009), 1–11.
- [213] SCARTON, A., GUIOTTO, A., MALAQUIAS, T. M., SINIGAGLIA, G., JONKERS, I., AND SAWACHA, Z. A methodological framework for detecting ulcers' risk in diabetic foot subjects by combining gait analysis, a new musculoskeletal foot model and a foot finite element model. *Gait & Posture* 49 (2016), 6–7.

- [214] SCHEPERS, T., KIEBOOM, B., DIGGELE, P. V., PATKA, P., AND LIESHOUT, E. M. M. V. Pedobarographic Analysis and Quality of Life After Lisfranc Fracture. *Foot & Ankle International* 31, 10 (2010), 857–864.
- [215] SCHERER, P. R., SANDERS, J., ELDREDGE, D. E., DUFFY, S. J., AND LEE, R. Y. Effect of Functional Foot Orthoses on First Metatarsophalangeal Joint Dorsiflexion in Stance and Gait. *Journal of the American Podiatric Medical Association* 96, 6 (2006), 474–481.
- [216] SCHMALZ, T., BLUMENTRITT, S., DREWITZ, H., AND FRESLIER, M. The influence of sole wedges on frontal plane knee kinetics, in isolation and in combination with representative rigid and semi-rigid ankle-foot-orthoses. *Clinical Biomechanics* 21, 6 (2006), 631–639.
- [217] SCOTT, S. H., AND WINTER, D. A. Biomechanical model of the human foot: Kinematics and Kinetics during the stance phase of walking. *Journal of Biomechanics* 26, 9 (1993), 1091–1104.
- [218] SEIREG, A., AND ARVIKAR, R. J. A mathematical model for evaluation of forces in lower extremities of the musculo-skeletal system. *Journal of Biomechanics* 6 (1973), 313–326.
- [219] SELBIE, W. S., AND CALDWELL, G. E. A simulation study of vertical jumping from different starting postures. *Journal of Biomechanics* 29, 96 (1996), 1137–1146.
- [220] SETH, A., SHERMAN, M., REINBOLT, J. A., AND DELP, S. L. OpenSim: a musculoskeletal modeling and simulation framework for in silico investigations and exchange. *Procedia IUTAM - Symposium on Human Body Dynamics* 2 (2011), 212–232.
- [221] SHERMAN, M. A., SETH, A., AND DELP, S. L. Simbody: multibody dynamics for biomedical research. *Procedia IUTAM - Symposium on Human Body Dynamics* 2 (2011), 241–261.
- [222] SHIH, Y. F., CHEN, C. Y., CHEN, W. Y., AND LIN, H. C. Lower extremity kinematics in children with and without flexible flatfoot: A comparative study. *BMC Musculoskeletal Disorders* 13 (2012).
- [223] SIEGLER, S., BLOCK, J., AND SCHNECK, C. D. The Mechanical Characteristics of the Collateral Ligaments of the Human Ankle Joint. *Foot & Ankle* 8, 5 (1988), 234–242.
- [224] SILVA, M. T., AND AMBRÓSIO, J. A. C. Kinematic Data Consistency in the Inverse Dynamic Analysis of Biomechanical Systems. *Multibody System Dynamics* 8 (2002), 219–239.

- [225] SIMON, J., DOEDERLEIN, L., MCINTOSH, A. S., METAXIOTIS, D., BOCK, H. G., AND WOLF, S. I. The Heidelberg foot measurement method: Development, description and assessment. *Gait and Posture* 23, 4 (2006), 411–424.
- [226] SPÄGELE, T., KISTNER, A., AND GOLLHOFER, A. Modeling, simulation and optimization of a human vertical jump. *Journal of Biomechanics* 32 (1999), 521–530.
- [227] STACOFF, A., DE QUERVAIN, I. K., DETTWYLER, M., WOLF, P., LIST, R., UKELO, T., STÜSSI, E., DE QUERVAIN, I. K., DETTWYLER, M., WOLF, P., LIST, R., UKELO, T., AND STÜSSI, E. Biomechanical effects of foot orthoses during walking. *The Foot* 17, 3 (2007), 143–153.
- [228] STAHELI, L. T. Planovalgus Foot Deformity. *Journal of the American Podiatric Medical Association* 89, 2 (1999), 94–99.
- [229] STEWART, S., DALBETH, N., VANDAL, A. C., AND ROME, K. Spatiotemporal gait parameters and plantar pressure distribution during barefoot walking in people with gout and asymptomatic hyperuricemia: Comparison with healthy individuals with normal serum urate concentrations. *Journal of Foot and Ankle Research* 9, 1 (2016).
- [230] SU, S., MO, Z., GUO, J., AND FAN, Y. The Effect of Arch Height and Material Hardness of Personalized Insole on Correction and Tissues of Flatfoot. *Journal of Healthcare Engineering* 2017 (2017).
- [231] SUN, P. C., SHIH, S. L., CHEN, Y. L., HSU, Y. C., YANG, R. C., AND CHEN, C. S. Biomechanical analysis of foot with different foot arch heights: A finite element analysis. *Computer Methods in Biomechanics and Biomedical Engineering* 15, 6 (2012), 563–569.
- [232] SYNGELLAKIS, S., A, A. M., AND RASSOULIAN, H. Assessment of the non-linear behaviour of plastic ankle foot orthoses by the finite element method. *Proceedings of the Institution of Mechanical Engineers. Part H, Journal of engineering in medicine* 214, 5 (2000), 527–539.
- [233] TAGA, G. A model of the neuro-musculo-skeletal system for human locomotion. *Biological Cybernetics* 73 (1995), 97–111.
- [234] TÄNDL, M., STARK, T., EROL, N. E., LÖER, F., AND KECSKEMÉTHY, A. An Object-Oriented Approach to Simulating Human Gait Motion Based on Motion Tracking. *International Journal of Applied Mathematics and Computer Science* 19, 3 (2009), 469–483.

- [235] TANG, S. F. T., CHEN, C. H. C. K., WU, C. K., HONG, W. H., CHEN, K. J., AND CHEN, C. H. C. K. The effects of total contact insole with forefoot medial posting on rearfoot movement and foot pressure distributions in patients with flexible flatfoot. *Clinical Neurology and Neurosurgery* 129, S1 (2015), S8–S11.
- [236] TELFER, S., ABBOTT, M., STEULTJENS, M., RAFFERTY, D., AND WOODBURN, J. Dose-response effects of customised foot orthoses on lower limb muscle activity and plantar pressures in pronated foot type. *Gait & Posture* 38, 3 (2013), 443–449.
- [237] TELFER, S., AND WOODBURN, J. The use of 3D surface scanning for the measurement and assessment of the huma foot. *Journal of Foot and Ankle Research* 3, 19 (2010).
- [238] THELEN, D. G., AND ANDERSON, F. C. Using computed muscle control to generate forward dynamic simulations of human walking from experimental data. *Journal of Biomechanics* 39 (2006), 1107–1115.
- [239] THEOLOGIS, T. N., HARRINGTON, M. E., THOMPSON, N., AND BENSON, M. K. D. Dynamic foot movement in children treated for congenital talipes equinovarus. *The Journal of Bone & Joint Surgery* 85-B, 4 (2003), 572–577.
- [240] TONG, J. W. K., AND NG, E. Y. K. Preliminary investigation on the reduction of plantar loading pressure with different insole materials (SRP - Slow Recovery Poron®, P - Poron®, PPF - Poron®+Plastazote, firm and PPS - Poron®+Plastazote, soft). *The Foot* 20, 1 (2010), 1–6.
- [241] TONON, F. Explicit Exact Formulas for the 3-D Tetrahedron Inertia Tensor in Terms of its Vertex Coordinates. *Journal of Mathematics and Statistics* 1, 1 (2004), 8–11.
- [242] TSUNG, B. Y. S., ZHANG, M., MAK, A. F. T., AND WONG, M. W. N. Effectiveness of insoles on plantar pressure redistribution. *The Journal of Rehabilitation Research and Development* 41, 6 (2004), 767.
- [243] TURNER, D. E., HELLIWELL, P. S., EMERY, P., AND WOODBURN, J. The impact of rheumatoid arthritis on foot function in the early stages of disease : a clinical case series. *BMC Musculoskeletal Disorders* 7, 102 (2006), 1–8.
- [244] TURNER, D. E., AND WOODBURN, J. Characterising the clinical and biomechanical features of severely deformed feet in rheumatoid arthritis. *Gait & Posture* 28 (2008), 574–580.

- [245] TWOMEY, D., MCINTOSH, A. S., SIMON, J., LOWE, K., AND WOLF, S. I. Kinematic differences between normal and low arched feet in children using the Heidelberg foot measurement method. *Gait & Posture* 32, 1 (2010), 1–5.
- [246] ULBRECHT, J. S., HURLEY, T., MAUGER, D. T., AND CAVANAGH, P. R. Prevention of recurrent foot ulcers with plantar pressure-based in-shoe orthoses: The CareFUL prevention multicenter randomized controlled trial. *Diabetes Care* 37, 7 (2014), 1982–1989.
- [247] VAN SOEST, A. J., SCHWAB, A. L., BOBBERT, M. F., AND VAN INGEN SCHENAU, G. J. SPACAR: a software subroutine package for simulation of the behavior of biomechanical systems. *Journal of Biomechanics* 25, 10 (1992), 1219–1226.
- [248] VICENZINO, B. Foot orthotics in the treatment of lower limb conditions: A musculoskeletal physiotherapy perspective. *Manual Therapy* 9, 4 (2004), 185–196.
- [249] VICON MOTION SYSTEMS. Plug-in Gait Reference Guide, 2017.
- [250] VISWANATHAN, V., MADHAVAN, S., GNANASUNDARAM, S., GOPALAKRISHNA, G., NATH DAS, B., RAJASEKAR, S., AND RAMACHANDRAN, A. Effectiveness of Different Types of Footwear Insoles for the Diabetic Neuropathic Foot. *Diabetes Care* 27, 2 (2004), 474–477.
- [251] VUILLERME, N., AND BOISGONTIER, M. Changes in the relative contribution of each leg to the control of quiet two-legged stance following unilateral plantar – flexor muscles fatigue. *European Journal of Applied Physiology* 110, 1 (2010), 207–213.
- [252] VUKOBRATOVIĆ, M., POTKONJAK, V., BABKOVIĆ, K., AND BOROVAC, B. Simulation model of general human and humanoid motion. *Multibody System Dynamics* 17 (2007), 71–96.
- [253] WARD, S. R., AND LIEBER, R. L. Density and hydration of fresh and fixed human skeletal muscle. *Journal of Biomechanics* 38 (2005), 2317–2320.
- [254] WESTBLAD, P., HASHIMOTO, T., WINSON, I., LUNDBERG, A., AND ARNDT, A. Differences in ankle-joint complex motion during the stance phase of walking as measured by superficial and bone-anchored markers. *Foot and Ankle International* 23, 9 (2002), 856–863.
- [255] WILD, S., ROGLIC, G., GREEN, A., SICREE, R., AND KING, H. Global Prevalence of Diabetes (Estimates for the year 2000 and projections for 2030). *Diabetes Care* 27, 5 (2004), 1047–1053.

- [256] WINDLE, C. M., GREGORY, S. M., AND DIXON, S. J. The shock attenuation characteristics of four different insoles when worn in a military boot during running and marching. *Gait & Posture* 9, 1 (1999), 31–37.
- [257] WISMANS, J., VELDPAUS, F., AND STRUBEN, P. A three dimensional mathematical model of the knee joint. *Journal of Biomechanics* 13 (1980), 677–685.
- [258] WOJTYRA, M. Multibody Simulation Model of Human Walking. *Mechanics Based Design of Structures and Machines* 31, June 2015 (2003), 357–379.
- [259] WOODBURN, J., NELSON, K. M., SIEGEL, K. L., KEPPEL, T. M., AND GERBER, L. H. Multisegment Foot Motion During Gait: Proof of Concept in Rheumatoid Arthritis. *The Journal of Rheumatology* 31, 10 (2004), 1918–27.
- [260] WREN, T. A. L., GORTON, G. E., ÖUNPUU, S., AND TUCKER, C. A. Efficacy of clinical gait analysis: A systematic review. *Gait & Posture* 34, 2 (2011), 149–153.
- [261] YAMAGUCHI, G. T., AND ZAJAC, F. E. Restoring Unassisted Natural Gaitto Paraplegics Via Functional Neuromuscular Stimulation: A Computer SimulationStudy. *IEEE Transactions on Biomedical Engineering* 37, 9 (1990), 886–902.
- [262] YURT, Y., SENER, G., AND YAKUT, Y. The effect of different foot orthoses on pain and health related quality of life in painful flexible flat foot: a randomized controlled trial. *European Journal of Physical and Rehabilitation Medicine* 2018 Mar 16 (2018), Epub ahead of print.
- [263] ZAJAC, F. E., NEPTUNE, R. R., AND KAUTZ, S. A. Biomechanics and muscle coordination of human walking Part I: Introduction to concepts, power transfer, dynamics and simulations. *Gait & Posture* 16, 3 (2002), 215–232.
- [264] ZAJAC, F. E., NEPTUNE, R. R., AND KAUTZ, S. A. Biomechanics and muscle coordination of human walking Part II: Lessons from dynamical simulations and clinical implications. *Gait & Posture* 17 (2003), 1–17.
- [265] ZAJAC, F. E., WICKE, R. W., AND LEVINE, W. S. Dependence of jumping performance on muscle properties when humans use only calf muscles for propulsion. *Journal of Biomechanics* 17 (1984), 513–523.
- [266] ZHANG, X. *Multi-segment foot kinematics and foot muscle morphology in recreatinal runners with a pronated foot posture*. Ph.d. thesis, KU Leuven, 2018.

- [267] ZHANG, X., AND LI, B. Influence of in-shoe heel lifts on plantar pressure and center of pressure in the medial-lateral direction during walking. *Gait & Posture* 39, 4 (2014), 1012–1016.
- [268] ZIFCHOCK, R. A., AND DAVIS, I. A comparison of semi-custom and custom foot orthotic devices in high- and low-arched individuals during walking. *Clinical Biomechanics* 23 (2008), 1287–1293.

Curriculum Vitae

Personal Data

Name: Tiago de Melo Malaquias
Date of birth: 7th of September, 1990
Place of birth: Lisbon, Portugal
Work address: Biomechanics Section
Department of Mechanical Engineering,
KU Leuven
Celestijnenlaan 300C, B-3001 Heverlee, Belgium
Email: melo.malaquias@kuleuven.be
Alt. email: melo.malaquias@gmail.com

Education

2015-Present: PhD candidate at the Biomechanics Section, Department of Mechanical Engineering, KU Leuven, Leuven, Belgium

2008-2013: Integrated Master's Degree in Biomedical Engineering, Instituto Superior Técnico (IST), Lisbon University, Lisbon, Portugal

2012-2013: Erasmus Exchange Program, Master of Science in Biomedical Engineering, Eindhoven University of Technology, Eindhoven, The Netherlands

Experience

- 2014: Researcher – NP Mimetic Project, Dynamics of Mechanical Systems Research Group, University of Minho, Guimarães, Portugal
- 2010-2014: Research Assistant (Volunteer) – Biomechanics of Movement Research Group, Instituto Superior Técnico (IST), Lisbon University, Lisbon, Portugal

Volunteering

- 2017-Present: Founder and Board President, Portuguese Association of Students, Researchers and Graduates in Belgium, The Netherlands and Luxembourg
- 2015-2017: Board Member – Webmaster, PhD Society Leuven
- 2009-2014: Board Member, Vice-President and General Assembly President Biomedical Students Union of Instituto Superior Técnico

Awards

Best Poster Award - National Committee on Biomedical Engineering
15th National Day on Biomedical Engineering, Brussels, Belgium, 2016
Malaquias T.; Weckx C.; Aerts W.; De Groot F.; Jonkers I.; Vander Sloten J.
Plantar pressure-based estimates of foot kinematics during gait – Optimization approach.

Best Paper Award - European Society for Movement analysis in Adults and Children (ESMAC)
25th ESMAC Annual Meeting, Seville, Spain, 2016
Scarton A., Guiotto A., Malaquias T., Sinigaglia G., Jonkers I., Sawacha Z.
A methodological framework for detecting ulcers' risk in diabetic foot subjects by combining gait analysis, a new musculoskeletal foot model and a foot finite element model.

List of publications

Publications in International Peer Reviewed Journals

Boey, Hannelore; **Malaquias, Tiago M.**; Natsakis, Tassos; Clockaerts, Stefan; Misselyn, Dominique; Coudyzer, Walter; Vander Sloten, Jos; Jonkers, Ilse. *4D CT scanning combined with a foot manipulator device allows to measure hind- and midfoot kinematics during simulated gait*. Submitted to the Journal of Orthopaedic Research.

Scarton, Alessandra; Guiotto, Annamaria; **Malaquias, Tiago M.**; Spolaor, Fabiola; Sinigaglia, Giacomo; Cobelli, Claudio; Jonkers, Ilse; Sawacha, Zimi. *A methodological framework for detecting ulcers' risk in diabetic foot subjects by combining gait analysis, a new musculoskeletal foot model and a foot finite element model*. Gait & Posture; 2018; Vol. 60; pp. 279 - 285

Malaquias, Tiago M.; Silveira, Carolina; Aerts, Wouter; De Groote, Friedl; Dereymaeker, Greta; Vander Sloten, Jos; Jonkers, Ilse. *Extended foot-ankle musculoskeletal models for application in movement analysis*. Computer Methods in Biomechanics and Biomedical Engineering; 2017; Vol. 20; iss. 2; pp. 153 - 159

Malaquias, Tiago M.; Gonçalves, S. B.; Silva, M.T. 2015. *A Three-Dimensional Multibody Model of the Human Ankle-Foot Complex*, book chapter in New Trends in Mechanism and Machine Science – From Fundamentals to Industrial Applications (P. Flores, F. Viadero, eds.), pp 445-453.

Conference Abstracts

Guiotto, Annamaria; **Malaquias, Tiago M.**; Ciniglio, Alfredo; Acquaviva, Marco, Wesseling, Mariska; Guarneri, Gabriella; Avogaro, Angelo; Jonkers, Ilse; Sawacha, Zimi. *Multiscale modelling in diabetic foot prevention: a muscle forces*

driven approach. Accepted to the 27th Congress of the International Society of Biomechanics/43rd Annual Meeting of the American Society of Biomechanics, July 31 – August 4, 2019, Calgary, Canada.

Malaquias, Tiago M.; Aerts, Wouter; De Groote, Friedl; Jonkers, Ilse; Vander Sloten, Jos. *Predictive simulations of the corrective effect of controlled stiffness 3D-printed insoles during the stance phase of gait.* 8th World Congress of Biomechanics, July 8 – 12, 2018, Dublin, Ireland.

Boey, Hannelore; **Malaquias, Tiago M.**; Natsakis Tassos; Clockaerts, Stefan; Vander Sloten, Jos; Jonkers, Ilse. *Validation of 4D CT scanning combined with a foot manipulator to measure individual foot bone kinematics.* 8th World Congress of Biomechanics, July 8 – 12, 2018, Dublin, Ireland.

Guiotto, Annamaria; **Malaquias, Tiago M.**; Spolaor, Fabiola; Jonkers, Ilse; Sawacha, Zimi. *A multi-scale framework for the prevention of plantar ulcers in diabetic subjects: a multidisciplinary approach combining gait analysis, musculoskeletal and finite element foot modeling.* 8th World Congress of Biomechanics, July 8 – 12, 2018, Dublin, Ireland.

Malaquias, Tiago M.; Aerts, Wouter; De Groote, Friedl; Jonkers, Ilse; Vander Sloten, Jos. *Plantar pressure based estimates of foot kinematics during gait – A least squares optimization approach.* 15th International Symposium on Computer Methods in Biomechanics and Biomedical Engineering, March 26 - 29, 2018, Lisbon, Portugal.

Guiotto, Annamaria; **Malaquias, Tiago M.**; Spolaor, Fabiola; Saurin, Martina; Jonkers, Ilse; Sawacha, Zimi. *The role of muscle forces on foot internal stresses and plantar pressure distribution: differences between healthy and diabetic neuropathic subjects.* 26th European Society for Movement analysis in Adults and Children Annual Meeting, September 6 – 9, 2017, Trondheim, Norway.

Guiotto, Annamaria; Scarton, Alessandra; **Malaquias, Tiago M.**; Jonkers, Ilse; Vander Sloten, Jos; Cobelli, Claudio; Sawacha, Zimi. *Foot FEM models for plantar ulcer prevention: Comparison between joint reaction forces and muscle forces as boundary conditions.* 26th Congress of the International Society of Biomechanics, July 23-27, 2017, Brisbane, Australia

Malaquias, Tiago M.; Weckx, Cederic; Aerts, Wouter; De Groote, Friedl; Jonkers, Ilse; Vander Sloten, Jos. *Plantar pressure based estimates of foot kinematics during gait – A least squares optimization approach.* 7th Portuguese Congress on Biomechanics, February 10 - 11, 2017, Guimarães, Portugal.

Malaquias, Tiago M.; Weckx, Cederic; Aerts, Wouter; De Groote, Friedl; Jonkers, Ilse; Vander Sloten, Jos. *Plantar pressure based estimates of foot*

kinematics during gait – Optimization aproach. 15th Belgian National Day on Biomedical Engineering, November 25, 2016, Brussels, Belgium.

Scarton, Alessandra; Guiotto, Annamaria; **Malaquias, Tiago M.**; Sinigaglia, Giacomo; Jonkers, Ilse; Sawacha, Zimi. *Combination of gait analysis, musculoskeletal modeling and finite element modeling: an improved approach for the biomechanical analysis of the diabetic foot.* 17th Meeting of the Società Italiana di Analisi del Movimento in Clinica, October 5-8, 2016, Milan, Italy.

Scarton, Alessandra; Guiotto, Annamaria; **Malaquias, Tiago M.**; Sinigaglia, Giacomo; Jonkers, Ilse; Sawacha, Zimi. *A methodological framework for detecting ulcers' risk in diabetic foot subjects by combining gait analysis, a new musculoskeletal foot model and a foot finite element model.* 25th European Society for Movement analysis in Adults and Children Annual Meeting, Date: September 26 – October 1, 2016, Seville, Spain.

Malaquias, Tiago M.; Silveira, C.; Aerts, W.; De Groote, F.; Dereymaeker, G.; Vander Sloten, J.; Jonkers, I. 2015. *Development of a new CT scan-based Foot-Ankle Multibody Model.* 13th International Symposium on Computer Methods in Biomechanics and Biomedical Engineering, September 1-5, 2015, Montreal, Canada.

Malaquias, Tiago M.; Goncalves, Sérgio B.; Tavares da Silva, Miguel. *A Three-Dimensional Multibody Model of the Human Ankle-Foot Complex.* 5th European Conference on Mechanism Science. September 16 – 20, 2014, Guimarães, Portugal.

Malaquias, Tiago M.; Gonçalves, S. B.; Silva, M. T. 2014. *Development of a Three-Dimensional Multibody Model of the Human Leg and Foot for Application to Movement Analysis.* 3rd Joint International Conference on Multibody System Dynamics and the 7th Asian Conference on Multibody Dynamics, June 30-July 3, 2014, Busan, South Korea.

FACULTY OF ENGINEERING SCIENCE
DEPARTMENT OF MECHANICAL ENGINEERING
BIOMECHANICS SECTION
Celestijnenlaan 300C box 2419
B-3001 Leuven
melo.malaquias@kuleuven.be
<https://www.mech.kuleuven.be/en/bme>

